Stability Analysis of the Spine Pertaining to Idiopathic Scoliosis

by

Micheline Reimbold

Department of Civil Engineering and Applied Mechanics

McGill University, Montreal, Quebec, Canada

June, 1992

A Thesis submitted to the Faculty of Graduate Studies and Research
in partial fulfilment of the requirements of the degree of
Master of Engineering.

0-612-44102-4

Dedicated to those suffering

from idiopathic scoliosis

Abstract

A three-dimensional structural analysis model of the human thoracolumbar spine and rib cage has been developed in order to investigate its stability in relation to adolescent idiopathic scoliosis. Idiopathic scoliosis is one of the most puzzling deformities of the spine, due to the fact that there is no known initiating cause. From the viewpoint that it can be explained in a purely biomechanical manner, one particular hypothesis as to its etiology is investigated in this thesis. The hypothesis is that a lordosis-inducing growth of the thoracic spine [34,100,115] in conjunction with spinal asymmetries in the lateral or horizontal plane [34] is the primary cause of the deformity.

Analyses are performed on the constructed model using the MSC/NASTRAN finite element program. The model consists primarily of interconnected beam elements to represent a realistic geometry of the spine and rib cage. The various stiffness properties needed in the model were obtained from the published literature. Simulations of analyses and experiments performed by other researchers produced comparable results, thereby validating the present model, which is then used to investigate the above hypothesis.

Lordosis-inducing growth, in which the anteriors of the thoracic vertebrae grow faster than the posteriors, is simulated in a geometric nonlinear analysis by differential thermal loading of these parts. Results show that under such loading, the model of the normal spine with its natural asymmetries of the thoracic region, gradually deforms into a shape with displacements and rotations typical of thoracic idiopathic scoliosis. These results therefore constitute a validation of the stated hypothesis, and indicate that a lordosis-inducing growth of the thoracic vertebrae is a likely cause of thoracic idiopathic scoliosis.

Résumé

Un modèle d'analyse structurale tridimensionnelle de la colonne vertébrale dorso-lombaire et de la cage thoracique a été developpé dans le but d'étudier sa stabilité en relation avec la scoliose idiopathique chez l'adolescent. La scoliose idiopathique est une déformation de la colonne vertébrale qui est des plus énigmatiques: sa cause demeure inconnue. En tenant compte du fait que cette déformation peut être expliquée d'une façon purement biomécanique, cette thèse explore une hypothèse étiologique particulière. Selon cette hypothèse, la cause primaire de la déformation consiste en la conjonction de la croissance de la colonne dorsale, responsable d'une lordose [34,100,115], et d'asymétries vertébrales dans les plans latéral ou horizontal [34].

Des analyses on été effectuées sur le modèle en utilisant le logiciel d'analyse avec éléments finis MSC/NASTRAN. Le modèle est constitué essentiellement d'éléments de poutre interconnectés qui représentent une géométrie réaliste de la colonne vertébrale et de la cage thoracique. Les différentes rigidités nécessaires à la construction du modèle ont été trouvées dans la littérature existante. Des simulations d'analyses et d'expériences faites par d'autres chercheurs ont produit des résultats comparables, validant par conséquent le modèle proposé. Ce modèle a alors été utilisé pour étudier l'hypothèse mentionnée ci-dessus.

La croissance provoquant la lordose, pendant laquelle la partie antérieure des vertèbres dorsales croît plus rapidement que leur partie postérieure, est simulée dans une analyse géométriquement non-linéaire par un chargement thermique différentiel. Les résultats ont démontré que sous un tel chargement, le modèle normal de la colonne vertébrale avec ses asymétries naturelles de la région dorsale, se déforme graduellement jusqu'à une forme ayant des déplacements et des rotations typiques de la scoliose dorsale idiopathique. Par conséquent, ces résultats constituent une validation de l'hypothèse énnoncée ci-dessus; de même, ils indiquent que la croissance provoquant la lordose des vertèbres dorsales est une cause probable de la scoliose dorsale idiopatique.

Acknowledgements

The author would like to take this opportunity to express her sincere thanks to her advisor Professor S.C. Shrivastava for his guidance and invaluable time offered throughout this project. In addition, appreciation is extended to Dr. H. LaBelle of Hôpital Sainte-Justine, Montreal, for suggesting references which helped focus the direction of this work.

The author acknowledges her gratitude to the Natural Sciences and Engineering Research Council of Canada for the scholarship support, and to the Computing Center of McGill University for granting generous computer funding and consultations. Without their assistance, the project would not have been possible.

Finally, the writer wishes to thank her family, friends, and fellow students for their continual support and encouragement. A special thanks is extended to Mr. N. Riverin for the use of his computer, and Miss G. Romero, Miss P. Conner, and Miss J. Shaw for their assistance in preparing the thesis.

Table of Contents

List of Figures

List of Tables

List of Symbols

A	cross-sectional area
a	transverse radius
a_0	amplitude of curve
b	sagittal radius
C_w	warping torsion constant
E	Young's modulus of elasticity
eq	denotes equivalent
G	shear modulus of elasticity
I_1,I_2	area moments of inertia in planes 1 and 2 respectively, where planes 1, 2, and the cross-sectional plane are mutually perpendicular.
I_{12}	area product of inertia
I_x,I_y,I_z	area moments of inertia about axis x, y, z respectively
I_o	polar moment of inertia of cross-section about the shear center O
J	torsional constant
K_1,K_2	shear area factors for planes 1 and 2 respectively, where planes 1, 2, and the cross-sectional plane are mutually perpendicular.
L	length, height (of vertebrae, disc, etc.)
M_{cr}	critical buckling moment
P_{cr}	critical buckling load
R	radius of curvature
t	thickness
U	internal strain energy
V	potential energy of external loads
u,v,w	represent displacements of a point in x,y,z axes directions respectively
β	axial rotation about the longitudinal axis, i.e. horizontal plane rotation
λ	effective length or equivalent length of Euler column
υ	Poisson's ratio

Chapter 1
Introduction

1.1 The Clinical Problem

Scoliosis has been found to be the most common spinal deformity in North American children and adolescents [96,134]. It is defined as an abnormal lateral curvature of the spine [96]. Approximately eighty percent of the reported cases are what is known as *idiopathic scoliosis* [41,61,94,96,99]. The name idiopathic derives from the fact that these curves have no known cause or etiology [61,94,96,99]. In other words, the deformity is found to develop in otherwise healthy children and adolescents with no apparent spinal abnormalities or associated musculoskeletal conditions [29,34].

Idiopathic scoliosis may be classified according to the age of onset or of detection of the deformity. The majority of the cases of idiopathic scoliosis, particularly in North America (75% in many clinics [99]), occur and progress during the adolescent growth spurt, and hence they are termed *adolescent idiopathic scoliosis* (abbreviated as AIS) [34,94,96,135]. The rates of incidence as well as the distribution of the type of idiopathic scoliosis, e.g. the age of onset, are found to vary among countries. The variance in incidence is compounded by the fact that different detection techniques with varying sensitivity (e.g. visual rib hump test or radiograph), different populations of children, and different definitions of scoliosis (i.e. the degree or the severity of curve) are used in the clinical studies of scoliosis [70]. Generally, AIS is reported to have an incidence of 1.4 to 4.1 per 1000 persons, and it is predominantly found in girls over boys by a ratio of 9:1 [19,53,55]. It is estimated that about 15% of the adolescent population has idiopathic scoliosis to some degree [33,104].

Of the cases diagnosed, approximately 20% have curves that eventually progress or worsen [66,71]. The progressive cases lead to a poorer quality of life, filled with emotional and psychological anguish, as well as physical pain. Severe cases, particularly those of early onset, may lead to serious cardio-pulmonary disorders and even early death [41,66,99].[1]

The development of surgical procedures has outpaced the understanding of scoliosis [41]. Modern surgical techniques, such as the implantation of the Harrington rod, and the Cotrel-

[1] These early-onset cases, often classified as infantile scoliosis, are quite rare in North America. However, they appear frequently in Europe. Fortunately, a large percentage of these infantile cases correct themselves and only 10% have the potential to progress to such severe forms [41,66,99].

Dubousset and Zielke instrumentations, are available to treat the severe curves [52]. However, they are only partially successful in that a correction of up to 50% of the lateral deformity may be achieved [66]. Together with bracing devices like the Milwaukee brace, approximately 80% of curves treated show improvement [61]. Since the chances of correction are improved by early detection [41], screening programs have been instituted in schools for detection of the curves in their early stages. As a result, a larger number of curves are now found, but of less severity [94].

The problem lies not so much in the detection of curves but in the prediction of their progression, i.e. in determining which ones are going to progress. Only the progressive curves require extensive treatment. However, the factors causing progression are not entirely understood. This uncertainty of prognosis renders the current approach to treatment a conservative one. In one study [77], it was found that only 1 out of every 4 curves braced was progressive. In order to eliminate unnecessary treatments, since only a small percentage of the cases diagnosed progress, an understanding of the etiology of AIS is necessary [41,94].

Knowledge of the etiology will help determine the factors responsible for curve progression. Patients may then be evaluated properly and prescribed the most appropriate treatment with greater confidence. As a result, significant costs and acute discomforts, due to these unnecessary treatments, may be minimized [94]. In addition, the understanding of the primary lesion will help in the development of the most effective methods of bracing and surgery. Clinically, it is felt that the correction of the primary deforming mechanism, if possible, is the best approach for treatment because secondary effects, responsible for gross deformity, are likely to correct themselves as a result [24,34,35,41,100]. Patients with progressive cases may then be effectively treated, and better corrective results may be attained.

Before one can hope to understand the etiology of AIS, a thorough understanding of the three-dimensional deformity is necessary [26,66]. In addition, a knowledge of the anatomy of the normal spine is helpful to better understand the abnormal one. The anatomy of the spine, which may be unfamiliar to the reader, is explained extensively in Chapter 2. Definitions of terms denoted with an asterisk (*) may be found in the glossary, Appendix A.

The lateral curve is the most obvious feature of the deformity. The frontal* view of a normal spine is basically straight, whereas the same view of a scoliotic spine reveals the lateral curve. The region of the spine in which the abnormal lateral curve is located, and the side to which it deviates defines the curve pattern. Various curve patterns exist. For example, common curve patterns are the single thoracic* curve (curve in thoracic region, convex to the right, i.e. away from heart), and the right thoracic - left lumbar* double curve [4,61,70]. The severity of the deformity is classified according to the degree of curvature of the lateral curve which is commonly measured by Cobb angle. Cobb angle is defined as the angle, on the radiograph of the spine, between the lines drawn on the endplates of the vertebrae at the inflection points of the curve [96].

The majority of the AIS cases are found to be right thoracic. Curves in the thoracic region produce the most significant visual deformities, and are the most dangerous. The ribs, which are connected to the thoracic vertebral column, deform in accordance with the rotation and lateral deviation of the vertebrae. As a result, a rib hump protrudes posteriorly on the convex side of curve; a rib valley appears anteriorly on the concave side; and more importantly, the space for vital organs is reduced [32,41]. The typical deformity of thoracic scoliosis is shown in Fig. 1.1. Due to the fact that thoracic curves are both a common and serious form of the deformity, they are addressed specifically in this study.

All idiopathic curves are classified as structural curves.[1] The term structural implies that there is a significant rotation of vertebrae about their longitudinal axes associated with the lateral curve such that the anterior* aspect of a vertebra rotates towards the convexity of the lateral curve and the posterior* side towards the concavity [23,34,96,135].[2] From now on, following the terminology used in the literature, the direction of the axial rotation will be described with respect to the anterior aspect of the vertebrae. For example, the rotation found in idiopathic scoliosis will be denoted convex-sided rotation since the anteriors of vertebrae go towards the convexity of the curve. This convex-sided rotation is found in all cases of idiopathic scoliosis, regardless of the curve pattern. This type of rotation, illustrated in Fig. 1.2(b), is opposite to the usual type of rotation accompanying lateral bending of the normal spine, shown in Fig. 1.2(a) [72,129].

The magnitude of the convex-sided rotation is found to reach a maximum at the apex of the lateral curve, i.e. the point most laterally deviated point from the vertical axis. Both the direction and magnitude of the rotation are illustrated in Figs. 1.3 (a) and (b), which show posterior views of a thoracic scoliosis. In both figures, it is obvious that the spinous processes located on the posterior of the vertebrae, denoted with lines on radiograph in Fig. 1.3(a), rotate towards the concavity of the

---

[1]Structural curves are distinguished from other lateral curves known as compensatory and functional curves. Compensatory curves have little or no rotation compared to structural curves and arise to maintain vertical alignment of the spine, and as such, they have little chance of progression [66,96]. Functional curves have a rotation which is in the opposite direction to that which is found in structural curves [23]. These curves arise as a result of known causes such as a tilted pelvis or unequal leg lengths. This rotation type is the same as that accompanying lateral bending of the normal spine.

[2]In engineering terms (using the right-hand rule), this means that the axial rotation vector is directed downwards along the vertebra for the right-convex curves, and directed upwards for the left convex curves.

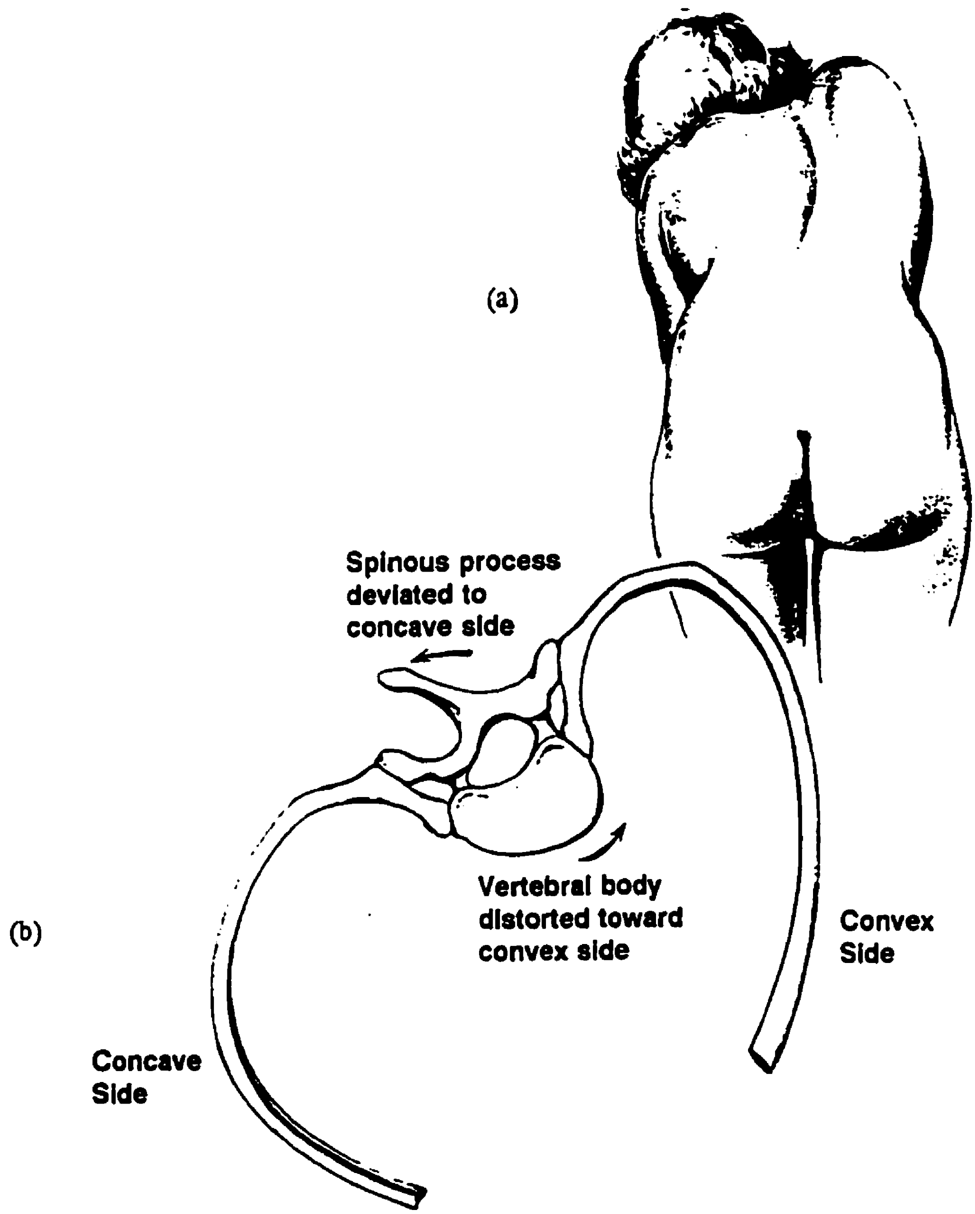

Fig. 1.1 An example of advanced right thoracic scoliosis. (a) View of the patient from behind showing the characteristic rib hump. (b) View of a horizontal section from below indicating key characteristics. After Keim [61].

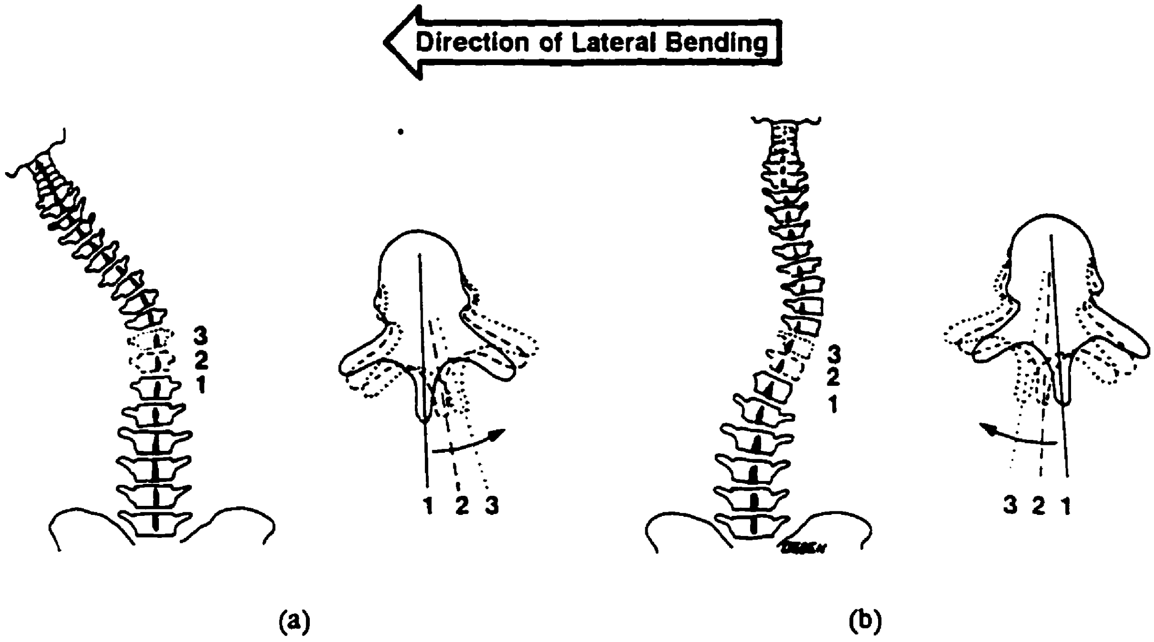

Fig. 1.2 Posterior views of the spine illustrating the coupling of lateral bending and axial rotation. In normal lateral bending (a), the spinous process rotate towards the convexity of the lateral curve and the anterior of vertebrae rotate towards the concavity, i.e. concave-sided rotation. In the scoliotic deformity (b), the spinous process rotate towards the concavity of the lateral curve and the anterior of vertebrae rotate towards the convexity, i.e. convex-sided rotation. After White and Panjabi [130].

lateral curve. The coincidence of the maximum lateral deviation and axial rotation is indicated by the closeness of the posterior elements to the inside of the lateral curve at the apex of the curve. The vertebra most rotated and most deviated from the vertical is often referred to as the apical vertebra. The nature of these rotations seem to give the curves their progression potential [66], and hence they are of great concern clinically.

Implied by the above described combination of lateral curve and convex-sided rotation is another feature of the scoliotic deformity: a lordosis*, i.e. a longer anterior length than posterior length of spine. Since the rotation in idiopathic scoliosis is always as described above, with the anterior aspect of spine rotating towards the outside of lateral curve and posterior aspect towards the inside, particularly at the apex, geometrically, the anterior length *must* be longer than the posterior in the section with the lateral curve, in order to obtain such a rotation. A longer anterior than posterior spine length implies a curve convex towards the anterior of the spine which by definition is known as a *lordosis*. Thus, regardless of the location of the curve, there is always a lordosis in the apical region of the lateral curve.

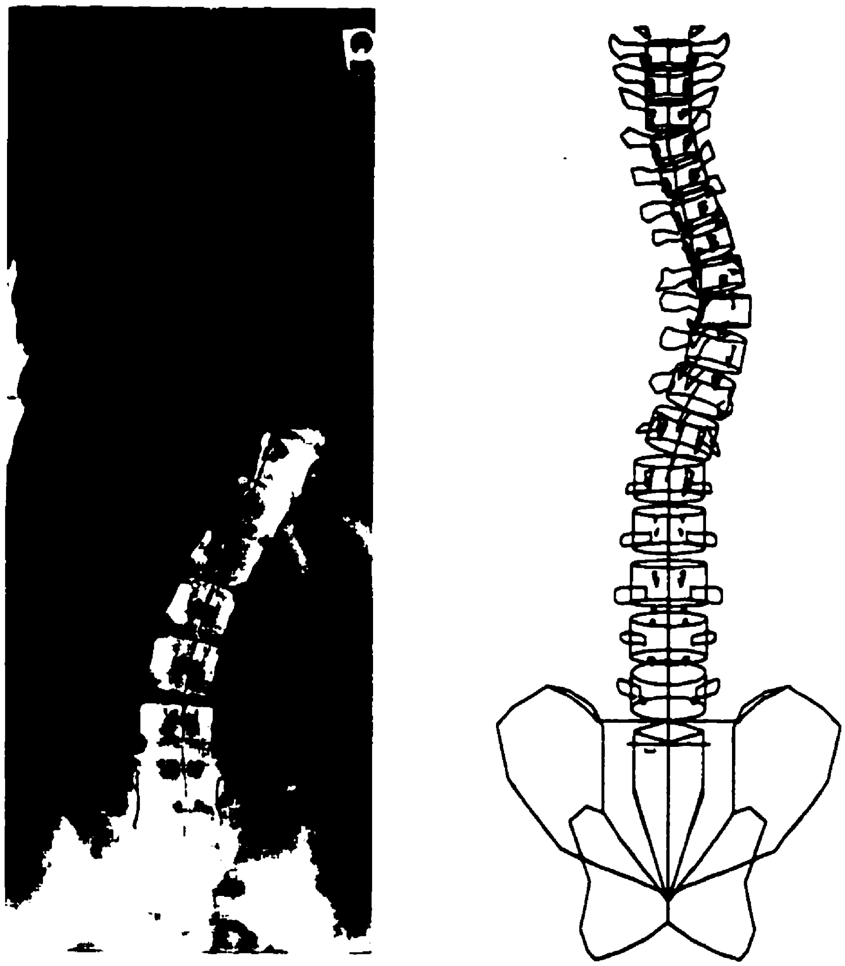

(a) (b)

Fig. 1.3 Posterior view of right thoracic scoliosis illustrating convex-sided rotation. (a) Radiograph of the deformity with markings indicating the spinous process line. (b) Computer graphics drawing of the deformity. After Herzenberg et al. [52].

The rotational component of the deformity gives the impression that the scoliotic patient has a severe kyphosis* or hunchback rather than a lordosis. However, close examination of the deformity, taking into account the large amount of axial rotation, does reveal that there is in fact a lordosis at the apex of the lateral curve [34]. This lordotic tendency of the spine at the apex of thoracic scoliotic curves was first noted by Adams in 1865 [1]. Adams described scoliosis as a product of rotation and lordosis. Thus, a lateral curve, convex-sided vertebral axial rotation, and a lordosis combined with an unexplained etiology to their development characterize idiopathic scoliosis.

As mentioned before, the factors of progression are not entirely known. Currently, the risk factors of progression are considered to be skeletal immaturity, young chronological age, female gender, curve magnitude, curve pattern, family history, and noticeable thoracic lordosis [41,70,96]. Skeletal immaturity and young chronological age at the time of detection, both present risks for progression since they imply a large amount of growth remaining[1] for potential progression. Curves have the ability to progress significantly during growth [32]. Generally, the earlier is the onset, the worse is the prognosis [34,96,99]. Female gender is an obvious risk since the deformity predominantly occurs in girls, as mentioned earlier. Curve magnitude and curve pattern are factors which must be taken into consideration. A study conducted by Lonstein and Carlson [71] reveals that patients whose initial curvatures are greater than 20 degrees by Cobb angle* measurement, or who have double or thoracic curves, have greater probability of progression. Family history becomes an important factor in the face of the evidence indicating that scoliosis is hereditary [135]. The last factor, thoracic lordosis, is a risk because, as explained above, it is a feature which is noted in patients with thoracic scoliosis and is *not typical* of the normal thoracic region.

Although the presence of the thoracic lordosis at the apex of the scoliotic curve has been known for some time [1], it was only later emphasized by Somerville in 1952 [115], Roaf in 1966 [100], and more recently brought into prominence by Dickson et al. in 1986 [34]. Somerville, Roaf, and Dickson et al. all formulated hypotheses concerning the etiology of AIS based on the development of a primary lordosis in the thoracic region of the spine. Somerville [115] and Leatherman and Dickson [66] referred to the deformity, perhaps more appropriately, as rotational lordosis and lordoscoliosis, respectively. Dickson et al. [34] expanded upon the hypothesis by stating that a lordosis coupled with another asymmetry in either the lateral or horizontal plane, which he termed *biplanar spinal asymmetry*, superimposed during growth produces scoliosis.

These related theories appear promising since a lordosis must exist in order to obtain the lateral deviation and axial rotation of the kind noted in idiopathic scoliosis. Thus, either the thoracic lordosis results from, or is a factor causing the development of the spinal lateral displacement and rotation. In addition, the lordosis hypothesis has explanations for many of the clinical findings of scoliosis. As such, this factor must not be overlooked and it, in fact, becomes the focus of this study. For simplicity, the hypothesis investigated will be referred to as the lordosis hypothesis. This and other etiological theories and correlating clinical investigations pertaining to idiopathic scoliosis are discussed in Chapter 3.

[1]Spinal growth is suspected to continue until approximately the age of 25 years [56].

1.2 Biomechanical Approach to Idiopathic Scoliosis

The mechanics of the spine has been a challenging topic in the field of biomechanics, for some time now. Understanding the initiating factor of idiopathic scoliosis has been the particular aim of many studies. It is one of the most sought-after problems.

The spine may be idealized as a column. It is the main load-bearing structure in the human body, analogous to the column in a building structure. However, it is a very complex column. It is composed of discrete elements, i.e. discs and vertebrae, with very different linear and nonlinear material properties; has complex kinematics and interactions between elements due to the presence of facet joints and ligaments; is subjected to growth (material and geometric changes) and large deformations; and has complex rib cage and muscle interaction forces.

The fact that scoliosis is a deformity, whereby a once straight spine (basically straight when viewed in the frontal plane) deviates into a curved configuration, leads one to suspect that scoliosis is a *buckling or structural instability phenomenon* [48]. The initial curve present in the sagittal* plane, and the deformations involving lateral displacement and axial rotation suggest more particularly, *torsional-flexural buckling* of the spine. From this viewpoint, factors decreasing its stability would increase the rate of progression of scoliosis [26,31]. Results of a buckling analysis would throw light on the subject of scoliotic progression.

It is well known [123] that the stability of a circular curved column of thin rectangular cross-section subjected to a pure moment about the strong axis of bending is dependent on the direction and the amount of curvature, with respect to the direction of the moment loading. The curved column is more stable, i.e. it can be subjected to a greater moment prior to buckling, if the moment is applied in the sense to increase the curvature than to decrease it. The kind of loading is analogous to the thoracic spine subjected to flexion*, i.e. forward bending. In this bending, the thoracic spine can be expected to be more stable with a kyphosis than with a lordosis. This observation lends support to the conjecture that a thoracic lordosis renders the spine less stable and hence more susceptible to (scoliosis) buckling.

Due to the complex nature of the spine structure, modelling is very difficult and requires many approximations. Lucas and Bresler [73] investigated the stability of the ligamentous thoracolumbar* spine. Theoretically, they analyzed the spine as a homogeneous column with stiffness effectively equivalent to the stiffness of the whole non-homogeneous column. Their theoretical results were in good agreement with their experimental results.[1] Belytschko et al. [10] simulated the experiment conducted by Lucas and Bresler using a finite element model of the spine and made correlations between the buckled spine and the scoliosis deformity. Andriacchi et al. [4] conducted a similar study, including the rib cage in their model. These and other spinal modelling and analyses, performed for the purpose of understanding the mechanical factors influencing scoliosis, are discussed in detail in Chapter 3.

1.3 Focus of the Present Study

In this study, a structural analysis model of the thoracolumbar spine and rib cage is constructed, and is then used to investigate the lordosis hypothesis concerning the etiology of thoracic AIS. As mentioned earlier, the basis of the hypothesis was formulated by Somerville [115] and later refined by Dickson et al. [34]. To reiterate, the hypothesis is that during adolescent growth, a thoracic lordosis coupled with an asymmetry in a plane other than the sagittal* plane produces scoliosis [34].

The hypothesis is simulated in two different ways using the geometric nonlinear analysis program capability of the MSC/NASTRAN finite-element analysis package. In the first approach, a slight lordosis is imparted to the spine prior to the nonlinear analysis, in which its response to increasing gravity-type load is studied. In the second approach, the growth of the thoracic spine into a slight lordosis is modelled as part of the nonlinear analysis. In this latter approach, the initial spinal shape is normal, and the response under incremental loading arising due to lordosis-inducing growth of the thoracic vertebrae and body weight forces is analyzed. The study is limited to attempting to develop a right thoracic scoliosis with an apex at the T8-T9 level, because this form of AIS has been found to be the most common [34,83]. Thus, the objectives of the present study can be summarized as follows:

(1) Development of a structural analysis model of the human thoracolumbar spine and rib cage representing overall geometry, and linear approximations of nonlinear stiffness properties of the typical normal spine. Although the anatomy is simplified, care is taken to include the pertinent elements necessary to conduct a sufficiently accurate analysis of the overall spinal behaviour. In the first instance the spine and rib cage are considered to be symmetric with respect to the sagittal plane.

(2) Validation of the constructed model by comparison of its predictions with the results obtained by previous researchers. Comparison is made of the critical buckling loads and the buckling

[1]Their experimental results are of significance because they are only ones that are based on an experimental study of a complete thoracolumbar spine specimen.

mode shapes of the symmetric spine model under compressive loading.

(3) Construction of a symmetric model with a slight lordosis in the thoracic spine. Based on the data of a real scoliotic spine, the anterior and posterior heights of the thoracic vertebrae in the normal spine are increased and decreased, respectively, such that the resulting thoracic spine has a slight lordosis with an apex at T8-T9, which is the usual location of the scoliosis apex.

(4) Comparison of the buckling loads and mode shapes of the symmetric models with the normal and the lordotic spines under compressive loading. Results of the linear bifurcation analyses should indicate which configuration is more stable, and provide insight regarding the hypothesis concerning lordosis as a possible etiology.

(5) Comparison of the deformed shapes of the models resulting from the geometric nonlinear imperfection growth analyses with a scoliotic spine, in the hope of validating the lordosis hypothesis, using:

(a) the lordotic model, with anatomical horizontal and frontal plane asymmetries (i.e. imperfections) incorporated, under increasing load proportional to gravity up to the vicinity of the structure's approximate bifurcation buckling load, and

(b) the normal model, again with asymmetries incorporated, under compressive loading modelling body weight and a deformation loading simulating accelerated anterior growth and constrained posterior growth of the thoracic vertebrae.

Chapter 2

Anatomy and Kinematics of the Normal Spine and Rib Cage

In order to understand and address the clinical problem of adolescent idiopathic scoliosis, a knowledge of the components comprising the spinal structure and their kinematics is necessary. The purpose of this chapter is to familiarize the reader with the relevant anatomy and kinematics of the normal spine and rib cage.

2.1 Spinal Column

The spinal column provides the intrinsic support to the human body, Fig. 2.1. It is basically composed of 3 element types: vertebrae, intervertebral discs, and ligaments. Together, they constitute what is known as the ligamentous spine, which is the spine without muscles and the rib cage. The vertebrae and discs are in alternating order in the column. The vertebrae are hard bony elements while the discs are made up of soft tissue. Thus, discs are the deformable elements which give mobility and flexibility to the spine. The heights of the vertebrae are substantially larger than those of the discs and in all, the vertebrae comprise approximately 3/4 of the total length of the spine [44,105]. The size of both elements increase caudally*.[1] This has biomechanical significance since the loads also increase in descending over the vertebral column [44]. The ligaments interconnect adjacent vertebrae. Their resistance to stretching provides additional stiffness to the spine by limiting its motion. The participation of the individual ligaments is dependent on their location with respect to the vertebra and the type of motion the intervertebral joint undergoes.

The normal spinal column may be sub-divided into 5 regions as shown in Figs. 2.1 and 2.2. The 7 superior vertebrae (C1-C7) found in the neck make up the *cervical* region. The following 12 vertebrae (T1-T12) have attachments for the ribs and therefore make up what is called the *thoracic* region. The next 5 vertebrae (L1-L5) make up the *lumbar* region. The fourth and fifth regions are the sacral and coccygeal regions. They consist of fused vertebrae, 5 in the sacral region and 4 in the coccygeal region. These two regions are unlike the other three because their vertebrae cannot move relative to one another (there are no intervertebral discs between these vertebrae). In this study, only the thoracic and the lumbar regions, known as the thoracolumbar spine, will be considered since scoliosis occurs predominantly in these regions.

---

[1]Terms indicated with an asterisk (*) are defined in the Glossary in Appendix A.

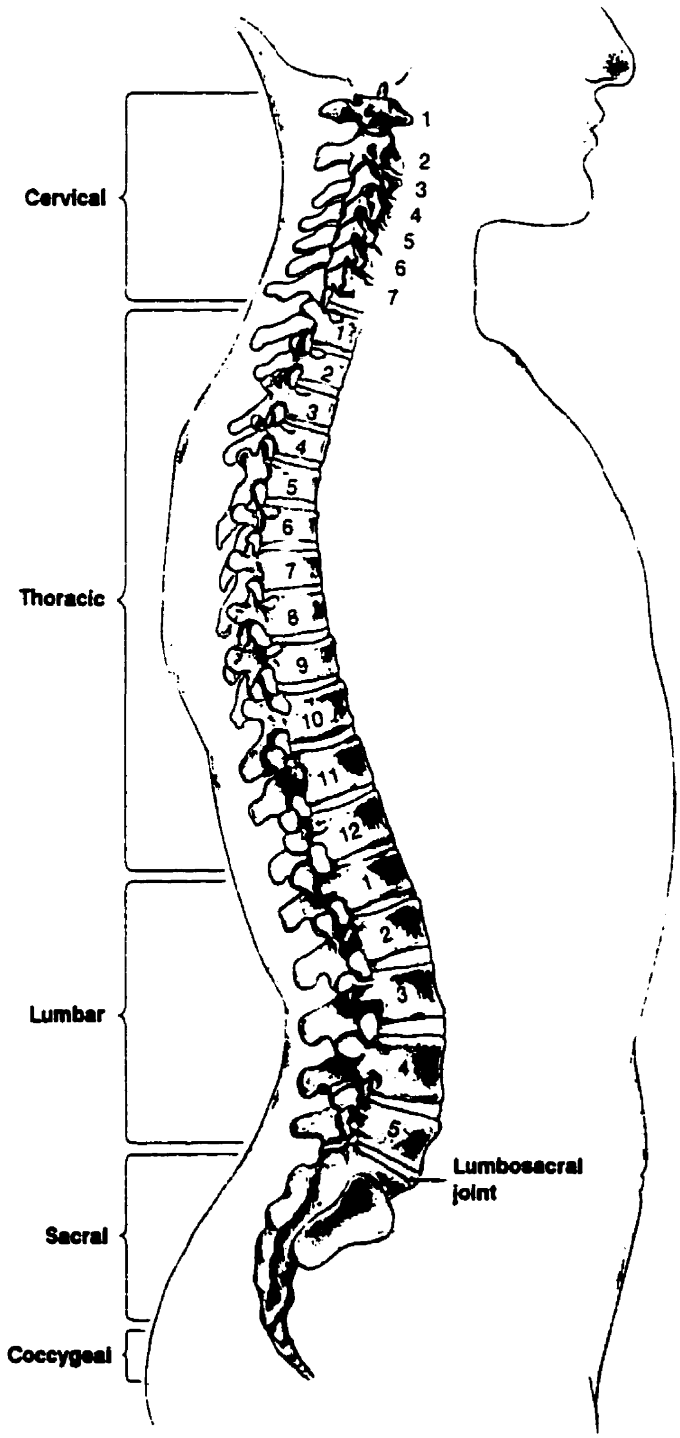

Fig. 2.1 Right lateral view of spinal column in relation to body outline. After Jacob et al. [57].

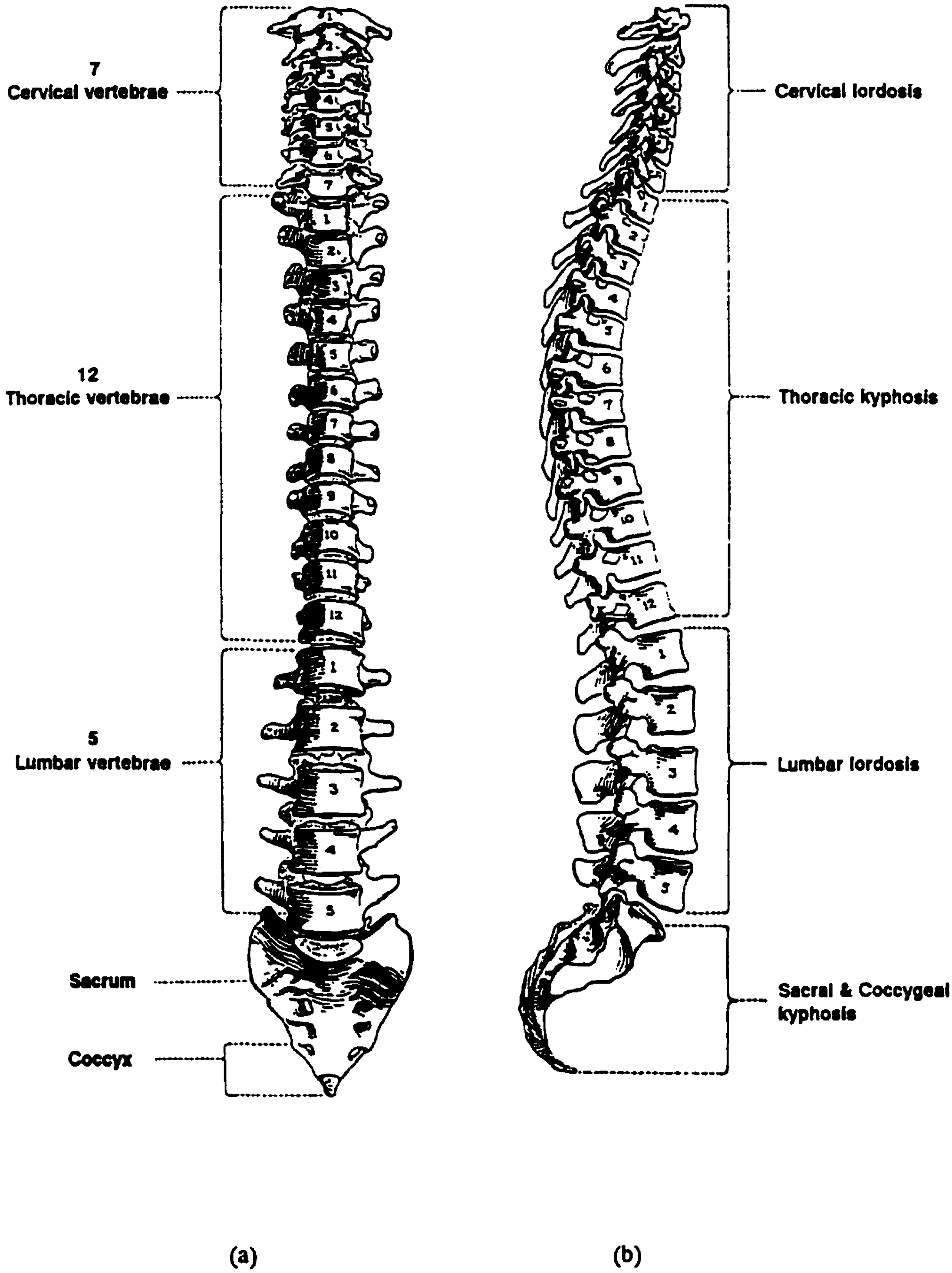

Fig. 2.2 Vertebral column (a) anterior (frontal plane) view and, (b) right lateral (sagittal plane) view. After Grant [43].

In the frontal plane, Fig. 2.2(a), the normal spine is relatively straight except for a slight physiological right thoracic curvature which may be due to the position of the aorta [117] or right-handedness [28,39,46]. The sagittal plane has 4 curves, each associated with a particular region of the spine as shown in Fig. 2.2(b). In both the cervical and lumbar regions, there is a sagittal curvature with a posterior concavity known as *lordosis*. Inversely, in the thoracic and sacral region, there is a curvature with a posterior convexity known as *kyphosis*. The degree of curvature varies from one individual to the next and also with respect to age and sex. As previously mentioned, the degree of curvature may be measured by Cobb angle*, which is expressed in degrees. A normal range of thoracic curvature (kyphosis) is between 20-50° [5,12,130] with an average of 37° [116]. The thoracic curvature is primarily due to smaller anterior vertebral body heights than posterior ones. The degree of curvature is found to increase with age. The thoracic curve tends to be straighter (with less curvature) in females than in males below the age of 40. However, the difference becomes negligible after age 40 when the thoracic curve of females becomes as curved as males [130]. The average normal lumbar curvature is 50° (lordotic) [116] with an accepted normal range of 20-60° [12]. This curvature is found to be slightly more pronounced in females [130]. This curvature is mainly due to the inclination of the sacrum (approximately 40°), the wedge-shaped lumbosacral intervertebral disc (13°), and the 5th lumbar vertebra, L5 (8°) [15,60,116].

Although the spinal column is the major load-bearing structure, it cannot withstand the external forces it is subjected to alone. Lucas and Bresler [73] found that the ligamentous spine cannot even support the weight of the head (> 2 kg) without buckling. The spinal column requires additional supporting structures. These structures providing the extrinsic support include muscles, fascial envelopes, abdominal and thoracic cavity pressures and rib cage [40]. Among these, rib cage is the most important part of the spinal skeleton and is included in the present investigation. Its major roles are to protect the vital organs and increase spinal stability. Andriacchi et al. [4] have shown that the introduction of the rib cage increases the load carrying capacity of the ligamentous spine in compression approximately 3-fold (see Fig. 3.1).

2.2 Components of Spine [15,43,60,130]

2.2.1 Vertebrae

The vertebrae are bony structures which give rigidity to the spinal column. Each vertebra has many parts, but essentially there are two main parts. They are the vertebral body and the vertebral arch [60], see Fig. 2.3, page 16.

The vertebral body is the main load-bearing component of the vertebrae carrying approximately 80% of its compressive load. The actual percentage is dependent on the position of the spine during the time of loading. The vertebral body is composed of spongy, cancellous bone surrounded by a thin, cortical bone shell. The density and elastic modulus of the cortical bone are much higher than those of the cancellous bone. However, both carry significant loads, with the relative share of the load varying with age. In the young adolescent, the cancellous bone is found to carry 55% of the load; this percentage decreases on average to 35% by the age of 40 [130]. Cortical bone, surrounding the perimeter of the body, gives high bending and torsional strength to the vertebrae.

Cancellous bone is both advantageous and necessary. Aside from helping support the load, it decreases the weight of the vertebrae, since it is not solid bone. It's sponge-like openings enable nutrients to seep through to the cortical bone. Secondly, it acts as an energy absorber. It gives resilience to the vertebrae and allows it to be subjected to sudden forces without damage to its constituents [15,61,130].

The vertebral arch attaches to the posterior side of the vertebral body. It is composed of two pedicles and two laminae. The pedicles are at the anterior ends of the arch and join the vertebral arch to the vertebral body. The laminae comprise the posterior section of the arch. From the vertebral arch, seven processes emerge, as shown in Fig. 2.3.

A spine-like process, appropriately named spinous process, projects posteriorly and slightly inferiorly* from the point where the two laminae merge. From the junction of the lamina and the pedicles on each side of the arch, project a superior articular process upward, an inferior articular process downward, and a transverse process laterally and slightly posteriorly.

When the vertebrae are stacked as in the vertebral column, the vertebral body, its posterior bony features and the connecting ligaments completely enclose a space known as the vertebral canal, through which the spinal cord passes. Thus, these elements provide the spinal cord with necessary protection.

Aside from creating bony protective arch for the spinal cord, the processes increase the stiffness of the intervertebral joint, both by direct and indirect means. The processes act indirectly by providing attachments for the ligaments which adjoin adjacent vertebrae. They are advantageous in that they provide the ligaments with longer moment arms to make them act more efficiently, and with various orientations so that they can participate in restricting various types of motions.

(a)

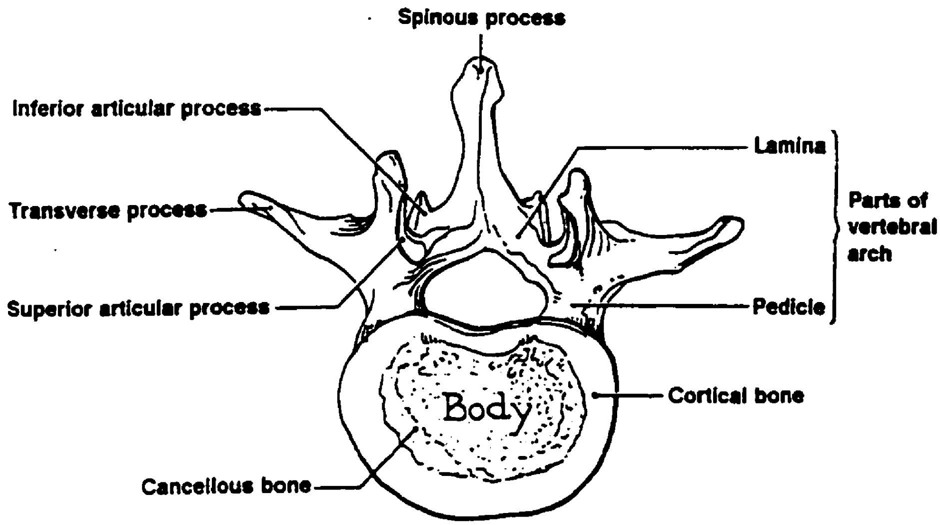

(b)

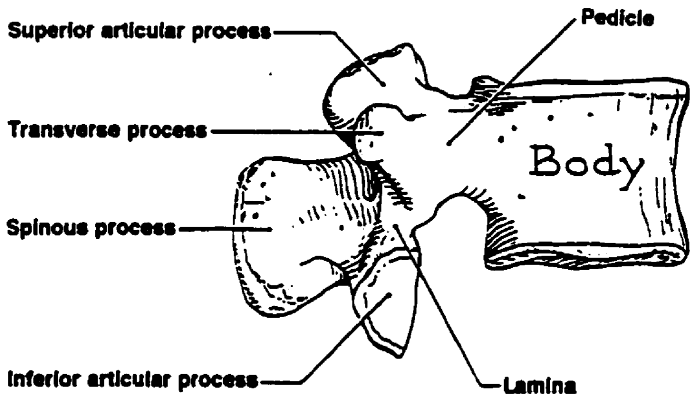

Fig. 2.3 Typical vertebra: vertebral body and vertebral arch with its 7 bony processes (a) top view, and (b) right lateral view. After Grant [43].

The processes themselves restrict particular motions due to impingement. For example, extension is limited by the impingement of the inferior articular processes on the laminae of the vertebrae below and the spinous processes on one another. Likewise, the ipsilateral* articular processes limit lateral bending. However, their contribution is highly nonlinear; only having a stiffening effect on intervertebral joint motion upon impingement or contact.

The inferior articular processes and the superior articular processes of the underlying vertebra form a joint between the vertebrae. The joint, shown in Fig. 2.4, is called a zygapophyseal joint, commonly referred to as facet joint. These joints carry the remaining 20% of the compressive load applied to the vertebra. Of great importance is the orientation of the facet joint (cartilaginous face of the joint) which determine the type of motion permitted between the vertebrae [15,60].

The different spinal regions have different ranges of motion. This is partly due to the variations in size, shape, and orientation of the above mentioned features of the vertebra found in the various regions of the spine. In addition to these variations, vertebrae from each region of the spine, e.g. thoracic or lumbar, have distinguishing features [43,60,130].

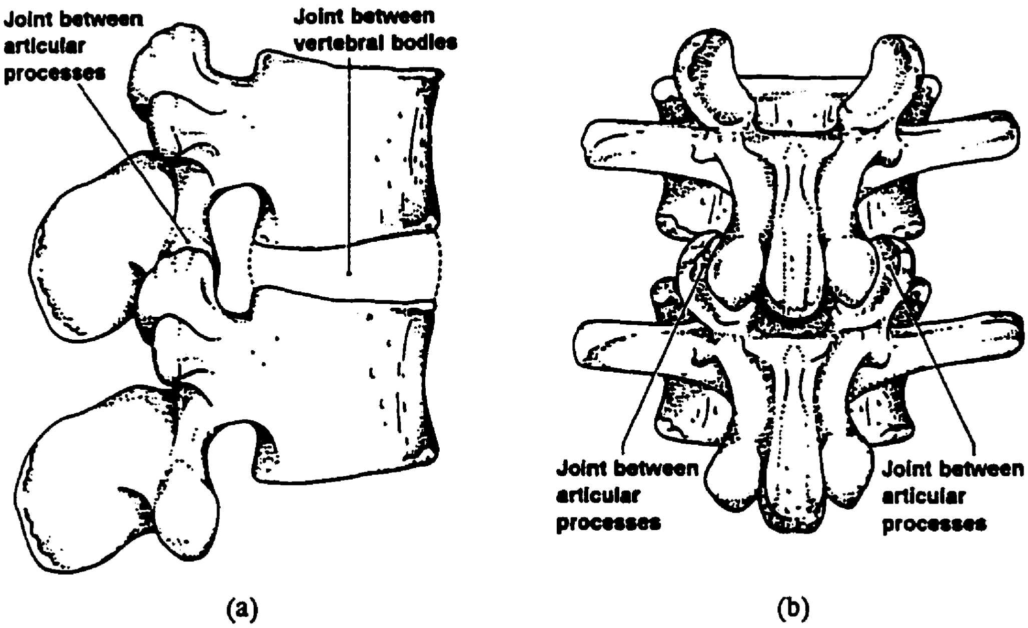

Fig. 2.4 Zygapophyseal (facet) joint (a) right lateral view, and (b) posterior view. After Bogduk and Twomey [15].

The thoracic vertebrae, shown in Fig. 2.5, are differentiated from the other vertebrae due to their articular facets located on the vertebral body and on the transverse processes for the attachment of the head and the tubercle of the ribs, respectively (see Fig. 2.12). They have wedge-shaped vertebral bodies, having larger posterior heights, giving thoracic kyphosis. In cross-section, the thoracic vertebrae are heart-shaped and generally have transverse and anteroposterior diameters of approximately equal dimensions. Many of the thoracic vertebrae are known as transition vertebrae because the superior ones resemble the cervical vertebrae, while the inferior ones resemble the lumbar vertebrae, in both structure and function.

The orientation of the facets of the articular processes of the thoracic vertebrae, Fig. 2.6(a), is such that it permits axial rotation. The superior articular facets face posteriorly (slightly superiorly and laterally) and the inferior articular facets face anteriorly (slightly inferiorly and medially). As a result, axial rotation is the predominant motion in the thoracic region [44,65,130].

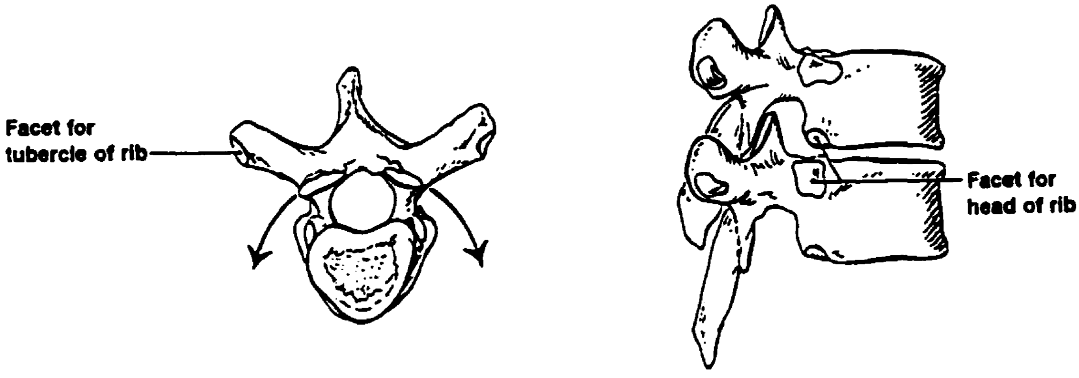

(a) (b)

Fig. 2.5 Typical thoracic vertebra (a) top view, and (b) right lateral view. After Grant [43].

(a)

(b)

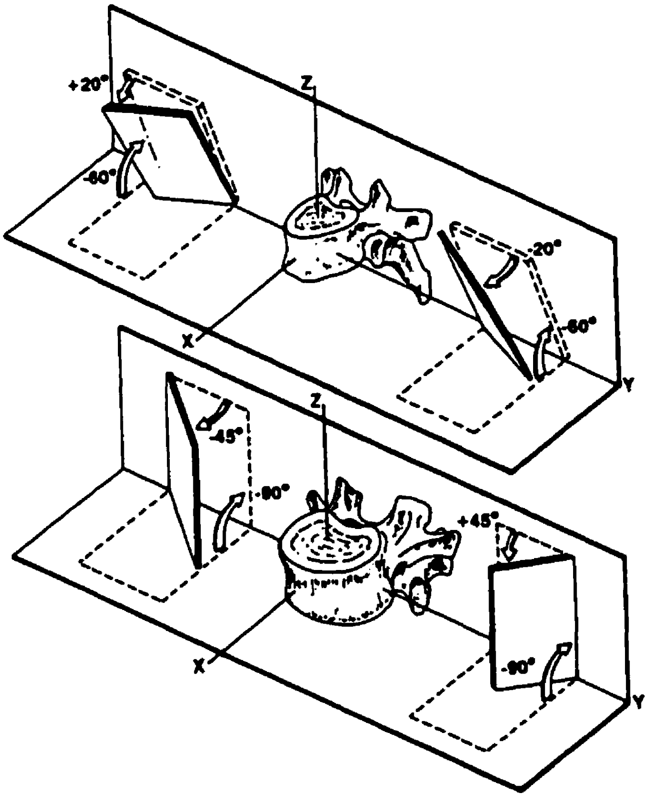

Fig. 2.6 Orientation of the facet joints in the (a) thoracic, and (b) lumbar regions of the spine. After White and Panjabi [130].

Mammary processes and accessory processes are distinctive of the lumbar vertebrae, see Fig. 2.7. In comparison to thoracic vertebrae, the spinous process are shorter and more oblong (ie. less spine-like) and the transverse process are thinner and oriented more laterally. In cross-section, the vertebral bodies are kidney-shaped with a transverse diameter which is approximately 50% larger than the anteroposterior one. In addition, the vertebral bodies are larger in size and mass in this region, as shown earlier in Fig. 2.2. The cross-sectional area is found to increase caudally throughout spine to accommodate the increasing compressive load.

As shown in Figs. 2.6(b) and 2.7, the facets of the superior articular processes are orientated medially* and posteriorly and have a concave shape. The inferior articular facets face laterally and anteriorly. This configuration with vertical orientation in the sagittal plane allows flexion* and extension* but does not permit much axial rotation. Comparatively little flexibility in axial rotation exists in the lumbar region. It is mainly the thoracic region which accommodates most of the axial rotation in the thoracolumbar spine [60,65].

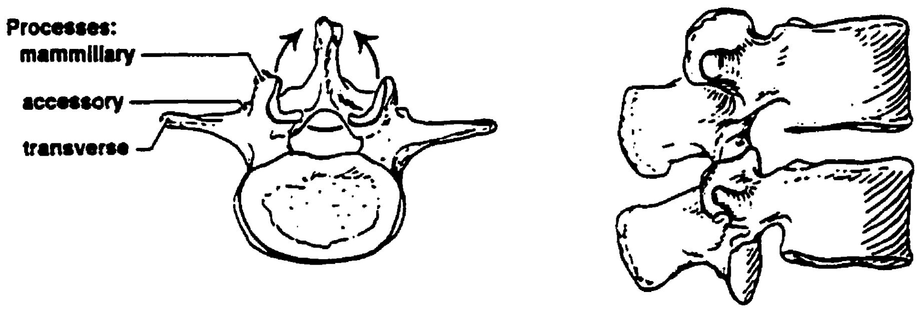

(a) (b)

Fig. 2.7 Typical lumbar vertebra (a) top view, and (b) right lateral view. After Grant [43].

For the reasons explained above, the posterior elements of the vertebrae contribute to the stiffness of the intervertebral joint. This is confirmed by the fact that in in-vitro studies, removal of the posterior elements indicates an increase in the flexibility of the vertebral joint [11,75,113]. By limiting the range of motion of adjacent vertebrae, hence the spine, the posterior elements act as a safety mechanism protecting intervertebral disc (annulus) from undue stress and deformation as well as other body parts from damage due to hyperextension and hyperflexion [42].

2.2.2 Intervertebral Discs

The intervertebral discs are the "highly" deformable components between adjacent vertebral bodies (Fig. 2.4). Their chief role is to provide flexibility and load transfer between vertebral bodies. The intervertebral discs are best suited to resist compressive loads, as reflected in their stress-strain curves. Their importance is illustrated by the fact that they must provide the competing attributes of both flexibility and stability to the spine. The disc are composed of strong, soft tissue, the properties of which, effectively determine the stiffness of the whole spine.

The discs have visco-elastic properties, meaning the amount of deformation is dependent on the rate of loading (stress or strain rate). In addition, continued deformation is found to occur during sustained loading, and permanent deformation upon unloading. These represent two well known phenomena associated with visco-elastic materials, namely creep and hysteresis [61,126].

The intervertebral disc is composed of two main parts, Fig. 2.8. They are the nucleus pulposus and the annulus fibrosus. The nucleus pulposus makes up the center portion of the disc and is composed of a semi-fluid ground substance with some collagen fibers and a few cartilage cells dispersed within. The annulus fibrosus surrounds the periphery of the nucleus, although there is no clear boundary between the two portions.

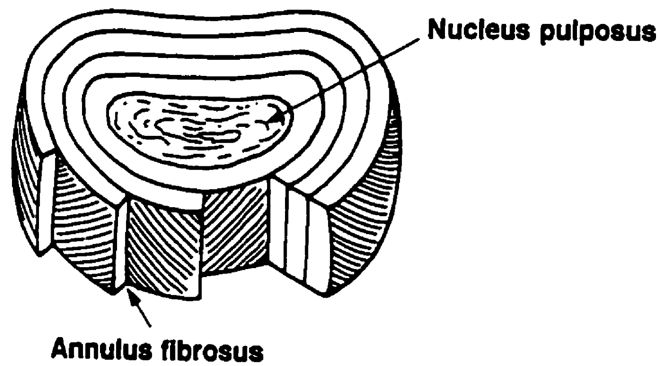

Fig. 2.8 Intervertebral disc. After White and Panjabi [130].

The inner portion of the annulus attaches to the cartilaginous vertebral end-plates which separate the disc from the adjacent vertebrae, Fig. 2.9(a). The end plates do not extend over the complete disc. The outer portion of the annulus fibers attach directly to the vertebral body, providing a strong connection between vertebrae and disc.

The annulus is composed of concentric laminated bands of collagen fibers, Fig. 2.9(b). The orientation of these fibers is the same in alternate bands and opposite in adjacent bands. But, both are approximately 30° to the horizontal such that two adjacent bands have a 120 degree angle between the orientation of their fibers. The orientation of the fibers has mechanical significance. Since the annulus is only strong in tension along the direction of the fibers, this alternation in orientations allows the annulus to resist all types of loading, even if only half the layers are working such as in torsion [15]. With this knowledge, it is not surprising to find that torsional forces often injure annulus [38,130].

The annulus is capable of carrying loads by itself due to its densely packed bands, while the nucleus, with its fluid-like properties cannot. However together, they provide a system capable of supporting loads that would otherwise have buckled the annulus alone, and also a system capable of absorbing and storing energy, i.e. cushioning impact type loads. Thus, the nucleus-annulus structure is mechanically advantageous, especially in compression [15,60].

The size of the intervertebral discs is also found to increase caudally (as do the vertebrae) as shown in Figs. 2.1 and 2.10. The larger cross-sectional area in the lumbar region bears the large compressive loads while their increased height maintains flexibility [15,61,130].

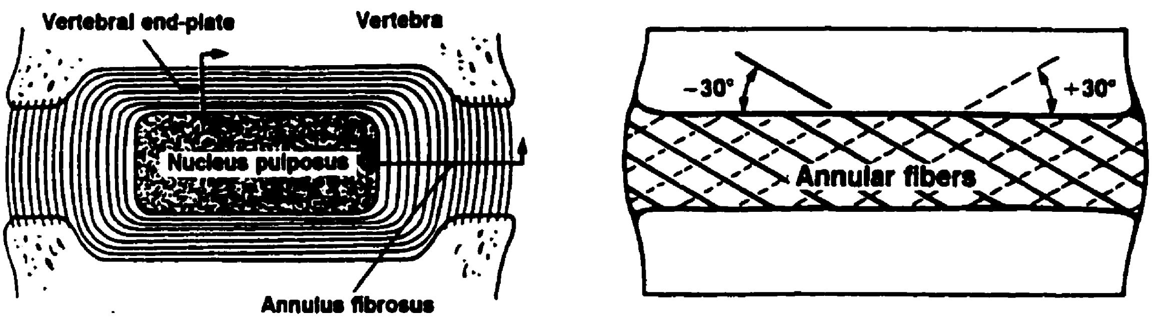

(a) (b)

Fig. 2.9 Annulus fibrosus. (a) Section through the disc, illustrating connection of annulus to adjacent vertebra. After Bogduk and Twomey [15]. (b) Fiber orientation of concentric bands of annulus. After White and Panjabi [130].

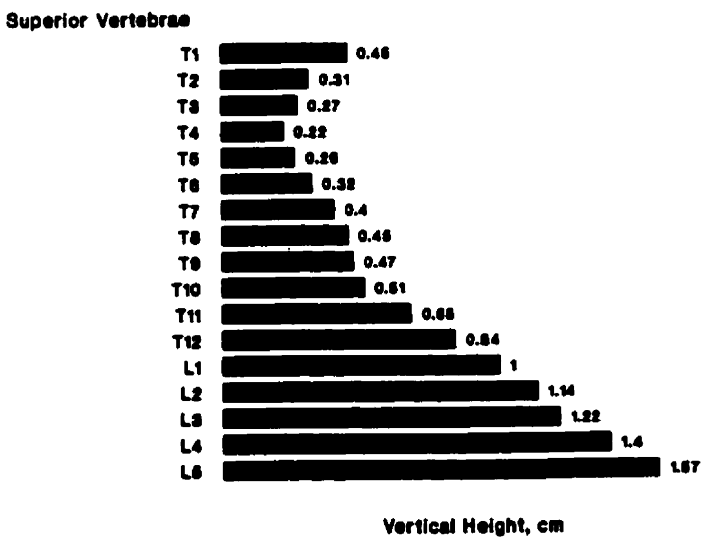

Fig. 2.10 Graphical representation of intervertebral disc heights [44,124].

2.2.3 Spinal Ligaments

The spinal ligaments, as shown in Fig. 2.11, connect adjacent vertebrae in the vertebral column. They are strong uniaxial soft tissue structures, which resist tensile forces but buckle under compressive loads. Hence, they increase stiffness of the intervertebral joint by limiting its motion in directions depending on their location of attachment between vertebrae. Like the intervertebral disc, their material is visco-elastic; thus their deformations are time-dependent [126].

There are seven major spinal ligaments [15,44,60,130]. The anterior and posterior longitudinal ligaments, as their names indicate, run the full length of the spine along the anterior and posterior portions of the vertebral bodies, respectively. The former is composed of long collagen fibers, running the full length of the ligament, and short fibers, attaching to anterior side of vertebral body and intervertebral disc. The latter is composed of only short fibers which insert into the posterior aspect of the disc and span over the posterior surface of vertebral body. They limit extension and flexion respectively. They are stretched due to the separation of the vertebrae as well as the bulging of the intervertebral discs [42].

The remainder of the spinal ligaments are segmental, meaning they are made up of short fibers and run between adjacent vertebrae (vertebral arches & processes).

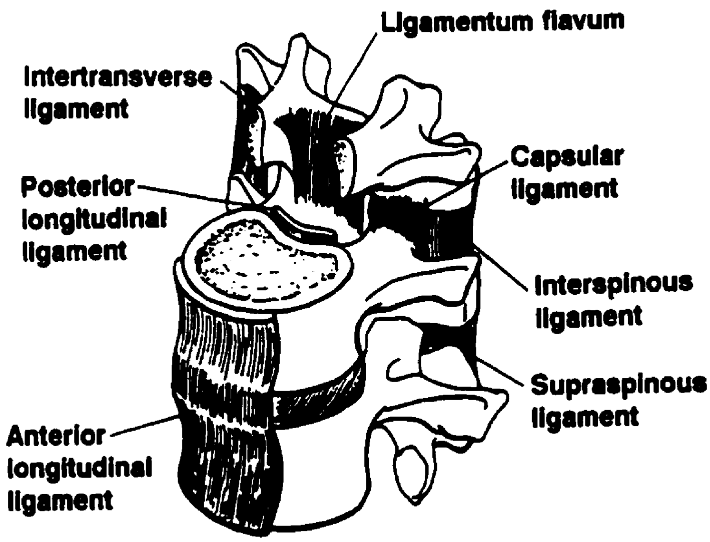

Fig. 2.11 Ligaments of the spine. After White and Panjabi [130].

The ligamentum flavum is a very thick yellow ligament which connects laminae of adjacent vertebrae. It extends the full length of the laminae and fully encloses the vertebral canal. Due to its anatomical position, it mainly limits flexion and to some degree lateral bending.

The interspinous and supraspinous ligaments connect the spinous processes of adjacent vertebrae. The interspinous ligament extends the full length of the spinous process, from tip to root, while the supraspinous connects the posterior ends. However, they both provide stiffness in flexion to the joint.

The intertransverse ligament connects transverse processes on the same side and limits lateral bending. The capsular ligament are very short and connect articular processes (superior to inferior). They limit the amount of flexion and lateral bending.

Additional ligaments which connect the ribs to the vertebrae will be discussed in the following section on the rib cage.

2.3 Rib Cage

The rib cage, shown in Fig. 2.12, provides additional stiffness to the thoracic region of the spinal column. The main components are the ribs, the sternum, the costal cartilage, the intercostal tissue, and the costovertebral and costotransverse joints.

The sternum is located anterior to the spinal column. It is a hard bone, of composition similar to the vertebral body. It provides an anterior attachment for the ribs on both sides of the body. The ribs are curved hollow bones with an elliptical cross-section. The posterior end of the rib is known as the head. The adjacent section is called the neck or tubercle. The anterior portion articulates with costal cartilage. Costal cartilage is the soft tissue connector for anterior attachment of the ribs.

Humans have 12 pairs of ribs approximately symmetric with respect to the sagittal plane. The anterior seven pairs are known as true ribs. They attach anteriorly, via the costal cartilage, directly to the sternum. The next five pairs do not attach directly to the sternum and are known as false ribs [44]. The first three pairs attach to the costal cartilage of the rib above it by means of its costal cartilage. The last two pairs have no anterior attachment hence are known as floating ribs.

Posteriorly, ribs are attached to the spine by costovertebral and costotransverse joints, as shown in Fig. 2.13. Articular facets are found on the inferior and superior borders of the lateral-posterior surfaces of the vertebral body and on the transverse processes as well as on the head and tubercle of the rib. Ligaments of the costovertebral joint, i.e. radiate and intraarticular ligaments, connect the head of the rib to the spinal column. Radiate ligaments connect the head of the rib to two adjacent vertebral bodies, i.e. the superior facet of the corresponding vertebra and the inferior facet of superior vertebra, with the exception of the 1st, 10th, 11th and 12th ribs which are only connected to their corresponding vertebra. Intraarticular ligament connects the head to the intervertebral joint. The costotransverse ligaments connect the tubercle of the rib to the transverse process, except for ribs 11 and 12, which have no costotransverse joint [65]. In addition, there are soft tissues which run in between adjacent ribs in the intercostal spaces.

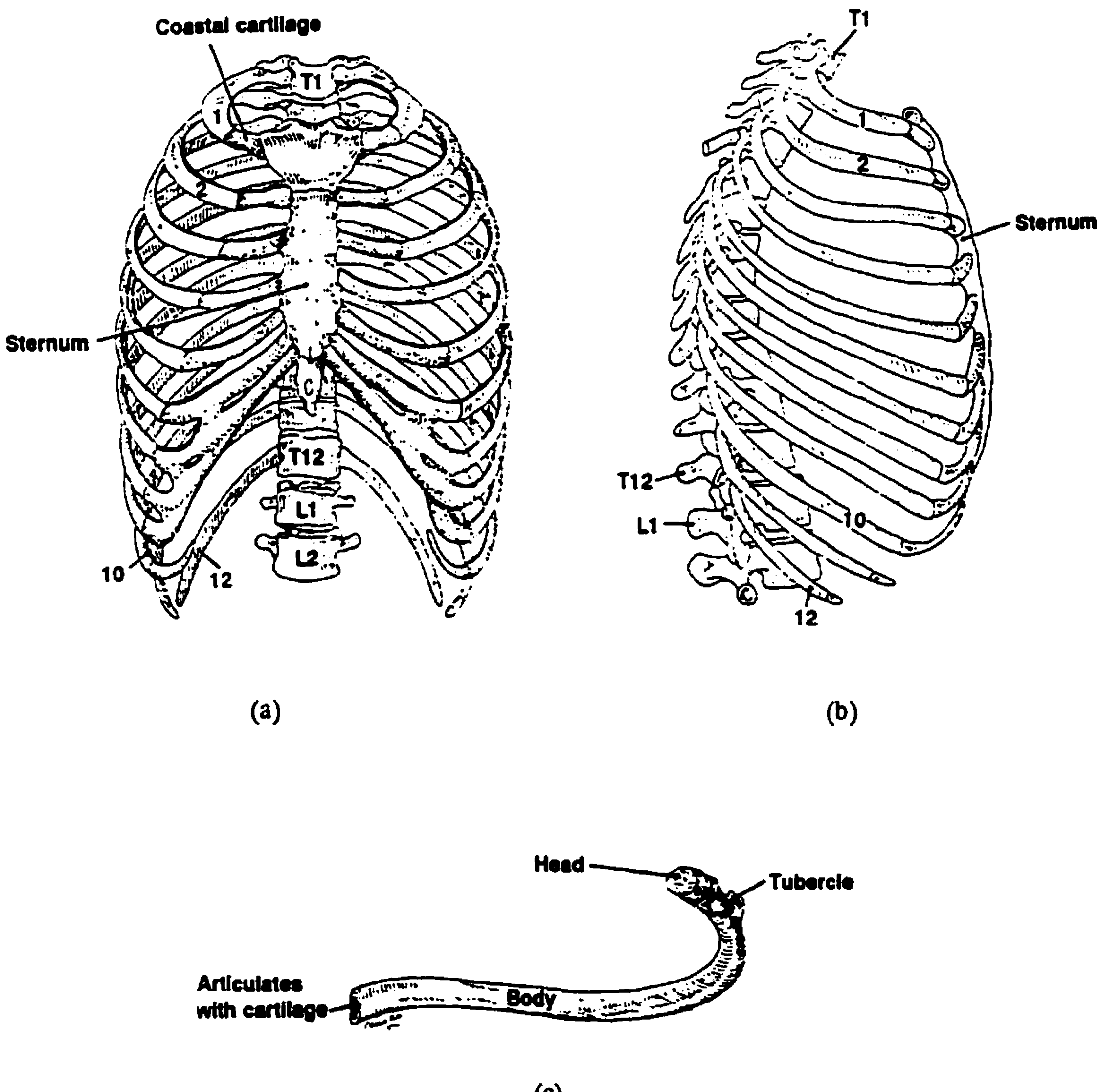

Fig. 2.12 Rib cage structure illustrating (a) anterior view, (b) right lateral view, and (c) view of a typical rib from the inside. After Pansky [92].

(a)

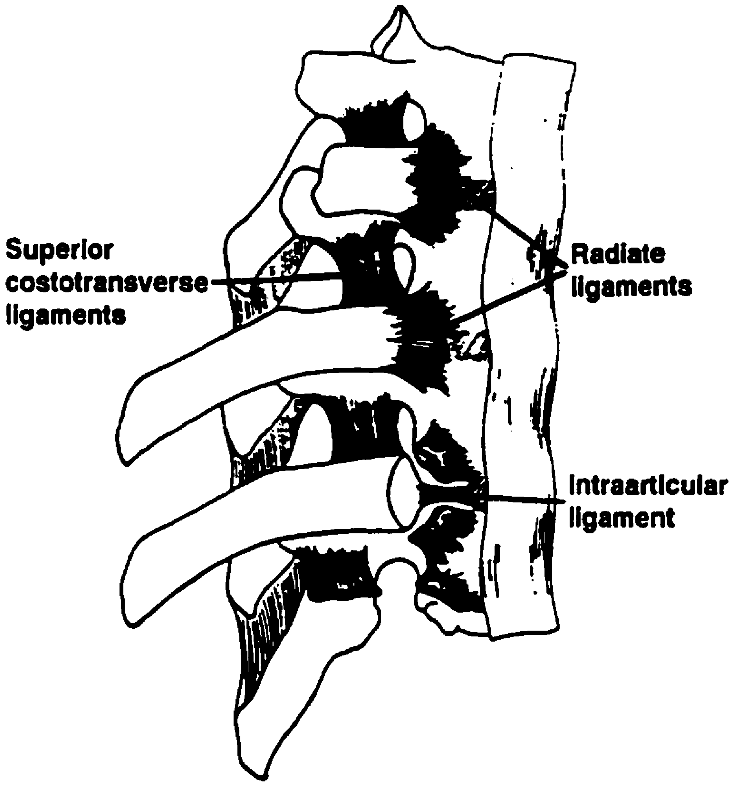

(b)

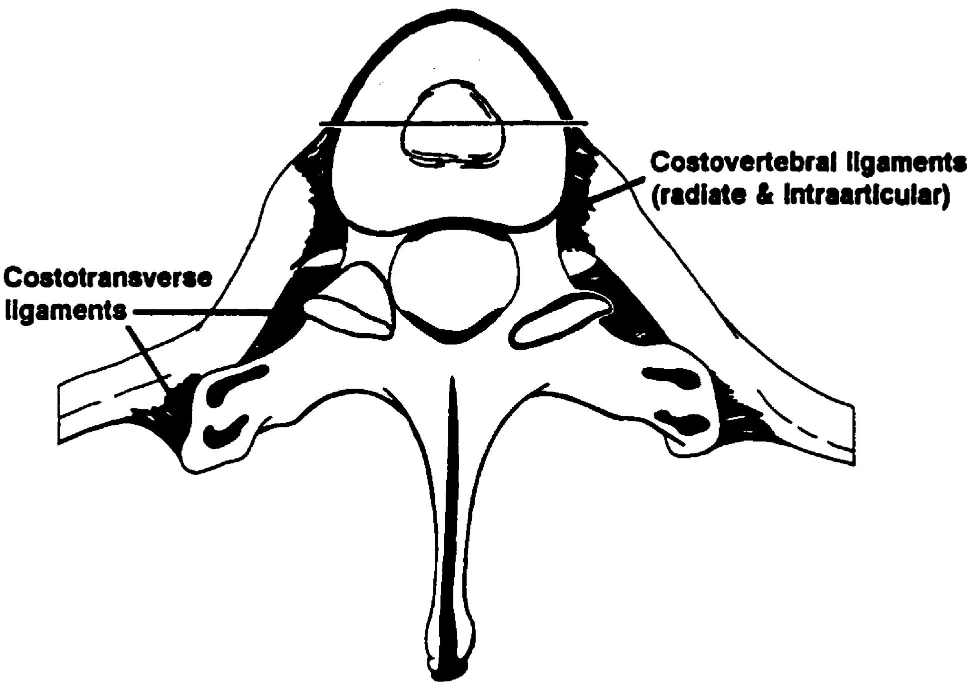

Fig. 2.13 Ligaments connecting ribs to the spine (a) right lateral view, and (b) top view. After White and Panjabi [130].

These strong ligaments are the only connections between the rib cage and the spinal column. The costal cartilage joins the ribs to the sternum making the cage continuous. Therefore, the stiffening effect of the rib cage on the thoracic spine depends entirely on the strength of these soft tissue elements; the chain is only as strong as its weakest link. Any movement that occurs between the thoracic vertebrae must also occur between the ribs of corresponding vertebrae. Deformations occur primarily in the costal cartilage, and less pronounced in the rib [60]. As a result, the rib cage mechanism limits the range of motion in bending and twisting in the thoracic spine. This range of motion decreases with age as costal cartilage ossifies [61].

Although individual components of the rib cage are flexible, the rib cage, as a whole is found to have a stiffening effect on the spine. This increase in stiffness is attributed to the additional stiffness provided by the ligaments of the costovertebral and costotransverse joints, and more importantly to the increased cross-sectional dimensions of the thoracic spine provided by the rib cage, as illustrated in Fig. 2.14. The increased dimensions provide thoracic spine with a larger moment of inertia and torsional constant to resist bending and torsion. As a result, the rib cage contributes approximately 40% of the bending strength and stability of the thoracic spine [5,61,130]. Based on a finite element model study [4], inclusion of the rib cage increases the stiffness of the normal thoracic spine in all four physiological motions (lateral bending, torsion, flexion, and especially extension) as shown later in Fig 3.5. In addition, as mentioned earlier and as shown subsequently in Table 3.1, the stability of the spine is found to increase 3-fold with the inclusion of the rib cage [4].

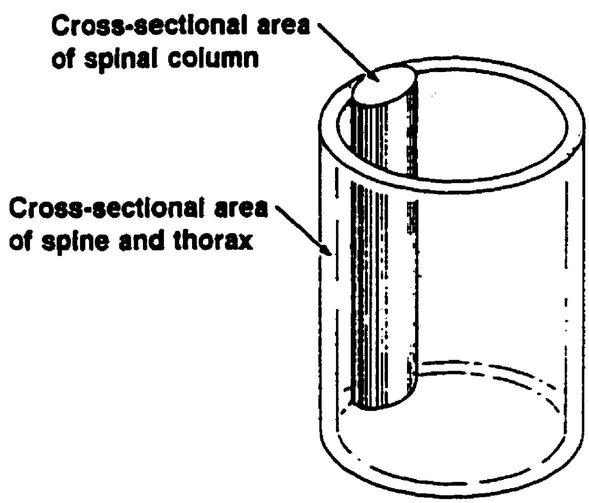

Fig. 2.14 Schematic diagram showing increase in transverse (horizontal) plane dimensions of thoracic spine by virtue of rib cage. After Apuzzo et al. [5].

2.4 Coupling* in a Normal Spine

Significant coupling is found between lateral bending and axial rotation in the normal spine. This type of coupling means the vertebrae rotate axially when the spine is subjected to lateral bending, and vice versa. Coupling is an important part of the kinematics of the normal spine and as such needs to be discussed. It is particularly interesting in this study because idiopathic scoliosis consists of a lateral curve with convex-sided rotation. A study of normal coupling can help understand the type typical of scoliosis.

Coupling is influenced by many factors involving different aspects of the spine anatomy. As a result, it is a very complex phenomenon, and consequently there are conflicting in vivo results. White [129] found concave-sided rotation in motion segments of the thoracic spine when subjected to lateral bending, see Fig. 1.2(a). Significant coupling was found in the upper thoracic and cervical regions of the spine. In the middle and lower thoracic regions, the coupling was found to be less significant and sometimes in the opposite direction i.e. convex-sided [129]. Observations of convex-sided rotation have also been reported in the lumbar spine [61].

Lovett [72] studied the rotation of the spine associated with lateral bending using cadaver and live specimens. He found that the erect spine rotates predominantly with concave-sided rotation during lateral bending. However, he found the characteristic direction of the rotation varied with respect to the region of the spine. Arkin [7], on the other hand, found the living spine to rotate in convex-sided rotation when subjected to lateral bending. However, both agreed that the direction of axial rotation is dependent on the amount of flexion or extension. Flexion during lateral bending produced convex-sided rotation, and conversely, extension produced concave-sided rotation. Arkin [7] explained this behaviour by stating that structures under greater tension will assume the straighter line, i.e. the inside of a lateral curve.

Despite the different results, these findings together with the results of a biomechanical analysis by Veldhuizen and Scholten [125] indicate that both the direction and the strength of the coupling are influenced by:

(1) sagittal inclination of the spine in the sagittal plane [125],
(2) facet joint orientation (the inclination in the sagittal plane, as illustrated in Fig. 2.6) [125],
(3) amount of flexion and extension forces in the spine [7,72].

An additional consideration is the centers of rotation or shear centers of the motion segments [84]. As illustrated in Fig. 2.15, the centers of rotation vary for the different regions of the spine due to the various facet orientations and they do not coincide with the centroid [47,60]. The location of the centers of rotations could possibly influence coupling effect. Factors which are found to influence convex-sided rotation may be possible links to idiopathic scoliosis. Possible etiological factors are discussed in Chapter 3.

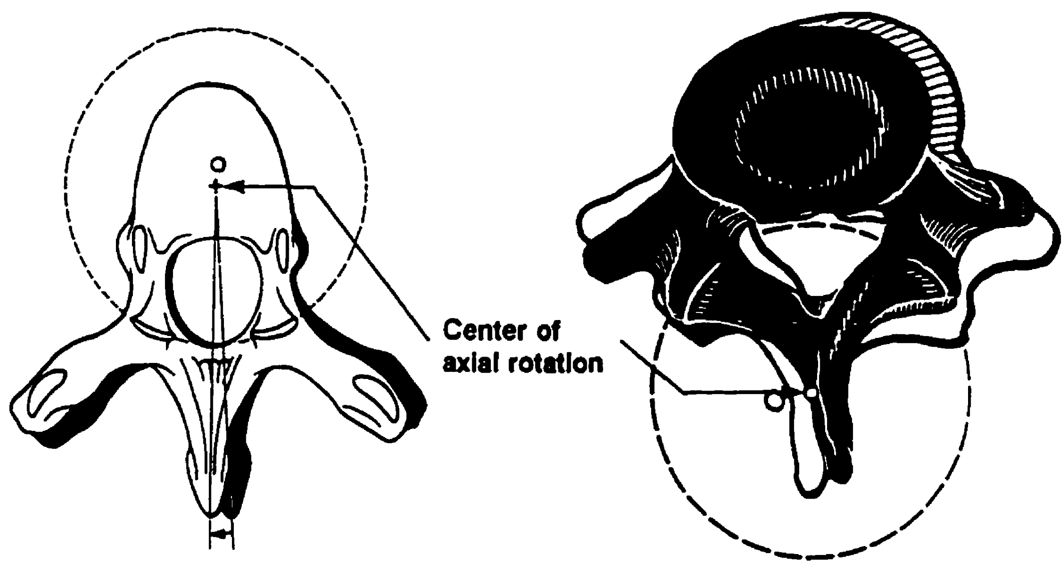

(a) (b)

Fig. 2.15 Centers of rotation of the (a) thoracic, and (b) lumbar vertebrae. After Kapandji [60].

Chapter 3
Literature Review

The purpose of this chapter is to bring the reader up-to-date on the present status of knowledge and modelling of the spine pertaining to scoliosis. It first includes a brief discussion of the etiological theories of AIS. Particular attention is focused on the lordosis hypothesis [34]. Secondly, it describes the development of spine models aimed at achieving an understanding of spinal stability and mechanics with relations to scoliosis.

3.1 Etiological Theories of Adolescent Idiopathic Scoliosis

For many years, the etiology of AIS has been sought. Theories of biochemical, genetic, neuromuscular, and hormonal origins have been formulated, but have been unsuccessful in pin-pointing the cause. It is now suspected to be a combination of many factors [26]. However, whatever the cause, the deformation must be explainable *biomechanically* [49,98].

Two factors known to play a role in the pathogenesis and progression of scoliosis are growth and genetics. A survey conducted in the 1960's by Wynne-Davies [135] on patients from the Edinburgh Scoliosis Clinic, Scotland, indicates peak incidence of idiopathic scoliosis during infancy and adolescence. These two periods coincide with the two growth spurts experienced during one's life; the first following birth, the second during puberty. In addition, progression of existing lateral (scoliotic) curves has been noted to accelerate and become clinically significant during the adolescent growth spurt [94,106]. Some suspect growth to be the primary cause of scoliosis with gravity and susceptibility of skeletal tissue to the Heuter-Volkmann effect (increased pressure leads to decreased growth) acting as secondary factors [8,17]. Whatever the case, the simultaneous occurrence of growth and onset or progression is considered too high to be coincidental and, therefore, it follows that growth must be linked to etiology of the disease.

In the same study [135], the rates of incidence of idiopathic scoliosis among 1st, 2nd, and 3rd degree relatives of 114 patients from the Edinburgh clinic were recorded and compared with the incidence in the general population, determined by screening 11,087 Edinburgh children. The results showed that the incidence of scoliosis is much higher among the relatives of the index patients than in the general population. It was particularly high among 1st degree relatives (parents, siblings, children) of the adolescent girl patients (6.9% compared to population incidence of 0.1%). The study found that the highest incidence (12%) was among female relatives of adolescent girl patients. Two important points were drawn out of this study. First, the families were found to have both infantile and adolescent scoliosis, which suggests they both have the same etiology. Second, the strong familial trend of the disease found in this study suggests idiopathic scoliosis is hereditary, i.e. affected by genetics related factors [135].

Aside from explaining its correlation with growth and genetics, the etiology of AIS must be able to explain other characteristics of the disease, e.g. its predominant occurrence in girls compared to boys, and of course, the peculiar character of the deformity (lateral curve with spinal rotation). From the biomechanical point of view, progression of the lateral curve with rotation may be likened to torsional-flexural (lateral) buckling of a column curved in one plane, as discussed in greater detail in Chapter 4. For the time being, knowledge of the theory pertaining to the buckling of a simple Euler column[1] is sufficient. The formula giving the buckling load of an Euler column is

$$P_{cr} = \frac{\pi^2 EI}{\lambda^2}$$

where P_{cr} is the critical buckling load, E is the Young's modulus of the column material, I is the weak-axis moment of inertia of the column cross-section, and λ is the effective length[2] of the Euler column.

It is clear from the above equation, that buckling occurs if the column becomes too slender[3] (that is, λ^2/I too large), too flexible (value of E too small), or is subjected to loads (gravity loads, muscle action forces) which are too large [49]. With these general conclusions as their basis, many researchers have investigated these stability factors as possible explanations for the progression of the scoliotic curve. Results of the clinical studies conducted to substantiate these hypotheses are as follows.

Slenderness

In one study [132], scoliotic girls were found to be significantly taller than structurally normal girls of the same ages. In another study [112], girls were found to have spines significantly slenderer than those of boys. However, when slenderness was compared between scoliotic and normal girls,

---

[1]Euler column here represents an idealized column which is straight, homogeneous, and has a constant cross-section. Also, it assumes small deformation theory and linear elastic material behaviour.

[2]Effective length, as explained in Chapter 4, is dependent on column length and end support (boundary) conditions.

[3]Slenderness is measured by slenderness ratio, which may be defined as the ratio of column length to a cross-sectional dimension (e.g. radius) of the column.

there were some differences, but they were not consistent [112]. The evidence that the scoliotic girls are taller than normal girls makes the buckling theory plausible since column length is one of the influential parameters in column stability. If all other variables were kept constant, taller would mean more slender. However, the slenderness study [112] found no consistent differences. In light of these findings, the excessive slenderness would explain the dominant occurrence in girls but it does not justify conclusively why some girls are more susceptible to scoliosis than others.

Flexibility

Flexibility of the spine is dependent on the flexibility of the soft tissue constituents (primarily the discs). Spines with abnormal lateral bending flexibility are more susceptible to buckling, hence, possibly to scoliosis. With respect to studies investigating lateral bending flexibility of the spine, motion segments* of the female were found to be generally more flexible than those of the male [48,78,81], while scoliotic girls were found to have significantly less flexibility than structurally normal girls [76]. Similar to slenderness, flexibility hypotheses may explain progression prevalence in girls. However, the finding that scoliotic girls have stiffer spines in lateral bending than those of normal girls seems to go against the hypothesis and makes the excessive flexibility an unlikely cause.

Abnormal Loads

Biomechanically, abnormal sets of forces and moments could increase the likelihood of lateral buckling of the spine. The abnormal load of concern in scoliosis is an unbalanced lateral moment since compressive forces alone do not produce significant amount of lateral bending of motion segments [11]. The possibility of unilateral weakness or abnormalities of trunk muscles were investigated in 93 scoliotic and 109 structurally normal adolescent girls [97]. Measurements of the maximum voluntary trunk strengths indicate that there is no consistent difference in mean muscle strengths between scoliotic girls and normal girls. Based on these results, AIS is not likely a result of gross weaknesses or imbalances in the major muscles of the trunk.

Since trunk muscles of scoliotic girls prove *capable* of producing normal strength forces, another study was conducted by Reuber et al. [98] to investigate the possibility of lateral asymmetric trunk muscle contraction forces as a cause of curve progression. Myoelectric activities[1] of trunk muscles were measured in adolescent girls, 20 scoliotic and 12 structurally normal, during various

---

[1]The nerve transmits a signal that stimulates a muscle to contract. The magnitude of the signal, known as the myoelectric activity, determines the strength of the muscle contraction (i.e. the muscle contraction force) [98].

exercises to determine the muscle contraction forces. Muscle force asymmetries significantly different from normal girls were found only in patients with severe cases of double curves, with one Cobb angle larger than 25°. The fact that the larger trunk muscle forces were consistently found on the convex side of the severe lateral curves indicated that the lateral muscle force asymmetries are a result of scoliosis, developed to balance the lateral moment created by lateral offset,[1] rather than its cause. This conclusion of the study then suggested that scoliosis may be a result of a lack of force asymmetry in the spine which has a slight lateral offset. To this end, two other hypotheses have been proposed [98].

These hypotheses for the progression of scoliosis involve a malfunction in the neural network responsible for maintaining upright postures of the trunk. This malfunction, as suggested by Reuber et al. [98], includes the inability to detect an unbalanced lateral moment or to direct the necessary asymmetrical response in trunk muscles to counteract moment. In the first hypothesis, as a result of contraction forces in the trunk muscles being too symmetric, the soft tissues of the motion segments, particularly the intervertebral discs, in the curve region must provide resistance to most of the unbalanced moment. Hence, discs deform, motion segments rotate (i.e. tilt) further, and the lateral curve increases. This behaviour is said to be a necessary condition for curve progression but not a sufficient one [98]. The second hypothesis explains the curve progression. It pertains to possible long-term behaviour of discs to unbalanced lateral moments resulting from motor control defects. It hypothesizes that if the tilts continue to increase and in time become more or less permanent under sustained lateral moment, then an irreversible progression would occur. Although experiments conducted with animals support the hypothesis, it requires long-term testing of human discs, involving the monitoring of creep and hysteresis effects [98].

A study was performed on spine models [49], to investigate the possible sources of unbalanced lateral bending moments that could lead to curve progression, support clinical findings concerning muscle forces previously discussed, and substantiate the neural control defect hypothesis. The effects of possible abnormal trunk muscle forces and righting mechanisms, resulting from neuromuscular system malfunctions, on lateral curves were examined in this study. Results indicate that if progression of the scoliotic curve is due to trunk neuromuscular failure, then it is most likely in the malfunction of the neural control system, which senses imbalances and stimulates responses, rather than in the functional capabilities of the muscles to respond to appropriate signals. However,

[1]The lateral offset creates lateral moments in the spine due to (1) the weight of body segments above the apex of the curve and (2) the shortening and lengthening of the moment arm, on the convex and concave sides respectively, through which trunk muscles act [98].

neural control defect seems a plausible cause, it too fails to correlate growth and female gender bias to the disease.

Another hypothesis, pertaining to asymmetrical growth of spinal components, was proposed by Lindahl and Raeder [68]. Using a straight column theoretical model, they found that the type of external forces necessary to produce the lateral displacement and rotation, typical of scoliosis, would be vertical restricting forces acting on the spine, located in the quadrant lateral and posterior to the affected vertebral bodies, see Fig. 3.1. Possible sources of restricting force in this quadrant would be the restriction of the vertical growth of some or all the elements present in the quadrant i.e. transverse process, posterior section of ribs, and long dorsal muscles.

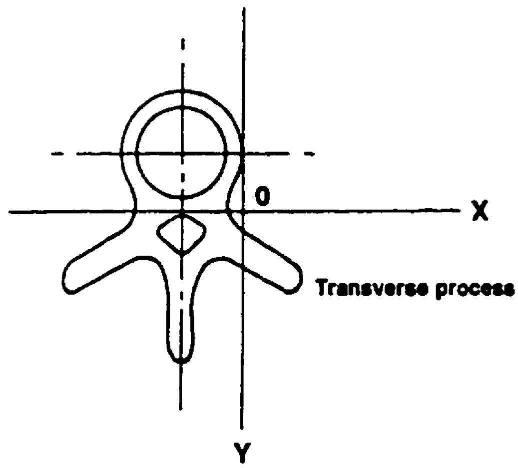

Fig. 3.1 Quadrant X O Y. The binding forces must be located in this quadrant in order to produce a lateral displacement and a convex-sided rotation similar to the type found in scoliosis. After Lindahl and Raeder [68].

The theory is based on the idea that since the anterior section of the spinal column, composed of stacked vertebral bodies, provides the majority of the stiffness of the spinal column, the deformed configuration of the spine is such that the anterior of the column will undergo the least amount of deformation in the column. He suggested that the muscles and ligaments interconnecting the transverse process on one side grow at a slower rate than the rest of structure. As a result, they would produce restraining forces between the transverse process on one side, i.e. in the quadrant, and cause lateral deviation and convex-sided rotation of the column so that the vertebral bodies experience a minimal bending deformation. It was conjectured that, if the ends of the spine were restrained in rotation, a deformation typical of scoliosis, with maximum rotation at the apex of the lateral curve, would result [68].

An attempt was made to clinically test the hypothesis by removing the transverse process on the concave side of 13 idiopathic patients and determining whether or not the progression would stop [67]. However, due to the unpredictable nature of scoliosis, whether it will progress or be stationary at any point in time, the effects of the treatment were difficult to establish (there was no conclusive proof of reduction in the scoliosis angle). Evidence of scoliosis developing in patients with unilateral paresis of the intercostal muscles located in the quadrant [58] and in patients following the surgical removal of the transverse processes (convex towards the side of the resection) [127,128], gives promise to the theory. Although this hypothesis explains the occurrence of disease during growth, it fails to explain the high frequency in females.

Lastly, abnormalities in the collagenous matrix of intervertebral discs, thought to cause a decrease in the resistance of the passive tissue component, were investigated as a possible factor in curve progression. Harrington [50] and Ponsetti et al. [95] have suggested that a collagen defect in the invertebral disc is the principal factor. Collagen content, extractability and distribution across disc were studied in both normal and scoliotic spines. Collagen abnormalities were found in scoliotic discs. However, results are conflicting as to whether they are primary or secondary effects[1] [18].

3.1.1 Lordosis Hypothesis and "Biplanar Spinal Asymmetry" [34]

The lordosis at the apex of the lateral curve in thoracic scoliosis has been noted as early as 1865 by Adams [1]. Although researchers such as Somerville [115] and Roaf [100] felt that scoliosis could not occur without the initial development of a lordosis, this aspect of scoliosis has been largely overlooked [66]. It is only over the recent years that the sagittal curvature of the spine in scoliotic patients has been receiving increasing interest [83], particularly by Dickson et al. [6,30,34].

The deformity is often misunderstood, because severe cases of thoracic scoliosis give the appearance of a severe kyphosis i.e. hunchback[2]. However, this is misleading due to the large axial rotation accompanying the deformity. As shown in the graphs and radiographs in Fig. 3.2 from Deacon et al. [30] of a specimen with severe thoracic scoliosis, the degree and direction of curvature varies according to the angle of view. Figure 3.2(a) indicates the variation of the curvature according to the angle of rotation of the specimen. Figure 3.2(b) shows the usual A-P view of the specimen, while Fig. 3.2(c) illustrates the true A-P view of the deformity. The "true" A-P is the view orientated

---

[1]Abnormalities in the collagen content of the scoliotic discs were found to be dependent on curve location. These results suggest that abnormality is of a secondary nature. However, contrasting results from pepsin extractability tests indicate abnormalities in all scoliotic discs [18].

[2]This deformity is often described as a kyphoscoliosis by many surgeons and physicians [100], implying mistakenly, that it consists of an excessive kyphosis as well as a lateral curve.

with respect to the apical vertebrae, which gives the maximum view of the lateral deformity. The lateral curvature is generally of a magnitude 41% greater in the true view of the deformity than that in the A-P view of the specimen [30]. Figure 3.2(d) shows the usual lateral view of the specimen which indicates a false kyphosis. It is only in the "true" lateral view, Fig. 3.2(e), that the actual lordosis becomes evident. This true lateral view is perpendicular to the true A-P view.

Studies by Öhlen et al. [83] and Willner [131] showed that scoliotic patients have significantly smaller thoracic kyphosis than normal persons. Statistically, a radiographic study by Dickson et al. [34], of over 70 patients with idiopathic thoracic scoliosis showed a true lordosis at the apex of their lateral curves in 75% of the cases, with the remaining ones having significantly reduced or absent kyphosis. The mean was a 3° lordosis at the apex. Results are contradictory at this point in time regarding whether or not there exists a correlation between the degree of lordosis and the degree of scoliosis (i.e. lateral curve) [30,34,83].

The results indicating the presence of lordosis are not surprising, for as mentioned before, geometrically, the convex-sided rotation, characteristic of scoliosis, requires a longer anterior length of spine than posterior i.e. true lordosis, throughout the lateral curve. In morphometric analyses conducted by Deacon et al. [30] and Roaf [100], it was found that the mean anterior length of the spine was longer than its posterior length. The vertebrae in the affected region were found to be lordotic, implying *asymmetric* vertebral growth [30,34]. Thus, it seems that the spine, even in regions typically kyphotic, ie. thoracic region, must be lordotic to some degree in order to obtain scoliotic rotation [29].

The above geometrical evidence and its interpretation constitutes the basis of the *lordosis hypothesis* as to the etiology of thoracic scoliosis. Somerville [115], Roaf [100], and more recently Dickson et al. [34] have been the most prominent proponents of this hypothesis. Somerville [115] was one of the first to propose, on the basis of his physical model and experimental studies, that the relative faster growth of the anterior portion of the spine forces it into a configuration with lordosis, rotation and lateral deviation. Roaf [100] supported the hypothesis by stating that there are two possible results from relative anterior overgrowth of the spine. They are: (1) a severe lordosis, or (2) a sideways deviation of the longer anterior portion, i.e. scoliosis. He suggested that the severe lordosis is prevented by the sternum and abdominal muscles and thus the scoliotic-type deformations accommodate the asymmetrical growth. Dickson et al. [34] extended the hypothesis by pointing out that in addition to the thoracic lordosis, there must be some sort of spinal asymmetry in a plane other than the sagittal plane, i.e. the horizontal or frontal plane, for AIS to develop. Without the asymmetry, under symmetrical loading, the spine would remain in the sagittal plane until the point

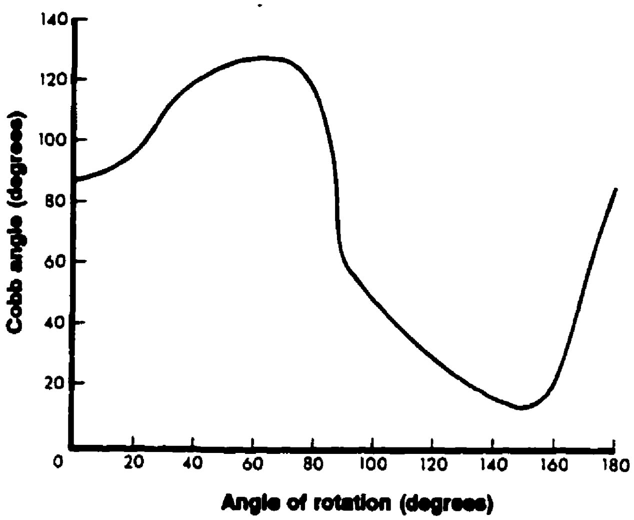

(a)

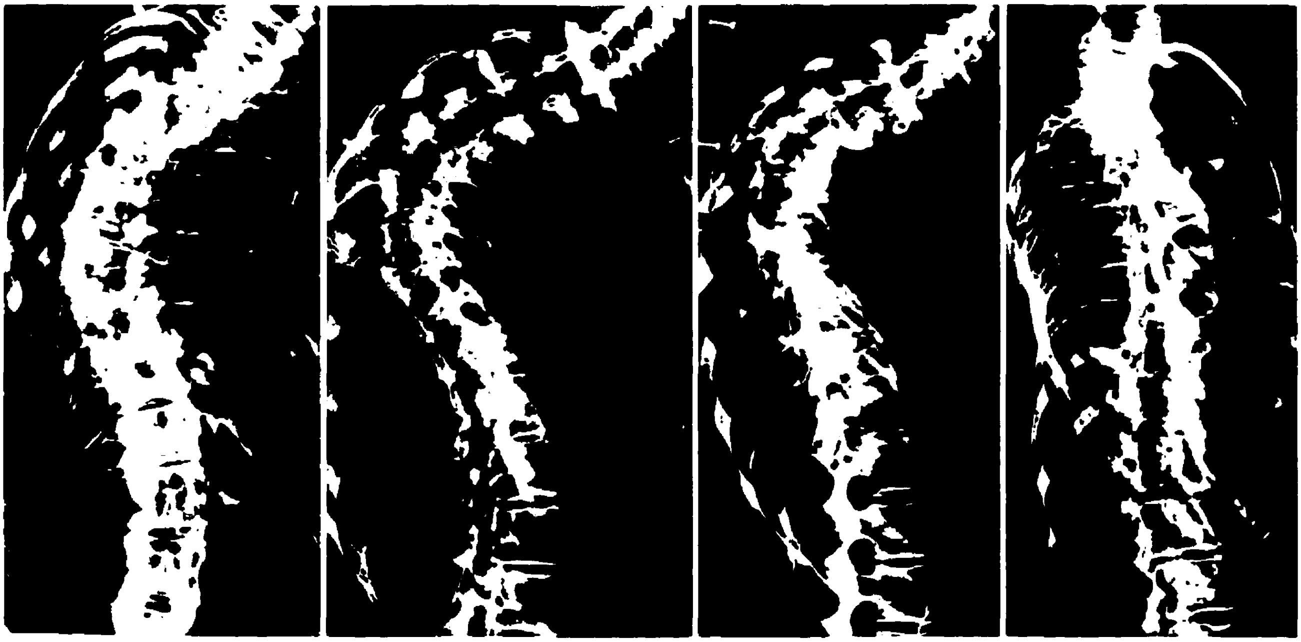

(b) (c) (d) (e)

Fig. 3.2 Variation of the degree of curvature (Cobb angle) with respect to the view of the thoracic scoliotic deformity. (a) Graph of the Cobb angle measured versus the angle of rotation from the frontal view of the scoliotic specimen. Radiographs of the specimen taken at 4 views. (b) A-P view of the specimen indicating a lateral curvature of 87°. (c) *True* A-P view of the deformity revealing a true lateral curve of 128°. (d) Lateral view of the specimen giving an impression of a kyphosis of 61°. (e) *True* lateral view of the deformity revealing a true 14° lordosis at the apex of the lateral curve. This view is 90° to the plane of maximum lateral deformity. All figures are from Deacon et al. [30].

of excessive loading. Therefore according to Dickson et al. [34], the combination of the thoracic lordosis and the additional asymmetry, which they termed "biplanar spinal asymmetry", is the crucial factor giving instability to the spine. They suspect that its presence during growth is the primary cause; while the lateral curvature and rotation of the AIS spine are secondary effects.

Experimental and Biomechanical Support

Results of experimental and biomechanical model studies support the hypothesis. Somerville [115] produced progressive idiopathic thoracic scoliosis in 3 young rabbits by surgically creating a lordosis over a short segment of their spine. Considerable amount of rotation, in the scoliotic direction, was developed in animals in which the disease is unknown and in which gravity can have no effect. Dickson [34] performed a biomechanical study in which a model with a short-segmented biplanar asymmetry (lordosis and slight frontal curve) was created using spines of rabbits. Upon forward flexion, these spines deformed in a manner similar to scoliosis. The normal rabbit spine, when subjected to flexion, did not rotate. Conclusions drawn from the experiments were that a significantly reduced kyphosis and an asymmetry in the horizontal or the frontal plane are necessary for scoliosis. Since Somerville was unaware of the necessity of such an asymmetry and attempts by other investigators to repeat his experiment were unsuccessful, Dickson et al. [34] suggests that Somerville must have accidentally created a slight frontal plane asymmetry[1] in his experiment.

It may also be recalled that in the work dealing with the restricting forces [68], the analysis determined the position of binding forces, necessary to achieve scoliotic deformity, to be lateral and posterior to the vertebral bodies of the hypothetical straight column. The posterior positioning of the load creates a lordosis and the lateral offset of the load creates a lateral asymmetry. Therefore, it seems that this theoretical analysis obtains scoliotic-type rotations by effectively imposing biplanar spinal asymmetry due to the location of the loading.

Two other related studies were performed to investigate the lordosis hypothesis. Jarvis et al. [59] conducted an experiment on human and calf spines to study the effect of a localized lordosis or tethering of the posterior elements of the spine on the behaviour of the normal spine. Ligamentous spines, with and without posterior tether, were loaded by axial displacement. Slight asymmetry in the mounting gave spines a tendency to deflect laterally in a certain direction. Upon loading, significant lateral curves were produced, convex to the side determined by the asymmetry. A fixed length tether was placed posteriorly of the spine and slightly laterally to the convex side of the of this lateral curve,

[1]Children, unlike animals, have inherent frontal and horizontal plane asymmetries [34].

in the lower thoracic region of the spine. The tether was found to increase the convex-sided rotation. Without the tether, the rotation was found to be non-existent or in the opposite direction (concave-sided). Geometrically, convex-sided rotation in which the tether moves towards the inside of the lateral curve, accommodates the "inextensible" tether. Thus, according to Jarvis, the posterior tether explains the rotation characteristic of scoliosis, but the cause of the tether is uncertain.

Stokes and Gardner-Morse [118] simulated the experiment performed by Jarvis et al. [59] using a simple homogeneous finite element model of the ligamentous thoracolumbar spine. Under loads contracting the postero-lateral tether in the thoracic region 3% and a compressive force of 250 N applied at the top, lateral displacements and convex-sided rotations resulted. However, the axial rotation was very small, with a relative magnitude at the apex of 0.09°/mm of lateral deflection. Tethering in the lumbar region produced poor results with rotations of a kind opposite to scoliosis.

Explanation of Clinical Evidence

The lordosis hypothesis [34] also has explanations for the clinical findings. Logically, regardless of the initiating factor, scoliosis requires growth. It is only during growth periods, that such large deformations or changes may develop. Since according to the hypothesis the lordosis arises from asymmetrical anterior-posterior vertebral growth in the hypothesis, it is not surprising to find high incidence of AIS during the adolescent growth spurt. It is during the periods of peak growth, that asymmetrical growth rates would alter spine configuration most drastically, and consequently, its effects would become obvious at this time.

Lateral spinal profiles (sagittal curvatures) are determined genetically [116]. This is demonstrated by the fact that some families have a tendency to have flat backs while others have round backs. Thus, the strong familial trend noted in AIS [135] may be explained by the fact that the essential lesion of AIS according to the hypothesis, namely a reduced thoracic kyphosis, is an inherited feature [6,34].

As found by Willner [131], during the normal growth process, the thoracic kyphosis reduces in magnitude between the ages of 8 and 12 and becomes a minimum at about the age of 10. This period of reduced curvature coincides with the adolescent growth spurt of girls, as shown in Fig. 3.3(a). Boys, on the other hand, Fig. 3.3(b), have their peak growth velocity, on average, 2 years later than girls when spine has maximum kyphotic curvature. Based on the fact that girls have a reduced kyphosis while boys have a maximum kyphosis during period of peak growth (i.e period when AIS develops), the hypothesis explains the susceptibility of girls to the deformity [34].

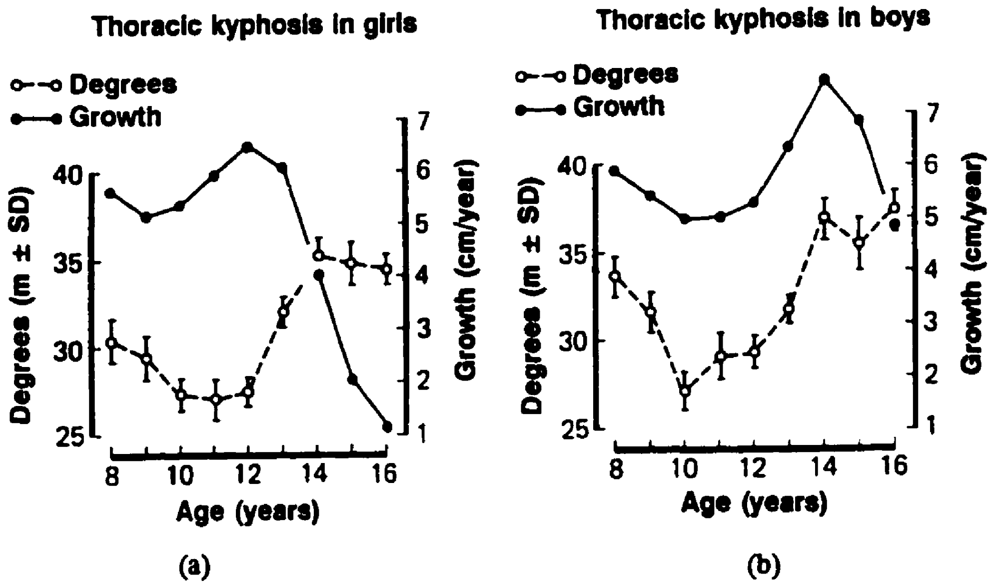

Fig. 3.3 Graphs illustrating the correlation between growth rates and the degree of thoracic kyphosis in (a) girls and (b) boys, ages 8 - 16 years old [131]. Figures are from Leatherman and Dickson [66].

A kyphosis on the small side of the normal range produces a straighter hence taller spine. Thus, the reduced thoracic kyphosis resulting from asymmetrical vertebral growth explains the finding that scoliotic girls (with mild cases) are taller on average than normal girls, in the absence of any adolescent growth abnormalities [6]. Biomechanically, a reduction in the curve amplitude of the spine increases its length without a change of its cross-sectional properties and therefore produces a less stable configuration of spine. The effect of the magnitude of curvature or curve amplitude on column stability will be discussed in Chapter 4.

To illustrate the precarious balance of the sagittal profile of the spine in late childhood, the middle thoracic vertebrae need only change their curvature by about 3° each, for the thoracic spine to become lordotic [31]. In addition, the thoracic region is also the site of the natural frontal and transverse plane asymmetries due to the presence of the aorta on the left side. In the frontal plane, the thoracic spine has a slight right curve and in the horizontal plane, the thoracic vertebrae T4 to T9 have an asymmetrical cross-section, as shown in Fig. 3.4. Anatomically, the flatter the thoracic kyphosis, the greater the effect of the aorta on the vertebrae [45].

The T9 vertebra is one of the thoracic vertebrae (with considerabe rotational freedom) which is located close to point of inflection between kyphosis and lordosis. Recalling that the crucial factors of AIS, according to the "biplanar spinal asymmetry" hypothesis, are lordosis plus a frontal or horizontal asymmetry, the hypothesis explains why T9 is a frequent apex of the deformity [83].

Sagittal curvature varies substantially from person to person. An average lateral profile is very difficult to construct as was found during modelling. However, since thoracic scoliotic patients have in common a lordotic tendency in their thoracic curvature [66], it is important to investigate its effect carefully. In light of the experimental and biomechanical model studies offering support of the lordosis hypothesis as well as the clinical evidence explainable by the hypothesis, it follows that this hypothesis as expounded by Somerville [115], Roaf [100], and Dickson et al. [34] must be capable of explaining the scoliotic deformity on a rational basis.

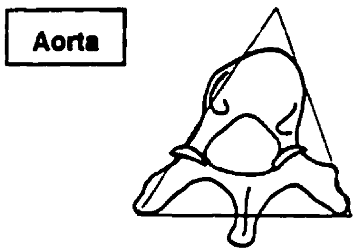

Fig. 3.4 Top view of transverse or horizontal plane asymmetry of middle thoracic vertebrae due to pulsation of the descending aorta of the left side of spinal column. After Leatherman and Dickson [66].

3.2 Spinal Modelling

A vast variety and number of studies have been conducted to understand the biomechanics of the spine. Significantly relevant to the present work were the studies which:

(1) experimentally determined stiffness properties of the various components of the spine,

(2) determined the geometry of spine and rib cage by direct measurement from human specimens,

(3) involved experimental and/or clinical procedures to evaluate possible causes of AIS,

(4) developed (mathematical) structural analysis models of the complete thoracolumbar spine.

To avoid repetition, the first two categories are discussed in detail in Chapter 5. The third one has already been discussed in the previous section. Discussion of the last (fourth) category is limited to those models which were concerned specifically with the study of scoliosis and/or spinal stability. In particular, no reference is made to the numerous model studies on dynamic analysis. Also, some of the discussion in this category overlaps with that in the section on possible etiology of AIS, since many studies involved testing hypotheses using appropriate structural analysis models.

Mathematical models are often used to simulate complex systems such as biological systems, which are difficult to study using standard experimental techniques [110]. Spine structural analysis models have long been used to gain an understanding of spinal behaviour, in particular, scoliosis. The chief advantage of mathematical models over physical models [7,20,101,115], is the ease of changing various parameters (i.e. size and shape of vertebrae, soft tissue properties, sagittal curvature) in order to predict the effects of such changes [10]. However, due to the complexity of the structure, and the lack of hard data on the living (in-vivo) spine,[1] unavoidable assumptions must be made in order to construct a feasible and useful model [42].

3.2.1 Continuum Models

Continuum models are the simplest way to represent the spine. In these models, the spine is idealized as a continuous beam.

Lucas and Bresler [73], determined the stability of the ligamentous spine both theoretically and experimentally. In their study, the spine was conceptualized to behave like an elastic beam with constant sectional properties along the length. For this purpose, the average lateral bending flexibilites of each elastic segment, $k = \theta/M$, were determined experimentally from lateral load studies on three ligamentous spines. The effective lateral flexibility, K, of the entire spine (of length L) was then calculated as $K = \Sigma k/L$. Using this value of K, the theoretical critical loads for various end support conditions were calculated according to the Euler buckling formula for straight elastic columns.

Next, the upright spine, constrained from displacement in the sagittal plane at the mid-thoracic and mid-lumbar levels to prevent A-P bending and securely fixed at the sacrum, was loaded vertically at the top until lateral buckling occurred. Buckling loads were determined for the conditions in which T1 was free and also when T1 was constrained from lateral and anterior-posterior displacements and axial (horizontal plane) rotation.

Comparisons were made between the theoretical critical loads and experimental critical loads for the same constraint conditions, see Table 3.1. Results were in close agreement, and indicated that the ligamentous spine behaves similarly to an elastic beam. The critical loads for the spine length of 47.9 cm, were found to be 2 kg and 17 kg for the T1-free and T1-constrained (as described above)

---

[1]Data on human spine found in literature are obtained from in-vitro spine. Properties etc. may very well be different in-vivo. In-vivo properties would be difficult if not impossible to measure. Therefore, present study is based on in-vitro measurements and does not account for postmortem effect.

conditions, respectively.

The work of Lucas and Bresler is significant in the field of stability of spine, since they were the only ones to have conducted an experimental *stability* study on a human spine. Their results provide researchers a basis for comparison.

Works by Hjalmars [54] and Lindbeck [69] indicate that in some circumstances a mathematically simple continuum model may be sufficient for the analysis of the mechanical response of the spine at an overall level. Hjalmars [54] developed an anisotropic beam model for the lateral bending of the human spine. Lindbeck [69] used this model to reproduce the characteristic form of a spine with functional scoliosis[1] by means of a buckling analysis. However, in view of the highly idealized assumptions necessary to arrive at a continuum model, they can provide at best, only a qualitative picture of the real behaviour.

3.2.2 Discrete-Parameter Models

More realistic and complex models were developed as computer technology improved [42]. Representation of the spine in three-dimensions is required in order to study very basic problems in orthopaedics such as scoliosis and effects of instability [87]. The discrete-parameter structural analysis model[2] is composed of discrete elements representing various anatomical elements of spine (discs, ligaments, vertebrae, etc.) each assigned its own sectional and material properties. Generally, the vertebrae, ribs, and sternum are idealized as rigid bodies, while the discs, ligaments, and cartilage are modelled as deformable elements.

Comparatively complex computations make these models less easy to work with than continuum models for the purpose of drawing general conclusions (e.g. effect of curvature) on the mechanical responses of the spine [54]. However, continuum models are too unlike the real spine structure because of their inability to account for important anatomical features (e.g. differences in properties of discs and vertebrae, presence of rib cage on thoracic vertebrae) [87]. Local effects and deformations are important in the present study, hence the model chosen for the present study is a discrete-parameter model. A discussion of past three-dimensional thoracolumbar spine models relating to the study of scoliosis now follows.

---

[1]Defined as a lateral curvature of the spine caused by tilt of pelvis.

[2]This is not a F.E.M. model, in which for example, discs and vertebrae are modeled in detail by 3-d finite element meshes. The interest here is in the behaviour of each distinct anatomical element which makes up spine rather then in the stress fields of each element. Thus, distinct elements are modeled using beam elements.

Schultz and Galante [110] constructed a three-dimensional mathematical model of the human vertebral column to study the geometry of the motions of the spine in flexion, extension, lateral bending, and axial rotation. This work is important because it describes motion in three-dimensions. The model used in the study was strictly a geometric one. Although force-deformation relationships are important in the mechanics of the spine, only geometrical compatibility was enforced in their study. The 24 vertebrae comprising the full mobile spine (C1 to S1) were modeled using rigid bodies, and the intervertebral discs and connecting ligaments were represented with fixed length elements which were attached to coordinates defined on the rigid bodies (i.e. vertebrae). Motion was simulated by altering the lengths of the fixed length elements. Resulting deformations were within reasonable anatomical values and they compared well with those from previous in vivo studies, indicating that the model was a good representation of the real spine. The most important conclusion from this study [110] was that within the restrictions imposed, the spine showed its ability to assume many different geometric configurations from a variety of different ways, not belonging to any one pattern of motion.

More pertinent to the present study is the application made of the above model to determine the geometric changes required to alter normal spine into a configuration typical of idiopathic scoliosis. Using 5 different models, Schultz et al. [111] studied the effect of the changes in the lengths of the various intervertebral connecting elements as well as in the position of (rigid) body coordinates defining their attachment (i.e. simulating change in vertebral geometry), on the geometric configuration of the models. The resulting configurations were then compared to radiographs of patients with idiopathic scoliosis. It was found [111] that "no single set of kinematic changes resulted in all of the geometric characteristics of the scoliotic deformity. The length changes are complex and suggest that they are secondary. However, it was concluded that regardless of the etiology of the disease, the posterior structures may have an important role in reaching the geometry of idiopathic scoliosis."

Panjabi and White [91] also developed a mathematical method to analyze three-dimensional motion of the spine. The method is based on roentgenograms[1] reflecting incremental motion of autopsy specimens of spine segments subjected to the three principal rotations (i.e. in sagittal, frontal, and horizontal planes). The method describes the motion about its "helical axis of motion", which according to these authors allows the comparison of the motion of 2 or more rigid bodies regardless of their shape or positions of their measuring points [91]. White [129] used the same method to analyze his experimental data based on two and three dimensional testing of motion segments of the

---

[1]*Roentgenograms* are defined as photographs made with x-rays [122].

normal thoracic spine. Their research on the kinematics of the normal thoracic spine is included in this review because of the following correlation made by them between the results and the etiology of scoliosis.

Significant coupling was found to exist between lateral bending and axial rotation. In most instances, the thoracic vertebrae were observed to experience concave-sided rotation, that is, the anterior aspect of vertebral body rotates towards the concavity of the lateral curve. However, in some cases, the middle thoracic vertebrae were observed to rotate in the opposite direction (i.e. convex-sided rotation, in which the anterior of the vertebral body rotates in the convexity of the lateral curve), which is characteristic of scoliosis.

With respect to this finding, the study suggested that the direction in which the middle thoracic vertebrae have a tendency to rotate may be a critical factor in the development of AIS. As stated by White [129], "any slight disturbances in the delicate balance of the normal thoracic motion may cause middle vertebrae which tend to rotate towards the convexity, to rotate too much. This rotation would lead to asymmetric loading on epiphyseal plates, muscle and ligament imbalances, and eventually scoliosis. Possible factors responsible for upsetting the balance could be malaligned facets, traumatic event, chemical hormonal change, and over-dominance of left or right handedness". The facts that (1) the mid-thoracic region is a frequent site of scoliosis and, (2) there is a slight anatomical lateral curve already present in this region, give promise to the theory.

Also of relevance to the present work is the study by a group of researchers [10,107] in which a three-dimensional model was developed for the purpose of conducting nonlinear (geometric) analysis of forces acting on the spine. This study was the first to report such a model. Analyses predicted the response of the spine to lateral load, the stability of the spine under compressive load, and the effect of tractive load on a scoliotic spine (model constructed of a scoliotic spine for this analysis). Both the construction of the model and the results of the stability analysis are important to the current work, and they will be referenced often in Chapter 5 and Chapter 6.

The modelling procedure and the results of the study were reported by Belytschko et al. [10]. The complete thoracolumbar spine was modeled with rigid bodies to represent vertebrae and deformable elements to represent soft tissue intervertebral elements. Beam elements were used to represent intervertebral discs with its longitudinal ligaments, and spring elements to model each of the major ligaments connecting posterior elements of vertebrae and the facet joints. This representation distinguished the model from previous ones such as the one by Roberts and Chen [103][1] in which the overall stiffness of the intervertebral joint was lumped in one element. Geometric nonlinearities were accounted for by using the incremental linearization technique of nonlinear analysis. This enabled them to analyze the normal motions of the spine, accompanied by large deformations.

Schultz et al. [107] described the construction of the model. This included the details of the geometry and force-deformation properties along the spine. The geometry was based on cadaver measurements [64,124]. Similar to the model constructed by Schultz and Galante [110], the geometry of the spine was defined using the local coordinates on vertebrae (rigid body) giving points of attachment for the intervertebral elements and using the lengths of the various intervertebral elements. Beam elements representing intervertebral discs and longitudinal ligaments were assigned bending, axial, shear, and torsional stiffnesses. Spring elements representing ligaments connecting posterior elements were assigned a tension stiffness, and those modelling facet joints were assigned both compression and tension stiffnesses. All the deformable elements were assigned linear isotropic elastic properties.[2] Stiffnesses assigned to these elements were chosen to simulate the behaviour found for cadaver motion segments, as best as possible.

Only the results from the lateral load and stability analysis are mentioned here, due to their relevance to the present study. In these two analysis, the conditions were set to simulate the experiments by Lucas and Bresler [73]. Frontal plane rotations resulting from a 0.5 kg lateral load, and lateral buckling loads for 3 different fixity conditions at the top i.e. (1) T1 free, (2) T1 fixed in horizontal displacements and rotation, and (3) T1 fixed against all degrees of freedom except for vertical displacement (see Table 3.1) were in good agreement with the results of Lucas and Bresler. In addition, the buckled configurations were scaled so that the resulting average lateral displacement would be the same as those of the scoliotic spine. Comparison of the buckled configuration to the scoliotic spine revealed similar lateral displacements and frontal rotations but very different *axial rotations*. The scoliotic spine used as reference was found to have a maximum axial convex-sided rotation of 25° while the buckled spine showed hardly any axial rotation. Based on these results, Belytschko et al. [10] suggested the investigation of the effect of the posterior muscles and rib cage

[1]Roberts and Chen [103] conducted a dynamic analysis and therefore their work is not included in this review. However, their model is very important to the current study as explained in Chapter 5.

[2]Ligament elements were assigned either a zero or non-zero axial stiffness depending if they were expected to experience compression or tension. It was found in the study that in conformity with the assumption, they either experienced tension or compression throughout the range of various types of loading [107].

on the axial rotations during buckling for future studies.

In their next attempt, the same group of researchers added a rib cage to their previous thoracolumbar spine model. The primary purpose this time was to study the mechanics of the human skeletal thorax [4]. Of particular interest is the results showing the stabilizing effect of the rib cage on the thoracolumbar spine.

Table 3.1 Lateral Buckling Loads Under Compressive Loads (N)*

T1 constraint	Ligamentous spine	Spine with rib cage intact
T1 free	19.13 (E) 20.50 (T) 20.60 (C)	78.48 (C)
T1 fixed in horizontal displacements and rotation	166.77 (E) 167.75 (T) 196.20 (C)	608.22 (C)
T1 fixed in all but vertical displacement	327.65 (T) 313.92 (C)	990.81 (C)

*Spine is constrained from displacements in the sagittal plane at the mid-thoracic and mid-lumbar levels to prevent anterior-posterior bending and sacrum is fixed.

E = experimental values obtained by Lucas and Bresler [73], spine length = 47.9 cm.
T = theoretical values obtained by Lucas and Bresler [73], spine length = 47.9 cm.
C = computed values by
- Belytschko et. al. [10] for buckling of the ligamentous spine, spine length = 49 cm.
- Andriacchi et. al. [4] for buckling of the spine with rib cage, spine length = 49 cm.

Andriacchi et al. [4] used thirty-nine rigid bodies to represent the skeletal thorax, i.e. ribs and sternum, in the model. Deformable elements were modeled using either spring or beam elements and were assumed to possess quasi-linear[1] properties. These elements include costal cartilage, intercostal ligaments, and costovertebral joint. The analysis was capable of having both geometric and material nonlinearities. Geometries of the elements were determined from cadaver measurements [108,109], and put in correct anatomical position with respect to spinal column with the aid of published anthropometric data [22,25]. Properties for deformable elements were determined by performing computer simulation of cadaver experiments [109]. Similar to the method used in assigning values

[1]Linear stiffness, although accounting for different stiffnesses in tension and compression [4].

for elements in the ligamentous spine model, stiffnesses were adjusted until reasonable agreement with experimental results was obtained.

The response of the spine and rib cage model was compared with available experimental results to determine if model was representative of the real structure. Results showed good agreement. Then using the validated model, the effect of the rib cage in bending and on the stability of the spine was investigated. Also, the model was modified into two different scoliotic configurations in order to study the effect of rib cage on scoliosis.

Once again, only the results of the bending and stability analysis are mentioned due to their relevance to the current study. First, the rib cage was found to increase the resistance of the spine to *all* modes of bending in the thoracic region, as shown in Fig. 3.5. As can be expected, removal of the sternum rendered the rib cage totally ineffective. Second, the experiments of Lucas and Bresler were again simulated, this time with the rib cage intact in order to demonstrate the effect of rib cage. For all three previously mentioned T1 constraint conditions, the rib cage was found to increase the buckling load of ligamentous spine 3 to 4 times[1] (see Table 3.1). These results along with those of the ligamentous spine, discussed previously, are shown in greater detail in Chapter 6, where they are used for comparison with the results from the present study.

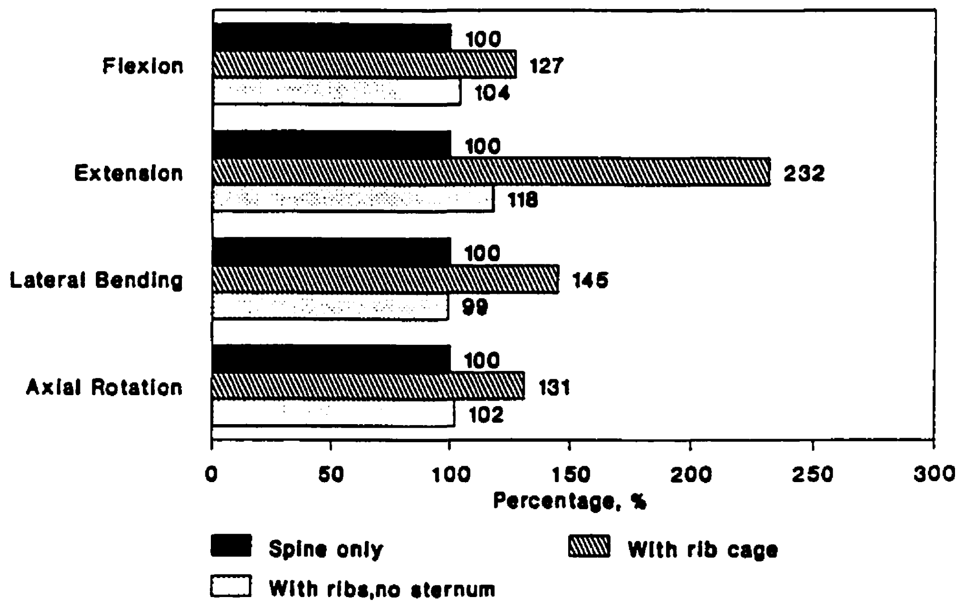

Fig. 3.5 Relative stiffening effect of the rib cage on the spine and the importance of rib cage continuity, i.e. sternum [4,130].

---

[1]The critical loads found in the study are still well below the in-vivo buckling loads. This is due to the other stabilizing components which are not accounted for in the model, e.g. muscles [4].

Haderspeck and Schultz [49] investigated the effect of various trunk muscle forces and support mechanisms, responsible for righting of the trunk, on the lateral curve of model spines using computer simulation. The study was conducted with the purpose of determining possible mechanisms that could produce abnormal loads (unbalanced moment) capable of lateral curve progression.

To this end, models of the spine, 5 with structurally normal configurations and 13 with scoliotic configurations, were used in the study [49]. The models were similar to those constructed by Belytschko [10], with the addition of trunk muscles. These muscles, capable of producing significant forces, were modeled using 68 individual model muscle slips. The muscles were assumed to behave linearly, and contract at a rather high intensity of 40 N/cm^2. Contraction was simulated by application of equal and opposite forces along muscle line of action. Actions of muscle groups (21 unilateral and 12 bilateral), i.e. erector spinae, were simulated by simultaneous contraction of combinations of individual muscle slips.

Results of the above analyses, as discussed in the previous section, indicated that if reason for the occurrence of abnormal forces is a defect in the neuromuscular system, then the malfunction is most likely to occur in the neural control, responsible for stimulating and sensing muscle actions to retain balance, than in actual muscle capabilities. This is evident by results showing that possible malfunctions intrinsic to muscles (excessive bilateral symmetry, unilateral weakness, and side-to-side muscle action asymmetry), under reasonable set of circumstances, cannot produce curves typical of scoliosis [49].

Chapter 4
Theoretical Considerations

This chapter provides an introduction to the general stability (or buckling) theory of columns [9,14,21,123] in the context of curved spine-like, albeit homogeneous, columns. The topics dealt with are: bifurcation buckling loads of Euler column, growth of the sagittal-plane curve of spine-like columns under increasing axial load, torsional-flexural stability of such columns, and effect of curvature on buckling loads.

In the analysis dealing with the torsional-flexural buckling, an approximate analytical solution is obtained for the torsional-flexural bifurcation buckling of a spine-like simply-supported column. This solution is then used to check the capability of the MSC/NASTRAN finite element program to solve torsional-flexural buckling problems numerically.

4.1 Flexural Buckling of Columns [21]

Like all slender structures, spinal columns can be expected to be susceptible to unstable (buckling) behaviour. To understand the theory involved in the stability of the curved, spine-like column, it is important to begin with the theory of the simple Euler column.

4.1.1 "Euler Column"

The Euler column, shown in Fig. 4.1(a), is a very idealized case. It may be used to demonstrate, in simple terms, the behaviour of a real column in axial compression. The Euler column is a straight, homogeneous (one material) column with constant cross-section. Its ends are simply-supported (i.e. hinged) and it is loaded axially along its centroidal line along the x-axis. It is assumed that the column material is linear elastic and the deformations are small. The column is restricted to deform in the x-y plane. Effect of gravity is neglected.

The critical compressive axial load, P, of the column is defined as the load for which equilibrium in the slightly bent configuration, as shown in Fig. 4.1(b), is possible [21]. To find this load, let $v = v(x)$ be the equilibrium deflection of the bent column axis in the y direction. According to Bernoulli-Euler theory, the internal resisting moment at any section a distance x from the origin, Fig. 4.1(c), is defined as

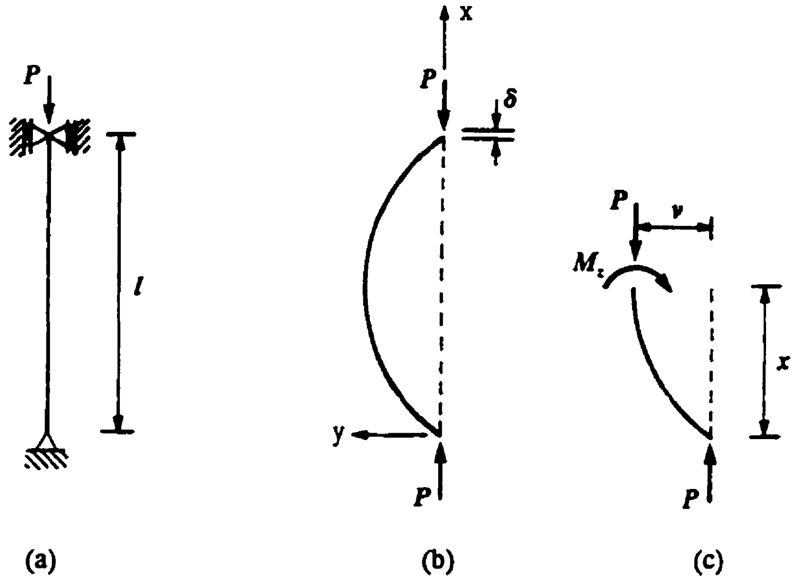

Fig. 4.1 Euler Column, (a) straight pre-buckling configuration, (b) buckled configuration, (c) free-body diagram (buckled column).

$$M_z = -EI_z\, v'' \tag{4.1}$$

where $v'' = d^2v/dx^2$ and EI_z is the flexural or bending stiffness of the column in the x-y plane.[1] The moment equilibrium of the free-body column of length x requires that $M_z = Pv$ which, by substitution of Eq. (4.1), leads to

$$EI_z\, v'' + Pv = 0 \tag{4.2}$$

Introducing

$$k^2 = \frac{P}{EI_z}, \tag{4.3}$$

the differential equation of equilibrium may be written as

$$v'' + k^2 v = 0 \tag{4.4}$$

The general solution of this equation is

$$v = A \sin kx + B \cos kx \tag{4.5}$$

[1] Actually, the correct expression is $M_z = -EI_z/R$ where $1/R$ = curvature = $v''/(1+(v')^2)^{3/2}$. However, for small deformation, $(v')^2 << 1$ and thus $1/R = v''$ is a permissible approximation.

where A and B are arbitrary constants to be evaluated by imposing the boundary conditions of the ends being restrained against displacements:

$$v(0) = 0, \quad v(l) = 0 \tag{4.6}$$

The first condition renders $B=0$; the second one demands that $A \sin kl = 0$, which can be satisfied by taking either $A=0$ (no buckling), or by taking $A \neq 0$ (buckling) but requiring

$$\sin kl = 0 \quad \Rightarrow \quad kl = n\pi \tag{4.7}$$

where $n = 1,2,3,...$ is an integer. Recalling that $k^2 = P/EI_z$, Eq. (4.3), the above condition is expressible as

$$P = \frac{n^2\pi^2 EI_z}{l^2} \tag{4.8}$$

Hence, at the axial loads given by Eq. (4.8), the column can assume deflected equilibrium shapes,

$$v = A \sin\frac{n\pi x}{l} \tag{4.9}$$

in which A, the amplitude of the sinusoidal buckling mode, is arbitrary, i.e. non-unique. This non-uniqueness is termed as bifurcation of equilibrium, and the loads at which this is possible are called bifurcation loads. The critical buckling load is the smallest load at which bifurcation of equilibrium is possible. Here it is obtained by setting $n=1$ in Eq. (4.8). Thus the formula for determining the critical load of a simply-supported Euler column is

$$P_{cr} = \frac{\pi^2 EI_z}{l^2} \tag{4.10}$$

which shows that the critical load is influenced by the length of column and its bending stiffness. Physically, at the critical load, the column can be in a deflected equilibrium shape of arbitrary (although small) amplitude $(-\epsilon < A < +\epsilon)$ without the presence of any lateral force. This behaviour of bending under zero lateral force is termed unstable, and hence the critical load is the smallest load at which this loss of stability occurs.

The Euler formula may be generalized, for determining the critical loads for columns with different end-conditions, provided the length of the equivalent Euler column, λ, is used. The expression for the generalized formula is

$$P_{cr} = \frac{\pi^2 EI_z}{\lambda^2} \qquad [4.11]$$

wherein the equivalent length, λ, is determined by the end-constraints on the column. These lengths determined by analyses similar to the one just described, are given in Fig. 4.2. From this figure it can be seen that, as expected, the greater is the degree of constraints, the smaller is the effective length, and thus the greater is the critical load. Thus Eq. (4.11) incorporates the influence of an additional parameter, the boundary conditions, on the critical load or stability of columns.

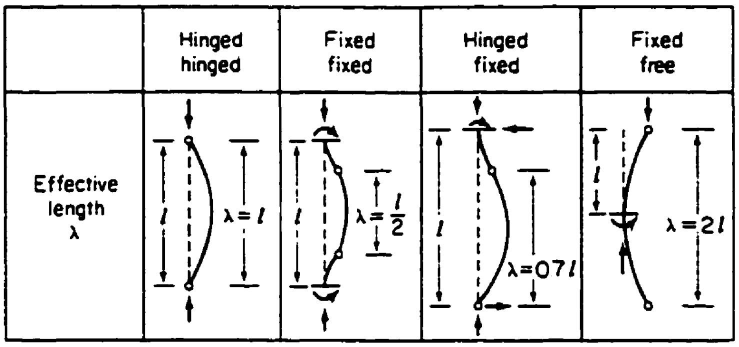

Fig. 4.2 Effective lengths for various boundary conditions. After Chajes [21].

4.1.2 Behaviour of Initially Curved Columns in Compression

In the case of the spine, the column is not straight. The curve present in the sagittal plane suggests the study of curved columns. For the moment, the out-of-plane movement is restrained, and only the sagittal plane behaviour is considered. Since there is already a curve present, the question of in-plane bifurcation from a straight configuration does not arise. Rather, there will be a growth, with increasing axial load, of the curve already present. For simplicity in solution, the column is given the same end conditions and assumptions as the simply-supported Euler column. The only difference is that the centroidal axis is curved. For the purpose of obtaining a useful solution and determining the effect of initial curvature on the spine, the shape of the sagittal curve of the spine-like column, shown in Fig 4.3, is approximated by

$$v_0 = a_0 \sin\frac{2\pi x}{l} \qquad [4.12]$$

where a_0 is the amplitude of the initial curve i.e. corresponding to $P=0$.

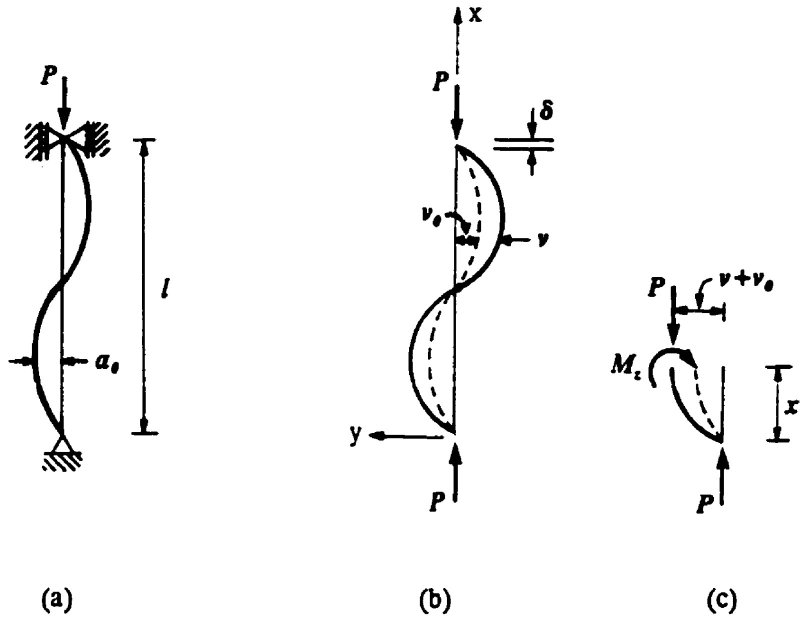

Fig. 4.3 Initially curved column under axial load.

Following the procedure outlined for the Euler column, the moment equilibrium of a portion of the column under an axial load P, Fig. 4.3(c), yields the following differential equation

$$EI_z\, v'' + P(v + v_0) = 0 \qquad [4.13]$$

where v is the additional deflection or the growth of the column curve in the sagittal (x-y) plane. Using the notation defined in Eq. (4.3), Eq. (4.13) can be rewritten as

$$v'' + k^2 v = -k^2 v_0 \qquad [4.14]$$

The general solution of the nonhomogeneous differential equation, Eq. (4.14), consists of a complementary solution, v_c , plus a particular solution, v_p . The complementary solution is the solution of the homogeneous equation, already obtained as Eq. (4.5). A particular solution for the v_0 given by Eq. (4.12), can be easily found as

$$v_p = \frac{a_0}{\dfrac{4\pi^2}{k^2 l^2} - 1} \sin\frac{2\pi x}{l} \qquad [4.15]$$

Hence, the general solution, $v = v_c + v_p$, is

$$v = A \sin kx + B \cos kx + \frac{a_0}{\frac{4\pi^2}{k^2 l^2} - 1} \sin\frac{2\pi x}{l} \qquad [4.16]$$

As in the Euler column case, boundary conditions determine the arbitrary constants, A and B. The end condition $v(0) = 0$ requires $B=0$, and $v(l) = 0$ requires $A \sin kl = 0$. Again, if $k=n\pi/l$, i.e. if $P = n^2\pi^2EI_z/l^2$, A can be taken as non-zero and arbitrary. However if $P \neq n^2\pi^2EI_z/l^2$ then A must be zero. The lowest loads at which A can be arbitrary, signalling unstable behaviour, is

$$P_z = \frac{\pi^2 EI_z}{l^2} \qquad [4.17]$$

Assuming $P < P_z$, hence taking $A=0$, and using the previously defined notation for k and relationship for P_z, the growth of the column curve may be expressed as the following function of P

$$v = \frac{a_0\, P}{4P_z - P} \sin\frac{2\pi x}{l} \qquad [4.18]$$

The total column deflection from the vertical, v_t, is therefore

$$v_t = v + v_0 = \frac{4\, a_0\, P_z}{4P_z - P} \sin\frac{2\pi x}{l} \qquad [4.19]$$

As P is increased the growth or displacement in the sagittal plane, v_t, and its rate, $dv_t/d\alpha$, both increase in a nonlinear manner.

4.2 Torsional-Flexural Bifurcation Buckling of a Curved Column Under Axial Load

If the spine-like column of Section 4.1.2 with perfect symmetry about the sagittal plane is allowed the freedom to displace out-of-plane (i.e. in the lateral or x-z plane), then once again the question of bifurcation of equilibrium arises. At sufficiently low axial loads, there is only the growth of the sagittal curve. However, at some higher load P, it may be possible for the column to bifurcate into an out-of-plane equilibrium shape. Such bifurcation will in general entail both twisting and lateral bending of the column in addition to the pre-buckling sagittal plane bending. This type of buckling is of common concern in the analysis and design of columns with thin-walled open-sections which are deemed to have low torsional stiffness.

The differential equations of equilibrium governing torsional-flexural buckling are quite cumbersome to derive from the first principles, in the manner of the previous sections. Here, it is more convenient to opt for the approach based on energy considerations [14].

It may be noted first of all that for bifurcation analysis, it is necessary to assume perfect symmetry about the sagittal plane. This renders the sagittal plane as one principal plane of bending. Secondly, for simplicity, it is assumed that the shear center of the column section coincides with the centroid of the cross-section. Thirdly, although the column is curved in the sagittal plane, integration or differentiation is performed with respect to x, the axial coordinate, rather than with respect to s, the length coordinate. In other words, the curvature effect on length is neglected and the analysis is restricted to cases where $(dv_i/dx)^2 << 1$, so that $ds \simeq dx$ along the centroidal line.

The strain energy of deformation due to an out-of-plane buckling displacement of the centroidal axis $w = w(x)$, and axial rotation $\beta = \beta(x)$ can be expressed as [14]

$$U = \frac{1}{2}\int_0^l \left[EI(w'')^2 + GJ(\beta')^2 + EC_w(\beta'')^2 \right] dx \tag{4.20}$$

where EI_y = lateral (x-z plane) bending stiffness, GJ = torsional stiffness, C_w = warping constant of the cross-section, and primes denote differentiation with respect to x. For circular cross-sections $C_w=0$, and for many other types of sections, the contribution of this term is small [14]. Accordingly, in the further analysis, it will be assumed that $C_w=0$. w and β are positive in the positive directions of the coordinate axes.

The loss in the potential energy of the axial load due to lateral buckling can be expressed as

$$V = -\int_0^l \int_A \sigma_{xx}^{o}\, \epsilon_{xx}\, dA\, dx \tag{4.21}$$

where A is the cross-sectional area, $\sigma_{xx}^{o} = (P/A) - (M_z y/I_z)$ is the pre-buckling axial compressive stress, and $\epsilon_{xx} = \{(w' + \beta' y)^2/2\} + \{(\beta' x)^2/2\}$ is the axial shortening strain due to buckling.[1] The expressions for σ_{xx}^{o} and ϵ_{xx}, when substituted in Eq. (4.21), give

$$V = -\left[\frac{1}{2}\int_0^l P\,(w')^2\, dx + \frac{1}{2}\int_0^l \frac{PI_o}{A}(\beta')^2\, dx - \int_0^l M_z w' \beta'\, dx \right] \tag{4.22}$$

where I_o is the centroidal polar moment of inertia of the cross-section. The first term in the square

[1] ϵ_{xx} is obtained by considering the geometry of deformation due to buckling where x, y are coordinates of a fiber with respect to the centroid.

brackets is the work of axial force due to axial displacement of ends, the second term is the work of axial stresses when the column twists, and the third term is the work of the pre-buckling bending moment in the sagittal plane. In the present case M_z arises due to eccentricity of P with respect to the centroid of column, and therefore $M_z = Pv_t$. The moment M_z is positive if it produces tension in the fibres with positive y coordinate.

The total potential energy due to torsional-flexural buckling may therefore be expressed as

$$\Pi = U+V = \frac{1}{2}\int_0^l \left[EI\,(w'')^2 - P\,(w')^2 + GJ\,(\beta')^2 - \frac{PI_o}{A}(\beta')^2 + 2M_z w'\beta' \right] dx \qquad [4.23]$$

Now, if the buckling configuration is to be an equilibrium one, the first-order variation of Π must vanish (i.e. $\delta\Pi = 0$) for arbitrary variation of w and β about the equilibrium configuration. Applying the standard calculus of variation procedure, the above condition can be shown to be equivalent to the following differential equations

$$(EI_y\, w'')'' + (Pw')' - \left(M_z\beta'\right)' = 0 \qquad [4.24]$$

$$\left[\left(\frac{PI_0}{A} - GJ\right)\beta'\right]' - \left(M_z w'\right)' = 0 \qquad [4.25]$$

and a choice of allowable natural and geometrical boundary conditions, which if needed can be derived by following the standard procedure.

With reference to the idealized spine-like column of the previous section, the variation of the bending moment along the length of the column due to the eccentricity of load P, is $M_z = P\,v_t$, which by virtue of the eccentricity defined in Eq. (4.19) is expressible as

$$M_z = M_0 \sin\frac{2\pi x}{l} \qquad [4.26]$$

where

$$M_0 = \frac{4P_z P a_0}{4P_z - P} \qquad [4.27]$$

Hence, the torsional-flexural buckling energy expression and the differential equations of equilibrium for the spine-like column of constant sectional properties and axial load P can be written as

$$\Pi = U + V = \frac{1}{2}\int_0^l \left[EI_y(w'')^2 - P(z')^2 + \overline{GJ}(\beta')^2 + 2M_0 \sin\frac{2\pi x}{l}\, w'\beta' \right] dx \qquad [4.28]$$

$$EI_y w^{IV} + Pw'' - M_0\left(\beta' \sin\frac{2\pi x}{l}\right)' = 0 \qquad [4.29]$$

$$\overline{GJ}\beta'' + M_0\left(w' \sin\frac{2\pi x}{l}\right)' = 0 \qquad [4.30]$$

where

$$\overline{GJ} = GJ - \frac{PI_0}{A} \qquad [4.31]$$

4.2.1 Closed Form Solution for a Simple Case

A solution of the above differential equations subjected to appropriate boundary conditions will yield the axial load P at which bifurcation of equilibrium of the column form the curved configuration in the sagittal plane to a curved three-dimensional configuration is possible. In general, the exact solution of these equations will be difficult or impossible to obtain because of (a) the presence of the variable coefficients, and (b) the nature of the boundary conditions. The purpose here is not to attempt an analysis for a realistic case, but rather to obtain a solution for an idealized simple case which can then be used to check the capability of the finite element program in solving such problems numerically. With this objective in mind, the boundary conditions chosen for a verification analysis are as follows:

$$\begin{aligned} \beta\,(0) &= \beta\,(l) = 0 \\ w\,(0) &= w\,(l) = 0 \\ w''(0) &= w''(l) = 0 \end{aligned} \qquad [4.32]$$

which correspond to fixity against axial rotation, fixity against lateral displacement, and absence of rotational restraints in the lateral plane, at the two ends.

However, even with these simplified boundary conditions, the exact solution of the differential equations is not a straight forward matter. Hence, a further approximation is made. Instead of solving the differential equations, the potential energy expression is made stationary with respect to a suitably chosen mode shape of the buckled column. This is the classical Rayleigh-Ritz method of approximate analysis of buckling problems [14,123].

Let the mode shape for the lateral displacement of the spine-like column be chosen as

$$w(x) = C_1 \sin\frac{\pi x}{l} \qquad [4.33]$$

where C_1 is an arbitrary parameter. This mode shape is consistent with the chosen boundary conditions on w, and may be considered as a "good" approximation of the unknown actual mode shape. Now, instead of arbitrarily choosing the mode shape for β, it is determined by solving Eq. (4.30) by substituting the above choice for w in that equation. The solution is

$$\beta = \frac{M_0 C_1}{6\,\overline{GJ}}\left[3\cos\frac{\pi x}{l} + \cos\frac{3\pi x}{l}\right] + C_2\,x + C_3 \qquad [4.34]$$

The two integration constants C_2 and C_3 are determined from the boundary conditions on β, Eq. (4.32), and the solution is expressible as

$$\beta = \frac{M_0 C_1}{6\,\overline{GJ}}\left[3\cos\frac{\pi x}{l} + \cos\frac{3\pi x}{l} + \frac{8\,x}{l} - 4\right] \qquad [4.35]$$

Using Eq. (4.33) and Eq. (4.35) for w and β in the expression for the potential energy, Eq. (4.28), and performing the integration yields:

$$\Pi = U + V = \frac{C_1^2\pi^2}{4l}\left[\frac{EI_y\pi^2}{l^2} - P - \frac{M_0^2}{\overline{GJ}}\left(\frac{1}{2} - \frac{32}{9\pi^2}\right)\right] \qquad [4.36]$$

The potential energy here is a function of the single parameter C_1. The condition $\delta\Pi = 0$ is equivalent to $d\Pi/dC_1 = 0$ for arbitrary C_1, which requires that the term in the square bracket of Eq. (4.36) must vanish. The bifurcation buckling load (consistent with the assumed mode shape) is therefore given by

$$\overline{GJ}\left(\frac{\pi^2 EI_y}{l^2} - P\right) - \left(\frac{1}{2} - \frac{32}{9\pi^2}\right)M_0^2 = 0 \qquad [4.37]$$

Recalling the definitions of $\overline{GJ}$, M_0 , and P_z , Eqs. (4.31), (4.27), and (4.17) respectively, and introducing

$$P_y = \frac{\pi^2 EI_y}{l^2}$$
$$P_\beta = \frac{GJA}{I_0} \qquad [4.38]$$

the above equation can be expressed as

$$\left(1-\frac{P}{4P_z}\right)^2\left(\frac{P_\beta}{P}-1\right)\left(\frac{P_y}{P}-1\right) = 0.1397\,\frac{a_0^2 A}{I_0} \qquad [4.39]$$

where it may be recalled that $P<P_z$ has been assumed.

This equation gives a critical torsional-flexural buckling load which according to Rayleigh's principle [14] is an upper bound on the true critical load associated with the exact mode shape. It can be expected that an assumed mode shape which is close to the true mode shape will yield an upper bound which is close to the true buckling load.

4.2.2 Verification of NASTRAN analysis

Now, in order to check the capability of the NASTRAN finite element program, and conversely the goodness of the above analysis, the bifurcation buckling analysis was performed on a computer model of the spine-like curved column of constant cross-section and homogeneous properties. The model consisted of approximately 23 straight beam elements to represent the sine-curved column. The amplitude of the curve was taken as $a_0/L = 0.0359$, where L is the curved length of the column. Using the discrete property values of the ligamentous spine as found in the literature and as discussed in Chapter 5, effective homogeneous bending and torsional properties were calculated according to the method used by Lucas and Bresler [73], and assigned to the elements of this column model. The bifurcation buckling load from NASTRAN was found to be 47.44 units of force while that obtained from the above analysis was 48.87 units. This means that the analytical result was 3.0% higher than the computer result. The mode shapes for w and β were also found to be in good agreement with their chosen functions Eq. (4.33) and (4.35) respectively. Hence it is concluded that the NASTRAN program is capable of handling torsional-flexural buckling problems correctly and conversely, the functions chosen for w and β are acceptable, and thus the above approximate analysis is a valid one.

4.2.3 Effect of the Curve Amplitude

Since a strong hypothesis as to the cause of AIS relates to the sagittal plane curvature of the spine, the characteristic equation resulting from the above analysis is now used to investigate the effect of the magnitude of the curve amplitude on the buckling load. A higher or lower buckling load would signify higher or lower stability.

If L is the curved length of the spine-like column, then the dependence of the axial length l on the curve amplitude a_0 may be expressed approximately by

$$l = L\left[1 - \left(\frac{\pi a_0}{L}\right)^2\right] \qquad [4.40]$$

provided $(\pi a_0 / L) << 1$. Therefore the buckling load P_y corresponding to pure lateral buckling of straight column of length l, Eq. (4.38) may be expressed as

$$P_y = \frac{\pi^2 EI_y}{L^2}\left[1 + \left(\frac{\pi a_0}{L}\right)^2\right] = P_{y_0}\left[1 + \left(\frac{\pi a_0}{L}\right)^2\right] \qquad [4.41]$$

where $P_{y0} = \pi^2 EI_y/L^2$ is the lateral buckling load of the column when $a_0 = 0$. Similarly, P_z, Eq. (4.17) may be expressed as

$$P_z = \frac{\pi^2 EI_z}{L^2}\left[1 + \left(\frac{\pi a_0}{L}\right)^2\right] = P_{z_0}\left[1 + \left(\frac{\pi a_0}{L}\right)^2\right] \qquad [4.42]$$

where $P_{z0} = \pi^2 EI_z/L^2$. As a_0 decreases, the column becomes straighter and P_y and P_z decrease. The smallest values of P_y and P_z are of course P_{y0} and P_{z0} respectively.

With these values of P_y and P_z, the characteristic equation determining the torsional-flexural buckling load can be written as

$$\left[1 - \frac{P\left(1 - \left(\frac{\pi a_0}{L}\right)^2\right)}{4 P_{z_0}}\right]^2 \left[\frac{P_\beta}{P} - 1\right]\left[\frac{P_{y_0}}{P}\left(1 + \left(\frac{\pi a_0}{L}\right)^2\right) - 1\right] = 0.1397\,\frac{a_0^2 A}{I_0} \qquad [4.43]$$

Since the right side of the above equation is positive, it follows that the smallest buckling load P_{cr} is less than both P_β or P_y. If P_β is much smaller than P_{y0} (i.e. a column weaker in torsion), then it can be inferred that P_{cr} will only be slightly smaller than P_β, and virtually unaffected by the magnitude of a_0/L. On the other hand, if P_{y0} is much smaller than P_β (i.e. a column weaker in lateral bending), then P_{cr} will be slightly smaller than $P_y = P_{y0}\,(1+\pi^2 a_0^2/L^2)$ with a_0/L playing a significant role. However, if $P_\beta \approx P_{y0}$, then there is a stronger interaction between torsional and lateral bending effects and P_{cr} is significantly different from P_β or P_y. Figure 4.4 illustrates these results by showing variation of P_{cr}/P_{y0} as a function of a_0/L for various $P_\beta/P_{y0} \geq 1$ ratios for a spine-like homogeneous column with $EI_z/EI_y = 2$ and $GJ/EI_y = 1.6$.

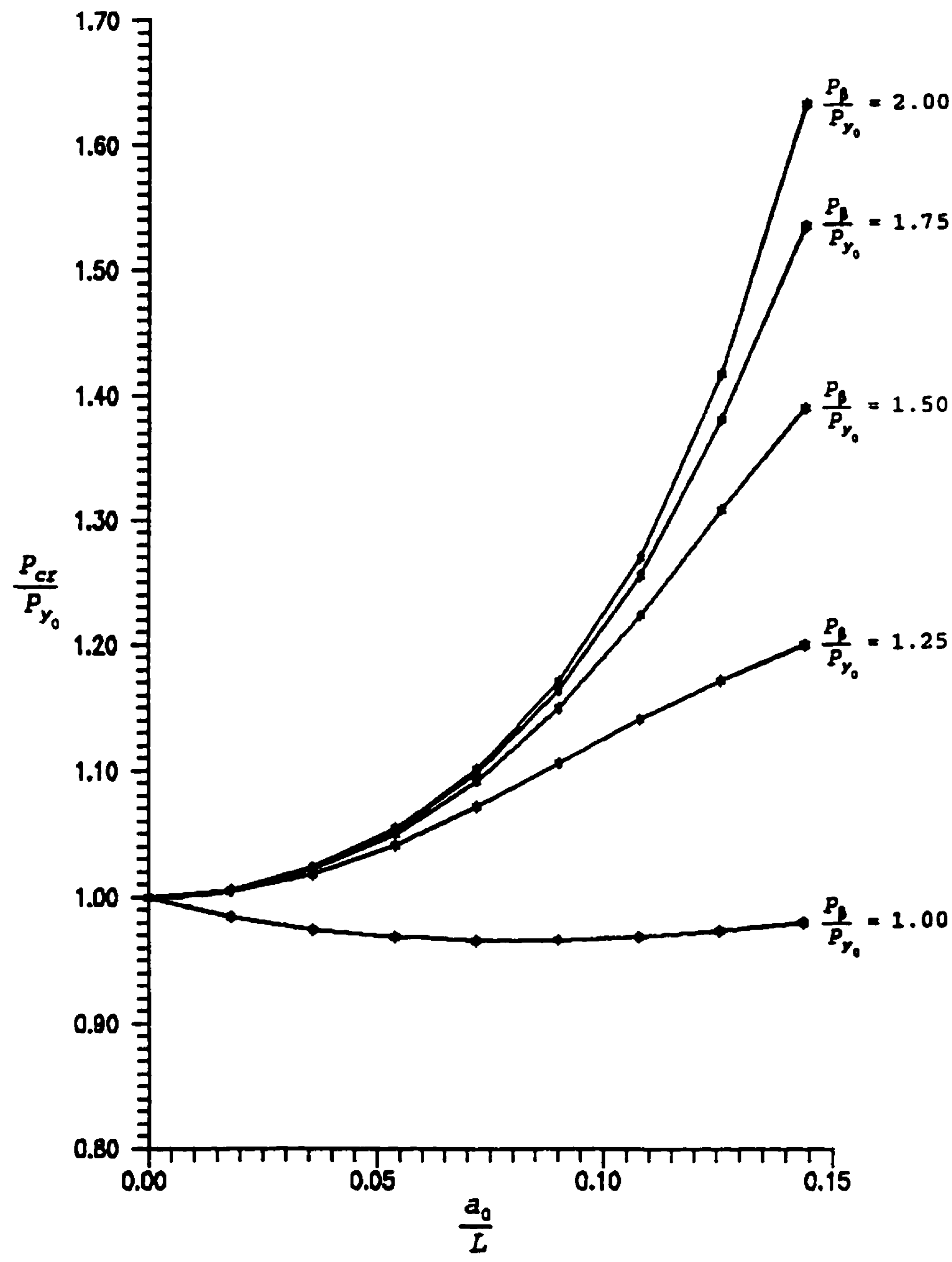

Fig. 4.4 Ratio of P_{cr}/P_{y_0} as a function a_0/L for a simply-supported spine-like column with fixed length, L, and initial sagittal curve, $y=a_0 \sin 2\pi x/l$. L = fixed curved length of column, a_0 = variable amplitude of curve, l = variable axial length of the column, P_{cr} = actual critical load, $P_\beta = GJA/I_0$ = pure torsional buckling load, $P_{y_0} = \pi^2 EI_y/L^2$ = flexural buckling load of the straight column in the lateral plane (i.e. with $a_0=0$).

The qualitative significance of the above analysis in the context of the lordosis hypothesis is that a reduction in the thoracic kyphosis of a real spine (with $P_g/P_{y0} >> 1$) will reduce its buckling load (thus making it less stable) and that the amount of reduction will be greater for spines with greater P_g/P_{y0} ratios.[1]

4.3 Effect of the Curvature and its Direction on Torsional-Flexural Buckling

In the above analyses, no account was taken of the curvature direction. Such an analysis would have required using the curved beam formulas and would have been complicated. However, the effect of curvature direction with regard to buckling may be understood by examining a simple case as follows.

Timoshenko [123] has analyzed the torsional-flexural buckling of a circular curved column of thin rectangular cross-section of radius of curvature R and curved length L, subjected to in-plane moment M_1 or M_2 as shown in Fig. 4.5. Again, EI_y represents the lateral (out-of-plane) flexural bending stiffness, and GJ the torsional stiffness. The arc length is approximated by $L = R\alpha$ for small α i.e. large R. The critical moment at which buckling occurs [123] is then

$$M_{cr_1} = \frac{EI_y + GJ}{2R} + \frac{\pi}{L}\sqrt{EI_y GJ} \qquad [4.44]$$

if the applied moment is in the same direction as the curvature (causing it to increase), Fig. 4.5(a), and is

$$M_{cr_2} = -\frac{EI_y + GJ}{2R} + \frac{\pi}{L}\sqrt{EI_y GJ} \qquad [4.45]$$

when it is applied in the opposite direction, Fig. 4.5(b). Thus, the stability is reduced when the applied moment acts to decrease the curvature. The reduction may be understood by noting that in the latter case, it is the longer fibres of the curved column which are subject to compression. Stated another way, in the former case, an increase in the curvature ($\downarrow R$) increases stability ($\uparrow M_{cr1}$), while in the latter, an increase in the curvature ($\downarrow R$) tends to decrease it ($\downarrow M_{cr2}$).

With reference to the real spine, the typical gravity loading is in the sense of forward flexion. Thus, according to the above formulas, the spine would be become less stable (i.e. more prone to buckling) as the thoracic kyphosis is reduced. This latter observation favours the lordosis hypothesis of AIS since it entails a reduction in the kyphotic curvature in the thoracic region of the spine.

---

[1]According to effective homogeneous properties of the spine, calculated as described in Section 4.2.2, $P_g/P_{y0} \approx 441$.

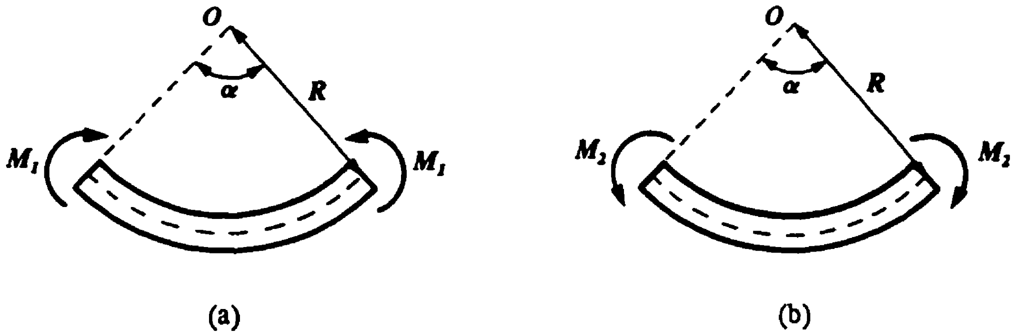

Fig. 4.5 Lateral buckling of a circular curved column subjected to pure moments.

4.4 Computer Simulation of Structural Behaviour of the Spine

One of the purposes of the foregoing analysis of simplified theoretical models was to present some basic concepts related to behaviour of slender structures under compressive loading. The real spine is too complex a structure to resemble the homogeneous theoretical column models. Therefore, no reliable quantitative information can be derived from the above type of analysis, although qualitatively, insight into the stability behaviour is gained from the explicit relations derived among the parameters of the models. A computer-aided numerical analysis of a suitable theoretical model is the only avenue available for a non-experimental quantitative investigation of the structural behaviour of the human spine.

The first requirement for any reliable biomechanical analysis of spine behaviour is that it must be based on a realistic modelling of the actual geometry and structural properties of the spine. However for a manageable model, a balance must be struck (depending on the purpose at hand) between which details to account for and which to ignore. In the present work, as will be subsequently seen, the spine with rib cage is modelled as a three-dimensional structure composed primarily of small straight beam elements of appropriate stiffness properties.

Structural stability analyses on the constructed models are performed using the MSC/NASTRAN finite element program. In the first instance, the model assumes the spine together with the loading to be perfectly symmetrical about the sagittal plane. The question is then asked at what load magnitude the spine will bifurcate into an out-of-plane (torsional-flexural) buckling mode. The answer to this question requires the program to perform the linear eigenvalue analysis, similar in principle to that done analytically in the preceding section for the homogeneous curved column.

The above bifurcation analysis indicates the load near which a realistic (slightly unsymmetric) spine would begin to experience lateral instability, and the mode shape in which initial buckling displacements and rotations would occur. Although helpful in establishing this load and the associate mode shape, this analysis provides no information on the actual amounts of displacements and rotations which the spine would experience as a function of the load.

To determine the buckling displacement and rotation magnitudes, one must perform the so-called post-buckling analysis. This is a geometric nonlinear analysis, and the simplest way to perform it is via an imperfection growth analysis. The spine model is assumed to be imperfect in that there is present, ab initio, a small geometrical asymmetry with respect to the sagittal plane, and is loaded in small load increments, taking into account the accumulated geometry changes at every increment. This type of analysis is similar in principle to that conducted for the imperfect (sine-shape) Euler column, Section 4.1.2. For small loads the effect of imperfection is small, meaning that the out-of-plane deformations remain small (and hence, in a sense, stable). However, as the load increases, the effect begins to grow in an accelerated nonlinear manner. Buckling is indicated when substantial (out-of-plane) geometry changes have occurred.

Nonlinear growth analyses performed on the models of this thesis are described in Chapters 5 and 6.

Chapter 5
Structural Modelling and Input Data

5.1 Description of Analyses

Stability analyses are performed on three-dimensional discrete parameter models of the human thoracolumbar spine and rib cage to determine if the hypothesis of the spinal lordosis as an initiating factor of the etiology of AIS is a valid one. The finite element analysis program MSC/NASTRAN (version 65C) is used to carry out the analyses. NASTRAN is run on the IBM/9000-230 mainframe computer at McGill University, using the MVS/XA operating system. Basically, two types of analyses are considered necessary for this study: linear buckling analyses and geometric nonlinear analyses.

Linear buckling analyses are performed to determine the bifurcation[1] (torsional-flexural) buckling loads of the symmetric spinal models under (a) compressive loading distributed along the column length, proportionately with the body weight distribution, and (b) a loading proportional to the resultant body weight acting at the center of gravity effectively lumped at the top of the spine (i.e. force and moment). Analyses are conducted on a model representing the typical normal spine, and also on one which has a slightly altered sagittal configuration by virtue of the introduction of a thoracic lordosis apical at T8. Bifurcation loads and corresponding mode shapes are compared in the hope of shedding some light on the lordosis hypothesis. This part of the investigation determines whether the lordotic spine model has a lower bifurcation load than the normal spine, i.e. less stable, as well as a mode shape similar to a scoliotic deformed configuration (convex-sided rotation),[2] to ultimately determine whether a lordotic configuration is more susceptible to scoliosis. Although mode shape deformations are indeterminate as to their amounts, they indicate the manner in which the spine deforms near the buckling load.

The second type of analyses, the geometric nonlinear analyses, comprise the heart of the study. They take into account large deformations[3], a category under which the scoliosis deformity

---

[1]Bifurcation here consists of a linear eigenvalue problem.

[2]Recall that the rotation is described in terms of the anterior portion of vertebrae. Convex-sided rotation implies anterior portion of vertebrae rotate towards the convexity of the lateral curve.

[3]By accounting of large deformations is meant the accumulated effects of the changing geometry of the model on its current behaviour.

falls. Here, they are used to simulate a possible instability of the spine, resulting in large deformations, by determining the growth of its initial geometry under increasing loading. Two distinct nonlinear growth analyses are carried out to test the lordosis hypothesis, which to reiterate, was stated by Dickson et al. [34] as a lordosis in combination with an asymmetry in another plane.

In the first growth analysis, the initial geometry is that of a spine which has the frontal and horizontal plane asymmetries (i.e. imperfections) of a normal spine, but which also has a lordosis in the thoracic region, in accordance with the hypothesis. Loading proportional to the resultant body weight acting at the center of gravity is applied as an equivalent force and moment at the top vertebra T1. As the load is increased incrementally, the spine changes its geometry, and it may be expected that as the total load nears the bifurcation buckling load of the linear analysis, the lateral imperfections would begin to grow significantly. The growth of the deformations achieved under the "full-load" are compared with a scoliotic configuration in order to test the hypothesis.

In the second growth analysis, the initial geometry is purely that of a normal spine, with the normal frontal and horizontal plane asymmetries, and the normal thoracic kyphosis and lumbar lordosis present. However, the loading consists of simulating the lordotic growth of the thoracic vertebra in addition to the body weight lumped at T1. The asymmetrical growth is simulated by thermal loading of the vertebra, by heating the elements positioned anterior to the thoracic vertebrae and by simultaneously cooling those positioned posterior to these vertebrae. The loading is increased until length changes in these elements correspond to those found in the thoracic vertebrae of a scoliotic patient, and gravity load equals a realistic value that restricts spine from elongation. The configuration of the gradually deformed spine under such loading is compared with that of a scoliotic spine.

5.2 Description of the Constructed Model

Discrete beam elements are used to construct the three-dimensional structural analysis model of the human thoracolumbar spine and rib cage. A large portion of time of this study was spent in modelling the geometry and structural properties. The aim is to construct a model representative of the normal spine and rib cage with particular attention focused on the sagittal curvature of the spine. With an alteration of this curvature being the basis of the hypothesis investigated in the present study, an accurate representation of a normal curvature is very important. Appendix C gives a full description of the model.

The complete thoracic and lumbar spine is modeled (from T1 to the top of the sacrum, inclusive). The spinal column, as mentioned earlier, is not uniform, and thus is modelled with 17 rigid elements representing vertebrae T1-L5, and 17 deformable elements representing intervertebral joints (composed of intervertebral discs, connecting ligaments, and posterior elements, e.g. facet joints) between T1 and sacrum.

The 10 superior pairs of ribs (ribs 1-10) are included in the model. The last 2 pairs, the floating ribs, are not modeled since they have virtually no structural relevance. Each rib is represented by 4 rigid elements for a total of 80 elements. The five nodes segmenting the rib, from the posterior to the anterior end, denote the head, tubercle, angle, midaxillary line junction, and costochondral joint of the rib [103,120]. At the costochondral joint, the rib attaches to costal cartilage (CC) represented by 1 or more elastic elements (36 elements in total) which attaches to the sternum represented by 18 rigid elements. Costovertebral joints (CV) and costotransverse joints (CT), which attach the posterior end of the ribs to the vertebral column, are included in the model. Deformable elements are used to represent the constraints imposed by the joints as well as the resistance to deformation provided by the connecting ligaments [4]. For each of the typical ribs, 2-9, 2 CV elements are used to model the connections between the head of the rib and the vertebra of its own number and the one above it. For ribs 1 and 10, only 1 CV element is used to model the costovertebral joint since they are only connected to their corresponding vertebra. In addition, for each rib, 1 CT element is used to represent the joint between its tubercle and the transverse process of the vertebra of the same number. There are 20 CT elements and 36 CV elements total. To provide points of attachment for the joints on the vertebrae, rigid elements stemming from the vertebral elements are modelled. Twenty rigid elements are used to model the transverse processes on vertebrae T1-T10 for articulation with the CT elements and 36 rigid elements are used to represent facets on posterior, lateral aspect of vertebral bodies T1-T10 for articulation with the CV elements. Midaxillary nodes on the ribs provide attachment points for the 18 IC elements representing the intercostal tissue which runs in between adjacent ribs.

All the elements in the model are represented with beam elements except the sternum, which is composed of 12 rigid quadrilateral plate elements along with 6 beam elements (included for programming compatibility between adjacent coplanar plate elements). As beam elements, they exhibit axial, shear, bending, and torsional stiffnesses with the exception of the IC and CV elements, which possess only axial stiffness.

The complete model is composed of 224 nodes, 288 beam elements, and 12 quadrilateral plate elements. An additional 26 beam elements and 22 nodes are required for applying loads at the centers of gravity of various body segments and slices about the inferior central node of the vertebrae (see Section 5.5). These loading elements are also useful in showing visually (by their displacement) the directions of axial rotation of vertebrae.

During graphical construction of the spinal column's sagittal curvature, it is helpful to use mean dimensions of the anterior, posterior, and central heights as well as the sagittal diameters of the vertebral bodies and discs. This results in a model representing each vertebra and each intervertebral joint with 3 elements; reflecting the anterior surface, the centerline, and the posterior surface of each vertebral body and each disc in the midsagittal plane. Rigid elements are used to connect the 3 elements transversely and provide them with continuity. Anatomically, these rigid elements represent the endplates found at the interface between the vertebra and intervertebral disc. This model with the 3-element representation, referred to as the 3-element model, represents the spinal column with 172 beam elements and an additional 70 nodes in comparison to the 1-element model, which uses 34 beam elements to represent the spine with central elements only.

Most of the analyses in this study are performed on the 1-element model. However, in addition to aiding in the construction of the sagittal curvature of the spine, the 3-element model is necessary to create the lordotic model from the normal one by increasing and decreasing the lengths on the anterior and posterior sides of the vertebrae, T4-T12, respectively. Likewise, the position of the anterior and posterior elements of vertebrae T4-T12 and the corresponding endplates are used in the nonlinear analysis for simulating lordotic growth of the spine.

Since there are 3-elements representing each vertebra and intervertebral joint, properties are assigned to the 3-elements such that together they have the equivalent stiffness of the element which they model. Equivalent sectional properties for the anterior and posterior elements and the central elements are calculated according to the formulas in Appendix B. Thus, theoretically, the 3-element model and the 1-element model are equivalent structures.

Although the geometry of the normal spine is almost symmetrical about the sagittal plane, it is necessary to model the complete three-dimensional structure for the buckling and geometric nonlinear analyses. A right-handed rectangular coordinate system, shown in Fig. 5.1, is chosen to globally define the structure such that the x-z plane defines the midsagittal plane, the x-y plane defines the transverse or horizontal plane, and the y-z plane defines the frontal plane.

5.3 Representation of Spine and Rib Cage Geometry

Constructing a model to represent a typical *normal* human thoracolumbar spine and rib cage is not an easy task. When dealing with the human body, modelling becomes very complex. Each structure is unique and there is tremendous variance of dimensions and properties from person to person. Anatomical studies related to the human spine reveal a large scatter of results making definition of *normal* very vague. Hence, *normal* characteristics can best be expressed using a range of values.

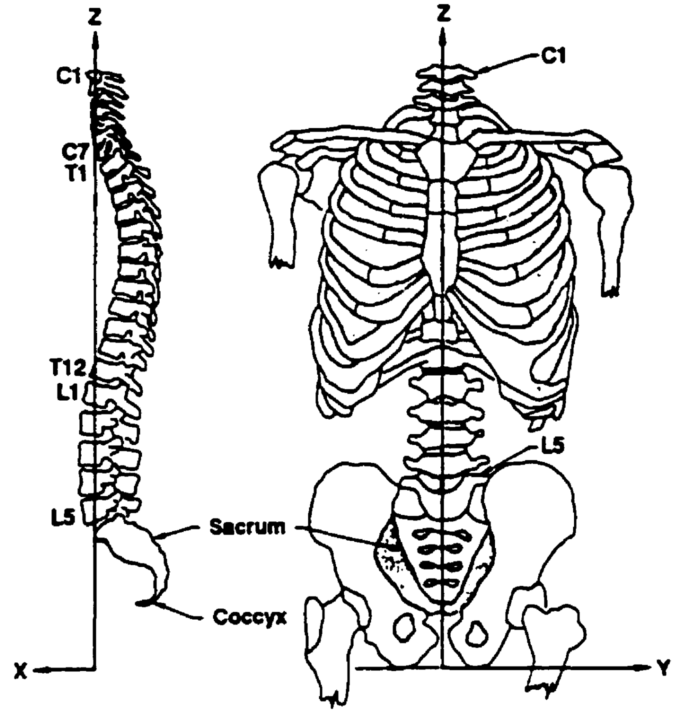

Fig. 5.1 Global coordinate system (a) left lateral view, and (b) anterior view. After Roberts and Chen [103].

The sagittal curvature, the critical parameter in the present investigation, can be described by the degree of kyphosis and lordosis and more accurately by the segmental sagittal angulations of the vertebrae[1] [12] and the reciprocal angulations[2] [16]. Segmental sagittal angulations and reciprocal angulations are important measurements because they reflect the intermediate changes in the curve. Two vastly different curves may have the same degree of kyphosis and lordosis [130]. The Cobb angle* measurement determines the angle between the endpoints or inflection points of the curve and does not determine the changes in the curve itself.

---

[1]Segmental sagittal angulations are angles measured between lines drawn parallel to the posterior aspect of the vertebral bodies [12].

[2]Reciprocal angulations are angles measured between lines drawn parallel to the endplates. The angulation between two vertebrae is measured between the inferior endplate of the inferior vertebra and the superior endplate of the superior vertebra.

Normal range of lumbar lordosis is accepted to be 20°-60° when measuring from the inferior face of T12 to the inferior face of L5 using the Cobb angle method. Normal thoracic kyphosis is 20°-50° when measuring from the top of T3 to the bottom of T12. It must be remembered that when specifying the degree of curvature, it is important to include the level and method of measurement to make valid comparisons [12].

A complete set of global coordinates describing the geometry of the thoracolumbar spine and rib cage was formulated and made available by Roberts and Chen [103]. However, no attempt was made by these authors to represent the *typical or normal* geometry. The data were obtained from direct measurement of a skeleton with a small frame. This fact makes the data seem advantageous; not only are the data consistent since they are obtained from the same person but they are based on a small frame, which is representative of the targeted population of AIS, the adolescent female. However, careful examination of the spinal column geometry reveals that the sagittal curvature is just outside the accepted "normal" range described above; a kyphosis of 52° is measured from the top of T3 to the bottom of T12. Also, the sagittal curvature does not reflect the spine found in anatomy books and other literature, which have many common characteristics among them. In addition, anterior and posterior disc and vertebrae heights, needed to alter the thoracic curvature, are not given. It was felt that this spine model could not be acceptable for the purposes of this study and that a new model must be constructed.

5.3.1 Normal Geometry

A new model, MOE, considered to be representative of the normal spinal column and rib cage is therefore developed by the present author. The spinal column is constructed graphically on the basis of anatomical data available in literature [15,60,107,116,119,124] and anatomical drawings [43,44,45,57].

Spinal Modelling

The mean measurements from an anthropometric study by Lanier [64], on the presacral vertebrae of 101 American white adult males, ages 40-50 years, are used to describe vertebrae geometry. The mean vertebral body anterior and posterior heights and superior and inferior sagittal diameters are used to draw the spinal sagittal configuration. Central heights are taken to be the average of the anterior and posterior heights. Intervertebral joint central heights are obtained from Schultz et al. [107] and the anterior heights, to some extent, from Todd and Pyle [124]. Vertebral height data presented by Todd and Pyle are used to check Lanier's values and make small adjustments when necessary. Comparison of the chosen data and the values used in the model are shown in Table 5.1. Discrepancies are due to strict adherence to the guidelines mentioned later.

Data on female vertebral dimensions were found in one study [114], but it did not contain a complete set of vertebra. Other studies [3,16,113] also giving an incomplete set of data were consulted and compared but were not used as guidelines. It was decided to use sources which provided a complete set of average vertebral data in the interest of reducing errors due to inconsistencies resulting from different measuring techniques, and from mixing data from different sample groups. Lanier's data [64], based on a large sample group (N = 101) and referenced by many researchers, for example Schultz et al. [107], were therefore chosen as the source for vertebral data.

The following criteria, found in the literature, appear to geometrically define the normal sagittal curvature of the spine. They were chosen to serve as guidelines in the construction of the spinal column model in the midsagittal plane:

(1) Mean segmental sagittal angulations of the normal thoracic and lumbar curves given by Bernhardt and Bridwell [12]. As mentioned before, these angulations are important parameters in describing a curve accurately.

(2) L1 as the intermediate vertebral body (IVB), i.e. the vertebra which is most tilted from the horizontal. Stagnara et al. [116] found one-third of all the cases studied to have L1 as the IVB.

(3) Apex of the kyphosis at T6-T7 disc. Apex of the lordosis at L3-L4 disc [12].

(4) Posterior aspect of T6 as approximately vertical [43,44,45,57].

(5) L1 as positioned directly vertical over the sacrum [15].

(6) Superior surface of the sacrum at 41° to the horizontal [116]. (Also found to be the averaged value from other sources [15,60]).

(7) Angulations of particular disc centerlines from the vertical [107] as:

T1-T2	16.5°	flexed
T12-L1	15.0°	extended
L5-S1	32.5°	flexed

(8) Normal kyphosis:

30°-50° with an average of 37° (top T4 - bottom IVB) [116].
20°-50° with an average of 36° (top T3 - bottom T12) [12].

Normal lordosis:

45°-70° with an average of 50° (bottom IVB -sacrum) [116].
20°-60° (female) with an average of 44° (bottom T12 - bottom L5) [12].

(9) Reciprocal angulations of thoracic and vertebral endplates according to Stagnara et al. [116].

Table 5.1 Comparison of Anatomical Measurements of Vertebrae and Discs with Model Values

Element: Alternating Vertebra & Disc	Anterior height (cm)		Central height (cm)		Posterior height (cm)		Avg. sag. radius, b (cm)	
	Lit.	MOE	Lit.	MOE	Lit.	MOE	Lit.	MOE
T1	1.62	1.63	1.68	1.68	1.73	1.73	0.854	0.853
Disc	0.44	0.44	0.45	0.45		0.46	0.866	0.887
T2	1.77	1.79	1.79	1.79	1.80	1.80	0.934	0.937
	0.31	0.32	0.31	0.31		0.31	0.987	0.994
T3	1.84	1.84	1.85	1.85	1.86	1.86	1.046	1.050
	0.27	0.27	0.27	0.27		0.27	1.104	1.106
T4	1.86 v	1.87	1.90	1.91	1.94 v	1.94	1.151	1.154
	0.21	0.21	0.22	0.22		0.24	1.197	1.200
T5	1.90	1.90	1.96	1.96	2.02	2.02	1.244	1.244
	0.25	0.23	0.26	0.25		0.27	1.291	1.289
T6	1.90	1.90	1.99	1.99	2.08	2.09	1.333	1.330
	0.30	0.30	0.32	0.32		0.34	1.376	1.376
T7	1.92 v	1.90	2.02	2.02	2.11 v	2.14	1.416	1.417
	0.38	0.38	0.40	0.40		0.42	1.452	1.454
T8	1.97	1.98	2.07	2.07	2.18	2.17	1.489	1.490
	0.43	0.43	0.45	0.44		0.45	1.518	1.516
T9	2.06	2.07	2.14	2.13	2.23	2.20	1.529	1.527
	0.45	0.45	0.47	0.47		0.49	1.537	1.540
T10	2.23	2.24	2.30	2.30	2.37	2.37	1.554	1.554
	0.49	0.50	0.51	0.51		0.51	1.572	1.573
T11	2.29	2.30	2.43	2.43	2.56	2.56	1.589	1.593
	0.66 d	0.72	0.68	0.68		0.65	1.611	1.611
T12	2.43	2.44	2.57	2.57	2.71	2.71	1.614	1.615
	0.92 d	0.93	0.84	0.84		0.76	1.624	1.630
L1	2.64 v	2.64	2.72	2.72	2.80 v	2.80	1.647	1.655
	0.97	1.18	1.00	1.01		0.83	1.668	1.676
L2	2.77 v	2.77	2.79	2.79	2.81 v	2.81	1.684	1.690
	1.13	1.41	1.14	1.15		0.88	1.708	1.710
L3	2.85 v	2.85	2.80	2.80	2.75 v	2.75	1.725	1.729
	1.52 d	1.51	1.22	1.22		0.93	1.736	1.742
L4	2.81	2.82	2.74	2.75	2.68	2.68	1.766	1.766
	1.48	1.79	1.40	1.40		1.02	1.781	1.778
L5	2.89	2.90	2.65	2.65	2.41	2.41	1.757	1.756
	1.87 d	2.00	1.57	1.57		1.14	1.734	1.733

- Vertebral heights are from Lanier [64]. Central heights [107] are taken to be the average of anterior and posterior heights. v = adjustments made using data from Todd & Pyle [124].
- Anterior disc heights are taken from Todd & Pyle [124]. d = adjustments made using segmental sagittal angulation data [12]. Central disc heights are from Schultz et al. [107], which are based on Todd & Pyle [124] values.
- Sagittal radius of vertebra = average of superior and inferior vertebra sagittal radii [64].
- Sagittal radius of disc = average of inferior sagittal radius of superior vertebra and superior sagittal radius of inferior vertebra [64].

In an effort to keep within the set guidelines, MOE satisfies criteria 2-6 above and its comparison with the other criteria is as follows:

- Segmental sagittal angulations of MOE are in good agreement with the established means, as shown in Fig. 5.2.
- Reciprocal angulations of the present model spine, shown in Table 5.2, are found to be close to the means established by Stagnara et al. [116]. Additionally, lumbar curvature is within the range for females established by Sullivan and Miles [119].
- Angulations of the particular discs from the vertical are as follows:

T1-T2	16.8° flexed	(0.3° diff.)
T12-L1	18.0° extended	(3.0° diff.)
L5-S1	32.8° flexed	(0.3° diff.)

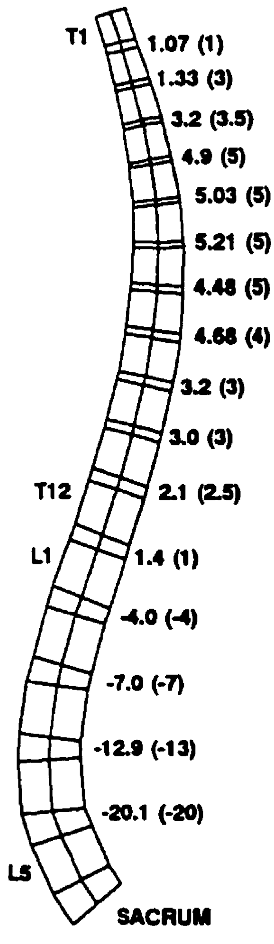

Fig. 5.2 Mean segmental sagittal angulations of MOE compared with normal values [12] shown in parentheses.

Table 5.2 Reciprocal Angulations of MOE in Comparison to Means (Degrees)

	S	L5	L4	L3	L2	L1	T12	T11	T10	T9	T8	T7	T6	T5	T4
S	0 (0)														
L5	-22 (-21)	-8 (-8)													
L4	-37 (36)	-23 (-23)	-2 (-1)												
L3	-48 (-47)	-34 (-33)	-13 (-12)	-2 (1)											
L2	-56 (-54)	-42 (-40)	-21 (-19)	-10 (-6)	1 (2)*										
L1	-60 (-56)	-46 (-42)	-25 (-21)	-14 (-8)	-3 (0)	3 (4)*									
T12	-58 (-55)	-44 (-41)	-23 (-20)	-12 (-7)	-1 (1)	5 (5)	5 (5)								
T11	-55 (-53)	-41 (-39)	-20 (-18)	-9 (-5)	2 (3)	8 (7)	8 (7)	5 (4)*							
T10	-53 (-51)	-39 (-37)	-18 (-16)	-7 (-3)	4 (5)	10 (9)	10 (9)	7 (6)	2 (3)						
T9	-49 (-48)	-35 (-35)	-14 (-13)	-3 (0)	8 (8)	14 (12)	14 (11)	11 (9)	6 (6)	3 (4)					
T8	-45 (-44)	-31 (-31)	-10 (-9)	1 (4)	12 (12)	18 (16)	18 (15)	15 (13)	10 (10)	7 (8)	4 (4)				
T7	-40 (-39)	-26 (-26)*	-5 (-4)	6 (9)	17 (17)	23 (21)	23 (21)	20 (18)	15 (15)	12 (13)	9 (9)*	5 (5)			
T6	-35 (-33)	-21 (-20)	0 (2)	11 (15)	22 (23)	28 (27)	28 (26)	25 (24)	20 (21)	17 (19)	14 (15)	10 (11)	4 (4)		
T5	-31 (-28)	-17 (-15)*	4 (7)	15 (20)	26 (28)	32 (32)	32 (32)	29 (29)	24 (26)	21 (24)	18 (21)	14 (16)	8 (9)*	3 (4)	
T4	-29 (-23)	-15 (-10)	6 (12)	17 (25)	28 (33)	34 (37)	34 (36)	31 (34)	26 (31)	23 (29)	20 (25)	16 (21)	10 (14)	5 (9)	3 (4)

Values in parentheses are means based on observation of 100 adults [116]. Positive values indicate kyphosis, negative values indicate lordosis. An asterisk indicates adjustment of one degree believed to be due to typographic error in the data of [116].

- A thoracic kyphosis of 35° is measured using both levels of measurement mentioned above in criteria #8. This constitutes a 5% difference from the mean calculated by Stagnara et al. [116] and only a 2.8% difference from the mean calculated by Bernhardt and Bridwell [12].
- A lumbar lordosis of 63° is measured from the bottom of IVB to S1. This is a 26% difference from the mean calculated by Stagnara et al. [116]. A lordosis of 49° is measured from the bottom of T12 to the bottom of L5, only an 11% difference from the results from Bernhardt and Bridwell [12].

Therefore, in conclusion, the spinal column represented by MOE is acceptable as normal.

Rib Cage Modelling

The main purpose of including the rib cage is to model the stiffness it contributes to the thoracic spine. Results from past modelling [4] show that the rib cage increases the stability of the spine by 300% on average (Table 3.1). Rather limited information is available on rib cage geometry [27,85,102,108,133]. An attempt was made to construct the rib cage using the data on rib geometry from Schultz et al. [108] and Grant's Atlas of Anatomy [43] for rib orientation and positioning. The result was unsatisfactory, and as a solution, the rib cage (ribs, costal cartilage, and sternum) geometry measured by Roberts and Chen [103] is attached to the constructed spine of model MOE. This is considered acceptable because although the dimensions are taken from a person with a smaller than average height, the spinal column of MOE is only 7.9% larger than the Roberts and Chen [103] column. The column of MOE is straighter as indicated in Table 5.3, and for this reason gives the appearance of being taller or larger. Thus, it seems reasonable to attach the rib cage of Roberts and Chen to the MOE spine model.

Table 5.3 Comparison of Column Lengths

	Roberts & Chen model [103]	Present model MOE	% Difference
Axial length, l (cm)	42.67	48.21	13
Curved length i.e. sum of central heights, L (cm)	46.27	49.93	7.9

In addition, Roberts and Chen's rib cage compares well with the mean dimensions from the average population [22], and those found in Grant's Method of Anatomy [44], as shown in Table 5.4. Examination of the author's own x-rays (chest depth Rib 7 to T9 = 13.97 cm) further instills the belief that Roberts and Chen have a good representation of the rib cage. The rib cage dimensions of MOE are also included in the table. Any discrepancies between the rib cage dimensions of MOE and from Roberts and Chen model are due to adjustments necessary for achieving compatibility between the rib cage from Roberts and Chen and the spine of MOE.

The position of the nodes representing the facets on the transverse processes, which connect to the tubercles of the ribs by means of costotransverse joints (CT), are taken from Schultz et al. [109]. The tubercle of the rib is determined by the position of the facet on the transverse process, as shown in Fig. 5.3. For ease in computer input and in calculations, CT elements are chosen to be 0.1 cm in length. The position of the node representing the tubercle is defined 0.1 cm lateral to the node on the transverse process. This constitutes a good anatomical representation.

Table 5.4 Comparison of Rib Cage Dimensions of Models with Mean Measurements

Item	Mean measurements (cm) and their source	Dimensions of Roberts and Chen model [103], (cm)	Dimensions of MOE, (cm)
Chest depth: (clear distance)			
Sternum @ Rib 1 to T3	5 [44]	9.45	8.20
Sternum @ Rib 2 to T5	≈10 (g) [44]	11.30	10.15
Sternum @ Rib 7 to T9	21.59 & 13 (g)[a] [44]	13.70	13.30
Largest rib cage depth	21.06 [22]	21.08	20.73
Largest rib cage breadth	29.99 [22]	24.79	24.79
Sternum body length:			
Rib 1 - Rib 2	5[b] [44]	3.42	3.40
Rib 2 - Rib 7	10+ [44]	11.45	11.43
Full height	20.33 [22]	13.97[c]	13.95[c]

g = graphically measured from [44]
a = discrepancy between graphically measured and printed values [44]
b = measurement includes section of sternum above Rib 1, not accounted for in MOE, with a length determined graphically = 2.7 cm (g)
c = measurement does not include xiphoid process (section of sternum below Rib 7) and section above Rib 1 again, with graphic adjustment = 19.87 (g)

The head of the typical rib is defined by the position of the facets on the vertebral bodies. As mentioned in Chapter 2 (Section 2.3), the superior facet on the vertebra corresponding to the rib of its own number, and the inferior facet on the superior vertebra articulate with the head of the rib by means of costovertebral joints (CV). As shown in Fig. 5.4, for each rib, the 2 nodes representing the vertebral facets which attach to the rib, are positioned in the y-direction (lateral) at the maximum inferior transverse radius of the superior vertebra, which is taken from Lanier [64]. In the x-direction (anterior-posterior), the coordinate of the vertebral facet is taken to be the average of the x-coordinates of the superior posterior node of the vertebra corresponding to its rib number and of the inferior posterior node of the superior vertebra. In the z-direction (vertical), their position is taken to be the average of the z-coordinates of the same 2 nodes ±0.1 cm. Thus, the head of the rib may be positioned in between the 2 nodes representing the vertebral body facets, which are given the same x and y coordinates as described above, so that all CV elements also have lengths of 0.1 cm.

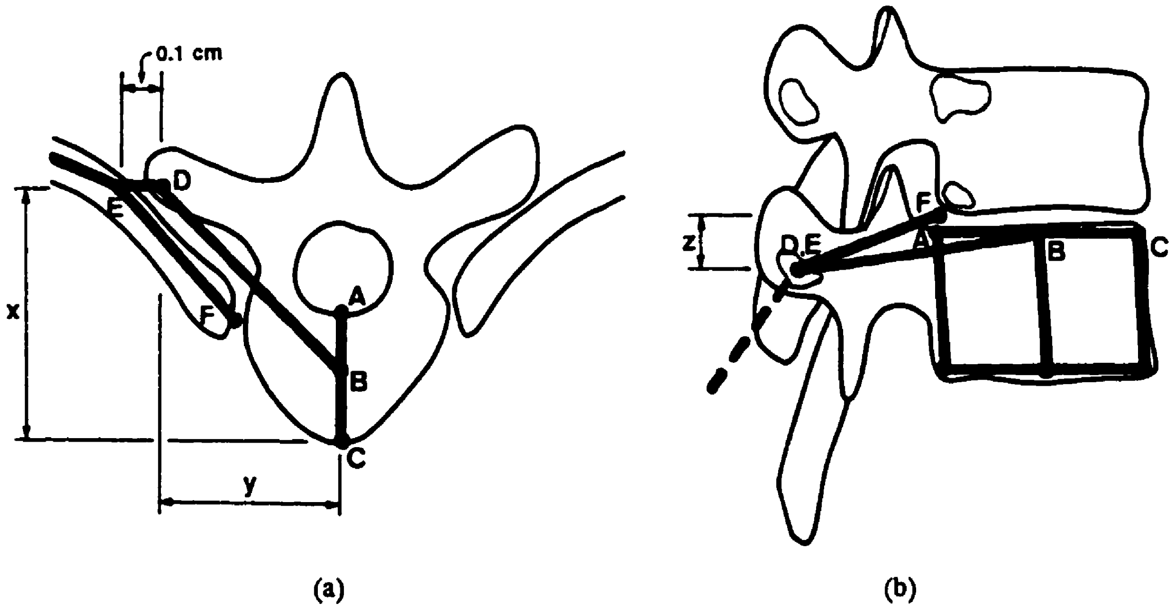

Fig. 5.3 Costotransverse joint: connection of the transverse process (vertebra) to the tubercle of the rib (a) top view, and (b) right lateral view. Values of x, y, and z for vertebrae T1 - T10 are obtained from Schultz et al. [109]. The node and element representation is as follows:

Node/ Element	Representation
A	superior, posterior node of vertebra in sagittal plane
B	superior, central node of vertebra in sagittal plane
C	superior, anterior node of vertebra in sagittal plane
D	facet on transverse process
E	tubercle of rib
F	head of rib
AB	posterior half of superior endplate of vertebra
BC	anterior half of superior endplate of vertebra
BD	transverse process
DE	CT joint
EF	rib (tubercle to head)

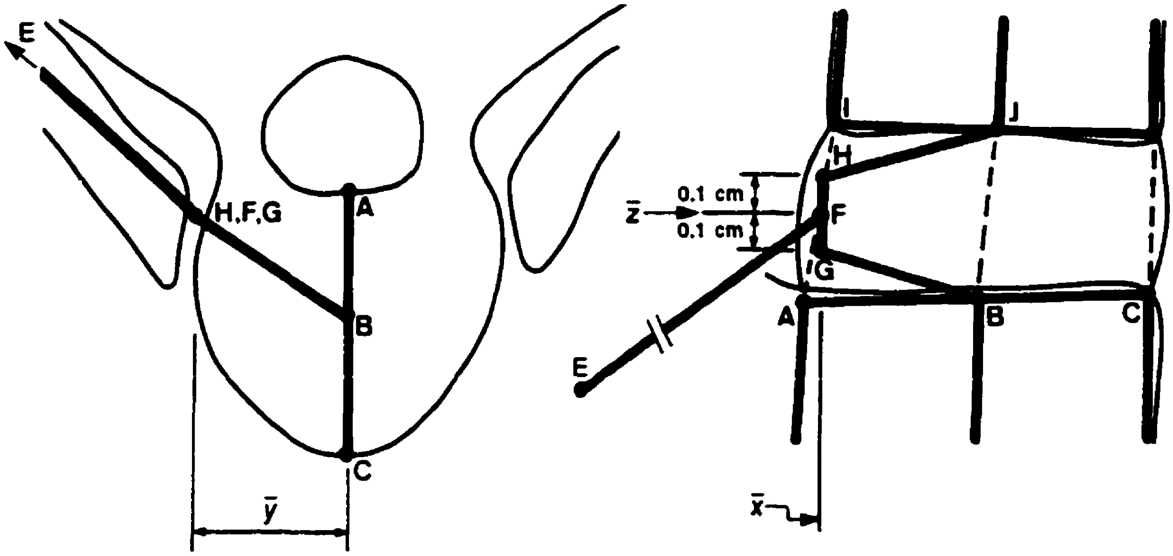

(a) (b)

Fig. 5.4 Costovertebral joint: connection of the vertebral bodies to the head of the rib (a) top view, and (b) right lateral view. Values of $\bar{y}$ are equal to the maximum inferior transverse radii of the superior vertebra of rib attachment obtained by Lanier [64], $\bar{x}$ and $\bar{z}$ = average x- and z- coordinates of nodes A and I. The node and element representation is as follows:

Node/ Element	Representation
A	superior, posterior node of vertebra in sagittal plane
B	superior, central node of vertebra in sagittal plane
C	superior, anterior node of vertebra in sagittal plane
E	tubercle of rib
F	head of rib
G	facet on vertebra corresponding to rib
H	facet on superior vertebra
I	inferior, posterior node of superior vertebra in sagittal plane
J	inferior, central node of superior vertebra in sagittal plane
AB	posterior half of superior endplate of vertebra
BC	anterior half of superior endplate of vertebra
BG	vertebrae (superior central node to facet)
EF	rib (tubercle to head)
FG	CV joint (attach rib to corresponding vertebrae)
FH	CV joint (attach rib to superior vertebrae)
HJ	superior vertebrae (inferior central node to facet)
IJ	posterior half of inferior endplate of superior vertebra

The model, MOE, representing the normal spine and rib cage is shown in Fig. 5.5. The global nodal coordinates defining its geometry are tabulated in Table 5.5. Appendix C offers a complete description of the model with all node and element numbers illustrated.

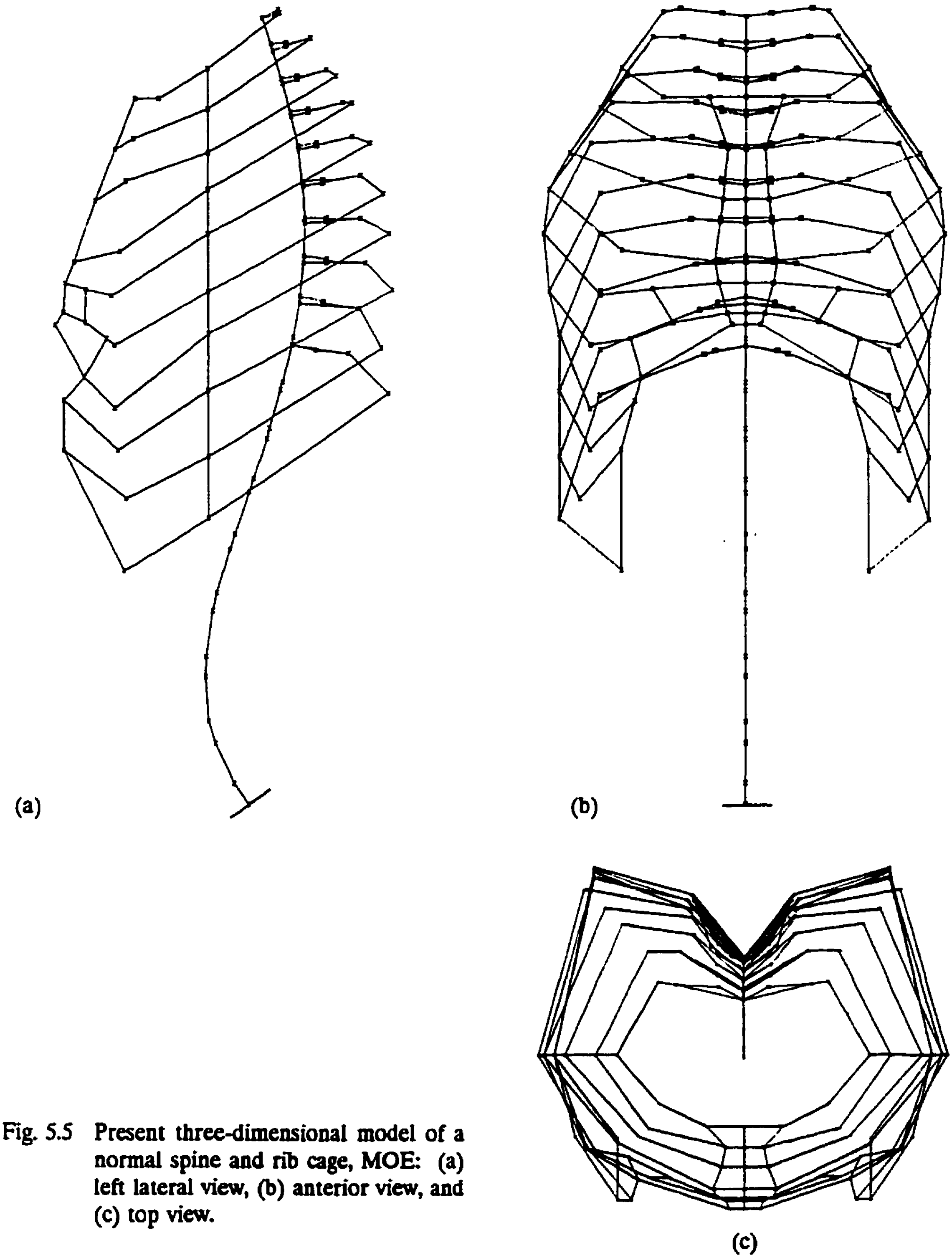

Fig. 5.5 Present three-dimensional model of a normal spine and rib cage, MOE: (a) left lateral view, (b) anterior view, and (c) top view.

Table 5.5 Global Nodal Coordinates of Normal Spine and Rib Cage Model: MOE

Node no.	Coordinates			Node no.	Coordinates			Node no.	Coordinates		
	X	Y	Z		X	Y	Z		X	Y	Z
1	-0.42	0.00	47.36	56	0.04	0.00	24.86	111	-3.23	1.55	41.73
2	-0.93	0.00	45.76	57	0.72	0.00	22.66	112	-3.23	1.55	41.53
3	-1.06	0.00	45.33	58	0.94	0.00	21.98	113	-3.79	1.52	39.61
4	-1.56	0.00	43.61	59	1.68	0.00	19.66	114	-3.79	1.52	39.41
5	-1.64	0.00	43.31	60	2.00	0.00	18.79	115	-4.17	1.55	37.37
6	-2.12	0.00	41.53	61	2.91	0.00	16.31	116	-4.17	1.55	37.17
7	-2.18	0.00	41.26	62	3.32	0.00	15.20	117	-4.38	1.59	34.98
8	-2.59	0.00	39.40	63	4.07	0.00	12.53	118	-4.38	1.59	34.78
9	-2.62	0.00	39.18	64	4.45	0.00	11.17	119	-4.38	1.67	32.46
10	-2.88	0.00	37.24	65	4.87	0.00	8.35	120	-4.38	1.67	32.26
11	-2.90	0.00	36.99	66	4.96	0.00	6.84	121	-4.17	1.76	29.87
12	-3.00	0.00	35.00	67	4.79	0.00	4.03	122	-4.17	1.76	29.67
13	-3.01	0.00	34.68	68	4.27	0.00	2.32	123	-3.67	1.87	26.89
14	-2.94	0.00	32.66	69	3.01	0.00	-0.29	124	-1.21	-1.45	47.59
15	-2.92	0.00	32.26	70	1.92	0.00	-1.97	125	-1.86	-1.58	45.84
16	-2.69	0.00	30.20	71	-1.21	0.00	47.59	126	-1.86	-1.58	45.64
17	-2.65	0.00	29.76	72	-1.79	0.00	45.96	127	-2.57	-1.61	43.78
18	-2.27	0.00	27.66	73	-1.93	0.00	45.52	128	-2.57	-1.61	43.58
19	-2.16	0.00	27.20	74	-2.52	0.00	43.82	129	-3.23	-1.55	41.73
20	-1.62	0.00	24.96	75	-2.62	0.00	43.53	130	-3.23	-1.55	41.53
21	-1.49	0.00	24.47	76	-3.19	0.00	41.76	131	-3.79	-1.52	39.61
22	-0.80	0.00	22.14	77	-3.27	0.00	41.50	132	-3.79	-1.52	39.41
23	-0.60	0.00	21.49	78	-3.76	0.00	39.62	133	-4.17	-1.55	37.37
24	0.19	0.00	19.04	79	-3.81	0.00	39.39	134	-4.17	-1.55	37.17
25	0.45	0.00	18.24	80	-4.15	0.00	37.40	135	-4.38	-1.59	34.98
26	1.37	0.00	15.68	81	-4.19	0.00	37.13	136	-4.38	-1.59	34.78
27	1.70	0.00	14.73	82	-4.36	0.00	35.05	137	-4.38	-1.67	32.46
28	2.45	0.00	12.04	83	-4.40	0.00	34.71	138	-4.38	-1.67	32.26
29	2.74	0.00	10.93	84	-4.38	0.00	32.57	139	-4.17	-1.76	29.87
30	3.15	0.00	8.16	85	-4.38	0.00	32.15	140	-4.17	-1.76	29.67
31	3.21	0.00	6.94	86	-4.19	0.00	29.99	141	-3.67	-1.87	26.89
32	3.02	0.00	4.20	87	-4.15	0.00	29.54	142	-1.38	4.00	47.90
33	2.58	0.00	2.87	88	-3.78	0.00	27.37	143	-3.39	3.81	46.14
34	1.45	0.00	0.47	89	-3.67	0.00	26.89	144	-4.40	3.00	44.15
35	0.60	0.00	-0.85	90	-3.14	0.00	24.58	145	-5.44	3.01	42.13
36	0.37	0.00	47.13	91	-3.02	0.00	24.08	146	-6.00	3.30	39.98
37	-0.07	0.00	45.56	92	-2.32	0.00	21.62	147	-6.50	3.33	37.57
38	-0.19	0.00	45.14	93	-2.14	0.00	21.00	148	-6.50	3.30	34.95
39	-0.60	0.00	43.40	94	-1.30	0.00	18.42	149	-6.83	3.02	32.20
40	-0.66	0.00	43.09	95	-1.10	0.00	17.69	150	-6.40	2.80	29.40
41	-1.05	0.00	41.29	96	-0.17	0.00	15.05	151	-5.75	2.53	26.70
42	-1.09	0.00	41.02	97	0.08	0.00	14.26	152	-1.38	-4.00	47.90
43	-1.42	0.00	39.18	98	0.83	0.00	11.55	153	-3.39	-3.81	46.14
44	-1.43	0.00	38.97	99	1.03	0.00	10.69	154	-4.40	-3.00	44.15
45	-1.61	0.00	37.08	100	1.43	0.00	7.97	155	-5.44	-3.01	42.13
46	-1.61	0.00	36.85	101	1.46	0.00	7.04	156	-6.00	-3.30	39.98
47	-1.64	0.00	34.95	102	1.25	0.00	4.37	157	-6.50	-3.33	37.57
48	-1.62	0.00	34.65	103	0.89	0.00	3.42	158	-6.50	-3.30	34.95
49	-1.50	0.00	32.75	104	-0.11	0.00	1.23	159	-6.83	-3.02	32.20
50	-1.46	0.00	32.37	105	-0.72	0.00	0.27	160	-6.40	-2.80	29.40
51	-1.19	0.00	30.41	106	-1.21	1.45	47.59	161	-5.75	-2.53	26.70
52	-1.15	0.00	29.98	107	-1.86	1.58	45.84	162	-1.21	1.55	47.59
53	-0.76	0.00	27.95	108	-1.86	1.58	45.64	163	-1.38	4.10	47.90
54	-0.65	0.00	27.51	109	-2.57	1.61	43.78	164	-1.50	5.08	47.67
55	-0.10	0.00	25.34	110	-2.57	1.61	43.58	165	3.00	7.62	44.23

Table 5.5 Global Nodal Coordinates Cont'd

Node no.	Coordinates			Node no.	Coordinates			Node no.	Coordinates		
	X	Y	Z		X	Y	Z		X	Y	Z
166	6.00	5.08	42.45	221	11.88	0.00	31.03	276	3.00	11.43	20.40
167	7.50	2.29	42.45	222	11.88	-1.65	31.03	277	8.10	10.16	17.84
168	7.50	0.00	42.45	223	10.56	-5.72	30.67	278	11.95	7.62	20.85
169	7.50	-2.29	42.45	224	9.00	-8.89	30.27	279	11.95	-7.62	20.85
170	6.00	-5.08	42.45	225	3.00	-12.40	34.03	280	8.10	-10.16	17.84
171	3.00	-7.62	44.23	226	-7.12	-9.53	39.58	281	3.00	-11.43	20.40
172	-1.50	-5.08	47.67	227	-6.00	-3.40	39.98	282	-7.76	-8.89	26.97
173	-1.38	-4.10	47.90	228	-3.79	-1.52	39.51	283	-6.40	-2.90	29.40
174	-1.21	-1.55	47.59	229	-4.17	1.55	37.27	284	-4.17	-1.76	29.77
175	-1.86	1.58	45.74	230	-6.50	3.43	37.57	285	-3.67	1.97	26.89
176	-3.39	3.91	46.14	231	-7.92	8.89	36.45	286	-5.75	2.63	26.70
177	-3.40	5.72	46.10	232	3.00	12.07	30.48	287	-8.20	8.89	24.20
178	3.00	8.89	41.75	233	8.83	9.53	27.24	288	3.00	11.43	16.65
179	7.60	5.72	39.90	234	9.30	6.99	27.64	289	8.20	7.62	13.42
180	8.73	1.14	39.28	235	10.60	4.45	28.64	290	8.20	-7.62	13.42
181	8.73	0.00	39.28	236	12.00	1.14	29.22	291	3.00	-11.43	16.65
182	8.73	-1.14	39.28	237	12.00	0.00	29.22	292	-8.20	-8.89	24.20
183	7.60	-5.72	39.90	238	12.00	-1.14	29.22	293	-5.75	-2.63	26.70
184	3.00	-8.89	41.75	239	10.60	-4.45	28.64	294	-3.67	-1.97	26.89
185	-3.40	-5.72	46.10	240	9.30	-6.99	27.64	500	-3.23	0.00	50.26
186	-3.39	-3.91	46.14	241	8.83	-9.53	27.24	501	-2.44	0.00	46.56
187	-1.86	-1.58	45.74	242	3.00	-12.07	30.48	502	-2.02	0.00	44.69
188	-2.57	1.61	43.68	243	-7.92	-8.89	36.45	503	-1.06	0.00	42.57
189	-4.40	3.10	44.15	244	-6.50	-3.43	37.57	504	-0.89	0.00	40.46
190	-5.00	7.24	43.78	245	-4.17	-1.55	37.27	505	-0.40	0.00	38.32
191	3.00	10.80	39.00	246	-4.38	1.59	34.88	506	0.59	0.00	36.12
192	8.05	6.35	37.34	247	-6.50	3.40	34.95	507	1.08	0.00	33.83
193	9.95	1.40	36.12	248	-8.30	8.89	34.00	508	1.50	0.00	31.43
194	9.95	0.00	36.12	249	3.00	11.43	27.88	509	2.06	0.00	28.93
195	9.95	-1.40	36.12	250	8.80	9.53	23.37	510	3.29	0.00	26.31
196	8.05	-6.35	37.34	251	10.65	6.35	25.30	511	4.42	0.00	23.55
197	3.00	-10.80	39.00	252	12.53	0.89	28.50	512	5.28	0.00	20.59
198	-5.00	-7.24	43.78	253	12.53	0.00	28.50	513	6.28	0.00	17.36
199	-4.40	-3.10	44.15	254	12.53	-0.89	28.50	514	6.88	0.00	13.86
200	-2.57	-1.61	43.68	255	10.65	-6.35	25.30	515	7.12	0.00	10.10
201	-3.23	1.55	41.63	256	8.80	-9.53	23.37	516	6.60	0.00	6.18
202	-5.44	3.11	42.13	257	3.00	-11.43	27.88	517	4.91	0.00	2.34
203	-6.00	8.26	42.08	258	-8.30	-8.89	34.00	518	4.25	0.00	-0.19
204	3.00	12.07	36.75	259	-6.50	-3.40	34.95	519	1.95	0.00	63.54
205	8.45	7.62	33.00	260	-4.38	-1.59	34.88	520	0.71	17.18	15.76
206	11.30	1.91	32.36	261	-4.38	1.67	32.36	521	0.71	-17.18	15.76
207	11.30	0.00	32.36	262	-6.83	3.12	32.20				
208	11.30	-1.91	32.36	263	-8.44	8.89	30.52				
209	8.45	-7.62	33.00	264	3.00	11.43	24.44				
210	3.00	-12.07	36.75	265	8.60	9.53	20.83				
211	-6.00	-8.26	42.08	266	11.95	6.73	23.88				
212	-5.44	-3.11	42.13	267	11.95	-6.73	23.88				
213	-3.23	-1.55	41.63	268	8.60	-9.53	20.83				
214	-3.79	1.52	39.51	269	3.00	-11.43	24.44				
215	-6.00	3.40	39.98	270	-8.44	-8.89	30.52				
216	-7.12	9.53	39.58	271	-6.83	-3.12	32.20				
217	3.00	12.40	34.03	272	-4.38	-1.67	32.36				
218	9.00	8.89	30.27	273	-4.17	1.76	29.77				
219	10.56	5.72	30.67	274	-6.40	2.90	29.40				
220	11.88	1.65	31.03	275	-7.76	8.89	26.97				

5.3.2 Lordotic Geometry

The lordotic model, LARRY, is created from MOE by altering its sagittal curvature. Using the structurally equivalent 3-element model, the central elements are kept of the same length while the anterior and posterior elements of the vertebrae T4-T12 are elongated and shortened respectively as indicated in Table 5.6, such that vertebrae T6 through T10 become lordotic. The amount of elongation and shortening is based on the measurements of lordotic vertebrae from a real scoliotic spine [30]. The ratios of the anterior and posterior lengths of the scoliotic vertebrae T4-T12 are used to calculate these lengths for the lordotic vertebrae of the present model, relative to their center lengths which are considered to remain unchanged and which are the averages of the anterior and posterior lengths. The procedure is accomplished by running a static structural analysis of MOE using the DEFORM[1] command available in NASTRAN. This command allows elements to be deformed axially. Constraints are placed on the structure so that the sagittal curvature is the main parameter altered. The analysis yields a structure with a lordosis in the thoracic region of the spine with an apex at T8, as shown in Fig. 5.6. This region is chosen specifically because, as mentioned previously, a very common form of AIS has an apex at the T8-T9 level, with lordosis present at the apex and at one or two levels above and below the apex [24,34]. The lordotic model thus created is used to study the effect of thoracic lordosis on subsequent spinal stability.

Table 5.6 Changes in Anterior and Posterior Lengths of Vertebrae

Vert.	Scoliotic specimen [30]	Normal lengths (cm)			Lordotic lengths (cm)		Change in length, (cm)		
	Ant./Post.	Post.	Central	Ant.	Post.	Ant.	Post.	Ant.	Average (±cm)
T4	0.966	1.943	1.905	1.869	1.938	1.872	-0.005	0.003	0.004
T5	0.989	2.019	1.957	1.899	1.968	1.946	-0.051	0.047	0.049
T6	1.103	2.087	1.993	1.900	1.895	2.090	-0.192	0.190	0.191
T7	1.480	2.140	2.021	1.904	1.630	2.412	-0.510	0.508	0.509
T8	1.304	2.168	2.073	1.979	1.800	2.347	-0.368	0.368	0.368
T9	1.443	2.201	2.134	2.067	1.747	2.521	-0.454	0.454	0.454
T10	1.227	2.370	2.304	2.239	2.069	2.539	-0.301	0.300	0.300
T11	0.959	2.558	2.430	2.303	2.481	2.379	-0.077	0.076	0.077
T12	0.912	2.713	2.574	2.435	2.693	2.456	-0.020	0.021	0.021

[1]The deform command may be used to load a structure by enforced specified axial deformation of one-dimensional elements within a structure. The only concern, at this point in the study, is the new geometry, without interest in the forces thus developed. This simple method achieves the desired geometry changes in conformity with the required geometric compatibility.

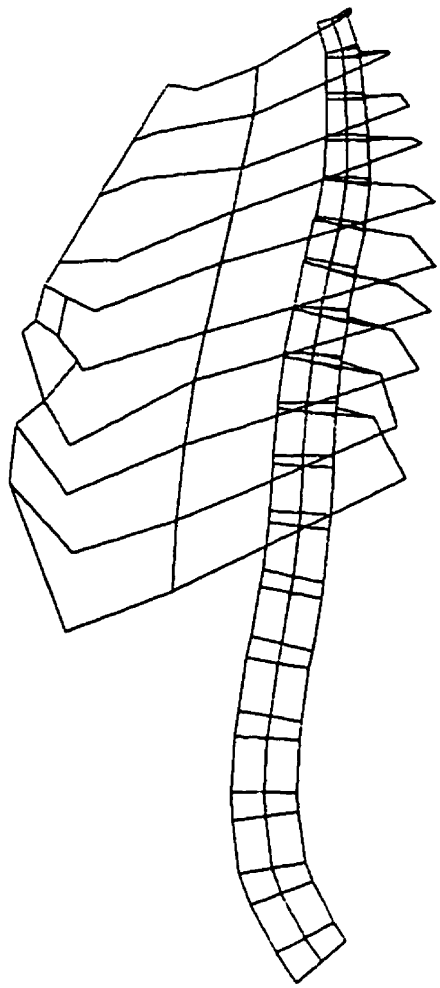

Fig. 5.6 Lordotic 3-element model of spine and rib cage, LARRY. Note the change in the thoracic curvature when compared to MOE in Fig. 5.5.

The desired anterior and posterior length changes of the vertebrae are also used in the calculation of temperature changes (ΔT) in these elements required as input in the nonlinear analysis which simulates lordotic growth of the spine by thermal loading the normal spine. Again, considering the center lengths to remain constant, relative faster anterior growth is simulated by heating the anterior elements and cooling the posterior elements. As shown in Table 5.7, using the desired length changes calculated above, the sagittal radii, and A-P bending stiffnesses of the designated vertebrae, the necessary forces in the anterior and posterior elements, to achieve such length changes (in an unrestrained system), may be determined. To obtain the axial force P, the elements may be thermally loaded by ΔT. The values of ΔT are dependent on the values of Young's modulus E, the area A, and the coefficient of expansion α, arbitrarily chosen for the axial elements. In order to facilitate calculations and to ensure that the anterior and posterior elements do not contribute to the stiffness of the vertebrae, a value of EA=1,000 N, small compared to the properties of the vertebrae, and an $\alpha=1$ were chosen.

Table 5.7 Temperature Changes Required to Simulate Asymmetrical Vertebral Growth

Vert.	Element No.		Change in length, ΔL Ant + Post - (cm)	Average sagittal radius, b (cm)	A-P rotation, $\theta=\Delta L/b$ (rad)	A-P bending stiffness, EI_y/L (N-cm/rad)	Moment, $M=EI_y\theta/L$ (N-cm)	Axial forces, $P=M/2b$ Ant-C Post-T (N)	Change in temp., $\Delta T=P/EA\alpha$ (± deg.)
	Ant	Post							
T4	41	75	.004	1.1535	0.0035	985,123	3,448	1,494.58	1.49
T5	43	77	.049	1.244	0.0394	1,232,632	48,566	19,520.10	19.52
T6	45	79	.191	1.3295	0.1437	1,532,338	220,197	82,811.96	82.81
T7	47	81	.509	1.4165	0.3593	1,899,970	682,659	240,966.82	240.97
T8	49	83	.368	1.4895	0.2471	2,268,683	560,592	188,181.27	188.18
T9	51	85	.454	1.527	0.2973	2,533,974	753,350	246,676.49	246.68
T10	53	87	.300	1.554	0.1931	2,692,127	519,850	167,261.90	167.26
T11	55	89	.077	1.5925	0.0484	2,982,337	144,345	45,320.25	45.32
T12	57	91	.021	1.615	0.0130	3,126,414	40,643	12,582.97	12.58

EA = 1000   C = compression   A-P = anterior-posterior
$\alpha = 1$ T = tension   Note: Bending stiffness properties explained in following section.

5.4 Representation of Stiffness Properties

As mentioned previously, discrete beam elements are chosen to make up the model. In reality, sectional and material properties vary throughout the spinal column and rib cage structure. Adding to this difficulty of non-homogeneity of properties within the same structure is the fact that properties vary tremendously from person to person. To keep the computer model simple yet adequate, new beam elements are introduced in the model only to represent a change in the geometry of the structure, e.g. a curve, and to account for a change in material, e.g. bone to ligament. It is assumed that the sectional and material properties are constant along the length of each individual element, but naturally, they are allowed to vary from element to element. For individual elements, sectional properties are assigned the averages of values along the length. Material properties are assumed linear, elastic and isotropic. Obtaining these properties to represent a typical normal spine and rib cage is a task in itself and will be discussed briefly.

Input for the program is in the form of sectional and material properties. The importance, is not focused on determining actual sectional and material properties but rather, on representing realistic stiffnesses, which are proportional to the product of the above two properties and which are usually the quantities reported in literature. Stiffnesses for the "rigid" or bony elements are based on the material properties of compact bone determined experimentally [103,120] and the actual sectional properties [64,103], when available in literature. Stiffnesses for the more deformable elements (intervertebral joints, ligaments, and cartilage) are based on results reported in literature from experiments on spinal motion segments [11,73,74,75,86,88,90,107,113] and soft tissue [4,109].

5.4.1 Rigid or Bone Elements

Sectional Properties

As mentioned above, the exact sectional properties of the rigid elements are not crucial for representing the actual behaviour of the spine and rib cage since they have comparatively large Young's moduli and shear moduli. When available in literature, true properties are generally assigned to the rigid elements, however assignments of equivalent sectional properties are made when appropriate to simplify input. In addition, approximations of properties are made when such data are not available.

Sectional properties of the rigid vertebral elements are calculated according to the data from Lanier [64]. For each vertebra, T1 - L5, the sagittal diameter was taken to be the average of the mean superior and the mean inferior sagittal diameters. The transverse diameter was taken to be the mean inferior transverse diameter. The cross-sectional area, moments of inertia, and torsional constants [51] are calculated according to the assumptions that (a) the vertebra is elliptical in shape, and (b) 100% of the cross-sectional area is effective. These properties are tabulated in Table 5.8. Element coordinate system for the vertebra and intervertebral joint elements is shown in Fig. 5.7.

Notations referred to in this chapter are as follows: A represents the cross-sectional area, I_1 and I_2 represent the area moment of inertia in the two perpendicular planes 1 and 2 (principal planes when cross-section is symmetrical) which are orthogonal to the cross-sectional plane, J represents the torsional constant, K_1 and K_2 represent shear area factors in planes 1 and 2 respectively, and I_{12} represents area product of inertia.[1] All symbols are defined in the List of Symbols. As noted in Table 5.8 and in Fig. 5.7, planes 1 and 2 are the principal planes. Plane 1 represents the lateral plane of the element and plane 2 corresponds to the A-P plane.

Since 3 elements are also used to represent 1 vertebra, equivalent sectional properties are calculated using the formulas derived in Appendix B. These equivalent values, used in the input data

[1]The nomenclature for inertia properties in terms of planes 1 and 2 is in accordance with that of NASTRAN. This is different from the axis-based convention normally used.

of the 3-element model, are shown in Table 5.8(a) and 5.8(b).

Table 5.8 Sectional Properties of Vertebrae*

Vertebra	E (N/cm^2)	G (N/cm^2)	A (cm^2)	I_1 (cm^4)	I_2 (cm^4)	J (cm^4)	K_1,K_2
T1	1030000	431000	4.24	2.651	0.773	2.395	1
T2	1030000	431000	4.72	3.061	1.030	3.083	1
T3	1030000	431000	5.08	3.036	1.390	3.813	1
T4	1030000	431000	5.50	3.181	1.822	4.633	1
T5	1030000	431000	6.05	3.631	2.342	5.695	1
T6	1030000	431000	6.68	4.240	2.965	6.980	1
T7	1030000	431000	7.44	5.198	3.728	8.685	1
T8	1030000	431000	8.23	6.386	4.566	10.650	1
T9	1030000	431000	8.98	7.853	5.250	12.586	1
T10	1030000	431000	9.97	10.407	6.022	15.258	1
T11	1030000	431000	11.15	13.896	7.036	18.684	1
T12	1030000	431000	12.00	16.789	7.813	21.327	1
L1	1030000	431000	12.81	19.659	8.692	24.108	1
L2	1030000	431000	13.57	22.346	9.624	26.908	1
L3	1030000	431000	14.58	26.430	10.853	30.774	1
L4	1030000	431000	15.25	28.846	11.896	33.690	1
L5	1030000	431000	14.73	26.207	11.366	31.710	1

* Values are based on the dimensions from Lanier [64].

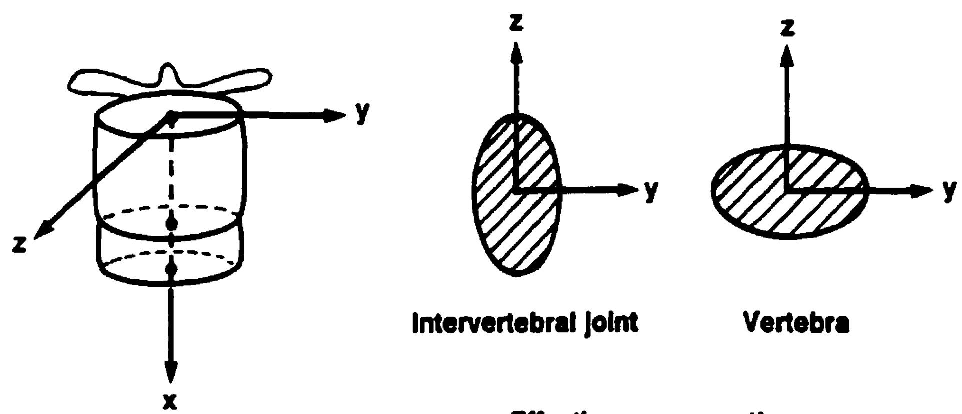

Fig. 5.7 Element coordinate system for vertebra and intervertebral joint elements. In this figure, the local y-axis coincides with the global Y-axis such that x-y plane defines element's lateral plane denoted by 1, and x-z plane defines the A-P plane denoted by 2. Cross-section is from bottom view.

Table 5.8a Equivalent Sectional Properties for Central Vertebral Elements (K_1=1.00)

Verterba	A (cm^2)	I_1 (cm^4)	I_2 (cm^4)	J (cm^4)	K_2
T1	3.222	2.015	0.025	1.755	-0.089
T2	3.587	2.326	0.027	2.235	-0.075
T3	3.861	2.307	0.035	2.692	-0.085
T4	4.18	2.418	0.05	3.192	-0.108
T5	4.598	2.76	0.072	3.857	-0.14
T6	5.077	3.222	0.1	4.654	-0.174
T7	5.654	3.95	0.11	5.709	-0.166
T8	6.255	4.853	0.14	6.977	-0.184
T9	6.825	5.968	0.171	8.333	-0.197
T10	7.577	7.909	0.185	10.35	-0.159
T11	8.474	10.561	0.19	12.86	-0.127
T12	9.12	12.76	0.229	14.88	-0.127
L1	9.736	14.941	0.21	16.903	-0.094
L2	10.313	16.983	0.249	18.93	-0.101
L3	11.081	20.087	0.303	21.689	-0.116
L4	11.59	21.923	0.371	23.675	-0.145
L5	11.195	19.917	0.353	22.131	-0.155

Table 5.8b Equivalent Sectional Properties for Anterior/Posterior Vertebral Elements (K_1=1.00, J=0.00)

Vertebra	A (cm^2)	I_1 (cm^4)	I_2 (cm^4)	K_2
T1	0.509	0.318	0.004	-0.089
T2	0.566	0.367	0.004	-0.075
T3	0.61	0.364	0.005	-0.085
T4	0.66	0.382	0.008	-0.108
T5	0.726	0.436	0.011	-0.14
T6	0.802	0.509	0.016	-0.174
T7	0.893	0.624	0.017	-0.166
T8	0.988	0.766	0.022	-0.184
T9	1.078	0.942	0.027	-0.197
T10	1.196	1.249	0.029	-0.159
T11	1.338	1.668	0.03	-0.127
T12	1.44	2.015	0.036	-0.127
L1	1.537	2.359	0.033	-0.094
L2	1.628	2.682	0.039	-0.101
L3	1.75	3.172	0.048	-0.116
L4	1.83	3.462	0.059	-0.145
L5	1.768	3.145	0.056	-0.155

Vertebral endplates, when included in model, are all given the same large (arbitrarily selected) sectional properties based on a circular cross-section, since they are modeled simply to provide rigid links between the 3 elements. The values selected are $A = 35.45\ cm^2$, $I_1 = I_2 = 100.0\ cm^4$, and $J = 200.0\ cm^4$.

For each rib, the sectional properties measured by Roberts and Chen [103] were averaged and assigned to all 4 segments of the rib. The properties were calculated on the assumption that the cross-sections have an elliptical shape but are only 50% effective (considering the compact bone contribution), and therefore are represented by an elliptical ring [103]. The properties are tabulated in Table 5.9, and the element coordinate system is illustrated in Fig. 5.8.

Table 5.9 Average Sectional Properties of Ribs [103]

Rib No.	Element No.	Property No.	A (cm)	I_1 (cm^4)	I_2 (cm^4)	J (cm^4)
1	285-292	153	0.4058	0.0267	0.0697	0.0519
2	293-300	154	0.2348	0.0084	0.0245	0.0199
3	301-308	155	0.3150	0.0127	0.0474	0.0337
4	309-316	156	0.3523	0.0150	0.0664	0.0392
5	317-324	157	0.2881	0.0128	0.0352	0.0297
6	325-332	158	0.3481	0.0204	0.0392	0.0434
7	333-340	159	0.4034	0.0277	0.0590	0.0591
8	341-348	160	0.4674	0.0225	0.0699	0.0551
9	349-356	161	0.3703	0.0264	0.0562	0.0580
10	357-364	162	0.3370	0.0181	0.0545	0.0426

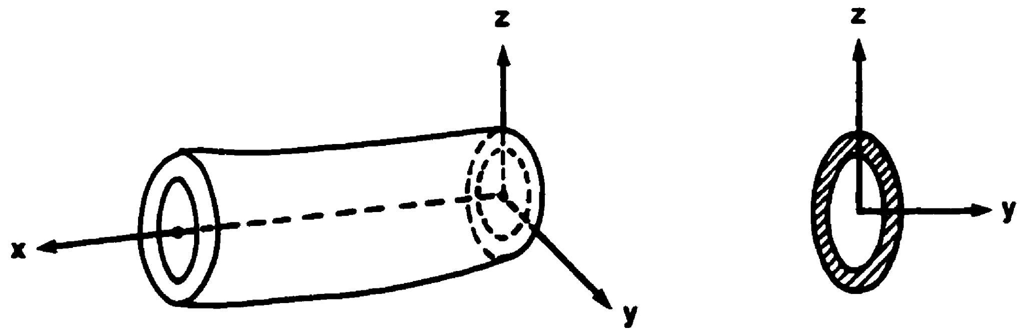

Fig. 5.8 Rib element coordinate system. The x-y plane coincides with the plane formed by the global Y-axis and the local x-axis. Here, the x-y plane defines plane 1, and the x-z plane, plane 2.

Similar to the endplates, the sternum beam elements are all given the same arbitrary property values, large enough to render them rigid. The sternum quadrilateral elements are assigned an average realistic thickness of 0.9 cm [103].

Sectional properties for elements representing the transverse processes and rigid posterior-lateral extensions of vertebral bodies needed to define positions of facets for articulation with the ribs by means of the CT and CV elements respectively, are arbitrarily selected to be the same for all similar element types in order to simplify input data. The assumption is appropriate since these elements are rigid links, providing anatomical positioning of the ligaments with respect to the vertebrae centers. The values, shown below, are chosen to reflect the true geometry and are based on the assumption of a circular cross-section.

Transverse:	$A = 1.0\ cm^2$	Elements defining:	$A = 3.545\ cm^2$
process	$I_1 = I_2 = 0.08\ cm^4$	vertebral body	$I_1 = I_2 = 1.0\ cm^4$
	$J = 0.16\ cm^4$	facets	$J = 2.0\ cm^4$

Material Properties

A lot of work has been done concerning properties of compact bone by Yamada [136] and Evans [36]. Based on their results, Sundaram and Feng [120] and Roberts and Chen [103] derived property values for particular types of compact bone as shown below in Table 5.10. These material constants were used for the bone elements of the present model, as indicated. The properties assume the material is isotropic and homogeneous, and as such the shear modulus G is related to Young's modulus E and Poisson's ratio ν by the relation $G = E/2(1+\nu)$.

Table 5.10 Material Properties for Bone Elements

Element type and source	Young's modulus, E (N/cm^2)	Shear modulus, G (N/cm^2)	Poisson's ration, ν
Vertebrae and elements defining facets on vertebral body [120]	1.03×10^6	4.31×10^5	0.20
Ribs, sternum, and endplate [103,120]	1.21×10^6	5.03×10^6	0.20
Transverse process [62]	3.50×10^5	1.40×10^5	0.25

5.4.2 Deformable Elements

The deformable elements in the model account for all the flexibility in the spinal structure. Therefore, in order to predict realistic behaviour, it is important to represent their true stiffnesses as accurately as possible. These deformable elements include the intervertebral joints, the ligaments, and the cartilage in the spine and rib cage. Stiffnesses are based on the best linear elastic approximation of the nonlinear, anisotropic, visco-elastic material. Whenever possible, actual sectional and material properties are used as the input data. However, due to the anisotropic nature of the material, many times the use of real stiffnesses and real cross-sectional areas A, and model lengths L, results in the calculation of other sectional (I and J values) and material properties (E and G values), far from real. Thus, the property values are treated simply as the appropriate quantities required for input in the program; it is the stiffness that must be realistic.

Stiffnesses of the costovertebral joints (CV), costotransverse joints (CT), intercostal tissue (IC), and costal cartilage (CC) attached to rib 6 are shown in Table 5.11. These stiffness values were obtained by simulating an experiment conducted on the ribs [109]. Stiffnesses were adjusted until the computed displacements agreed with the experimental results [4]. As noted in the table, and as mentioned earlier, the CT and CC elements exhibit axial, bending, torsional, and shear stiffnesses while the CV and IC elements only provide axial stiffness. Stiffness of the CV, CT, IC, and CC elements in the model are based on the stiffness values of these elements attached to rib 6.

Table 5.11 Stiffness Values for Deformable Elements Attached to Rib 6*

Element type	Axial, EA/L (N/cm)		Bending, EI/L (N-cm/rad)	Torsional, GJ/L (N-cm/rad)	Shear, GA/L (N/cm)
	ten.	comp.			
CV	49	490	0	0	0
CT	49	490	685	980	1225
IC	195	195	0	0	0
CC	735	735	245	980	80

* Values taken from Andriacchi et al. [4].

Typically, Young's modulus is 20 times higher in compression than in tension. Material property values for cartilage were determined by Yamada [136] to have elastic moduli in compression and tension respectively, of E_c=2,400 N/cm^2 and E_t=48,000 N/cm^2 and a Poisson's ratio of 0.1. Sundaram and Feng [120] determined an equivalent beam modulus for cartilage, E_{eq} = 6450 N/cm^2, using the tension and compression moduli. This equivalent modulus is used in determining sectional properties for the IC, CT, and CV elements.

The axial stiffness of 195 N/cm for the IC element attached to rib 6 is assumed for all other IC elements since no data on effective cross-sectional area were found. The cross-sectional area is therefore calculated using the equivalent modulus E_{eq} and the length of the element determined directly from the model. Properties of the IC elements are shown in Table 5.12.

Table 5.12 Cross-Sectional Area of Intercostal Tissue (IC elements)

Rib no.	Member no.	Property no.	EA/L, Axial stiffness [4] (N/cm)	E_{eq} [120] (N/cm^2)	Length (cm)	Area (cm^2)
1-2	421,430	62	195	6450	2.786	0.0842
2-3	422,431	63	195	6450	3.345	0.1011
3-4	423,432	64	195	6450	2.584	0.0781
4-5	424,433	65	195	6450	2.740	0.0828
5-6	425,434	66	195	6450	3.565	0.1078
6-7	426,435	67	195	6450	2.676	0.0809
7-8	427,436	68	195	6450	3.440	0.1040
8-9	428,437	69	195	6450	4.040	0.1221
9-10	429,438	70	195	6450	3.750	0.1134

Calculation of the CT and CV sectional properties is a bit more complex because their compressive axial stiffness is 10 times their tensile axial stiffness as seen in Table 5.11. However, the linearity of the program allows the input of only one (equal) stiffness. Information on the sectional properties of the ligaments at each rib level is unavailable. Thus, the stiffness values for these elements are assumed to be the same as the stiffness for the CT and CV elements of rib 6. The assumption is justified because the material is similar for the same element types and the same short length of 0.1 cm is chosen for each of these elements.

The procedure adopted to arrive at an equivalent axial stiffness, somewhere in between the value of the compressive and tensile stiffnesses is as follows. Multiplying the compressive stiffness and the tensile stiffness by their lengths L, and dividing by E_c and E_t, respectively, compressive and tensile areas are determined. The average of these two areas, 0.0015 cm^2, is used as the equivalent area. Then, a new equivalent axial stiffness of 96.75 N/cm is calculated based on the equivalent modulus E_{eq}, the equivalent area, and the true length. Based on these values, the remaining properties for the CT elements, I, G, and J, are determined from the bending, torsional, and shear stiffnesses respectively. The calculated properties are:

$$I_1 = I_2 = 0.0106 \ \ cm^4$$
$$J = 0.0012 \ \ cm^4$$
$$G = 81{,}666 \ \ N/cm^2$$

A Poisson's ratio of 0.1 is assigned to the elements [120,136]. The material is obviously not isotropic, however the realistic stiffness is modeled.

More information is found in literature concerning the costal cartilage. Roberts and Chen [103] give the sectional properties for the costal cartilage of all 10 ribs on the assumption they are elliptical and 100% effective. However, stiffnesses, which again are the important quantities to model, are unknown for the costal cartilage corresponding to ribs other than rib 6. Therefore, assuming all CC elements have the same Young's and shear moduli, stiffnesses for each CC element in the model are calculated by factoring the stiffness values determined for the cartilage of rib 6 (Table 5.11). The factor used is the ratio between the true sectional properties and the length (determined from model) of the CC element in question, and those of the cartilage of rib 6 (i.e. true sectional properties of the costal cartilage of rib 6 and the full length L_6 of the CC element attached to rib 6).

Although the calculation of the sectional properties of the costal cartilage is based on the assumption that they are elliptical, only one bending stiffness is given in [103]. Assuming it to be for bending about the weak axis, strong axis bending stiffness may be calculated in a manner similar to the above procedure, by factoring the weak axis stiffness using the true inertia about the strong axis of the cartilage in question (I_2) and the true inertia about the weak axis of the cartilage of rib 6 (I_1) along with the length factor. The formulas used to calculate the stiffnesses for each CC element are as shown on the following page. The factors are represented by α,λ,γ,and ξ. The subscript *6* denotes quantities belonging to the costal cartilage attached to rib 6. The subscript *k* denotes quantities belonging to a CC element in the model.

The E and G values used for all CC elements are 10,155 N/cm^2 and 1,105 N/cm^2, respectively. They are calculated using the axial and shear stiffnesses, and the true cross-sectional area corresponding to the cartilage attached to rib 6, as well as the full model length (L_6=9.271 cm) of the CC element attached to rib 6. The remaining sectional properties for all CC elements (I_1, I_2, J), tabulated in the last three columns in Table 5.13, are calculated using the corresponding factored stiffnesses, the lengths from the model, and the above E and G values. Figure 5.9 illustrates the element coordinate system.

$$\left(\frac{EA}{L}\right)_k = \frac{\alpha}{\lambda}\left(\frac{EA}{L}\right)_6 \qquad \alpha = \frac{A_k}{A_6}$$

$$\left(\frac{GKA}{L}\right)_k = \frac{\alpha}{\lambda}\left(\frac{GKA}{L}\right)_6 \qquad \lambda = \frac{L_k}{L_6}$$

$$\left(\frac{EI_1}{L}\right)_k = \frac{\gamma_1}{\lambda}\left(\frac{E\,I_1}{L}\right)_6 \qquad \gamma_1 = \frac{I_{1_k}}{I_{1_6}}$$

$$\left(\frac{EI_2}{L}\right)_k = \frac{\gamma_{21}}{\lambda}\left(\frac{EI_1}{L}\right)_6 \qquad \gamma_{21} = \frac{I_{2_k}}{I_{1_6}}$$

$$\left(\frac{GJ}{L}\right)_k = \frac{\xi}{\lambda}\left(\frac{GJ}{L}\right)_6 \qquad \xi = \frac{J_k}{J_6}$$

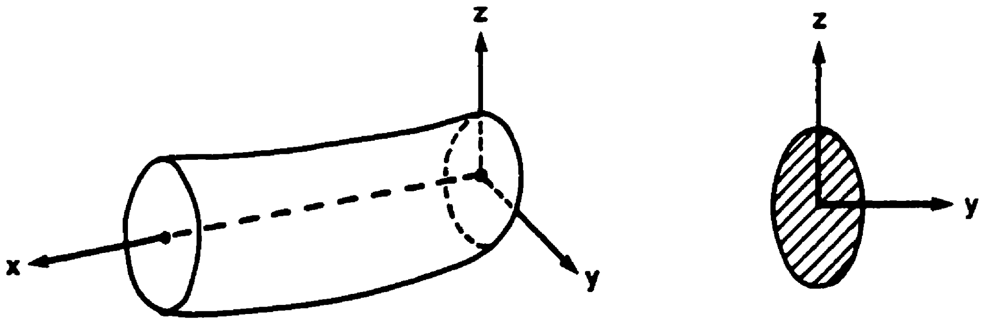

Fig. 5.9 Element coordinate system for CC elements. The x-y plane coincides with the plane formed by the global Y-axis and the local x-axis. Here, the x-y plane defines plane 1, and the x-z plane defines plane 2.

Intervertebral Joint Stiffness

The elements representing the intervertebral joints, in between the elements representing vertebrae, provide flexibility to the spinal column. The flexibility of these elements is dependent on (1) the size and shape of the cross-sections, the lengths (heights), and the material properties (moduli) of the intervertebral discs, (2) the action of the ligaments interconnecting the vertebrae, and (3) the shape of the articulating facets [73]. Since these variables differ at the various intervertebral joint levels, it cannot be assumed that the flexibilities are constant throughout the spine. Stiffnesses assigned to these elements have a great bearing on the results. Therefore, a thorough study of the prior works concerning testing of motion segments of the thoracic and lumbar spine is necessary.

Table 5.13 Sectional Properties of Costal Cartilage (CC elements)

Rib no.	Element no.	Prop. no.	Length (cm)	Real sectional properties [103]				Factored stiffness calculated based on stiffnesses of elements attached to rib 6 [4]					Model sectional properties; real area used for all CC elements		
				Area (cm^2)	I_1 (cm^4)	I_2 (cm^4)	J (cm^4)	EA/L (N/cm)	EI_1/L (N-cm /rad)	EI_2/L (N-cm /rad)	GA/L (N/cm)	GJ/L (N-cm /rad)	I_1 (cm^4)	I_2 (cm^4)	J (cm^4)
1	365,383	71	3.171	0.7458	0.0158	0.1169	0.0566	2388.46	725.49	5367.68	259.97	3088.97	0.2265	1.6761	8.8644
2	366,384	72	4.750	0.4129	0.0054	0.0373	0.0186	882.76	165.53	1143.36	96.08	677.66	0.0774	0.5348	2.9130
3	367,385	73	5.443	0.5419	0.0080	0.0706	0.0287	1011.05	214.00	1888.58	110.05	912.51	0.1147	1.0123	4.4948
4	368,386	74	6.418	0.6710	0.0110	0.1177	0.0549	1061.73	249.55	2670.21	115.56	1480.35	0.1577	1.6876	8.5981
5	369,387	75	3.560	0.5458	0.0101	0.0576	0.0343	1556.95	413.08	2355.81	169.46	1667.39	0.1448	0.8259	5.3719
"	370,388	76	4.288	0.5913	0.0124	0.0614	0.0421	1400.37	421.05	2084.88	152.42	1699.11	0.1778	0.8804	6.5935
6	371,389	77	2.395	0.6710	0.0156	0.0822	0.0525	2845.17	948.39	4997.29	309.68	3793.56	0.2237	1.1786	8.2222
"	372,390	78	2.614	0.6710	0.0156	0.0822	0.0525	2606.80	868.93	4578.62	283.73	3475.74	0.2237	1.1786	8.2222
"	373,391	79	3.024	0.6710	0.0156	0.0822	0.0525	2253.37	751.12	3957.84	245.26	3004.49	0.2237	1.1786	8.2222
"	374,392	80	3.633	0.6710	0.0156	0.0822	0.0525	1875.64	625.21	3294.39	204.15	2500.85	0.2237	1.1786	8.2222
"	375,393	81	2.775	0.6710	0.0156	0.0822	0.0525	2455.56	818.52	4312.98	267.27	3274.08	0.2237	1.1786	8.2222
7	376,394	82	4.151	0.8264	0.0250	0.1011	0.0805	2021.76	876.91	3546.23	220.05	3356.11	0.3584	1.4496	12.6074
"	377,395	83	6.603	0.8264	0.0250	0.1011	0.0805	1270.98	551.27	2229.35	138.34	2109.83	0.3584	1.4496	12.6074
8	378,396	84	1.963	0.8310	0.0230	0.1007	0.0809	4299.05	1705.99	7469.25	467.92	7132.17	0.3298	1.4438	12.6701
"	379,397	85	5.323	0.5935	0.0114	0.0710	0.0404	1132.28	311.83	1942.09	123.24	1313.46	0.1635	1.0180	6.3272
9	380,398	86	3.158	0.5290	0.0114	0.0422	0.0368	1701.12	525.61	1945.67	185.16	2016.64	0.1635	0.6051	5.7634
"	381,399	87	5.508	0.5290	0.0114	0.0422	0.0368	975.33	301.36	1115.54	106.16	1156.24	0.1635	0.6051	5.7634
10	382,400	88	8.323	0.4129	0.0066	0.0287	0.0217	503.80	115.46	502.08	54.84	451.206	0.0946	0.4115	3.3985

Note: E=10,155 N/cm2 L_6=9.271 cm (elements 372-374 or 390-392)
G=1,105 N/cm2

A motion segment is defined as consisting of an intervertebral disc and its two adjacent vertebrae with all connecting ligaments intact. It is important that the posterior elements of the vertebrae, in particular the facet joints, and the ligaments are included in the motion segment testing. They restrict movement between adjacent vertebrae, and hence contribute to the stiffness of the intervertebral joint. Their participation is evident because upon their removal, experiments [74,75,113] indicate significantly increased flexibility. Any deformation between the two vertebrae can be assumed solely due to the intervertebral joint.

Illustrated in Fig. 5.10 are the 12 principal directions in which the loads are applied and the deformations are measured when testing a motion segment. For the purpose of the stability analysis, motion segment testing may be reduced to loading in 8 physiological directions. They are axial compression; anterior, posterior and lateral shear; anterior, posterior, and lateral bending; and torsion. Due to the symmetry of the structure, lateral shear and bending, as well as torsion need to be tested in only one direction [121]. In addition, tensile stiffness is not important in compressive stability analyses [121]. By loading motion segments T1-T2 through L5-S1 in these 8 directions and measuring the displacements in those directions, the compressive, lateral, anterior and posterior shear, lateral, anterior (flexion), and posterior (extension) bending, and torsional flexibilities of the intervertebral joint at each level may be determined.

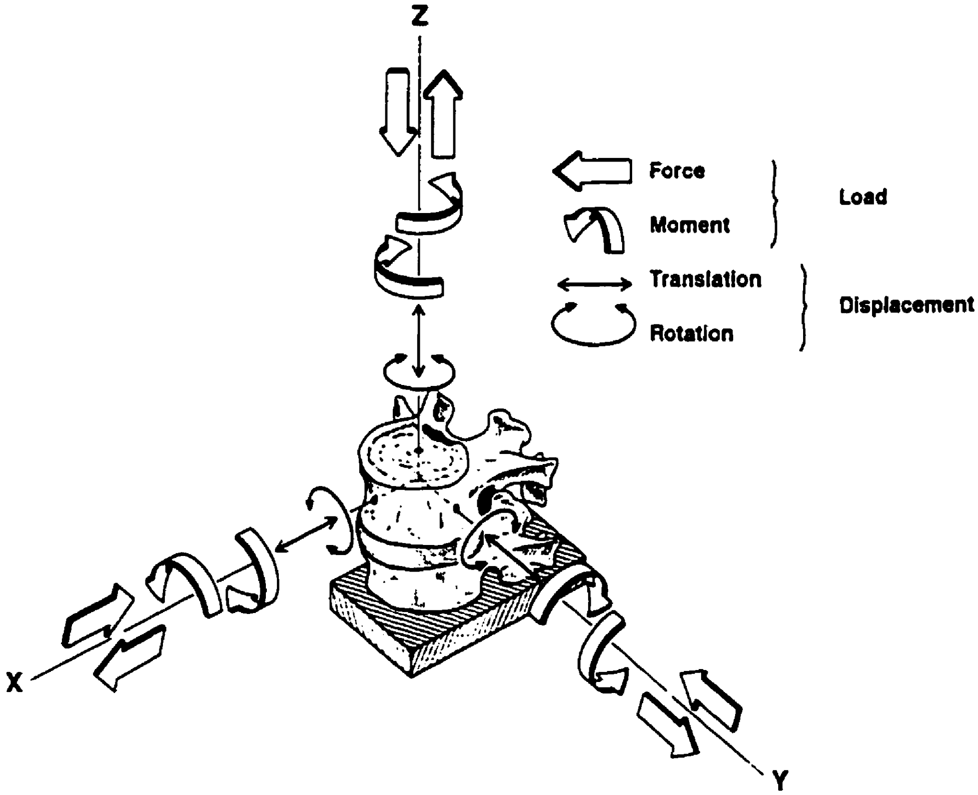

Fig. 5.10 Illustration of the principal directions of load application and deformation measurements in typical motion segment testing. After White and Panjabi [130].

Experimental determination of the appropriate stiffnesses is difficult due to the facts that:

(1) The post-mortem effect is not accounted for in the stiffness properties. All the tests are performed on in-vitro specimens. This type of testing is not possible on in-vivo specimens. However, the preservation technique seems to be quite effective.

(2) The material is human biological tissue. Firstly, it is highly nonlinear and visco-elastic. Its deformation is dependent both on the load and time. It becomes stiffer as the loads are increased. It is suspected to experience permanent deformation under sustained loads, although more testing is necessary. Secondly, in line with the characteristics of biological material, it is found to have a large variance of properties among specimens [88].

(3) Different experimental conditions and designs, i.e. testing procedures and displacement measuring devices, used by various researchers increase the large variation in results and makes comparison among them difficult [88]. Different procedures produce different experimental error. To add to the difficulty, some results are based on experiments which for example, take into account preload and coupling effects while others do not.

(4) It is difficult to conduct stiffness tests on the intervertebral joint. It is much easier to perform flexibility tests, in which the load is applied and resulting displacements are measured. The stiffnesses of the main motions[1] are approximated by inverting the main motion flexibilities. The approximation is acceptable as long as the coupled motions are small (negligible). Accurate stiffness values are reached by inverting the complete flexibility matrix, taking into account the coupled motion. Panjabi et al. [89] show a 10% error in neglecting the coupling effect. Since a larger variation is found among subjects, the above error is acceptable.

Experiments to determine the stiffness or flexibility of motion segments have been performed on a large scale. The large compilation of data is reduced by taking into account only those results which were obtained from experiments which tested many motion segments, individually, and in the principal directions [11,73,74,75,86,88,90,107,113]. Table 5.14 summarizes the motion segment experiments performed by various researchers which were used in determining the intervertebral joint stiffnesses used in this model. The reason for this is simply to limit unnecessary variance due to different procedures and to achieve some sort of consistency. In addition, emphasis is put on those

---

[1] *Main motion* [88] is defined as the motion produced in the same direction as the applied load.

Coupled motion is the motion produced in other directions other than the direction of main motion. It is defined [88] as a result of coupling which is the phenomenon in which motion along or about an axis is consistently associated with motion along or about another axis.

Table 5.14 Summary of In Vitro Motion Segment Flexibility Testing Studies used in determining Intervertebral (I.V.) Joint Stiffnesses

Experimenter(s), date, ref. no.	Motion segments tested	Conditions of Experiment	Results and comments
Lucas & Bresler, (1961), [73]	-T1/T2 through L5/S1, lateral bending stiffness only -1 specimen	-1 ligamentous spine of 32 yr old male subject to lateral loading from 0 - 2500 g at increments of 250 g. -Force applied laterally at T1, moment M at disc level determined by the force times distance from T1. Hence, moment increased caudally which is a realistic representation. -Rotation θ measured between adjacent vertebrae. -Time allowed for creep, and measurements also made upon unloading; which indicated no significant hysteresis.	-Flexibilities only determined from 1 specimen. -Stiffness in good agreement with Schultz [107] at T8/T9 and L3/L4 levels. -Flexibilities of spine determined at load levels of 500, 1000, and 1500 g. Any rotation between vertebrae assumed to take place at i.v. joint and flexibility at each level calculated as $f=\theta/M$. Flexibility at each level taken as average of 3 flexibilities. -Stiffness at each i.v. joint level approximated by $1/f_{avg}$.
Markolf, (1970 & 1972), [74,75]	-T7/T8 through L3/L4 -17 specimens (21-55 yrs old)	-Testing jig allowed unconfined motion. Measurements only made in principal directions. -Allowance for creep; readings after 1-2 mins. -Bending and torsion tests with articular facets and ligaments intact, then repeated with them removed. Pure moment applied. -Axial and shear tests: posterior structures removed. Lumbar segment only for shear test. Segment consisted of 3 vertebrae and 2 discs. Force applied at center of middle vertebrae, with end vertebrae fixed such that "pure" shear exists. Instron machine used for axial tests. Max. load 1400 - 2200 N, loading rate of 2.5 mm/min. -No preload.[1]	-Load-displacement curves for main motions. -Bending and torsion: no evidence of creep at moment levels tested. Non-linear deformations with stiffness increasing as moment is increased. Stiffer in extension than flexion (for all regions). Lumbar region more flexible for all bending. Lowest thoracic and lumbar i.v. joint much stiffer in torsion (due to facet orientation). -Shear: no creep, little displacement (stiff) hence loads applied are small to avoid damage. Initial stiffness = 1050 -5100 N/cm. -Axial: Observed hysteresis and non-linear stiffening with increased deflection. Final stiffness used for comparison, since spine subjected to constant compressive preload due to body weight. Stiffness range from 4200 - 10700 N/cm with average of 8690 N/cm. -Posterior structures have greatest stiffening effect in extension (in thoracic and lumbar region) and in torsion (in lumbar region).
Schultz, Belytschko, Andriacchi, (1973), [107]	-Simulated experiments using T8/T9 and L3/L4 model motion segments -determined disc stiffness for thoracolumbar region	-Conditions simulated: - no preload - unconstrained motion - loaded in all principal directions at geometric center of inferior surface of superior vertebrae - loading: forces - 100 kg for tension and shear, 300 kg for compression; moments - 150 kg-cm in thoracic and 200 kg-cm in lumbar for bending, 300 kg-cm for twisting.	-Low torsional stiffness compared to other cadaver material results. -Good agreement with normal motion ranges found in past. -Flexion found stiffer than extension, attributed to ligaments that work in flexion but not in extension, contrary to Markolf who found extension to be limited by impingement of facets. -Determined isolated disc stiffness in compression/tension, shear, bending, and torsion at all levels of thoracolumbar spine. Stiffness at model levels adjusted until results in agreement with cadaver results. Stiffness at other levels based on relative variations in geometry.

[1]Compressive preload of 400 N gives good representation of average body weight above L3.

Table 5.14 Summary of In Vitro Motion Segment Flexibility Testing Cont'd

Experimenter(s), date, ref. no.	Motion segments tested	Conditions of experiment	Results and comments
Panjabi, Brand, & White, (1976), [88,89]	-T1/T2 through T11/T12 -flexibility at each level based on 1 sample motion segment (segments obtained from 5 different specimens)	-No preload. -Coupling accounted for; force applied in 12 principal directions, displacements measured in 3 directions (1 main and 2 coupled), assuming symmetry about sagittal plane. -Loading: Forces - initial 10 N, increments of 30 N, up to max of 160 N. Moments - initial 100 or 150 N-cm, increments of 100 or 150 N-cm, to a max. of 600 or 750 N-cm. -36 load-displacement curves for main and coupled motions given for T10/T11 only. -Main and coupled flexibility coefficients determined at each level for principal loads of 100 N or 5 N-m. -Measurement after 4 mins. (approximately 97% deformed).	-No trend in thoracic flexibilities, possibly due to testing procedure; only 1 segment tested per level and segments obtained from different specimens. Allows no distinction between interlevel and intersubject variation. -Least flexible in axial direction. Less flexible in compression than tension, in extension than flexion. Equally flexible in A-P and lateral shear, in torsional and lateral bending. -Main motion always found to be greatest, except during axial compression which resulted in significant horizontal displacement. -[81] shows error (10%) in obtaining main stiffness coefficients by inverting main flexibility coefficients instead of inverting complete flexibility matrix (main and coupled coefficients).
Panjabi & White, (1977), [90]; Krag, (1975), [63]	-L1/L2 through L3/L4 -load-disp. curves given for L3/L4 segment of 58 yr. old man	-Compressive preloads of 0, 400, and 1000 N applied during physiological loading. -12 loads applied, 6 disp. measured at 0 load and 3 load increments. Max force 150 N, max moment 10 N-m. Reading analyzed for 3rd load cycle only (repeatable phase). -3 min. allowed for creep. -Posterior elements intact.	-72 load-displacement curves for L3/L4 segment (describes full motion) -Results show effect of compressive preload on segment behaviour - more flexible when subjected to forces directed laterally and anteriorly or to moments producing lateral bending and flexion - less flexible when subjected to axial tension and torsion - no effect when subjected to axial compression, posterior shear, or extension.
Schultz, Warwick, Berkson, & Nachemson, (1979), [113]; Berkson, Nachemson, & Schultz, (1979), [11]	-L1/L2 through L4/L5 -42 segments from 24 cadavers (mean age = 43), with and without posterior elements intact.	-Preload of 400 N applied during physiological loading -Loading: applied in 3 or more increments, maximum of 20.5 N-m for bending and torsion, 205 N for shear or motion limited to 8 deg. or 2 mm maximum. -Unconfined motion segment testing. -Displacement recorded in each of 6 directions for each of the 6 physiological loads applied, hence main and coupled motions accounted for. -Accounted for creep; readings after 15 sec. -Nonrepetitive static loading.	-Load-displacement curves of main motion reflect average response to loading of all segments tested; hence, no indication of inter-level variation and coupling. -Stiffest in torsion, 100% less in extension, 400% less in flexion and lateral bending -Posterior elements have greatest effect in extension and torsion -Strong coupling noted between bending and shear (could be the result of point of application of shear force causing moment on disc); *no consistent* coupling found between torsion and lateral bending which is believed to exist.
Tencer, Ahmed, & Burke, (1972), [121]	-L2/L3 and L4/L5 -14 segments from 8 subjects	-8 of 12 principal loads applied (due to symmetry w.r.t. sagittal plane) in 3 load steps. Max. loads: shear 90 N, comp. 823 N, flex.-ext. 11.2 N-m, lat. bend. 14.7 N-m, axial torque 12.9 N-m. -Allowance for creep: 1 min at 1st and 2nd step, 2 min at 3rd. -Unconstrained motion testing. -Posterior elements intact and then removed. -46 variations of combination loading performed. Preloaded with 1 of principal loads applied at max., then other principal loads applied in 3 steps with the exception of principal loads whose magnitudes are increased by the preload.	-Results in the form of load-disp. curves, main and coupled/main flexibility coefficients, and flexibility coefficient ratios for preload. -Anterior shear most flexible, posterior shear 50% and lateral shear 33% as flexible. Compressive preload decreased shear flexibility 61%, anteriorly and 73% posteriorly 73%. Contrary to Panjabi [90] but consistent with others. -Most flexible in flexion; in extension 60% and in torsion less than 30% as flexible. Lateral bending flexibility approximately the average of flexion and extension. Flexibility of axial torque decreased by 50% with compressive preload (good agreement with Panjabi [90]).

experiments which tested many motion segments from the same specimen. Again, this is done mainly to achieve consistency or a trend among various levels. If each motion segment tested is from a different specimen, it cannot be determined whether variance is an inter-level variation or a variation among different specimens, and consistency cannot be achieved [88].

An important factor in obtaining realistic stiffnesses is the application of compressive *preload* [90]. The spine is constantly subjected to compressive gravity loads due to body posture and superimposed body weight when it is under any other physiological load or load causing motion. Hence, results obtained when a preload is included as part of the testing environment are favoured. Obviously, preload is a more important factor for lumbar motion segments since they are subjected to more weight.

There is a difference of opinion whether compressive preload should be used in conjunction with lateral bending, flexion, and extension. The offset of the compressive preload may increase the effects of moments making the motion segment appear more flexible [121]. Testing by Panjabi et al. [90] indicates a significant increase in the flexibility of the segment in lateral bending and flexion when a compressive preload is applied. This increase may be due to the additional moment or the effect of compression in the element.

The assumptions made and criteria used to best approximate the stiffnesses used in this model are as follows:

(1) *Linear approximation*: Linear stiffness values for compression, and anterior-posterior bending and shear, are approximated from nonlinear load-displacement curves by determining stiffness at a point corresponding to the static load in that particular segment of the structure (determined approximately by a preliminary analysis) assuming a compressive buckling load, P_{cr}=600 N, from Andriacchi et al. [4]. Hence, more emphasis is put on studies which present results in terms of load-displacement curves rather than in terms of flexibilities at particular loads. For lateral bending, torsional, and lateral shear stiffness values, due to the geometry of the spine and the nature of the loading (i.e. axial compression and flexion moment), initial static stiffnesses are used since there is no deformation or loading in these directions prior to buckling. In addition, due to the linear property restriction, the same stiffnesses had to be assigned for flexion and extension as well as for anterior and posterior shear, although the stiffnesses are sometimes found to be significantly different.

(2) *Anatomical restraints*: Limitations on the motion in the different regions of the spine imposed by the respective vertebral geometry are kept in mind during the modelling of the properties. Recalling anatomical restrictions and freedoms, significant axial rotation is permitted in the thoracic

region. In the lumbar region, axial rotation is restricted while lateral bending is quite free. Both flexion and extension are allowed in each region.

(3) *Effect of preload*: In order to make a comparison of results, adjustments are made to the results which were obtained in experiments not including preload (when appropriate). The effect of the preload was determined for the L3-L4 motion segment by Panjabi et al. [90]. Assuming the effect varies linearly with respect to the weight on the segment, the effect of the preload at the other segments is interpolated.

The stiffness properties used for the intervertebral joints in the model are given in Table 5.15. They are based on the studies described in Table 5.14. Using the real cross-sectional areas, effective shear areas[1], and central lengths of the elements in combination with the axial and shear stiffnesses, the E and G values are determined respectively. Moments of inertia and torsional constant values are then calculated using the bending and torsional stiffnesses, real lengths, and E and G values previously calculated. This procedure enables proper modelling of the joint stiffness in quantities necessary for computer input. Sectional and material properties calculated for the intervertebral joint are given in Table 5.16. Equivalent sectional properties for the 3 element representation of the intervertebral joint are calculated using the formulas in Appendix B, and are given in Table 5.16a and 5.16b. The element coordinate system is shown in Fig. 5.7.

5.5 Loading and Boundary Conditions

The method of simulating the weight of upper body segments acting on the spine is adopted from Haderspeck and Schultz [49]. Horizontal slices of the trunk are made at the base of each vertebra. The weight of each slice is applied at the centroid of the slice, which is rigidly attached to the bottom center node of the vertebra.

The weight of each slice is calculated according to the volume of each slice and a constant density of 1019 kg/m^3 (specific weight γ=0.0099964 N/cm^3) [49]. The volume of each slice is calculated using the average area and thickness of the slice obtained from scaled sectional anatomical drawings [37]. Cross-sectional areas are measured from the drawings of various horizontal sections of the human body using a planimeter. The positions of the cross-sections do not correspond with the locations of the slices chosen (i.e. bottom of vertebrae). Therefore, with the aid of the sectional drawings indicating the vertical positions of the horizontal sections along the spine, the areas of the

[1]The effective shear area is calculated on the assumption that only the annulus and longitudinal ligaments resist shear, bending and torsion. The area factor for shear is taken = 0.4375 [38,80,107].

Table 5.15 Intervertebral Joint Stiffnesses

Superior vertebra	Axial (N/cm)	Torsional (N-cm/rad)	Lateral bending (N-cm/rad)	A-P bending (N-cm/rad)	Lateral shear (N/cm)	A-P shear (N/cm)	True area (cm^2)	Central length (cm)
T1	9090	2135	1710	4000	5886	5886	4.39	0.449
T2	11770	3305	3270	7000	10791	10791	4.98	0.310
T3	14715	4565	4710	10000	13734	13734	5.36	0.272
T4	20600	6925	7850	11460	18639	18639	5.71	0.222
T5	18640	7005	7550	11910	16677	16677	6.28	0.251
T6	17660	7090	7550	12590	15696	15696	6.89	0.320
T7	12285	7180	7730	7500	13734	13734	7.61	0.400
T8	14715	8595	8050	12000	12753	12753	8.38	0.442
T9	15385	10655	7985	9200	13734	13734	9.02	0.473
T10	15430	14035	11245	16500	13734	13734	10.09	0.507
T11	15300	23545	9220	12500	10791	10791	11.30	0.680
T12	15215	76660	9415	17315	9810	9810	12.07	0.841
L1	13455	53115	6400	16380	8829	8829	12.98	1.006
L2	12000	55290	4870	22165	7848	7848	13.78	1.147
L3	14715	61305	4965	23420	7848	7848	14.66	1.221
L4	13735	48685	5785	15000	6867	6867	15.38	1.401
L5	10790	39835	11505	11000	5886	5886	14.55	1.570

Table 5.16 Sectional Properties for Intervertebral Joint

Superior vertebra	E (N/cm^2)	G (N/cm^2)	A (cm^2)	I_1 (cm^4)	I_2 (cm^4)	J (cm^4)	K_1,K_2
T1	929.7	1376.0	4.39	0.826	1.932	0.697	0.438
T2	732.7	1535.4	4.98	1.384	2.962	0.667	0.438
T3	746.7	1593.0	5.36	1.716	3.643	0.779	0.438
T4	800.9	1656.4	5.71	2.176	3.177	0.928	0.438
T5	745.0	1523.5	6.28	2.544	4.013	1.154	0.438
T6	820.2	1666.3	6.89	2.946	4.912	1.362	0.438
T7	645.7	1650.0	7.61	4.788	4.646	1.741	0.438
T8	776.1	1537.5	8.38	4.584	6.834	2.471	0.438
T9	806.8	1646.2	9.02	4.681	5.394	3.062	0.438
T10	775.3	1577.4	10.09	7.353	10.790	4.511	0.438
T11	920.7	1484.3	11.30	6.810	9.232	10.787	0.438
T12	1060.1	1562.4	12.07	7.469	13.736	41.265	0.438
L1	1042.8	1564.1	12.98	6.174	15.802	34.163	0.438
L2	998.8	1493.1	13.78	5.592	25.453	42.473	0.438
L3	1225.6	1494.0	14.66	4.946	23.332	50.101	0.438
L4	1251.2	1429.8	15.38	6.478	16.797	47.705	0.438
L5	1164.3	1451.7	14.55	15.514	14.833	43.081	0.438

Table 5.16a Equivalent Sectional Properties for Central Intervertebral Joint Elements (K_1=0.4375)

Superior vertebra	A (cm^2)	I_1 (cm^4)	I_2 (cm^4)	J (cm^4)	K_2
T1	3.336	0.628	0.838	0.354	0.446
T2	3.785	1.052	1.354	0.164	0.441
T3	4.074	1.304	1.572	0.103	0.44
T4	4.34	1.654	0.916	0.074	0.442
T5	4.773	1.933	1.146	0.071	0.443
T6	5.236	2.239	1.355	0.017	0.446
T7	5.784	3.639	0.598	0.092	0.497
T8	6.369	3.484	1.683	0.501	0.454
T9	6.855	3.558	0.2	0.887	0.957
T10	7.668	5.589	3.646	1.957	0.447
T11	8.588	5.175	1.667	7.84	0.49
T12	9.173	5.676	4.594	38.095	0.457
L1	9.865	4.692	5.363	30.736	0.464
L2	10.473	4.25	11.999	38.88	0.448
L3	11.142	3.759	9.623	46.199	0.453
L4	11.689	4.923	3.902	43.432	0.527
L5	11.058	11.791	3.303	38.929	0.595

Table 5.16b Equivalent Sectional Properties for Anterior/Posterior Intervertebral Joint Elements (K_1=0.4375, J=0.00)

Superior vertebra	A (cm^2)	I_1 (cm^4)	I_2 (cm^4)	K_2
T1	0.527	0.099	0.132	0.446
T2	0.598	0.166	0.214	0.441
T3	0.643	0.206	0.248	0.44
T4	0.685	0.261	0.145	0.442
T5	0.754	0.305	0.181	0.443
T6	0.827	0.353	0.214	0.446
T7	0.913	0.575	0.094	0.497
T8	1.006	0.55	0.266	0.454
T9	1.082	0.562	0.032	0.957
T10	1.211	0.882	0.576	0.447
T11	1.356	0.817	0.263	0.49
T12	1.448	0.896	0.725	0.457
L1	1.558	0.741	0.847	0.464
L2	1.654	0.671	1.895	0.448
L3	1.759	0.594	1.519	0.453
L4	1.846	0.777	0.616	0.527
L5	1.746	1.862	0.521	0.595

top and bottom surfaces of each body slice are linearly interpolated using the calculated section areas, and the distances (thicknesses) between the horizontal sections and between the body slices made at vertebrae bases, measured directly from the drawings. The average area of each body slice is calculated, assuming linear variation of area between sections. The centroid of the slice is determined similarly by approximating the centroid of the area on the sectional drawings. All dimensions measured from the drawings [37] are increased linearly by 5% according to the suggestion by Haderspeck and Schultz [49]. They found the dimensions to be small when compared to a more recent and extensive study [22].

The weights of the upper extremities are applied at their centers of gravity and rigidly attached to the bottom center node of vertebrae T2, T3, and T4 [49]. Similarly, the weight of the head and neck are linked to T1 [22,49]. The weights assigned are adopted from Dempster sited in [25] with slight modifications based on adjustments of the percentage body weight of the segments [22]. The position of their center of gravity is based on data on the center of gravity of body segments [22] and scaled anatomy drawings [37].

Based on these calculations, the resultant weight on the sacrum is 376 N and the coordinates of its center of gravity (C.G.) is x_c=2.56 cm, y_c=0 cm, and z_c=27.78 cm. The results are in good agreement with Haderspeck and Schultz [49], who found the resultant weight to be 380 N and with Grant's Anatomy [44], which states that C.G. passes just in front of the sacrum. In addition, there is satisfactory agreement with the results found in literature [25,79] concerning weight supported by each vertebra level.

The weights of the upper body segments and slices, and their points of application are used to obtain a realistic loading condition proportional to the distribution of body weight along the spine length. For the purpose of the buckling analysis, the loads applied are expressed as a percentage of the total load applied to the structure. These loads are calculated in Table 5.17 and are applied to the structure as described above. It is felt that in the buckling analysis, distributed loading might produce more realistic results than loading with a lumped force at the top of the spine.

However, for the nonlinear post-buckling analysis, it was found that in NASTRAN the distributed loads could not be applied. The loaded nodes move and rotate with the structure and deviate far from the center of gravity. Hence, it was opted to apply the resultant body weight lumped at the C.G. by rigidly connecting the C.G. to the superior node of T1. As discussed below, the constraints on T1 are such that the weight stays in the center. Effectively, the loading is equivalent to a compressive force and a forward flexion moment (2.98 times the force) applied at T1.

Table 5.17 Body Weight Distribution at Various Levels

Slice level	Average calculated area, (cm^2) A scale=4/5*	Measured thickness, (cm) t scale=2/5	Real volume, (cm^3) $V=(5/4)^2(5/2)At$	Slice weight, (N) $W=1.05^3V\gamma$	Body weight distribution (%) $W/\Sigma W$	Measured moment arm in x-direction, (cm) scale=2/5	Real moment arm in x-direction, (cm) measured arm × 5/4 × 1.05
	170.730	1.05	700.260	8.103	0.021558	-1.750	-2.2969
T1	275.181	1.19	1279.162	14.803	0.039379	-1.150	-1.5094
T2	338.881	0.82	1085.478	12.561	0.033417	-0.035	-0.0461
T3	370.501	0.68	984.143	11.389	0.030297	0.806	1.0579
T4	388.662	0.73	1108.294	12.825	0.034119	1.292	1.6958
T5	357.191	0.62	865.072	10.011	0.026631	1.888	2.4780
T6	345.145	0.70	943.756	10.921	0.029054	2.737	3.5923
T7	351.458	0.65	892.374	10.327	0.027472	3.063	4.0202
T8	352.993	0.56	772.172	8.936	0.023771	3.191	4.1882
T9	359.677	0.74	1039.691	12.031	0.032007	3.299	4.3299
T10	361.756	1.00	1413.109	16.353	0.043503	3.740	4.9088
T11	358.633	0.94	1316.856	15.239	0.040540	3.977	5.2198
T12	359.333	1.16	1628.228	18.842	0.050125	3.875	5.0859
L1	356.939	1.22	1701.037	19.685	0.052367	3.744	4.9140
L2	336.705	1.33	1749.288	20.243	0.053852	3.376	4.4310
L3	313.249	1.26	1535.654	17.771	0.047275	3.026	3.9711
L4	298.077	1.52	1769.832	20.481	0.054484	2.730	3.5831
L5	291.018	1.62	1841.598	21.311	0.056694	2.638	3.4624
Disc	299.290	0.68	794.989	9.200	0.024474	2.779	3.6474
Trunk			23420.99	271.030	0.721018		
Head				46.369	0.1234		2.888 z=17.7775 (from T1 base)
Upper extremities				29.250	0.0778		1.640 y=±17.718 z=-30.005 (from T1 base)
				29.250	0.0778		
Sum				375.899	1.0000		

* Scale means the scale of the anatomical drawings.

Boundary conditions are chosen, in accordance with the literature, to reflect the anatomical constraints of an upright human spine. When possible in the analysis, the end-support condition at the top of the spine model (i.e. superior center node of T1) is chosen to be fixed in the x, y, θ_x, θ_y, and θ_z directions, constraining lateral and anterior-posterior displacements and rotations respectively, but allowing vertical displacement. In reality, the constraint at T1 is somewhere in between fixed as described above, and fixed only in horizontal displacements and rotation (with bending rotations released) [48]. This constraint is provided by the various mechanisms (i.e. muscles) involved in the righting reflex of the body [73]. The sacrum, at the base of the column, is fixed in all 6 degrees of freedom (i.e. completely fixed support). This constraint is provided anatomically by the level pelvis [48,73]. The remaining nodes in the model are generally given complete degrees of freedom. The boundary conditions are discussed more thoroughly in Chapter 6.

Chapter 6

Results and Discussion

This chapter presents results of the structural analysis performed on the spine and rib cage model constructed in Chapter 5. It consists of three main parts. The first part presents results of analyses conducted to establish the validity of the constructed model. This is accomplished by comparing the present results for some cases investigated by previous researchers. The second and third parts are original to this thesis. They present results of analyses performed to test the lordosis hypothesis corresponding to the author's two interpretations of it.

6.1 Model Validation

Since the present model, which is the basis of all the results, is constructed solely from literature data, it is important that the computed results compare reasonably well with those obtained from other validated spinal model studies and in vitro experimental studies. Unfortunately, there exists only a small number of studies on the behaviour of the complete thoracolumbar spine with rib cage which may be used for comparison. Three studies, discussed in Chapter 3, will be used in particular.

The first is the experimental investigations of Lucas and Bresler [73]. Much emphasize is put on these results since they are the only ones based on an actual human thoracolumbar spine. One shortcoming of these results is that they are limited to the ligamentous spine (devoid of the rib cage etc.). The other two studies are the structural analyses of discrete parameter models (as opposed to the gross continuum models) of the spine. Belytschko et al. [10] reported the results for the ligamentous spine, whereas Andriacchi et al. [4] performed the analysis on the same model but with the rib cage added.

6.1.1 Ligamentous Spine

To ascertain the correctness of the adopted stiffness properties of the motion segments, and of the geometry of the spine, the studies conducted on the isolated ligamentous spine by Lucas and Bresler [73] and Belytschko et al. [10] are simulated using the isolated ligamentous spine of the present model. In accordance with these references, perfect symmetry about the A-P plane is assumed.

The simulations are carried out using the MSC/NASTRAN finite element program. The computed results are compared with those reported in the above references. Items of comparison include (a) deformation response due to lateral loads, and bending and twisting moments applied at the top, and (2) the lateral buckling loads and associated mode shapes under a concentrated compressive load.

In the first simulation, the spine is considered like a cantilever. It is fixed at the base (i.e. sacrum) and is subjected to a 0.5 kg concentrated load in the lateral plane, applied at the top of the spine (at the bottom of T1). The response gives an indication of the effective lateral bending stiffness. As shown in Fig. 6.1(a), the computed structural response of the present ligamentous spine model in terms of frontal plane rotations, compares well with the results of Lucas and Bresler [73], and of Belytschko et al. [10]. Slight discrepancies between the rotations obtained by Lucas and Bresler [73] and in the present study may be attributed to the approximation of the intervertebral joint stiffnesses as being constants (independent of load or deformation) made in the present study. The rotations in the present study appear slightly larger in the lower spine, and slightly smaller in the upper spine in comparison to those found by Lucas and Bresler [73]. The resulting bending moments are smaller at the top and larger at the bottom. Thus, it appears that the linear approximation of motion segment behaviour slightly overestimates the stiffnesses at low loads, and slightly underestimates them at high loads. This point is highlighted when comparison is made between the responses at 2.5 kg lateral load. As shown in Fig. 6.1(b), a total frontal rotation of 64.43° at the T3 level obtained by the present model compares to a 41.9° rotation reported by Lucas and Bresler [73]. This discrepancy at the T3 level is again due to significantly larger rotations occurring in the lower spine under large loads in the present model. Thus, the linear approximations used in the present model appears to make the spine a bit too flexible in lateral bending at relatively large loads.

Next, effective bending and twisting stiffnesses[1] are compared with those reported by Andriacchi et al. [4] for the spine without the rib cage, Fig 6.2. As shown in the figure, the present model does not differentiate between flexion and extension behaviours since properties are assumed to be linear elastic. The overall lower bending stiffness of the present model is probably due to the use of somewhat lower stiffnesses of the motion segments. It may be recalled from Chapter 5, that these properties were obtained from tests conducted with a compressive preload. The presence of such preload can make these segments appear more flexible than they really are in lateral bending,

[1]Effective stiffness of the spine is used to describe the overall stiffness of the whole spine. For instance, in this case, the spine fixed at the base is subjected to bending and twisting moments applied at the top of the free end spine. The moments divided by the respective total rotation experienced by the top of the spine give the effective bending and twisting stiffnesses of the spine.

flexion and extension [121]. The effect is more likely to occur in the lumbar region, where

(a)

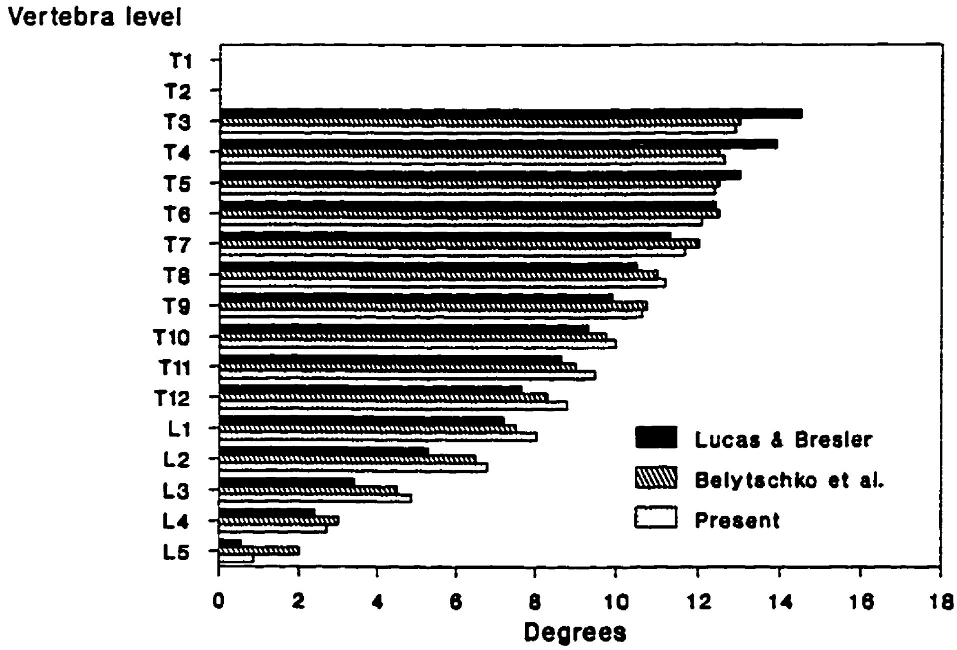

(b)

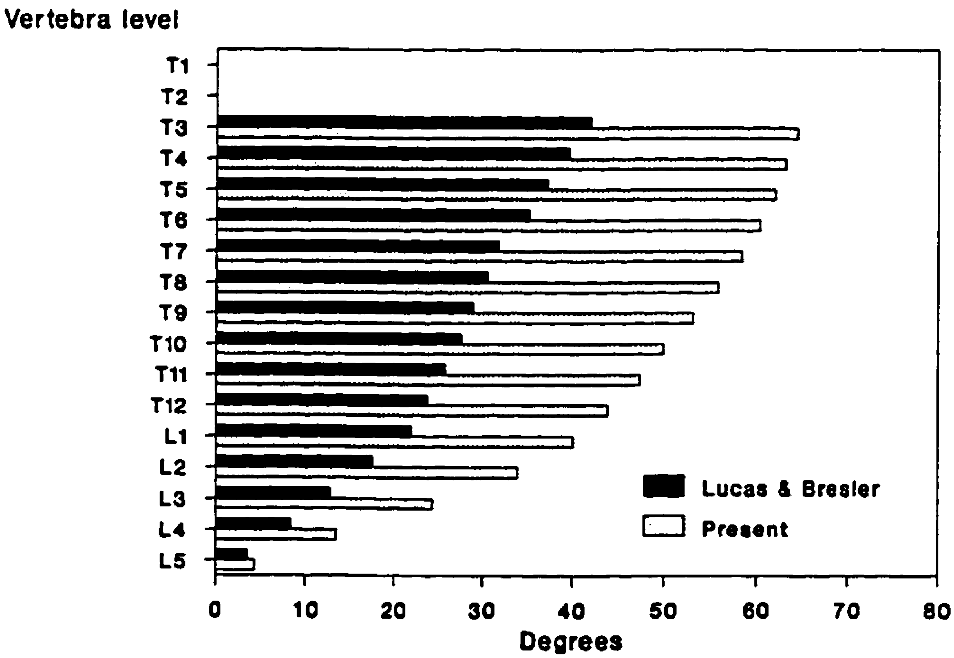

Fig. 6.1 Frontal plane rotations of vertebrae in the isolated ligamentous spine due to (a) 0.5 kg lateral load, and (b) 2.5 kg lateral load. Sacrum is considered fixed and application of the load is at the base of T1. Results for levels above T3 are not included because there are too many inaccuracies in the measuring of the small rotations in the in vitro study [73].

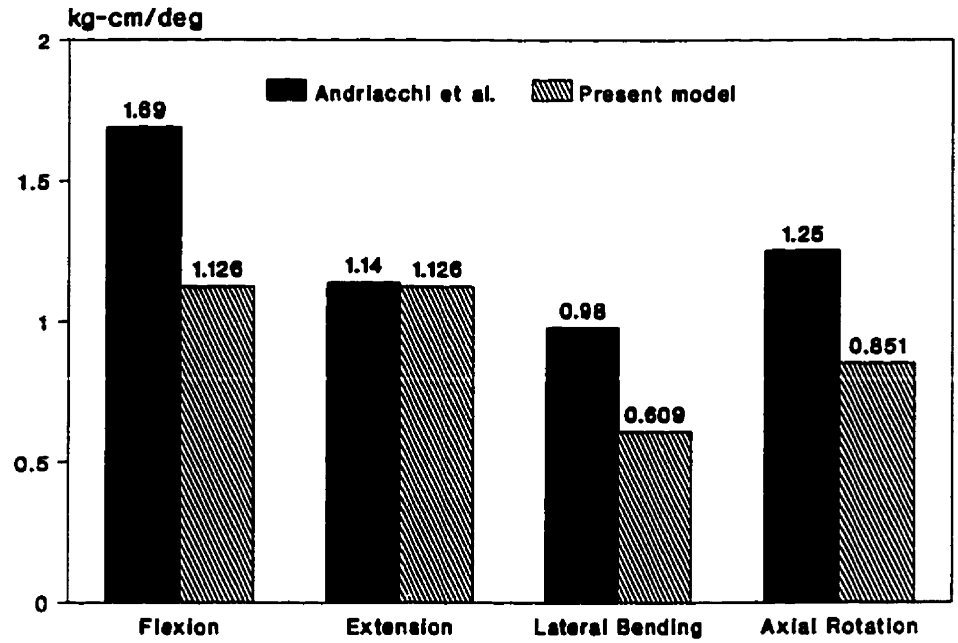

Fig. 6.2 Effective or overall bending and twisting stiffnesses of the ligamentous spine. Bending and twisting moments are applied at T1, while sacrum is fixed.

compressive load is larger and hence the simulated preload has a more significant effect on experimental results. Several lumbar motion segments with reduced lateral bending and flexion extension stiffnesses would tend to result in low overall lateral bending and flexion-extension stiffnesses. This may be another reason why the frontal plane rotations, Fig 6.1(a), in the lower spine are on the larger side.

Finally, the torsional-flexural bifurcation buckling loads of the spine model under compressive load at T1, for three different constraint conditions at T1, are determined. At the buckling load, the perfectly symmetrical spine, can assume an asymmetrical configuration involving lateral bending and twisting. The buckling mode gives some scaled magnitudes of the buckling deformations, but not their true or absolute magnitudes. (It may be recalled from Chapter 4, that this type of buckling analysis constitutes a linear eigenvalue problem).

The analysis considers the spine to be fixed at the sacrum and constrained in the mid-thoracic (node 13) and mid-lumbar (node 31) regions in the sagittal plane to simulate conditions of the experiments of Lucas and Bresler [73]. Using the global coordinate system defined in Fig. 5.1, the results for T1 free, T1 fixed in horizontal displacements and rotation (x, y, θ_z), and T1 fixed in all degrees of freedom except the vertical displacement (z) are shown in Table 6.1. Results are in good agreement. However, once again, it is apparent that the model tends to overestimate the stiffnesses at low loads, and underestimate them at high loads.

Table 6.1 Lateral Bifurcation Loads of Ligamentous Spine Under a Compressive Load (N)

Constraints at T1	Lucas and Bresler [73]		Belytschko et al. [10]	Present Study
	Exp.	Theor.*		
T1 free	19.13	20.50	20.60	24.06
T1 fixed in x, y, θ_z	166.77	167.75	196.20	168.55
T1 fixed in all but z displacement d.o.f.	-	327.65	313.92	297.90

* Theoretical results of Lucas and Bresler [73] are based on pure lateral buckling.

In the study by Belytschko et al. [10], the buckling mode shapes, resulting from the bifurcation analysis with T1 fixed in all but z displacement, were scaled by a factor such that the average lateral displacement would be the same as what is observed in a patient with thoracic idiopathic scoliosis in the study by Schultz et al. [111]. Since the main interest of this work lies in understanding scoliosis, the buckled mode shapes of the present ligamentous spine model corresponding to T1 constrained in all degrees of freedom but z displacement, denoted by condition 1, are similarly factored and compared to the factored mode shapes of Belytschko et al. [10] and the scoliotic patient. The factored frontal plane rotations and lateral displacements are shown in Figs. 6.3 and 6.4. It is evident that the presently computed results are similar to the results of Belytschko el. [10]. For the most part, the agreement is quite good for the frontal plane rotations, Fig. 6.3, except at the vertebral level T2 and T3. On the other hand, the lateral displacements, Fig. 6.4, are predicted to be significantly larger than in [10] especially in the lumbar region. These differences again confirm the fact that the present model is a bit too flexible in the lumbar region. In comparison to the scoliotic shape, the results differ in that the displacements and rotations are gradually increasing from zero from the end supports towards the middle.

Since the goal of the bifurcation analysis was to obtain scoliotic deformations, the accompanying axial rotation must be investigated. Belytschko et al. [10] report axial rotations, obtained by factoring axial rotation mode shape by the same factor used for other mode shapes, of negligible magnitudes compared to an apical axial rotation of 25° noted in the scoliotic patient [10].

The scaled mode shape of the axial rotation of the vertebrae in their model [10] is not given, nor is the data on the axial rotation of the vertebrae of the scoliotic patient. In the present study, the scaled axial rotations were noted to be concave-sided, i.e opposite to the rotation typical of scoliosis. According to the sign convention chosen, lateral displacements and horizontal (axial) rotations of the opposite sign indicate concave-sided rotation, while those of the same sign indicate convex-sided rotation.

However, the sagittal constraints at the mid-thoracic and mid-lumbar levels of the spine are artificial in comparison to the real spine. Thus, an analysis with T1 fixed in all but z displacement, without these constraints was performed. The results of this analysis, denoted as condition 2 in Figs. 6.3 - 6.5, are also compared with the scoliotic configuration. Release of the mid-sagittal constraints gives a slightly lower bifurcation load (289 N) and almost the same lateral displacement and frontal rotation mode shape as previously, Fig. 6.3 and 6.4. However, when the scaled axial rotations obtained from this latter analysis are compared with those in the case with the sagittal constraints (condition 1), the results are quite different, Fig. 6.5. The condition 2 scaled axial rotations are predicted to occur in the same direction as found in the scoliotic patient, with the maximum rotation coinciding with the maximum lateral displacement. However, the fact remains that these values are much smaller in comparison to the maximum rotation of 25° measured in the scoliotic patient [10].

In reality, the constraints at T1 are suspected to be somewhere between fixed in all directions except vertical displacement and fixed only in horizontal displacements and rotation [48]. It was found that the buckled spine achieved a lateral shape more similar to scoliosis when bending rotations at T1 were constrained than when they were allowed. For this reason, the bending constraints at T1 are imposed whenever possible in the present study. However, it is apparent that the buckling deformations are still not localized enough, and axial rotations are not large enough to correspond to deformations typical of idiopathic scoliosis.

It may be concluded that firstly, the above spinal model compares reasonably well with the results from previous researchers, indicating chosen stiffness properties and geometry of ligamentous spine are acceptable. Secondly, similar to previous findings, it appears that the bifurcation buckling of the normal spine cannot completely explain the localized deformations found in scoliosis.

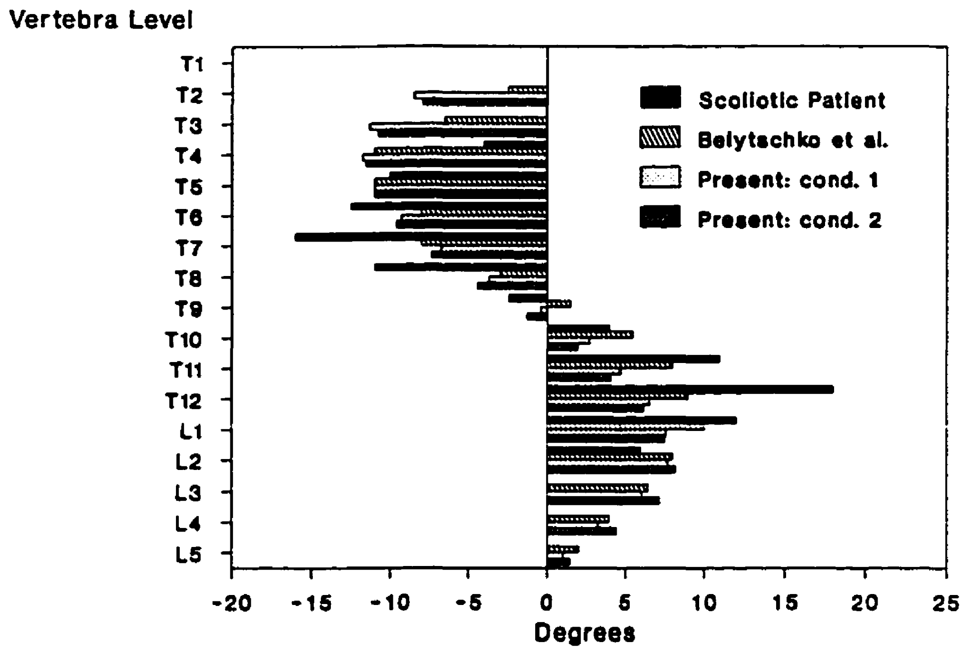

Fig. 6.3 Scaled mode shapes of frontal plane rotations of vertebrae in buckled ligamentous spine under compressive load at T1 compared with rotation of scoliotic patient. T1 is fixed in all but vertical (z) displacement, and sacrum is fixed. Condition 1 corresponds to additional sagittal plane constraints at the mid-thoracic and mid-lumbar levels. Condition 2 corresponds to no such additional constraints.

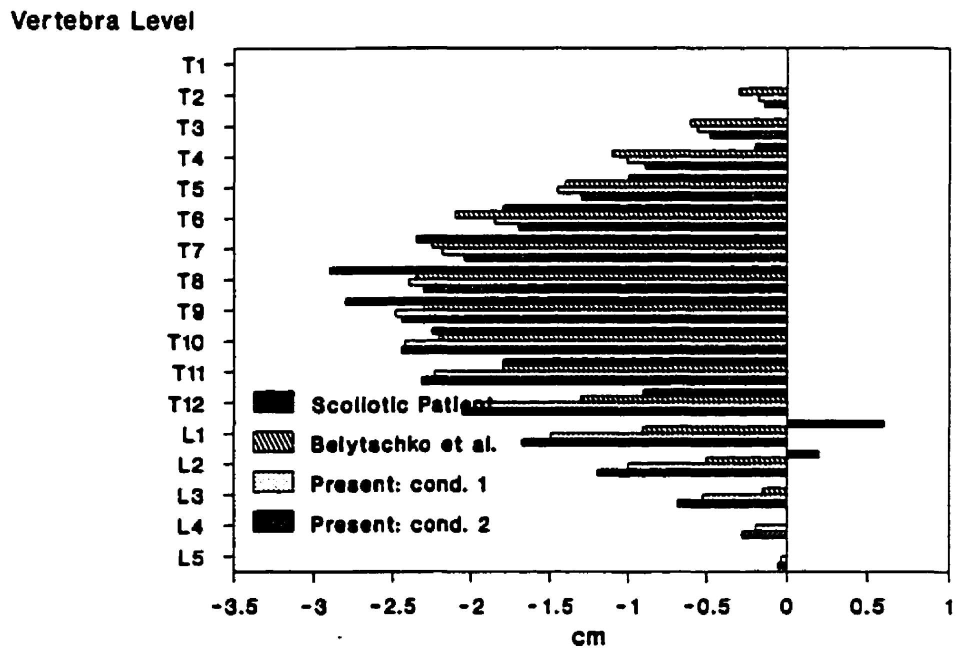

Fig. 6.4 Scaled mode shapes of lateral (frontal plane) displacements of vertebrae in buckled ligamentous spine under compressive load at T1 compared with displacements of scoliotic patient.

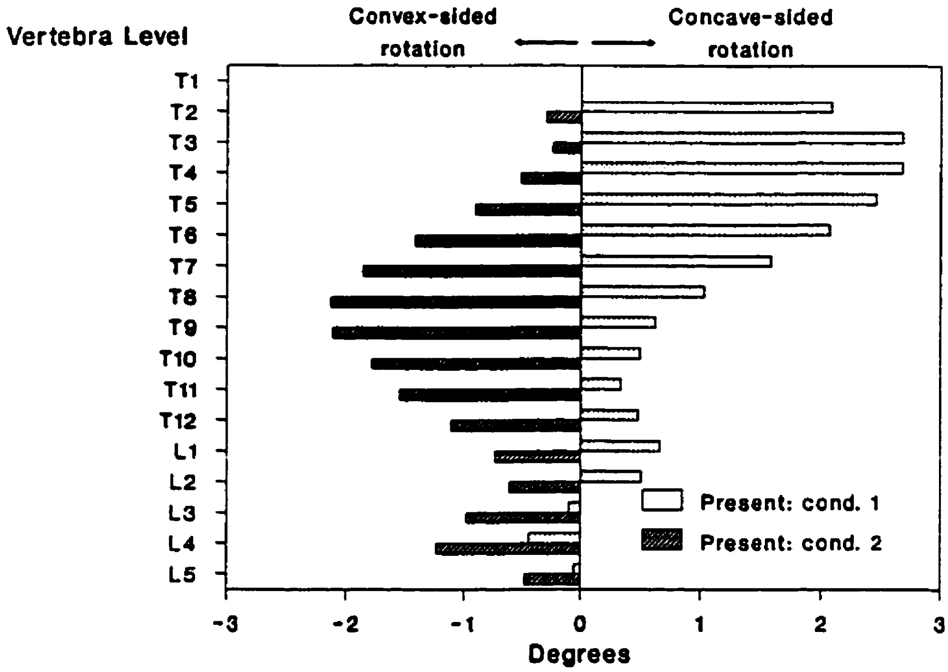

Fig. 6.5 Scaled mode shapes of axial (horizontal plane) rotations of vertebrae in buckled ligamentous spine under compressive load at T1.

6.1.2 Spine with Rib Cage Intact

Similar to the above analyses, experiments and analyses previously performed on the spine and rib cage structure are simulated and compared, in order to validate the properties and geometry of the rib cage used in the present work. Along with the study by Andriacchi et al. [4], which was used to compare the effective bending and twisting stiffnesses and the stability of the structure, two additional studies were used to validate the flexibility of the rib cage in the present model.

Agostoni et al. [2] subjected the relaxed rib cage of live subjects to a lateral squeezing force and measured resulting changes in the lateral and anterior-posterior diameters of the rib cage. The procedure is shown schematically in Fig 6.6. In the NASTRAN simulation of the procedure, the load was applied at the mid-axillary (IC) line, evenly distributed among the 5 lower ribs (ribs 6-10). Lateral displacements of the diameter are computed at the IC line of the middle ribs, i.e. rib 8 on both sides (nodes 264 & 269). Detailed description of the model with identification of nodes is given in Appendix C. The A-P displacements of the diameter are computed at the inferior end of sternum (node 253) and the most posterior points of rib 10 (node 273 & 284). With the sacrum fixed and T9 (node 17 & 18) constrained in the sagittal plane, the results are shown in Fig. 6.7. The A-P behaviour is apparently very similar to that observed in the real rib cage. However, the lateral deformation appears to be slightly small, indicating stiffer behaviour in this direction.

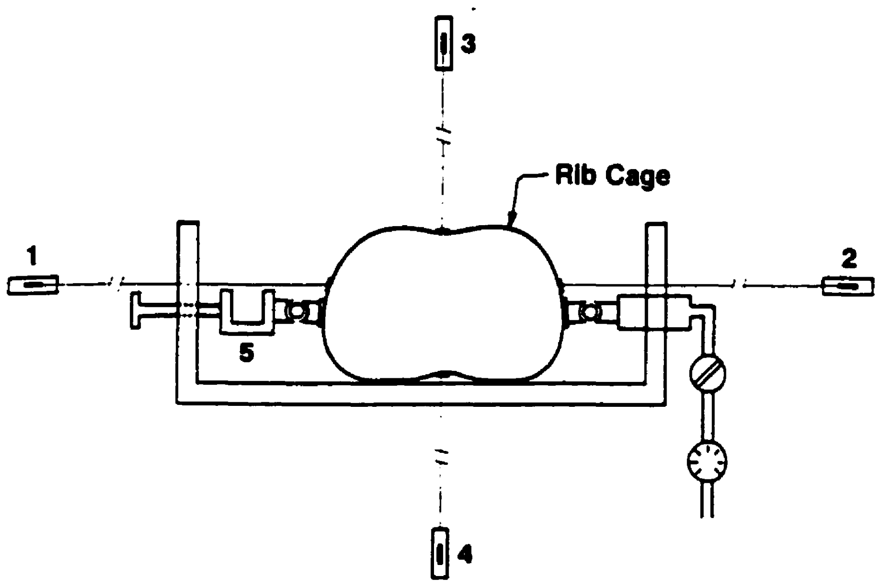

Fig. 6.6 Schematic diagram of the experimental set-up used by Agostoni et al. [2]. 1,2 = Lateral displacement transducer; 3,4 = A-P displacement transducer; 5 = Force transducer. Changes in the lateral and A-P diameters of rib cage are measured as functions of the applied lateral force.

Next, the sternum was loaded by horizontal forces directed posteriorly to simulate the experimental studies by Nahum et al. [82] and Patrick et al. [93]. Loads 0-12 kg in 4 kg increments were applied, half at the top of the sternum (node 168), half at the bottom (node 253) with T1 and T9 fixed in the A-P direction. Average posterior displacements of the sternum indicating A-P flexibility of the rib cage are shown and compared with the values from the above references and Andriacchi et al. [4] in Fig. 6.8. The figure shows the large scatter of experimental results. Both, Figs 6.7 and 6.8, reveal that the rib cage of the present model exhibits a generally stiffer behaviour than that of Andriacchi et al. [4] except in the A-P direction. However, in comparison to the experimental values and their scatter, the rib cage of the present spine model is similar to the Andriacchi et al. model [4] in that the model stiffness is between those obtained for the fresh and embalmed specimens.

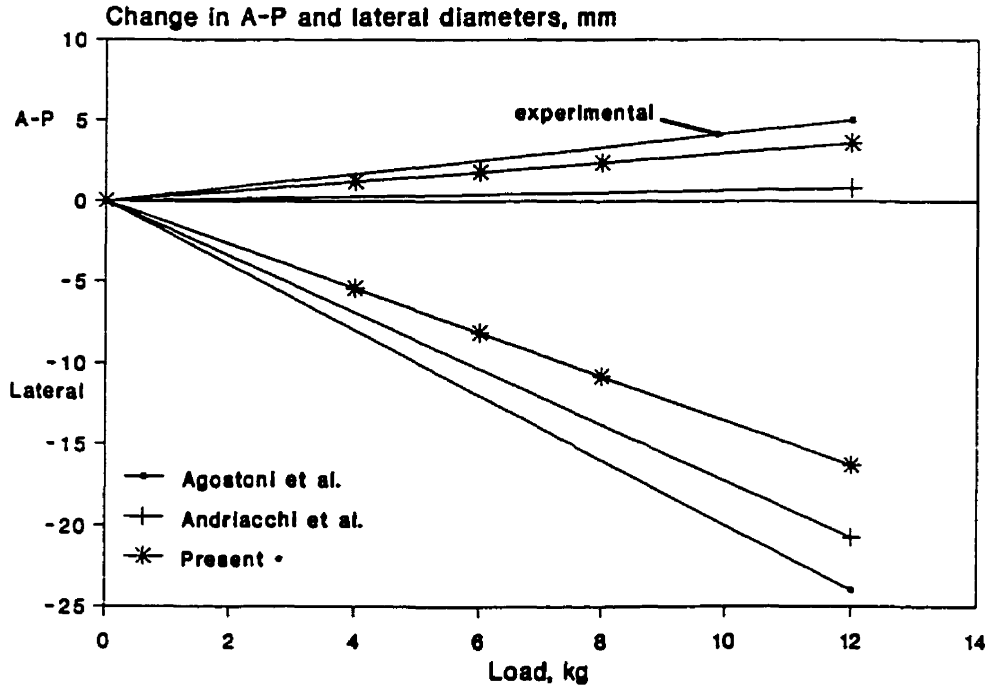

Fig. 6.7 Changes in A-P and lateral diameters of the rib cage resulting from lateral loading of rib cage. *Nodes used to determine changes in the diameters in present model are: 264 & 269 for lateral change, 253 & 273 or 284 for A-P change.

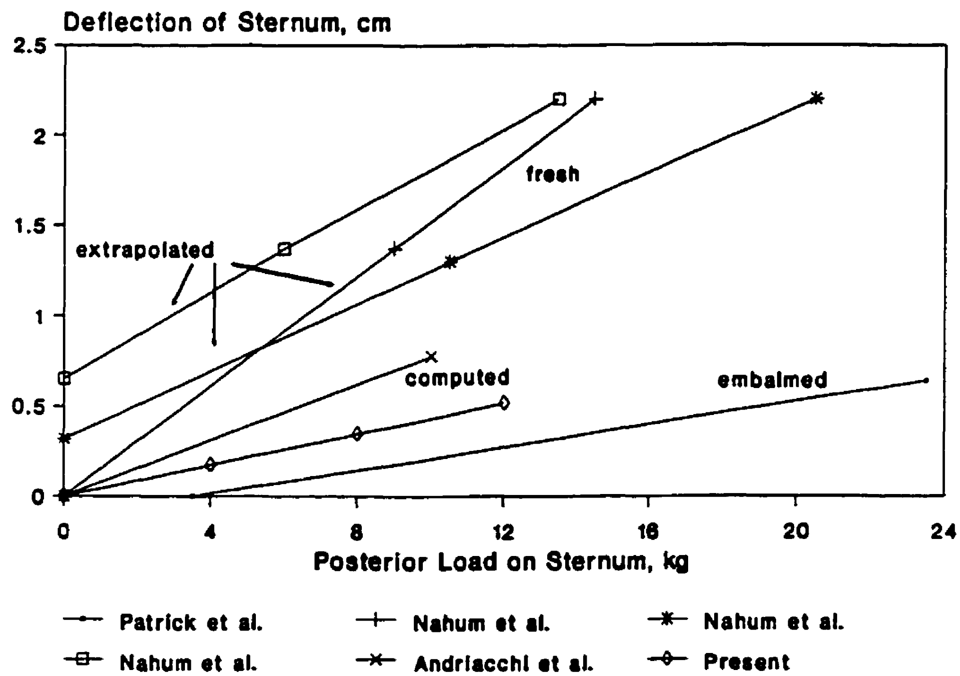

Fig. 6.8 Deflection of the sternum resulting from transverse loading of sternum in the posterior direction.

The effective bending and twisting stiffnesses of the spine with rib cage intact are illustrated in Fig. 6.9. The relative stiffening effect of the rib cage is shown in Fig. 6.10. The percentage in the figure represents the relative amount by which the effective stiffness of the spine with rib cage model is higher than the stiffness of the respective ligamentous spine model. It is apparent that the rib cage in the present model has a greater stiffening effect on the spine in lateral bending and especially in axial rotation than the one in the model by Andriacchi et al. [4]. Since the stiffnesses in flexion and extension must be the same in the present model, it is interesting to note that the rib cage stiffening effect of 172% compares very well with the average of such stiffening effects in flexion and extension (179%) in Andriacchi's model. Thus, it appears that the ligamentous spine of the present model (which is more flexible than the Belytschko et al. model [10]) and the rib cage of the present model (which is stiffer than the rib cage of Andriacchi et al [4]) combine themselves to produce a total spine and rib cage model which may be considered quite realistic, and not too different from the previous model [4].

The torsional-flexural bifurcation buckling loads under compressive load (a) concentrated at T1, and (b) distributed along the spine length proportional to weight distribution (Section 5.5) are shown in Table 6.2. Again the sagittal plane is artificially constrained from motion in the sagittal plane at the mid-thoracic and mid-lumbar levels so that a comparison with the results of Andriacchi et al. [4] can be made.

Table 6.2 Lateral Bifurcation Loads of Spine with Rib Cage Under a Compressive Load (N)

T1 Constraints	Andriacchi et al. [4]	Present study	
		Conc.	Dist.
T1 free	78.48	27.19 (65)*	58.25 (26)
T1 fixed in x,y,θ_z	608.22	307.75 (49)	543.35 (11)
T1 fixed in all d.o.f but z displacement	990.81	453.94 (54)	764.27 (23)

* The values in the parentheses give the percent difference from Andriacchi et al. [4].

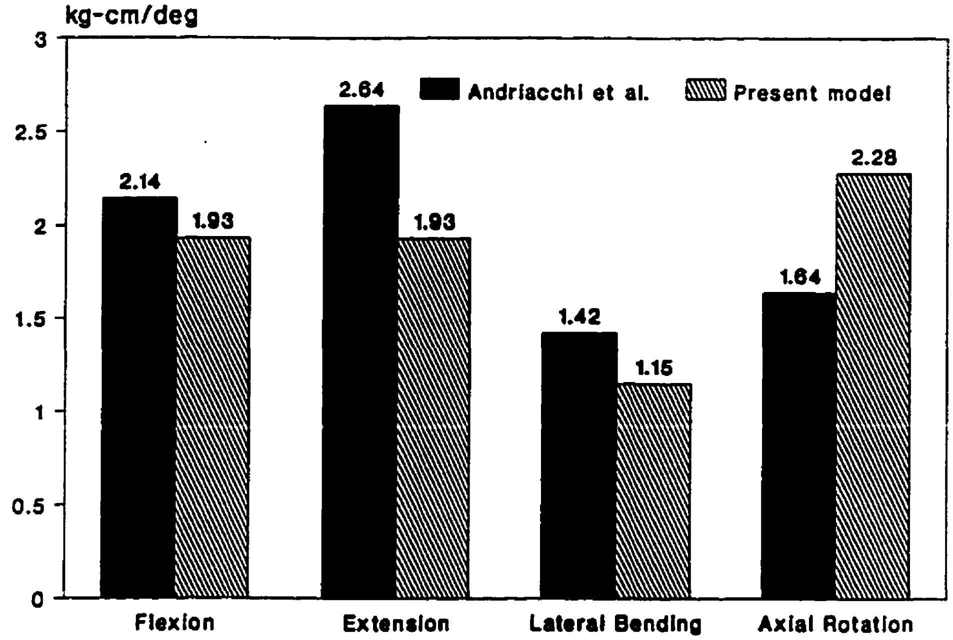

Fig. 6.9 Effective (i.e. overall) bending and twisting stiffnesses of the spine with rib cage.

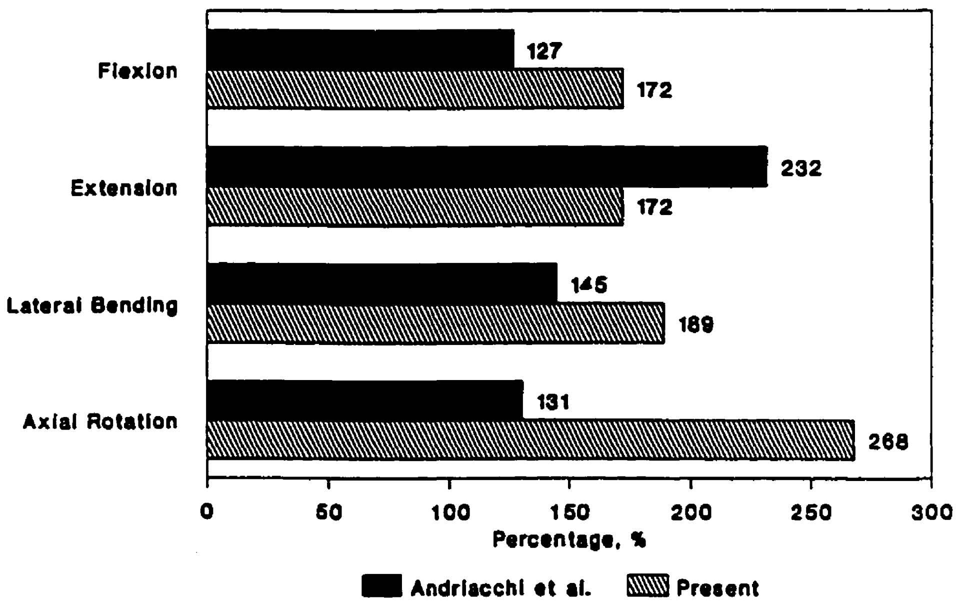

Fig. 6.10 Relative stiffening effect of rib cage on the ligamentous spine, in percentage.

It is apparent that in each case the buckling load is smaller than that obtained by Andriacchi et al. [4]. The discrepancy is larger for the lumped load case than for the distributed one. Possible explanations for large discrepancy between the results of the present model and that of Andriacchi et al. [4], may be the small size of the rib cage of the present model, an underestimate of the stiffnesses of soft tissue connections, and the linear approximations of stiffnesses. Unfortunately, there are no results from real specimens, which could be used for comparison. However, Andriacchi et al. [4] do state that based on the experimental studies on rib cage used for comparison, their model appears to be representative of spine and rib cage; although they do feel that more data on rib cage are necessary in order to fully validate it. Considering the large variation between subjects and the difficulty of defining "normal", it is felt that present model is an acceptable representation of the spine and rib cage structure. It is this structure on which structural analyses are performed in this thesis.

With respect to the resulting mode shapes, it can be seen that the imposition of bending constraints at T1 slightly lowers the apex of the lateral buckling curve but, as mentioned before, results in an overall shape closer to the scoliotic shape. The distributed loading lowers the apex most appreciably in comparison to that due to the concentrated loading. The reason is quite obvious, since in the former case less loading is applied at the top, and it increases gradually with descent along the spine. Apart from the lowered apex of the lateral curve and slight differences in direction of the axial rotation, the mode shapes between the concentrated and distributed cases are quite similar. Finally, in comparison to the ligamentous spine, the inclusion of the rib cage also effectively lowers the apex of the buckled lateral curve by one vertebral level.

6.2 Effect of Thoracic Lordosis on Spine Stability and Scoliosis

The results of this section are concerned with the testing of one interpretation of the lordosis hypothesis. The premise is that a spine with lordosis in the thoracic region is less stable than the normal spine (with the usual kyphosis in this region). The inference from reading the literature [34] is that a precondition to the subsequent development of scoliosis is that a spine has a lordosis along with a horizontal or frontal plane asymmetry in the thoracic region. It is conjectured that this lordosis has the potential to turn into a scoliotic spine. If true, this finding will have the diagnostic value in that adolescents with lordosis in the thoracic region would be classified as having high potential of developing scoliotic spines, and could be recommended for a corrective treatment.

The finite element simulation of the above interpretation of the hypothesis is performed in the following way. First, as previously mentioned, a so-called lordotic spine model is created by lengthening the anterior and shortening the posterior heights or lengths of the thoracic vertebrae of the normal spine and rib cage model, while maintaining strict symmetry about the sagittal plane. Second, this lordotic model and the normal model are loaded with distributed and lumped gravity loads to find and compare their torsional-flexural bifurcation buckling loads in an attempt to show that the spine with the lordosis in the thoracic region is less stable than the normal one. In addition, the results from the analysis on the lordotic model are used to determine the approximate load near which relatively large deformations would begin to occur in the imperfection growth analysis, and the expected mode in which they would grow. The third step is to subject the lordotic model, which has lateral and horizontal plane spinal asymmetries imparted, to a nonlinear imperfections growth analysis by increasing the gravity-like load in small increments starting from zero.

6.2.1 Creation of Lordotic Model

As discussed in Chapter 5, a spine and rib cage model with a thoracic lordosis is created for the use in the bifurcation analysis and in the imperfection growth analysis. This is accomplished, as may be recalled, by subjecting the normal spine to lordosis inducing changes in the dimensions of the thoracic vertebrae. The resulting, structurally deformed, configuration is adopted as the initial (unloaded) geometry of the lordotic model, i.e. with a spine with a lordosis in the thoracic region. As explained in Section 5.3.2, the creation of the lordotic model by the above procedure requires the 3-element normal model, which to reiterate, represents each vertebra and intervertebral joint element with 3 beam elements representing their anterior, central, and posterior parts in the sagittal plane. The lordotic geometry is obtained by loading the normal 3-element model with appropriate [30] shortening of the posterior and lengthening of the anterior beam elements of the thoracic vertebrae T4-T12. The formulas used for determining the equivalent properties of the anterior, posterior and central intervertebral joint and vertebra elements in the 3-element model, shown in Appendix B, use the approximation that the 3 element lengths are equal.

The structural equivalence of the 3-element model is checked by comparing the analysis results with the corresponding 1-element model for the cases of the ligamentous spine, and the spine with rib cage. Items used for comparison are (1) the critical buckling loads and the buckled mode shapes of the models, and (2) the effective bending and twisting stiffnesses. For the bifurcation buckling analysis, the spine is constrained in all degrees of freedom at T1 except the vertical displacement, fixed at the sacrum, and constrained against displacement at the mid-thoracic and mid-lumbar levels in sagittal plane. For the ligamentous spine, compressive loading is concentrated at T1, and for the spine with rib cage, the loading is distributed. The comparison is shown in Table 6.3. In the case of the ligamentous spine, the buckling loads differ by 0.3% and for the spine with rib cage, 0.5%. The buckled mode shapes of the 1-element and 3-element models are practically identical for both cases. Similarly, the effective stiffnesses are in agreement. This agreement then demonstrates that the 3-element representation is equivalent to the 1-element representation, and hence the 3-element spine and rib cage model may be used to construct the lordotic model, i.e. spine and rib cage model with lordosis in thoracic region.

Table 6.3 Comparison of 3-element models to 1-element models

Spine model	Critical load, P_{cr} (N)	Effective stiffness (kg-cm/deg.)		
		Flex.-exten.	Lat. bend.	Axial rot.
Ligamentous spine				
1-element	297.9	1.126	0.609	0.851
3-element	297.0	1.126	0.609	0.855
Spine with rib cage				
1-element	764.3	1.934	1.155	2.281
3-element	760.4	1.934	1.163	2.281

The lordotic spine and rib cage model so created is named LARRY, and is shown in Fig. 5.6. The new vertical length of the spine is 49.44 cm compared to the previous length of 48.21 cm of the normal spine. The elongation of 1.23 cm is mainly due to the straightening effect of the spine since the change in the curved length is only 0.67 cm. By representing the resulting 3-element lordotic spine with center vertebra and intervertebral joint elements only and assigning them the full stiffness of the vertebra and intervertebral joint elements, the 1-element lordotic model used in subsequent analyses is obtained.

6.2.2 Comparative Linear Bifurcation Analyses

Bifurcation analyses are performed on the (1-element) normal and lordotic models. As previously mentioned, they are carried out for two purposes: (1) to compare bifurcation buckling of normal and lordotic models, and (2) to determine the approximate load near which the spinal imperfections in the lordotic model would begin to grow.

As part of the analysis, the buckling mode shapes are scaled as previously described in section 6.1.1 and compared with scoliotic shape. Although data on the lateral displacements and frontal rotations of the vertebrae of a scoliotic patient were given by Belytschko et al. [10], data on the axial rotation of the vertebrae were not. Belytschko et al. stated that the scoliotic patient had an apical (maximum) rotation of 25°. The data from this one patient with thoracic scoliosis were again used for comparison in these analyses. Two loading cases are considered in the bifurcation analyses. One is the distributed loading which was considered in validating the model. The other is a lumped compressive load at the center of gravity of the body weight above the sacrum; the center of gravity is rigidly connected to the top vertebra T1. In both cases, the mid-sagittal plane is free from all artificial constraints.

Distributed Loading Case

The spine is considered fixed at the sacrum, and fixed in all but vertical directions at T1. This loading case with these constraints is felt to be the most realistic for reasons mentioned previously. For the normal spine, the lowest bifurcation buckling load is a sum of 762 N. Once again, the mode shapes scaled by a factor which gives lateral displacements comparable to scoliotic shape, are compared to scoliosis shape, Fig. 6.11 - 6.13. It appears that the deformations are not localized enough and axial rotations are not significant enough to be scoliotic. However, it should be noted that the directions of the axial rotations and their pattern (i.e. location of their maximum at the apex of the lateral curve) are similar to scoliosis below the T6 level.

In comparison, the lordotic spine is approximately 2.5% less stable in the sense that its critical bifurcation load is a sum of 743 N. This is not a significant decrease from the normal spine load and may be explained as primarily due to the lengthened spinal column without significant influence of the reduced curvature. Likewise, the mode shapes from the normal and lordotic model are quite similar as indicated in Figs. 6.11 - 6.13 except that the axial rotations of the scoliosis kind (Fig. 6.12) occur through the full length of the spine in the lordotic model.

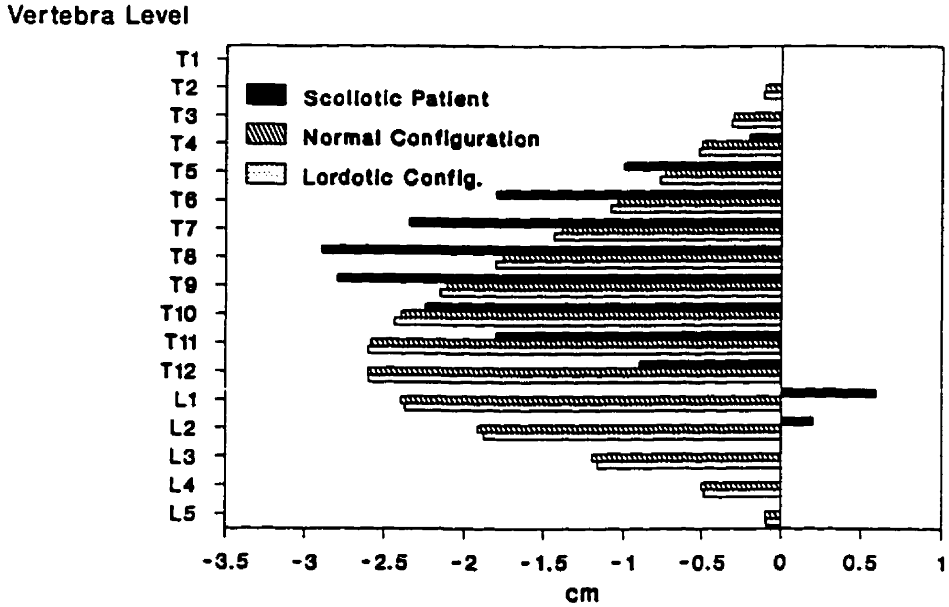

Fig. 6.11 Scaled mode shapes of lateral displacements of vertebrae of buckled spine with rib cage in normal and lordotic models under distributed loading compared with displacements of scoliotic patient. The models are considered fixed at T1 in all but vertical displacement, and completely fixed at the sacrum.

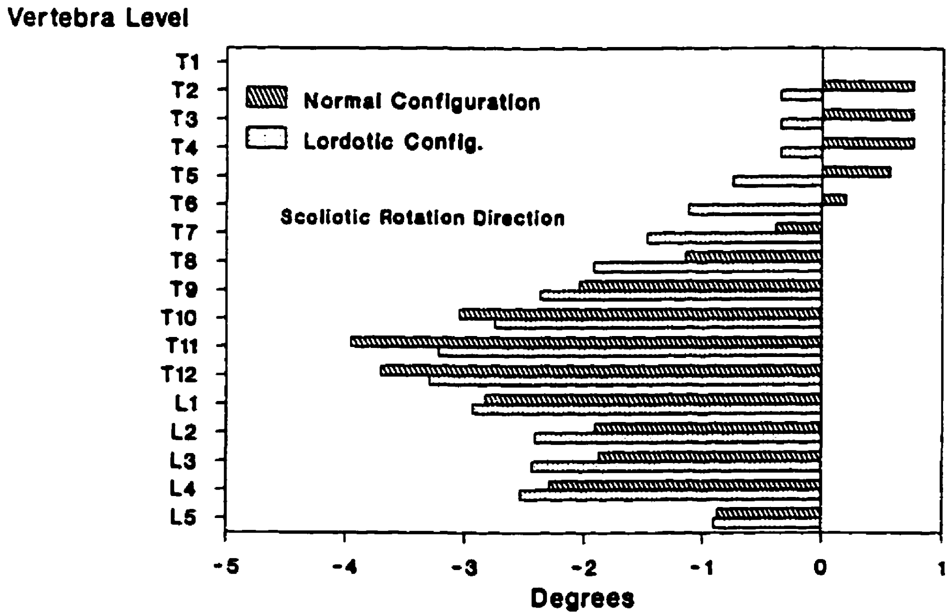

Fig. 6.12 Scaled mode shapes of axial (horizontal plane) rotations of vertebrae of buckled spine with rib cage in normal and lordotic models under distributed loading. T1 is fixed in all but vertical displacement, and sacrum is completely fixed.

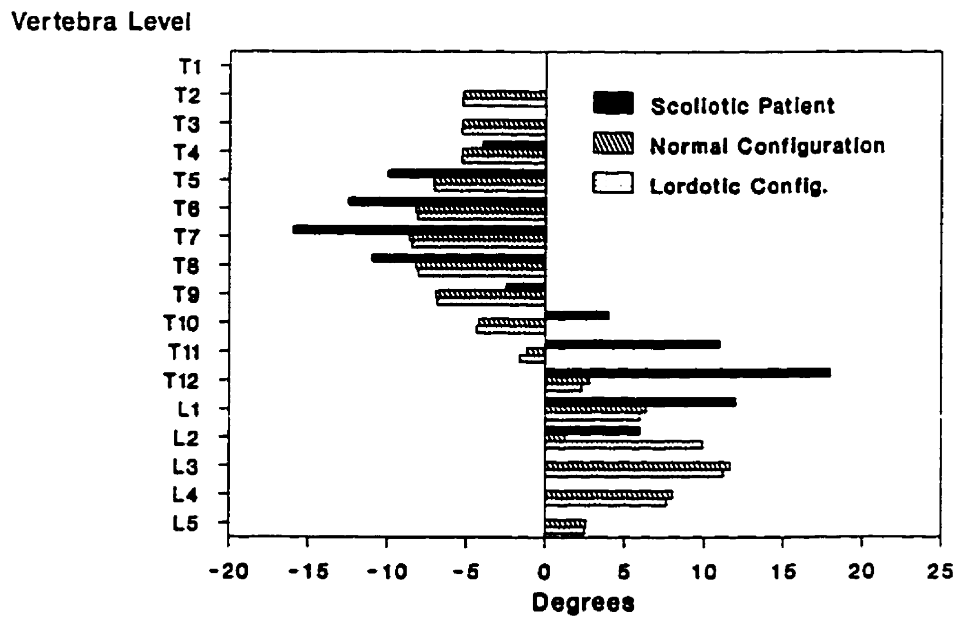

Fig. 6.13 Scaled mode shapes of frontal plane rotations of vertebrae of buckled spine with rib cage in normal and lordotic models under distributed loading compared with rotations of scoliotic patient. The models are considered fixed at T1 in all but vertical displacement, and completely fixed at the sacrum.

Center of Gravity (Lumped) Loading Case

In reality, the spine is loaded by the distributed body weight which is eccentric relative to the spine. Similar to the loading previously seen, a realistic modelling would therefore require that the spine be loaded at each vertebral level by a slice of body weight acting eccentrically at its center of gravity. However, as noted previously, in scoliosis this eccentricity varies with the deformation by virtue of the fact that while the spine displaces and rotates relative to the body, the weight distribution continues to maintain its position relative to the body. This stationary gravity loading is important in attaining scoliotic deformation. The upper body weight remaining in the sagittal plane causes lateral bending moments in existing lateral curves, which subsequently causes continual growth of lateral deformity. In the nonlinear analysis procedure of NASTRAN, the loads applied to the structure move with the structure. Hence it appears that NASTRAN cannot be used to model the distributed gravity loading in the nonlinear analysis of the spine attempting to simulate scoliotic deformation.

Since one objective of the present bifurcation analysis is to find the approximate load at which imperfections would begin to grow significantly in a nonlinear imperfection growth analysis, the bifurcation analysis (which is a linear analysis) should be carried out for the same type of loading as permitted and used in the growth analysis. Hence as a compromise with the limitations of NASTRAN, the distributed load is replaced by an equivalent concentrated force and moment at the top (vertebra T1) of the spine. It may be recalled from Chapter 5 that the eccentricity of the weight acting on the spine works out to be 2.98 cm anterior to T1. Hence the applied load for bifurcation analysis, as well as the subsequent growth analysis, is an axial compressive force P (N) and a flexion moment M = 2.98 P (N-cm). This approximation is not a bad one since a significant percentage of weight is in the upper region by virtue of the weight of the head and upper extremities.

With T1 fixed against horizontal (x, y) displacements and horizontal (θ_z) rotation[1], the critical bifurcation load corresponding to torsional-flexural buckling of the normal model is 278 N axial force and 827 N-cm flexion moment compared to 261 N and 779 N-cm for the lordotic model. Thus, in this case, the lordotic model turns out to be 5.8% less stable in torsional-flexural buckling. This result is in support of the lordosis hypothesis according to which a lordotic spine is more susceptible to scoliosis. As discussed in Chapter 4, the reduced stability in the lordotic model may be explained by the decreased curvature in the thoracic spine in the direction of the applied forward flexion moment [123] in addition to a longer effective length. Although the loading, since it is lumped at T1, is not very realistic for the human body, it is used here for relative comparison. The scaled buckling mode shapes of the models with normal and slightly lordotic spines, shown in Fig. 6.14 - 6.16, are practically identical with the exception of the axial rotations. The axial rotations of the lordotic spine although of a similar pattern as that of the normal spine are predicted to be smaller by approximately 25% at the T9-T10 levels, Fig. 6.15. In comparison with the scoliotic shape, the spines in both models lack localization of deformity and relative magnitudes of axial rotation. Nevertheless, the rotational mode shapes are scoliotic-like, i.e. convex-sided rotations with the maximum rotation occurring at the apex of the lateral curve.

---

[1]The two bending degrees of freedom are released at T1. Sagittal bending is released because moment is applied at T1; moment would have no effect on the column if T1 were fixed. Bending in lateral plane is free because anatomical constraint is same in both planes, somewhere between fixed and free bending degrees of freedom [48]. In the nonlinear analysis, a greater rotational constraint in the lateral plane may cause predominant growth to occur in the A-P plane.

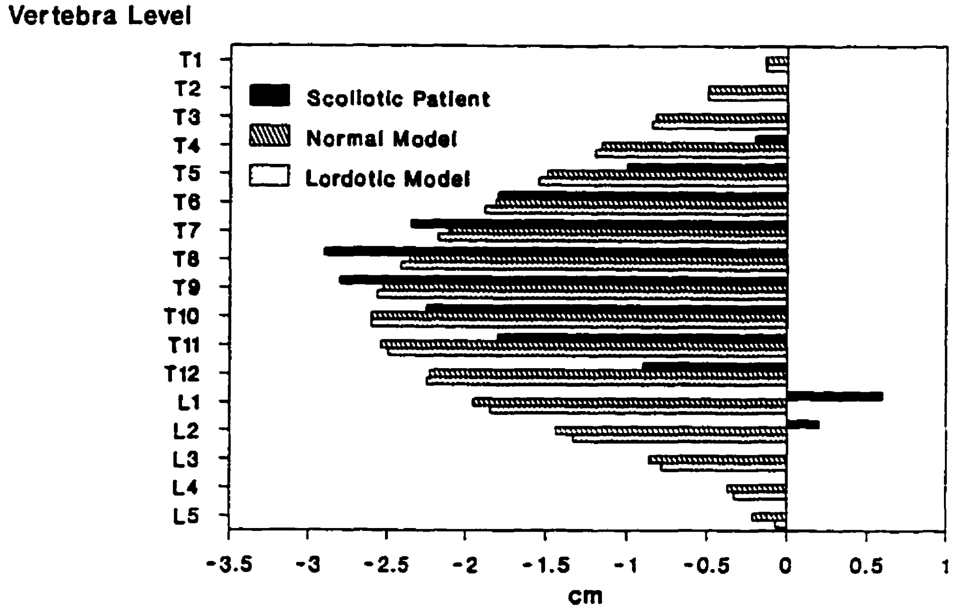

Fig. 6.14 Scaled mode shapes of lateral displacements of vertebrae of buckled spine with rib cage in normal and lordotic models under lumped force and moment loading at T1 compared with displacements of scoliotic patient. The models are considered fixed at T1 in horizontal displacements and rotation, and completely fixed at sacrum.

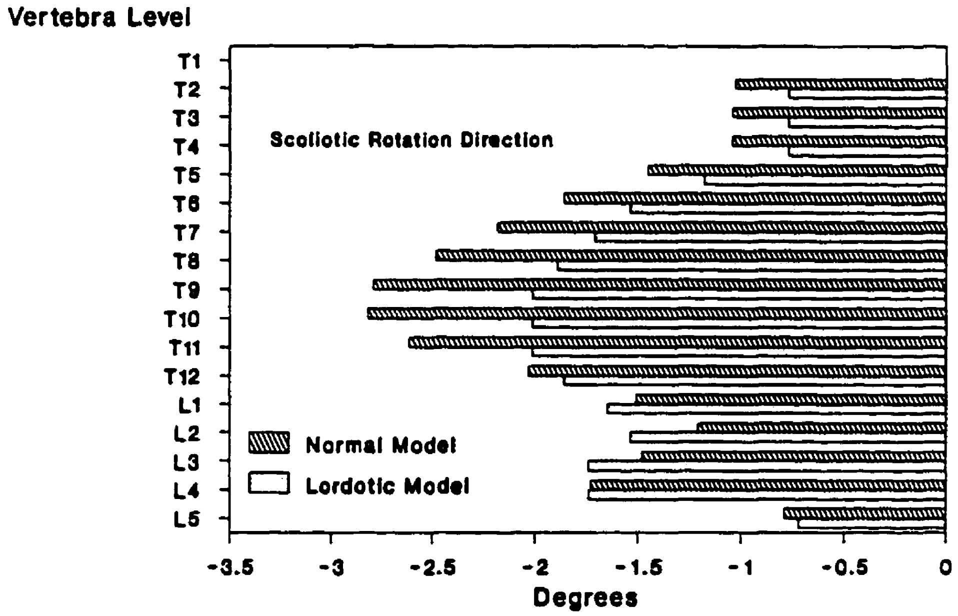

Fig. 6.15 Scaled mode shapes of axial (horizontal) rotations of vertebrae of buckled spine with rib cage in normal and lordotic models under lumped force and moment loading at T1. The models are considered fixed at T1 in horizontal displacements and rotation, and completely fixed at sacrum.

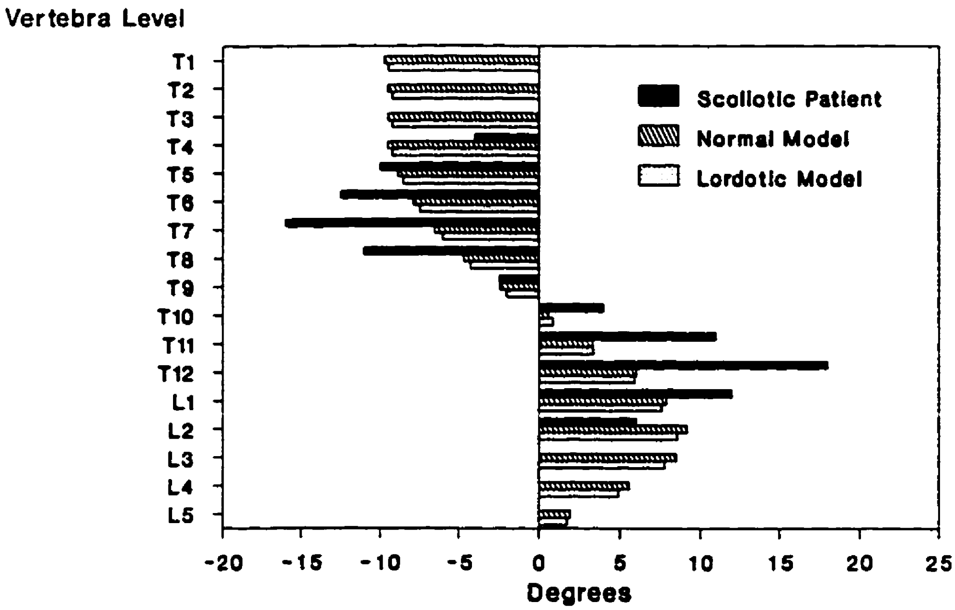

Fig. 6.16 Scaled mode shapes of frontal plane rotations of vertebrae of buckled spine with rib cage in normal and lordotic models under lumped force and moment loading at T1 compared with rotations of scoliotic patient. The models are considered fixed at T1 in horizontal displacements and rotation, and completely fixed at sacrum.

Thus, based on these bifurcation results, it appears that although the presence of the thoracic lordosis has some effect on lowering the critical bifurcation load, it has little effect on the resulting mode shapes. In both loading cases, the mode shapes of the normal and lordotic models are very similar, with the maximum lateral displacement occurring at the same level as the maximum convex-sided rotation. Thus, lordosis has little influence on creating deformations more similar to scoliosis than those produced in the absence of it. In fact, the magnitudes of the convex-sided rotations are of a smaller magnitude relative to the lateral displacements in the model with the lordotic spine in both distributed and lumped loading cases. In addition, although relatively large axial rotations were found at the L3 and L4 levels (which are not near the apex of the lateral curve) for both normal and lordotic models under both loadings, these rotations in the lordotic model tend to be significantly closer to the maximum magnitudes than those in the normal model, especially under lumped loading condition. It was also noted that the lordosis had a greater effect in reducing the critical load when the loading was comprised of the compressive force and forward (flexion) moment, although this loading produced less axial rotation relative to the lateral deviation in both models.

Conclusions drawn from the above bifurcation analyses are similar to those derived from the analysis of the ligamentous spine. The most important one is that buckling due to compressive (gravity-type) loading cannot explain scoliosis. Results give very diffused buckled mode shapes and, it appears that the introduction of a lordosis in the initial geometry has no influence on localizing the deformations or increasing the magnitudes of the axial rotations (in fact, it reduces them). On the other hand, deformations of the type revealed by the buckling analyses (lateral deviation and convex-sided axial rotation) are the same as those found in a localized manner in scoliosis. Thus, it appears that although scoliosis is related to the buckling phenomenon, it is not a result of buckling under compressive loading of the type considered above.

6.2.3 Imperfection Growth Analysis

The bifurcation buckling analyses of the preceding section predicted the critical load at which a perfectly symmetrical normal or lordotic spine would buckle laterally. It also predicted the mode shapes of ensuing infinitesimal buckling deformations. However, it does not provide any information on the actual amount of buckling deformations as functions of load. To obtain such information, a nonlinear post-buckling analysis is called for.

As already has been indicated, the usual way to obtain such information is to abandon the approach of bifurcation analysis of a perfect system, and instead perform a nonlinear growth analysis of a system which is initially slightly imperfect. The imperfections begin to grow with the increase of the load from zero. However, generally speaking, the rate of growth remains small, until the load approaches (from below) a value close to the critical bifurcation load. As the bifurcation load is approached the rate of imperfection growth increases and the accumulated imperfections begin to impart the column an increasingly buckled configuration. An example of such approach has been present in Chapter 4 when the growth of an initially curved column was studied.

The advantage of a growth analysis is obviously the fact that the actual deformations may now be determined uniquely as functions of load. However, there is no precise value for a buckling load; it can be taken as any load at which imperfections are deemed to have become excessive. The major disadvantage is that an expensive, iterative, nonlinear analysis is required in which load is applied incrementally, and the spine geometry is updated at each increment of the load consistent with the equilibrium of the structure in its deformed state. As is usual in nonlinear problems, convergence problems may arise, either because the load increment is too large, or because the maximum load the system is capable of sustaining is reached. In this work convergence problems were averted by keeping the load increments sufficiently small, and by keeping within only moderately large deformations. The convergence criteria used in the geometric nonlinear analysis in this study are the load equilibrium error test and the work error test with error ratio tolerances of $5x10^{-3}$ and $5x10^{-7}$ respectively. This means that convergence is considered to be achieved when the ratios of the unbalanced load error and the unbalanced work error to the increment of the load or the work in the load step are smaller than the tolerances.

In this part of the investigation, growth analysis was performed on the lordotic model. The initial spinal imperfections imparted to the model correspond to asymmetries with respect to the sagittal plane, of two kinds: (1) a slight right lateral curve in the thoracic region of the spine in the frontal plane, and (2) slight asymmetrical orientation of the cross-sections of thoracic vertebrae in the horizontal plane. As mentioned previously, both imperfections can be considered naturally present to some degree in all spines due to the position of the aorta [31,34,117].

The right lateral curve considered in the present model is tabulated in Table 6.4, and shown graphically in Fig. 6.17. It can be seen that the imperfection is taken to extend from vertebrae levels T4 - T10, with a maximum amplitude of 8 mm (in comparison to the length of the spine 48.2 cm) at the T8 level. The cross-sections of vertebrae T4 - T10 themselves are also distorted due to the presence of the aorta on the left side. This asymmetry is such that one of the principal planes no longer coincides with the sagittal plane. In the absence of any guiding data, the transformed principal axes are taken to be maximum of 10° from symmetrical principal axes, again at the T8 level in view of the fact that the vertebrae most affected by the aorta will have maximum lateral as well as horizontal plane distortions. Figure 6.18 illustrates the bottom view of the asymmetry of a typical vertebra. Keeping consistent with local coordinate system defined earlier for symmetrical vertebrae/intervertebral joints in Fig. 5.7, where local x-y plane defines plane 1 and local x-z plane defines plane 2 which coincides with the A-P or sagittal plane, the distorted cross-section requires specifications of transformed moments of inertia in the those same planes (now denoted 1′ and 2′), I_1' and I_2' as well as the product of inertia I_{12}'. The vertebrae being rigid are structurally unaffected by this small rotation. However, the intervertebral joints, which are greatly affected by the posterior elements and connecting ligaments of the vertebrae, effectively have new principal axes. These quantities calculated for the superior and inferior ends of the intervertebral joint are listed in Table 6.5.

Table 6.4 Initial Frontal Plane Asymmetries: Lateral Curve of Spine (Y-coordinates, cm)

(a) Y-Coordinates of Spine: Normal and Lordotic Models

Spine Element	Central line		Anterior line*		Posterior line*	
	Node No.	Y, cm	Node No.	Y, cm	Node No.	Y, cm
T4	7	0	42	-.03	77	0
	8	-.15	43	-.18	78	-.13
T5	9	-.18	44	-.20	79	-.15
	10	-.37	45	-.38	80	-.36
T6	11	-.40	46	-.42	81	-.38
	12	-.60	47	-.60	82	-.60
T7	13	-.63	48	-.63	83	-.62
	14	-.80	49	-.80	84	-.80
T8	15	-.80	50	-.80	85	-.80
	16	-.72	51	-.74	86	-.70
T9	17	-.65	52	-.70	87	-.60
	18	-.20	53	-.26	88	-.14
T10	19	-.12	54	-.16	89	-.08

* Necessary for nonlinear analysis in which lordosis-inducing growth is simulated, Section 3.2.

(b) Y-Coordinates of Costovertebral Joint on Vertebrae Side and Rib Side: Normal Model

Rib No.	CV on left vertebrae		CV on right vertebrae		CV on left rib		CV on right rib	
	Node no.	Y, cm	Node no.	Y, cm	Node no.	Y, cm	Node no.	Y, cm
5	113,114	1.38	131,132	-1.66	214	1.38	228	-1.66
6	115,116	1.18	133,134	-1.92	229	1.18	245	-1.92
7	117,118	.98	135,136	-2.20	246	.98	260	-2.20
8	119,120	.87	137,138	-2.47	261	.87	272	-2.47
9	121,122	1.11	139,140	-2.41	273	1.11	284	-2.41
10	123	1.79	141	-1.95	285	1.89	294	-2.05

(c) Y-Coordinates of Costovertebral Joint on Rib Side: Lordotic Model*

Rib No.	CV on left vertebrae		CV on right vertebrae		CV on left rib		CV on right rib	
	Node no.	Y, cm	Node no.	Y, cm	Node no.	Y, cm	Node no.	Y, cm
5	113,114	1.38	131,132	-1.66	214	1.386	228	-1.666
6	115,116	1.18	133,134	-1.92	229	1.236	245	-1.976
7	117,118	.98	135,136	-2.20	246	1.023	260	-2.243
8	119,120	.87	137,138	-2.47	261	0.906	272	-2.516
9	121,122	1.11	139,140	-2.41	273	1.085	284	-2.385
10	123	1.79	141	-1.95	285	1.851	294	-2.011

* Y-coordinates of CV on vertebral side are the same as in the normal model.

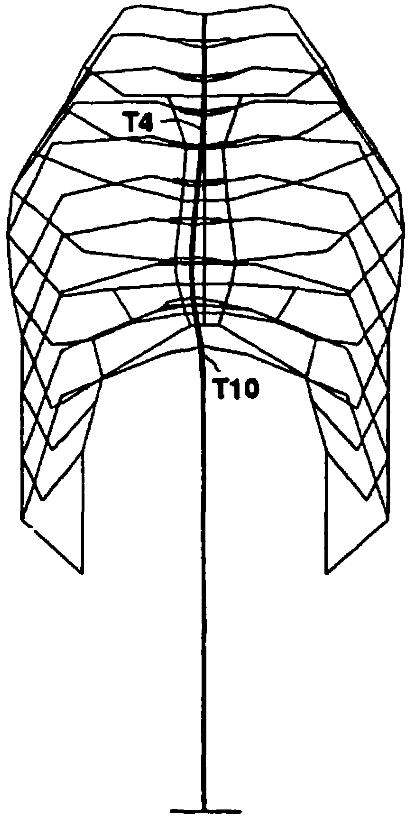

Fig. 6.17 Anterior view of initial lateral curve of spine used in the nonlinear growth analyses. The heavy line shows the lateral curve introduced.

Table 6.5 Initial Horizontal Plane Asymmetries: Transformed Sectional Properties of Intervertebral Joints

Superior Vert. of I.V. Joint	I_1 (cm^4)	I_2 (cm^4)	Nodes, sup. inf.	θ degree	I_1' (cm^4)	I_2' (cm^4)	I_{12}' (cm^4)
T3	1.716	3.643	5 6	0 2	1.716 1.718	3.643 3.641	0 –.067
T4	2.176	3.177	7 8	2 4	2.177 2.181	3.176 3.172	–.035 –.070
T5	2.544	4.013	9 10	4 6	2.551 2.560	4.006 3.997	–.102 –.153
T6	2.946	4.912	11 12	6 8	2.967 2.984	4.891 4.874	–.204 –.271
T7	4.788	4.646	13 14	8 10	4.785 4.784	4.649 4.650	.020 .024
T8	4.584	6.834	15 16	10 10	4.652 4.652	6.766 6.766	–.385 –.385
T9	4.681	5.394	17 18	10 4	4.702 4.684	5.373 5.391	–.122 –.050
T10	7.353	10.790	19 20	4 0	7.370 7.353	10.773 10.790	–.239 0

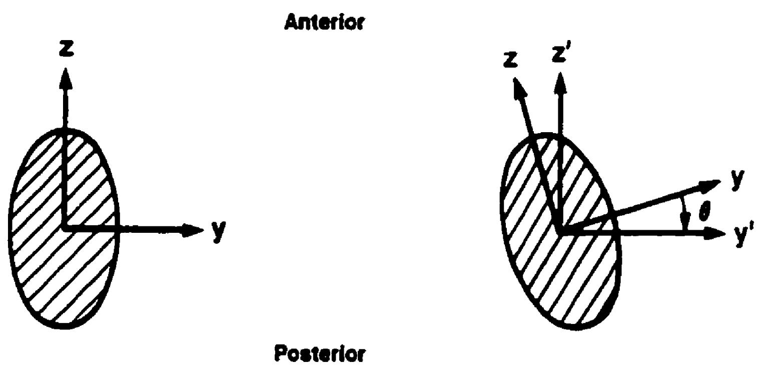

(a) (b)

Fig. 6.18 Bottom view of effective cross-section of intervertebral joint in horizontal plane (a) symmetric, and (b) asymmetric.

Growth analysis was performed on the lordotic model under lumped loading. As mentioned previously, limitations of the NASTRAN program, made it necessary to model the load as a lumped force P (N) and a flexion moment 2.98 P (N-cm) applied at the top vertebra T1. In the first instance, the constraints were chosen to be the same as those for the bifurcation analysis. In particular, movement in the sagittal plane was allowed. Although the mode shapes from the bifurcation analysis indicated rather diffused lateral displacements and relatively small convex-sided rotations, it is interesting to study the growth of a localized imperfection on the behaviour of the spine near the bifurcation load.

The load was incremented slowly in small steps ($\Delta P=0.5$ N, $\Delta M=1.5$ N-cm). However, instability in the form of convergence breakdown was encountered (at 68.5 N, 204.1 N-cm) well before the bifurcation load for lateral buckling (261 N, 779 N-cm) could be reached. The reason for this instability was that the displacements in the sagittal plane had become excessive and there was a loss of stiffness for bending in the sagittal plane. Although the convergent solution indicated scoliosis-like displacements and rotations, they had not sufficiently developed due to the load being rather far from the bifurcation load.

Therefore, in view of the above, another attempt was made by performing an analysis in which displacements in the sagittal plane along the entire spine length were constrained. In this case, using initial load steps of 5 N and 15 N-cm and much smaller ones as bifurcation load neared, the lateral bifurcation load could be reached without encountering any solution instabilities. The lateral imperfections grew as the load was increased. At a load ($P=261.75$ N, $M=780.06$ N-cm) near the bifurcation load previously determined, significant lateral displacements were obtained, with a maximum total lateral displacement of 5.5 cm occurring at the T8 level. Fig. 6.19 shows the resulting lateral deformation of the vertebrae in comparison to those of the scoliotic patient. Fig. 6.20 illustrates the growth of the lateral imperfection. However, axial rotations, Fig. 6.21, although in the scoliotic direction were found to be small, being a maximum of 2.59° at the L4 level, and 1.8° at the apex of the lateral curve at the T8 level. Thus, the maximum axial rotation did not coincide with the maximum lateral displacement, and also the pattern of deformation was not localized enough, which are both characteristics of scoliosis. As a reminder, data on vertebral axial rotation of the scoliotic patient other than a maximum rotation at the apex of 25° were unavailable for comparison.

Analysis was also performed without the horizontal plane asymmetries. Results of eventual growth were practically identical (< 5% different) to those obtained with this asymmetry present, indicating that the horizontal plane asymmetry has little effect on the results. On the other hand, the effect of the lateral asymmetry is evident in the shape of the lateral displacements i.e. maximum at the T8 level.

In conclusion, it appears the first interpretation of the lordosis hypothesis, requiring simulations of the buckling behaviour of a spine and rib cage with a slight lordosis in the thoracic region of the spine fails to explain deformation typical of thoracic idiopathic scoliosis. The imperfection growth analysis basically confirms what was indicated by the mode shapes in the bifurcation analysis, namely that (1) lateral displacements and convex-sided rotations would be produced but not localized enough as seen in scoliosis, (2) axial rotations would be of a relatively small magnitude in comparison to the lateral displacements and in comparison to those found in scoliosis, and (3) greatest axial rotations would occur near the T11 and the L4-L5 levels, which are not consistent with the site of the apex of the lateral curve in the nonlinear analysis.

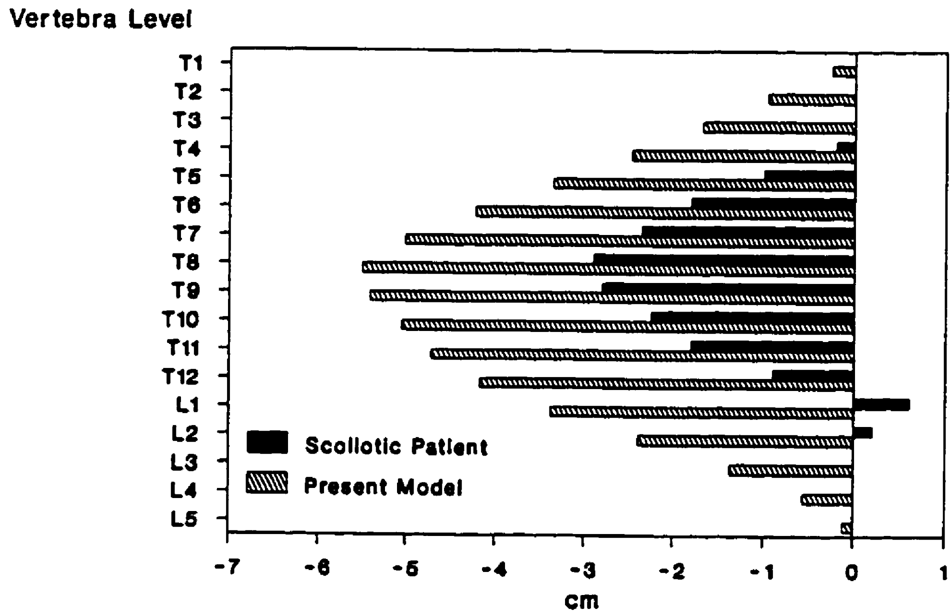

Fig. 6.19 Lateral deformations of vertebrae in lordotic model under lumped loading predicted by imperfection growth analysis and their comparison with displacements observed in a scoliotic patient. The models are considered fixed at T1 in horizontal displacements and rotation, completely fixed at sacrum, and constrained from displacement in the sagittal plane along the entire length of spine.

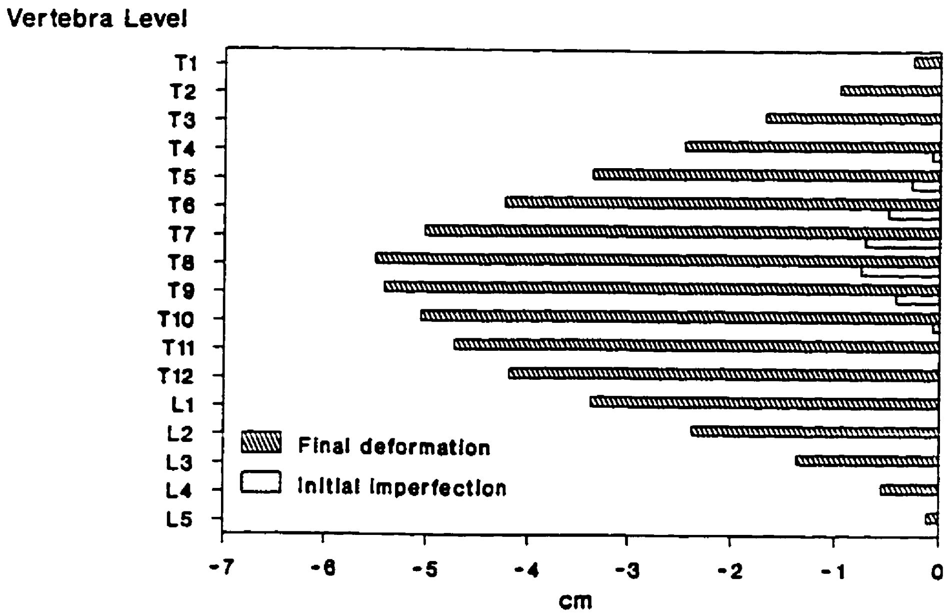

Fig. 6.20 Growth of initial lateral imperfection of spine under lumped loading.

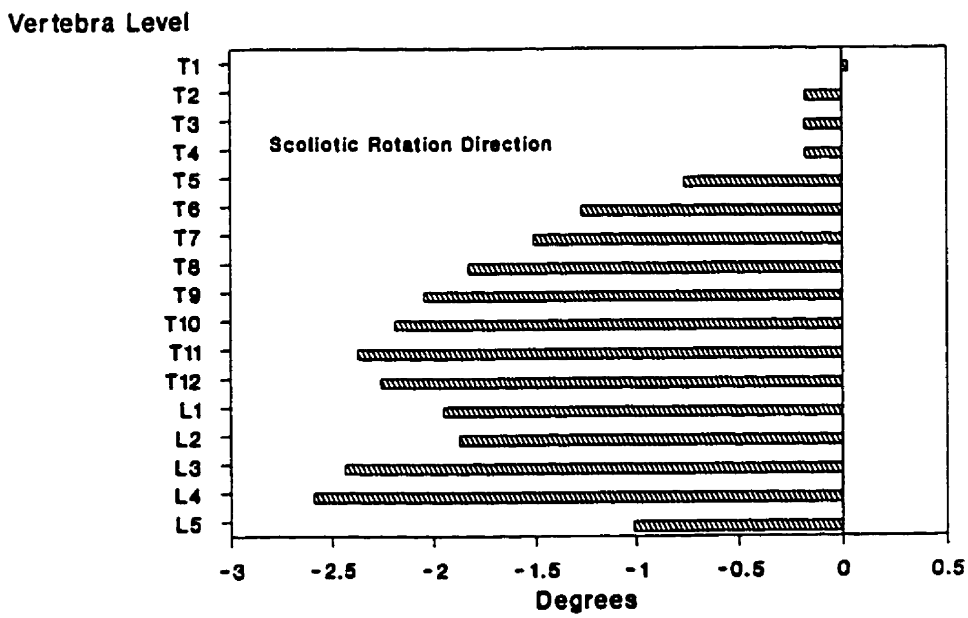

Fig. 6.21 Axial (horizontal plane) rotations of vertebrae in lordotic model under lumped loading predicted by imperfection growth analysis. The models are considered fixed at T1 in horizontal displacements and rotation, completely fixed at sacrum, and constrained from displacement in the sagittal plane along the entire length of spine.

6.3 Lordosis-Inducing Growth Study

This section is concerned with the testing of another interpretation of the lordosis hypothesis. The basic premise here is that the spine is liable to assume a scoliotic configuration during (not after) the lordosis inducing asymmetrical growth of the thoracic vertebrae while full gravity loading keeps acting on the spine. It is assumed that while the vertebrae undergo almost a natural (stress-free) dimension change the discs do not. Therefore, structurally speaking, the spine discs are being loaded by virtue of presenting deformable obstacles to the stress-free growth of vertebrae. As mentioned in Chapter 5, the above loading is simulated in the present work by the device of subjecting the vertebrae to temperature changes.

The nonlinear growth analysis is performed on the normal spine and rib cage model in which all spine elements are represented with 1 element with the exception of thoracic vertebrae T4-T12, which are represented by 3-elements. In contrast to the previous structurally equivalent 3-element model, the anterior and posterior elements of the 3-element representation used here have small axial stiffnesses only. Their purpose is to impose self-equilibrating loads on the vertebra to which they belong to simulate growth, without contributing to the stiffness of the spine. Therefore, the central element of this 3-element modelling retain the total stiffness of the vertebrae. As in the previous representations, the end plates of these vertebrae are modelled by stiff beam elements connecting the central element to the anterior and posterior elements.

The lordosis-inducing growth of the thoracic vertebrae is modelled by lengthening (i.e. heating) the anterior elements and shortening (i.e. cooling) the posterior elements. The temperature changes, and hence the length changes, are taken to be such that the lengths of the central elements are unchanged. This ensures that the central curved length of the spine remains almost unaltered by the vertebral growth. The amounts of temperature changes in the anterior ($+\Delta T$) and posterior ($-\Delta T$) elements have been given in Table 5.7. It may be recalled that these temperature changes were calculated on the basis of A-P stiffnesses of vertebrae and the measurements from a specimen with thoracic scoliosis [30].

The lateral imperfections required for the growth analysis consisted, as previously, of the frontal asymmetry in the form of a lateral curve, and of the horizontal asymmetry in the form of asymmetrical orientation of the intervertebral joints with respect to the sagittal plane. The structure is considered completely fixed at the sacrum, and partially fixed at T1 in that frontal plane rotation (θ_y) and vertical displacement (z) are allowed. The gravity loading is modelled by a single vertically downward force acting at T1 (with no accompanying sagittal moment).[1] The incremental loading program employed for the analysis is shown Table 6.6. A total of 196 load steps were required to reach complete subcase 8.

The same convergence criteria as used in the preceding imperfection growth analysis, Section 6.2, were employed in this nonlinear analysis. It may be noted that as deformation progressed, smaller load steps became necessary for obtaining convergence. However, no convergence could be achieved for the temperature loading of subcase 9, even after employing 100 load steps. This subcase required subjecting the T7 and T9 vertebrae to an additional temperature change from 188.2° (of subcase 8) to respectively 241° and 247°. Constraints of time and money prevented an analysis for this subcase with still smaller load steps.

Table 6.6 Loading Program Used in the Incremental Nonlinear Growth Analysis

Subcase	Increments of temperature		Increments of force	No. of load steps
	Temperature change ΔT, degrees	Vertebrae, anteriors $+\Delta T$ posteriors $-\Delta T$	Compressive force at T1, N	
1	1.5	T4-T12	0	1
2	18.0, 11.1	T5-T11, T12	0	10
3	0	-	100	25
4	25.8	T6-T11	0	15
5	0	-	50	25
6	37.5	T6-T10	0	20
7	105.4, 84.5	T7-T9, T10	50	50
8	0	-	50	50
9*	58.5, 52.8	T7, T9	0	100

* No convergent solution (with 100 load steps) could be found for the loading in subcase 9.

[1] The reason for not conducting an analysis with forward flexion moment present (to simulate application of weight at the center of gravity) was mainly the constraint of time.

Under the conditions and loading described above, the nonlinear imperfection growth analysis yielded results, at the final loading step of subcase 8, shown in Figs. 6.22-6.24. This load step corresponds to a total compressive load at T1 of 250 N (≈ 65% of the body weight above sacrum) and a total temperature change of ±188.2°, or an average enforced anterior/posterior length change of vertebrae T7-T9 of ±0.37 cm (≈ 20% of the vertebral lengths).

Fig. 6.22 shows the predicted lateral deformation of the vertebrae and their comparison with those observed in a scoliotic patient. It can be seen that predictions match quite well with the scoliotic displacements for T7-T11 vertebrae. The differences lie in the fact that whereas the actual scoliotic deformations are quite localized, the predicted curve is of a gradual type. This difference in detail is due, without much doubt, to the changes in stiffness which takes place by virtue of facet interaction between the vertebral bodies. These stiffnesses are modelled here rather grossly by considering the intervertebral joint stiffnesses to remain constant.

The variance of the axial rotation accompanying the lateral deformations is shown in Fig. 6.23. Although the variation in vertebral rotations of the scoliotic patient is not available, as mentioned previously, the resulting rotations in this analysis are convex-sided rotations which is characteristic of scoliosis. The maximum convex-sided rotation compares well with the maximum rotation of 25°, known for the thoracic scoliotic patient [10]. Moreover, the rotations display a localization typical of this type of scoliosis.

The important finding, evident from Figs. 6.22 and 6.23, is the convex-sided axial rotations of significant magnitudes and the correct pattern, with the site of maximum rotation coinciding with the apex of the lateral curve. At the apex, which is at the T8 level, the axial rotation attains a maximum value of 20.15°, and likewise the total lateral displacement attains a maximum value of 4.07 cm. Expressed in relative terms, this deformation equals an apical vertebral rotation of 0.5° per mm of lateral displacement.

Naturally, the direction of the eventual lateral displacements is determined by the direction of the initial lateral curve. Fig. 6.24 shows the amount of growth experienced by the lateral curve in the present case of analysis. In contrast, the direction of the axial rotation is not necessarily determined by the direction of horizontal plane asymmetries. It was found that a total absence of these asymmetries, or even asymmetries of the opposite kind, did not have any significant qualitative or quantitative effect on the eventual axial rotation. In other words, the analysis results indicate that the scoliotic rotations are rather insensitive to the asymmetrical or rotated cross-sections of vertebrae in the presence of a lateral curve asymmetry. Given the lateral asymmetry, asymmetrical vertebral growth inducing lordosis produces convex-sided rotations regardless of small horizontal asymmetry.

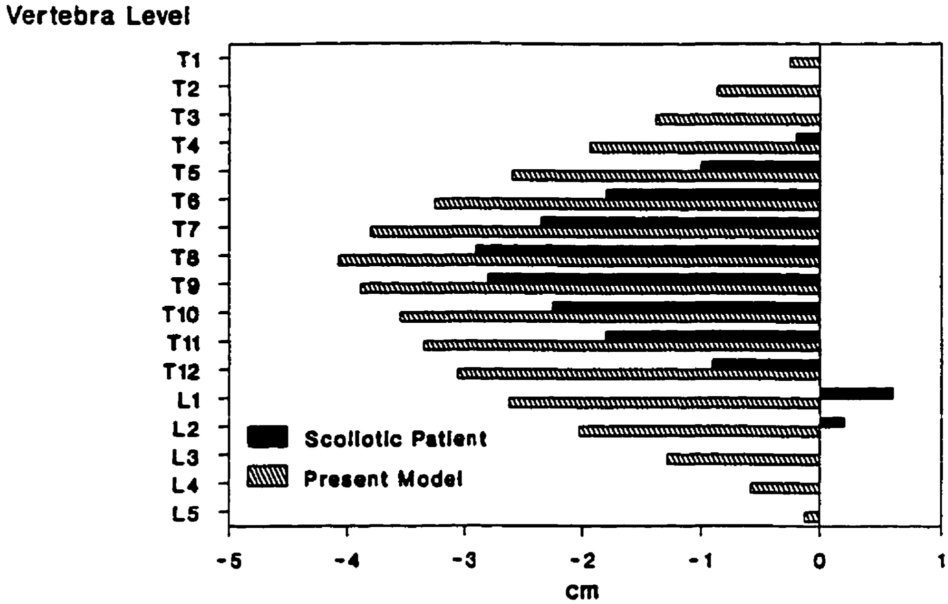

Fig. 6.22 Lateral deformations of vertebrae of normal spine with rib cage under asymmetrical vertebral growth and gravity loading (end of subcase 8, Table 6.6) predicted by imperfection growth analysis and their comparison with deformation observed in a scoliotic patient. The model is considered free in axial displacement and frontal plane rotation at T1, and completely fixed at sacrum.

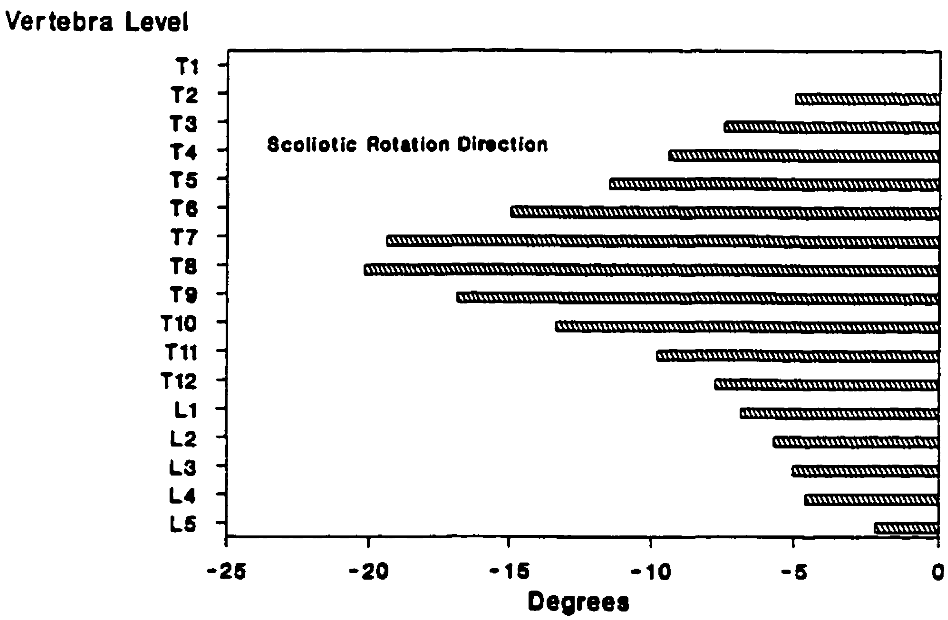

Fig. 6.23 Axial (horizontal plane) rotations of vertebrae of normal spine with rib cage under asymmetrical vertebral growth and gravity loading (end of subcase 8, Table 6.6) predicted by imperfection growth analysis. The model is considered free in axial displacement and frontal plane rotation at T1, and completely fixed at sacrum.

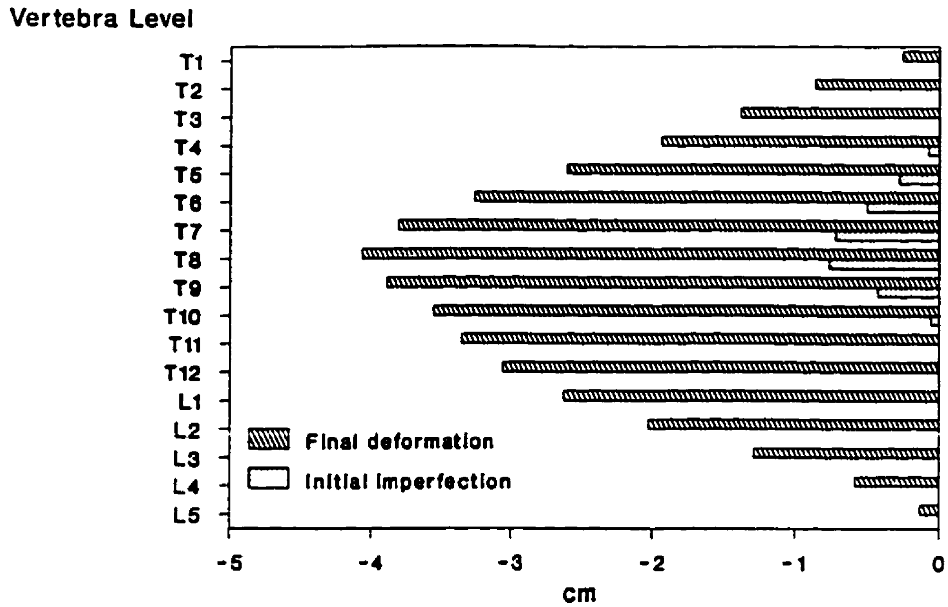

Fig. 6.24 Growth of initial lateral imperfection of spine under asymmetrical growth.

Figure 6.25 shows the plot of undeformed geometry of the spine with rib cage used in the analysis, in left lateral and A-P views. Figure 6.26 gives the deformed geometries at the end of load subcase 8. Comparing Fig. 6.26(a) with 6.25(a), it can be seen that the deformed spine has become straighter as a result of the vertebral growth. Figure 6.26(b) shows the convex-sided rotation typical of scoliosis; clearly the anterior vertebral bodies rotate into the *convexity* of the lateral curve.

The true lateral and frontal views of the deformity are obtained when it is viewed in and perpendicular to the plane obtained by rotating the sagittal plane by the amount of the apical rotation. These views are shown in Fig. 6.26(c) and 6.26(d). In the true lateral view, Fig. 6.26(c), it is found that the thoracic spine has lost its kyphosis and has become slightly lordotic. The vertebra T5-T8 now have longer anterior lengths than posterior lengths. The true A-P view, Fig. 6.26(d) shows the scoliotic deformation in its maximum. Referring back to Fig. 3.2, these characteristics are typical of thoracic scoliosis.

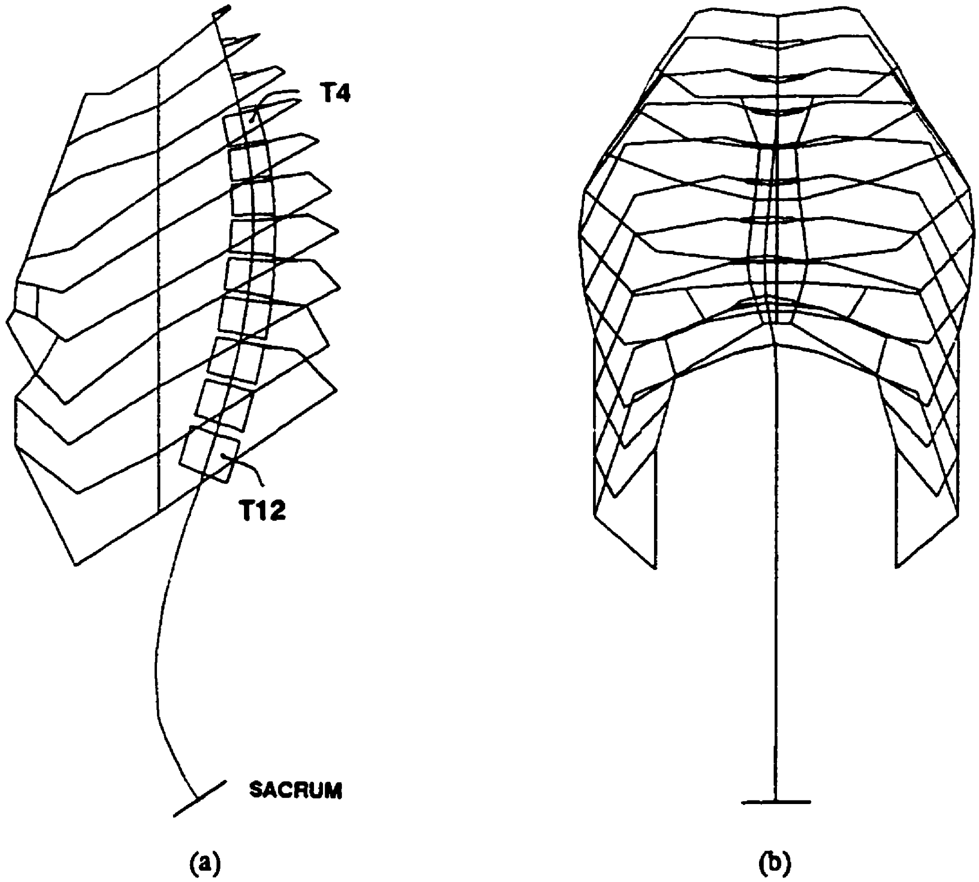

Fig. 6.25 Undeformed model of normal spine and rib cage used in the nonlinear analysis simulating lordosis-inducing growth of the thoracic vertebrae. (a) left lateral view, and (b) A-P view.

Similar analyses were performed in which thermal loading simulating the asymmetrical vertebral growth was considered alone, without the gravity loading, and under various constraint conditions at T1. When T1 was considered free in vertical displacement and frontal rotation, significant axial rotations resulted similar to those found in the above analysis in which the gravity load was superimposed. However, lateral displacements were extremely small in comparison. Next, an analysis with an additional constraint fixing vertical displacement was performed. It was found that in the latter case, axial rotations were slightly smaller, but the lateral displacements were larger than in the former. However, lateral displacements were still small in comparison to those found in the analysis with gravity load and those found in scoliosis. The small lateral displacements are attributed naturally to the fact that in both cases no appreciable lateral bending could take place since the spine did not or could not shorten. Another analysis was performed with T1 completely fixed. The resulting axial rotations were basically unaffected by the addition of the frontal rotation constraint. The lateral displacements, on the other hand, although they appeared more localized, had significantly

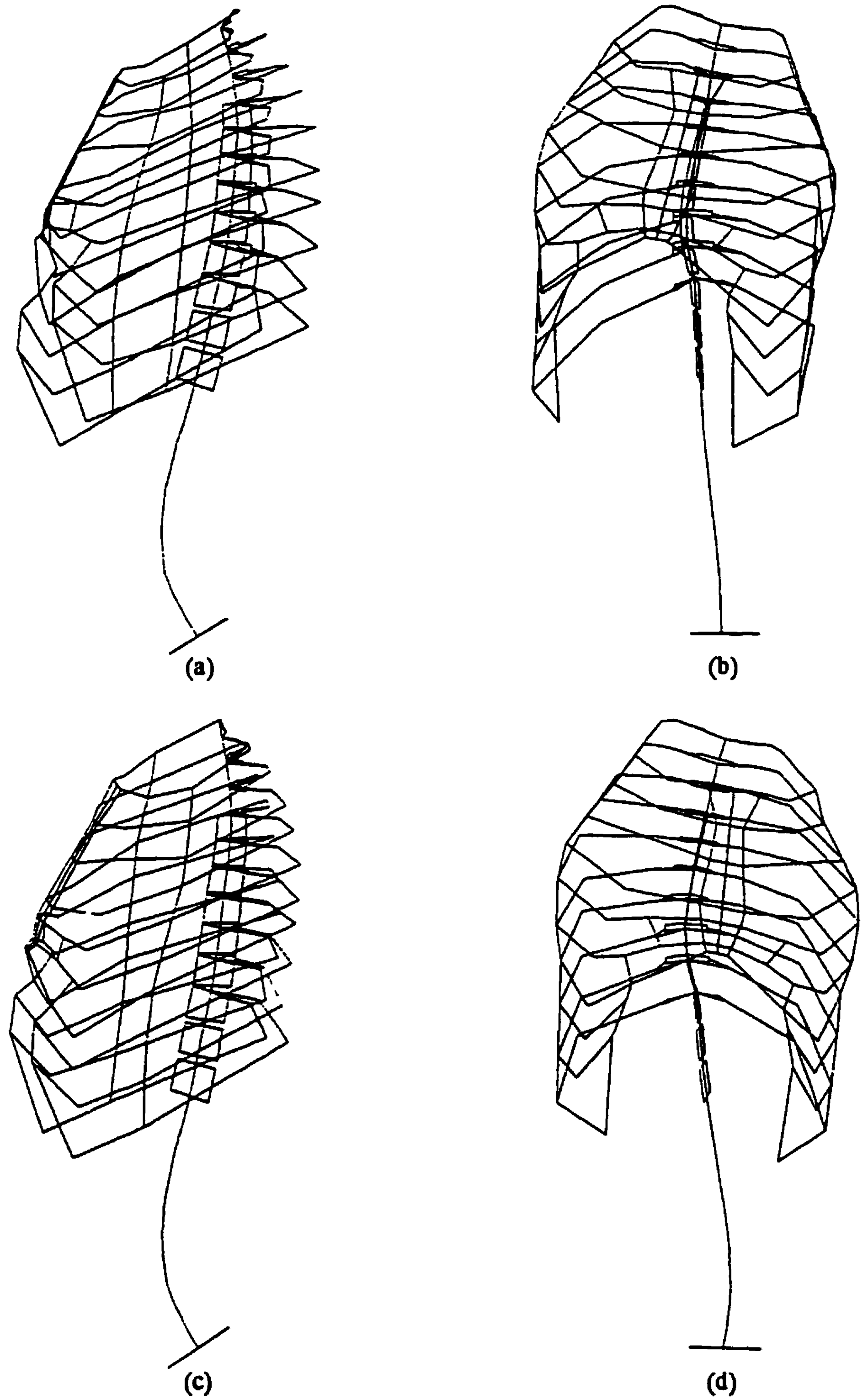

Fig. 6.26 Deformed configuration of spine and rib cage model after 250 N gravity compressive force and lordosis-inducing growth of the thoracic vertebrae. (a) left lateral view, (b) A-P view, (c) true lateral view of the deformation, (d) true A-P view of the deformation. True views are obtained at oblique angles to A-P and lateral views equivalent to the rotation of the apical vertebrae, here by $-20°$.

reduced (negligible) magnitudes.

Therefore, an important conclusion arising from the results of these additional analyses is that the axial rotation of the scoliosis type is mainly due to the asymmetrical growth of the vertebrae; the compressive gravity loading has little influence on the axial rotation. However, the author suspects that the constraint in sagittal plane rotation (θ_y) at T1 is crucial to the success of the analysis, although analysis was not attempted without it. This constraint is not artificial because the reaction moment is found to be a flexion moment approximately 1.5 times the gravity force which may be interpreted as being due to an anterior offset of the center of gravity from T1.

However, the significant lateral displacements resulting in analysis are due to gravity forces. As noted in analyses without gravity force, resulting lateral displacements were small. The structure must shorten in order to obtain lateral displacements of the magnitude seen in scoliosis. On the other hand, the effect of the asymmetrical growth was found to lengthen the column, i.e. straighten it, since central vertebral lengths were basically unchanged. The fact that gravity loads produce significant lateral displacements has also been demonstrated earlier in Section 6.2 by the nonlinear growth analysis on the lordotic model. Gravity forces are present in reality and in terms of the analysis are needed to counteract lengthening (straightening) effect of asymmetrical growth on spine. Thus, simultaneous presence of both asymmetrical vertebral growth and gravity loading is necessary to obtain lateral displacements and axial (convex-sided) rotations of magnitudes found in scoliosis.

As a measure of caution, it should be pointed out that the analysis results depend upon the loading path chosen between the starting and final values of loads. Analysis with different temperature and gravity loading paths produce quite different results. This means, for example, that one may not be able to obtain the same results by performing analyses with the following two sequences of loadings: (1) first loading the spine with only the gravity loading, and then loading it by temperature changes while keeping the gravity loads constant, and (2) by reversing the above sequence. A plausible reason for possibly different results is that in a nonlinear elastic system there may exist for the same load more than one deformed configurations; in other words, a uniqueness of loading does not guarantee the uniqueness of the displacement field.

Another feature of nonlinear analysis is that although convergence criteria may be satisfied within the selected tolerances at each load step, the accumulated unbalanced load errors may not yield a perfect equilibrium between applied forces and reactions in the deformed configuration. In the present analysis, these unbalanced forces remained small relative to the applied loads.

In conclusion, based on the nonlinear growth analysis of this section which yields the lateral displacements and axial rotations of essentially the same character and magnitude as observed in thoracic idiopathic scoliosis, it seems fair to say that the lordosis hypothesis in its second interpretation has now been validated. A particular pattern of asymmetrical lordosis-inducing growth of thoracic vertebrae can indeed deform the spine into a shape of thoracic idiopathic scoliosis. It also follows that an already present lateral curve of a more than normal magnitude will hasten the development of scoliotic deformation under such a vertebral growth.

Chapter 7
Summary and Conclusions

7.1 Summary of Analysis and Results

This study tests the lordosis hypothesis concerning the etiology of the development of adolescent idiopathic thoracic scoliosis. Two simulations, corresponding to two interpretations of the hypothesis, are modeled to investigate the hypothesis. The first modelling, corresponding to the first interpretation, conducts the nonlinear imperfection growth analysis of a *lordotic spine* (i.e. a spine which already has a thoracic lordosis) with the normally present anatomical asymmetries (i.e. imperfections) in the lateral and horizontal planes. The loading is by gravity loads alone, increasing incrementally from zero to near the expected bifurcation bucking load of the symmetric spine. The second modelling, corresponding to the second interpretation of the lordosis hypothesis, studies the nonlinear effect of asymmetrical growth of thoracic vertebrae (accelerated anterior and constricted posterior growth) [115] in a *normal spine*, with no pre-existing lordosis but again with the normal lateral and horizontal plane imperfections present [34].

Simulations are carried out using a lumped parameter structural analysis model of the human thoracolumbar spine and rib cage. MSC/NASTRAN finite element program was used to perform the analyses. Trunk and abdominal muscles, which are known to act on the spine, are omitted from the model. This omission greatly simplifies the modelling. On the other hand, this simplification perhaps exaggerates to some extent, the response of the spine to applied loads and asymmetrical growth.

Due to the limitation on resources and the complexity of the structure, many assumptions had to be made in constructing the analysis model. The data for the model were obtained solely from available literature. Material properties are assumed to be linear elastic. However, nonlinearities due to relatively large displacements are fully accounted for in the analyses. Best linear elastic approximations of stiffness properties are made to represent the experimentally determined behaviour of the various elements in the spine and rib cage structure (e.g. intervertebral joints). End constraints are chosen to simulate the anatomical constraints which maintain head in alignment with the pelvis. The top of the spine, vertebrae T1, is always constrained against displacements and rotations in the horizontal plane, and the sacrum is always considered completely fixed. The imposition of bending constraints at the top is included or excluded as deemed appropriate, for the real anatomical constraint is supposed to be somewhere between completely free and completely fixed bending degrees of freedom.

The analysis results from the presently constructed model are found to compare reasonably well with the results of previous researchers for cases investigated by them. In addition, as shown in Chapter 4, the ability of MSC/NASTRAN to perform torsional-flexural buckling analysis was verified by the fact that results obtained were in good agreement with the theoretical solution derived for this type of buckling for an ideal curved column of a sine wave shape. Similarly, the capabilities for geometric nonlinear analysis were verified by analysing simple nonlinear problems (e.g. bending of a beam under a pure end moment). Thus, the adequacy of both the structural model, and the method of analysis, implied by using MSC/NASTRAN, were validated.

Results of the First Approach

In the first approach, in which the effect of an existing lordosis in the thoracic region on spinal stability was studied, the results failed to support this interpretation of the lordosis hypothesis. It was apparent from the results of both the linear bifurcation analysis and the nonlinear imperfection growth analysis that a lordotic spine, by the way of pure torsional-flexural buckling, could not produce deformations, particularly the axial rotations, of magnitudes found in patients of idiopathic scoliosis. As discussed in Chapter 4, the spine-like structures with lower stiffness in lateral bending than in A-P bending are subject to torsional-flexural buckling. However, since the spine and rib cage model is apparently much stiffer in torsion than in lateral bending (Fig. 6.2 and 6.9), it follows that the buckling behaviour will be predominantly in the lateral bending mode. In other words, lateral deflections (or their growth) will dominate over the axial rotations. This is illustrated by the mode shapes obtained from the bifurcation analyses and by the imperfection growth obtained from the nonlinear analyses. Both show significant lateral displacements but comparatively small axial rotations.

Viewed in its own right without linkage to the lordosis hypothesis, it appears that a reduction in the kyphosis of the thoracic spine, or even a slight lordosis, has little effect on the stability of the spine. Buckling loads are lowered only slightly, and the mode shapes remain basically unaltered. This is also supported by the results of the theoretical study on the effect of spine curvature on its stability in Chapter 4. It was concluded there that a slight decrease in the amplitude of the sagittal curve resulted in slightly lowered buckling loads primarily due to the consequently increased spine length.

Results of the Second Approach

In the second approach, simulation of the lordosis-inducing (asymmetrical) growth of the thoracic vertebrae produced deformations in normal spines similar to those found in thoracic idiopathic scoliosis. The results therefore support this second interpretation of the lordosis hypothesis. Success of this approach can be attributed to the modelling of the asymmetrical growth of the thoracic spine, and its eventual transformation into a lordotic configuration, as a loading in the nonlinear imperfection growth analysis. The stresses induced in the discs due to elongation of the anterior elements and shortening of the posterior elements of vertebrae T4-T12 seem to be responsible for the large axial rotations obtained. In a somewhat constrained system, the elongation of the anteriors of vertebrae produces additional compressive stresses in the anteriors of the disc, and likewise, a shortening of the posteriors of vertebrae produces tensile stresses in the posteriors of the discs. The presence of the initial lateral curve which grows with increasing compressive loads, accommodates the growth by letting the spinal elements rotate in a convex-sided manner to avoid unnecessary stressing.

7.2 Conclusions

In this thesis, lordosis-inducing asymmetric growth of the thoracic vertebrae has been shown to produce thoracic scoliosis. To the author's knowledge, this is the first time that a structural analysis of a spine model with rib cage has successfully yielded deformations of the kind and amount found in scoliotic patients. The work therefore validates the lordosis-hypothesis, in its above interpretation, as being a possible etiology of adolescent idiopathic thoracic scoliosis.

To further substantiate the theory validating the hypothesis, it has been observed clinically that forward bending, which produces forces (anterior compression and posterior tension) similar to those produced as a result of lordosis-inducing vertebral growth, has a tendency to increase the rib hump, i.e. convex-sided rotation of thoracic spine, of scoliotic patients. In fact, forward bending is the test used to screen adolescents in order to detect cases of idiopathic scoliosis at an early stage. Even normal persons with slight right lateral thoracic curve are found to experience convex-sided rotation of thoracic vertebrae upon forward bending. In addition, it may be recalled that both Lovett [72] and Arkin [7] found that lateral bending produced convex-sided rotations in the normal spine when the spine was flexed forward. An imperfection growth analysis under a forward flexion moment and a compressive force (as was done in Section 6.2 to simulate the center of gravity application of the body weight) in combination with the thermal loading can be expected to produce scoliotic deformations of even larger magnitudes than found here.

The future research would undoubtedly improve the many approximations made in the spine models of this thesis. These approximations were necessary for the progress of the present work. However, the author feels that a significant advance has been made in demonstrating the lordosis-inducing asymmetrical growth as the key to obtaining scoliotic deformations. Axial rotations of significant magnitude found in this work are what had been lacking in the results of previous researchers concerning scoliosis [10, 118].

The salient conclusions may be reiterated as follows:

(1) Pure structural type torsional-flexural buckling of the spine and rib cage under increasing gravity-type loads cannot produce significant axial rotations due to the large effective torsional stiffness of the spine in comparison to its lateral bending stiffness.

(2) An existing lordosis in the thoracic region has minor effect on the subsequent stability characteristics of spine and rib cage.

(3) Forces developed due to lordosis-inducing (asymmetrical) growth of thoracic vertebrae are necessary to produce the convex-sided rotations with a maximum at the apex of the lateral curve as found in scoliotic patients.

(4) As suggested by Dickson et al. [34], the natural lateral asymmetry, present in all spines to some degree [31], is necessary for attaining correct scoliotic deformations. According to the present analysis, the lateral curve determines the direction of the deformity.

7.3 Suggestions for Further Research

For future, an interesting study would be to examine the effect of lordosis-inducing vertebral growths on the lumbar spine, and also on the complete thoracolumbar spine to determine whether or not other curve patterns (e.g. lumber and double curve) would develop. Additional suggestions for future research include (1) modelling of the nonlinear stiffness properties of spine elements, particularly of the motion segments, and (2) modelling of realistic gravity forces and muscle action forces.

A much more elaborate nonlinear finite element model, accounting correctly the geometric details of the spine, subjected to an imperfection growth analysis under the action of lordosis-inducing vertebral growth would provide very realistic answers to various questions concerning scoliosis.

References

1. Adams W: Lectures on the pathology and treatment of lateral and other forms of curvature of the spine. London, Churchill & Sons, 1865

2. Agonstoni E, Mognoni G, Torri G, Miserocchi G: Forces deforming the rib cage. Resp physiol 2:105-117, 1966

3. Andersson G, Schultz A, Nathan AK, Irstan L: Roentgenographic measurement of lumbar intervertbral disc height. Spine 6:154-158, 1981

4. Andriacchi T, Schultz A, Belytschko T, Galante J: A model for studies of mechanical interactions between the human spine and rib cage. J Biomech 7:497-507, 1974

5. Apuzzo MLJ, Watkins RG, Dobkin WR: Therapeutic considerations in the surgical management of lesions affecting the midthoracic spine. The Unstable Spine: Thoracic, Lumbar and Sacral Regions. Edited by SB Dunsker, HH Schmidek, J Frymoyer, A Kahn III. Philadelphia, WB Saunders, pp 107-109, 1986

6. Archer IA, Dickson RA: Stature and idiopathic scoliosis: A prospective study. J Bone Jt Surg 67B:185-188, 1985

7. Arkin AM: The mechanism of rotation in combination with lateral deviation in the normal spine. J Bone Jt Surg 32A:180-188, 1950

8. Arkin AM: The mechanism of the structural changes in scoliosis. J Bone Jt Surg 31A:519-528, 1949

9. Barsoum RS, Gallagher RH: Finite elements analysis of torsional and torsional-flexural stability problems. Inter J Numer Methods Eng 2:335-352, 1970

10. Belytschko T, Andriacchi T, Schultz A, Galante J: Analog studies of forces in human spine: Computational techniques. J Biomech 6:361-371, 1973

11. Berkson MH, Nachemson AL, Schultz AB: Mechanical proporties of human lumbar spine motion segments — Part II: Responses in compression and shear; influence on gross morphology. J Biomech Eng 101:53-57, 1979

12. Bernhardt M, Bridwell KH: Segmental analysis of the sagittal plane alignment of the normal thoracic and lumbar spines and thoracolumbar junction. Spine 14:717-721, 1989

13. Berry JL, Moran JM, Berg WS, Steffee AD: A morphometric study of human lumbar and selected thoracic vertebrae. Spine 12:362-367, 1987

14. Bleich F: Buckling of Strengths of Metal Structures. New York, McGraw-Hill, 1952

15. Bogduk N, Twomey LT: Clinical Anatomy of the Lumbar Spine. New York, Churchill Livingstone, 1987

16. Brandner ME: Normal values of the vertebral body and intervertebral disc index during growth. Am J Roentgenol Radium Ther 110:618-627, 1970

17. Burwell R: The relationship between scoliosis and growth. Scoliosis and Growth. Edited by PA Zorab. Baltimore, Williams & Wilkins, 1971

18. Bushell GR, Ghosh P, Taylor TKF, Sutherland JM: The collagen of the intervertebral disc in adolescent idiopathic scoliosis. J Bone Jt Surg 61B:501-508, 1979

19. Cailliet T: Scoliosis. Diagnosis and management. Philadelphia, FA Daves, 1975

20. Carey EJ: Scoliosis: Etiology, pathogenesis and prevention of experimental rotary lateral curves of spine. JAMA 98:104-110, 1932

21. Chajes A: Principles of Structural Stability Theory. Englewood Cliffs NJ, Prentice-Hall, 1974

22. Clauser CE, McConville JT, Young JW: Weight, volume, and center of mass of segments of the human body. Wright-Patterson Air Force Base, Ohio. AMRL-TR-69-70, 1969

23. Cobb J: Outline for the study of scoliosis. The American Academy of Orthopaedic Surgeons Instructional Course Lectures 5:261-275, 1948

24. Cruickshand JL, Koike M, Dickson RA: Curve patterns in idiopathic scoliosis: A clinical and radiographic study. J Bone Jt Surg 71B:259-263, 1989

25. Damon A, Stoudt H, McFarland R: The Human Body in Equipment Design. Cambridge MA, Harvard University Press, 1971

26. Danbert RJ: Scoliosis: Biomechanics and rationale for manipulative treatment. J Manipulative Physiol Ther 12:38-45, 1989

27. Dansereau J, Stokes IAF: Measurement of the three-dimensional shape of the rib cage. J Biomech 21:893-901, 1988

28. Davis GG: Applied Anatomy, 5th edition. Philadelphia, JB Lippincott, 1918

29. Deacon P, Dickson RA: Vertebral shape in the median saggital plane in idiopathic thoaracic scoliosis. Orthopedics 10:893-895, 1987

30. Deacon P, Flood BM, Dickson RA: Idiopathic scoliosis in three dimensions: A radiographic and morphometric analysis. J Bone Jt Surg 66B:509-512, 1984

31. Dickson RA: The aetiology of spinal deformities. The Lancet:1151-1155, 1988

32. Dickson RA: Idiopathic scoliosis: Pathogenesis and Biological Treatment. The University of Leeds Review 27:39-53, 1984-85

33. Dickson RA: Scoliosis in the community. Brit Med J 286:615-618, 1983

34. Dickson RA, Lawton JO, Archer IA, Butt WP: The pathogenesis of idiopathic scoliosis: Biplanar spinal asymmetry. J Bone Jt Surg, 66B:8-15, 1984

35. Dickson RA, Lawton JO, Archer IA, Butt WP, Jobbins B, Berkin CR, Bliss P, Somerville EW: Combined median and coronal plane asymmetry: The essential lesion of progressive idiopathic scoliosis. Proceedings and Reports of Universities, Colleges, Councils, Associations and Societies. J Bone Jt Surg 65B:368, 1983

36. Evans FG: Mechanical properties and histological structure of human cortical bone. ASME Publications 70-WA/BHF-7, 1970

37. Eycleshymer AC, Schoemaker DM: A Cross-Section Anatomy. New York, Appleton-Century-Crofts, 1970

38. Farfan HF, Cossette JW, Robertson GH, Wells RV, Kraus H: The effects of torsion on the lumbar intervertebral joint: The role of torsion in production of disc degeneration. J Bone Jt Surg 52A:468-497, 1970

39. Frazier JE: The Anatomy of the Human Skeleton, 4th edition. London, J & A Churchill, 1940

40. Frymoyer JW, Krag MH: Spinal stability and instability: Definitions, classifications, and general principles of management. The Unstable Spine: Thoracic, Lumbar and Sacral Regions. Edited by SB Dunsker, HH Schmidek, J Frymoyer, A Kahn III. Philadelphia, WB Saundersp, pp 1-16, 1986

41. Gillespie R: Juvenile and adolescent idiopathic scoliosis. The Pediatric Spine. Edited by DS Bradford, RM Hensinger. New York, Thieme, pp 233-241, 1985

42. Gracovetsky S: The Spinal Engine. New York, Springer-Verlag, 1988

43. Grant JCB: Grant's Atlas of Anatomy, 8th edition. Edited by JE Anderson. Baltimore, Williams & Wilkins, 1983

44. Grant JCB: Grant's Method of Anatomy: By Regions, Descriptive and Deductive. 10th edition. Edited by JV Basmajian. Baltimore, Williams & Wilkins, 1980

45. Gray H: Gray's Anatomy, 35th edition. Edited by R Warwick, PL Williams. London, Longman, 1973

46. Gray H: Anatomy of the Human Body, 23rd edition. Edited by WH Lewis. Philadelphia, Lea & Febiger, 1936

47. Gregeson GG, Lucas DB: An in vivo study of the axial rotation of the human thoracolumnbar spine. J Bone Jt Surg 49A:247-262, 1967

48. Gross C, Graham J, Neuwirth M, Pugh J: Scoliosis and growth: An analysis of the literature. Clin Orthop 175:243-250, 1983

49. Haderspeck K, Schultz A: Progression of idiopathic scoliosis: An analysis of muscle actions and body weight influences. Spine 6:447-455, 1981

50. Harrington PR: The etiology of idiopathic scoliosis. Clin Orthop 126:17-25, 1977

51. Harris PJ: Course notes for Structural Mechanics 303-514A, McGill University, Montreal, September, 1989

52. Herzenberg JE, Waanders NA, Closkey RF, Schultz AB, Hensinger RN: Cobb angle versus spinous process angle in adolescent idiopathic scoliosis: The relationship of the anterior and posterior deformities. Spine 15:874-879, 1990

53. Hildebrant R: Adolescent idiopathic scoliosis: A review of current concepts of etiology, incidence, pathophysiology and treatment. J Manipulative Physiol Ther 1:170-175, 1978

54. Hjalmars S: A continuum model of the human spine as an anisotropic beam. Proceeding of the 4th International Conference on Continuum Models of Discrete Systems. Stockholm, North-Holland Publishing Co, pp 167-170, 1981

55. Hoppenfeld S: Scoliosis. A manual of concepts and treatment. Philadelphia, JB Lippincott, 1967

56. Inkster RG: Osteology. Cunningham's Text-Book of Anatomy, 9th edition. Edited by JC Brash. London, Oxford University Press, 1951

57. Jacob SW, Francone CA, Lossow WJ: Structure and Function in Man, 5th edition. Philadelphia, WB Saunders, 1982

58. James J: Paralytic Scoliosis. Ann R Coll Surg Engl 21:21-42, 1957

59. Jarvis JG, Ashman RB, Johnston CE, Herring JA: The posterior tether in scoliosis. Clin Orthop 227:126-134, 1988

60. Kapandji IA: The Physiology of the Joints: Annotated diagrams of the mechanics of the human joints. Volume 3: The trunk and vertebral column, 2nd English edition. New York, Churchill Livingstone, 1982

61. Keim HA: The Adolescent Spine, 2nd edition. New York, Springer-Verlag, 1982

62. Kim YE, Goel VK: Effect of testing mode on the biomechanical response of a spinal motion segment. J Biomech 23:289-291, 1990

63. Krag MH: Three dimensional flexibility measurements of preloaded human vertebral motion segments. MD Thesis, Yale University School of Medicine, New Haven CT, 1975

64. Lanier Jr RR: The presacral vertebrae of American white and negro males. Am J Phys Anthrop 25:341-420, 1939

65. Larsan SJ: The thoracolumbar junction. The Unstable Spine: Thoracic, Lumbar and Sacral Regions. Edited by SB Dunsker, HH Schmidek, J Frymoyer, A Kahn III. Montreal, WB Saunders, pp 127-130, 1986

66. Leatherman KD, Dickson RA: The Management of Spinal Deformities. London, Wright, 1988

67. Lindah O: Resection of vertebral transverse processes in idiopathic scoliosis. Acta Orthop Scand 37:342-347, 1966

68. Lindah O, Raeder E: Mechanical analysis of forces involved in idiopathic scoliosis. Acta Orthop Scand 32:27-38, 1962

69. Lindbeck L: Analysis of functional scoliosis by means of an anisotropic beam model of the human spine. J Biomech Eng 107:281-285, 1985

70. Lonstein JE: Natural history and school screening for scoliosis. Ortho Clin North Amer 19:227-237, 1988

71. Lonstein JE, Carlson JM: The prediction of curve progression in untreated idopathic scoliosis during growth. J Bone Jt Surg 66A:1061-1071, 1984

72. Lovett RW: The mechanism of the normal spine and its relation to scoliosis. Boston Med Surg J 153(13):349-358, 1905

73. Lucas DB, Bresler B: Stability of the ligamentous spine. Biomechanics Lab Rpt #40, University of California, San Francisco, 1961

74. Markolf KL: Deformation of the thoracolumbar intervertebral joints in response to external loads: A biomechanical study using autopsy materials. J Bone Jt Surg 54A:511-533, 1972

75. Markolf KL: Stiffness and damping characteristics of thoracolumbar spine. Bioengineering Approaches to Problems of the Spine. National Institute of Health, Betheseda MD, pp 87-143, 1970

76. Mattson G, Haderspeck-Grib K, Schultz A, Nachemson A: Joint flexibilities in structurally normal girls and girls with idiopathic scoliosis. J Orthop Res 1:57-62, 1983

77. Miller J, Nachemson A, Schultz A: Effectiveness of braces in mild idiopathic scoliosis. Spine 9:632-635, 1983

78. Moll JMH, Wright V: Normal range of spinal mobility: An objective clinical study. Ann Rheum Dis 30:381-386, 1971

79. Nachmeson A: The load on lumbar disks in different positions of the body. Clin Orthop 45:107-122, 1966

80. Nachmeson A: Lumbar intradiscal pressure: Experimental studies on post-mortem material. Acta Orthop Scand Suppl 43, 1960

81. Nachemson A, Schultz A, Berkson MH: Mechanical properties of human lumbar spine motion segments: Inflences of age, sex, disc level, and degeneration. Spine 4:1-8, 1979

82. Nahum AM, Gadd CW, Schneider DC, Kroell CK: Deflections of the human thorax under sternal impact. International Automobile Safety Conference, Detroit & Brussels, pp 797-807, 1970

83. Öhlen G, Asro S, Bylund P: The sagittal configuration and mobility of the spine in idiopathic scoliosis. Spine 13:413-416, 1988

84. Olsen GA: New developments in the correction of scoliosis. Bioengineering Approaches to Problems of the Spine. National Institute of Health, Bethesda MD, pp 145,175, 1970

85. Openshaw P, Edwards S, Helms P: Changes in rib cage geometry during childhood. Thorax 39:624-627, 1984

86. Panjabi MM: Experimental determination of spinal motion segment behavior. Ortho Clin North Amer 8:169-180, 1977

87. Panjabi MM: Three-dimensional mathematical model of the human spine structure. J Biomech 6:671-680, 1973

88. Panjabi MM, Brand Jr RA, White III AA: Mechanical properties of the human thoracic spine: As shown by three-dimensional load-displacement curves. J Bone Jt Surg 58A:642-652, 1976

89. Panjabi MM, Brand Jr RA, White III AA: Three-dimensional flexibility and stiffness properties of human thoracic spine. J Biomech 9:185-192, 1976

90. Panjabi MM, Krag MH, White III AA, Southwick WO: Effects of preload on load displacement curves on the lumbar spine. Ortho Clin North Amer 8:181-190, 1977

91. Panjabi MM, White III AA: A mathematical approach for three-dimensional analysis of the mechanics of the spine. J Biomech 4:203-211, 1971

92. Pansky B: Dynamic Anatomy and Physiology. New York, MacMillian, 1975

93. Patrick F, Kroell C, Mertz H: Forces on the human body in simulated crashes. Proceedings of 9th Stapp Car Crash & Field Demonstration Conference, pp 237-259, 1965

94. Patwardhan AG, Bunch WH, Meade KP, Vanderby Jr R, Knight GW: A biomechanical analog of curve progression and orthotic stabilization in idiopathic scoliosis. J Biomech 19:103-117, 1986

95. Ponsetti IV, Pedrini V, Wynne-Davies R, Duval-Beaupere G: Pathogenesis of scoliosis. Clin Orthop 120:268-280, 1976

96. Pope MH, Stokes IAF, Moreland M: The biomechanics of scoliosis. Crit Rev Biomed Eng 11:157-188, 1984

97. Portillo D, Sinkora G, McNeill T, Spencer D, Schultz A: Trunk strengths in structurally normal girls and girls with idiopathic scoliosis. Spine 7:551-554, 1982

98. Reuber M, Schultz A, McNeill T, Spencer D: Trunk muscle myoelectric activities in idiopathic scoliosis. Spine 8:47-456, 1983

99. Roaf R: Spinal Deformities, 2nd edition. Tunbridge Wells, Kent, Pitman Medical, 1980

100. Roaf R: The basic anatomy of scoliosis. J Bone Jt Surg 48B:786-792, 1966

101. Roaf R: Rotation movements of the spine with special reference to scoliosis. J Bone Jt Surg 40B:312-332, 1958

102. Roberts SB, Chen PH: Global geometric characteristics of typical human ribs. J Biomech 5:191-201, 1972

103. Roberts SB, Chen PH: Elastostatic analysis of the human thoracic skeleton. J Biomech 3:527-545, 1970

104. Rogala E, Drummond D, Gurr J: Scoliosis: Incidence and natural history. J Bone Jt Surg 60A:173-176, 1978

105. Schultz AB: Biomechanics of the human spine and trunk. Handbook of Bioengineering. Edited by R Skalak, S Chien. Montreal, McGraw-Hill, pp 41.1-41.20, 1987

106. Schultz AB: Biomechanical factors in the progression of idiopathic scoliosis. Ann Biomed Eng 12:621-630, 1984

107. Schultz AB, Belytschko TB, Andriacchi TP, Galante JO: Analog studies of forces in human spine: Mechanical properties and motion segment behavior. J Biomech 6:373-383, 1973

108. Schultz AB, Benson D, Hirsch C: Force-deformation properties of human ribs. J Biomech 7:303-309, 1974a

109. Schultz AB, Benson D, Hirsch C: Force-deformation properties of human costo-sternal and costo-vertebral articulations. J Biomech 7:311-318, 1974b

110. Schultz AB, Galante JO: A mathematical model for the study of the mechanics of the human vertebral column. J Biomech 3:405-416, 1970

111. Schultz AB, Larocca H, Galante JO, Andriacchi TP: A study of geometrical relationships in scoliotic spines. J Biomech 5:409-420, 1972

112. Schultz AB, Sörensen SE, Andersson GBJ: Measurements of spine morphology in children, ages 10-16. Spine 9:70-73, 1984

113. Schultz AB, Warwick DN, Berkson MH, Nachemson AL: Mechanical properties of human lumbar spine motion segments — Part I: Responses in flexion, extension, lateral bending and torsion. J Biomech Eng 101:46-52, 1979

114. Scoles PV, Linton AE, Latimer B, Levy ME, Digiovanni BF: Vertebral body and posterior element morphology: The normal spine in middle life. Spine 13:1082-1086, 1988

115. Somerville EW: Rotational lordosis: The development of the single curve. J Bone Jt Surg 34B:421-427, 1952

116. Stagnara P, deMauroy JC, Dran G, Gonon GP, Costanzo G, Gimnet J, Pasquet A: Reciprocal angulation of vertebral bodies in a sagittal plane: Approach to references for the evaluation of kyphosis and lordosis. Spine 7:335-342, 1982

117. Steindler A: Kinesiology of the Human Body. Springfield, IL, Thomas, 1955

118. Stokes IAF, Gardner-Morse M: Analysis of the interaction between vertebral lateral deviation and axial rotation in scoliosis. J Biomech 24:753-759, 1991

119. Sullivan WE, Miles M: The lumbar segment of the vertebral column. Anat Rec 133:619-636, 1959

120. Sundaram SH, Feng CC: Finite element analysis of the human thorax. J Biomech 10:505-516, 1977

121. Tencer AF, Ahmed AM, Burke DL: Some static mechanical properties of the lumbar intervertebral joint, intact and injured. J Biomech Eng 104:193-201, 1982

122. The Random House College Dictionary, 1st edition (revised). Edited by JS Stein. New York, Random House, 1975

123. Timoshenko SP, Gere JM: Theory of Elastic Stability, 2nd edition. New York, McGraw-Hill, 1963

124. Todd TW, Pyle SI: A quantitative study of the vertebral column by direct and roentgenoscopic methods. Am J Phys Anthrop 12:321-339, 1928

125. Veldhuizen AG, Scholten PJM: Kinematics of the scoliotic spine as related to the normal spine. Spine 12:852-858, 1987

126. Waters RL, Morris JM: An in vitro study of normal and scoliotic interspinous ligaments. J Biomech 6:343-348, 1973

127. Wenger HL: Rib section in treatment of scoliosis. Arch Surg 44:119-128, 1942

128. Wenger HL, Herman M: Role of transverse process in thoracogenic scoliosis. Quart Bull Sea View Hosp 7:45-55, 1941

129. White III AA: Kinematics of the normal spine as related to scoliosis. J Biomech 4:405-411, 1971

130. White III AA, Panjabi MM: Clinical Biomechanics of the Spine. Philadelphia, JB Lippincott, 1978

131. Willner S: Spinal pantograph: A non-invasive technique for describing kyphosis and lordosis in the thoraco-lumbar spine. Acta Orthop Scand 52:525-529, 1981

132. Willner S: A study of growth in girls with adolescent idiopathic structural scoliosis. Clin Orthop 101:129-135, 1974

133. Wilson TA, Rehder K, Krayer S, Hoffman EA, Whitney CG, Rodarte JR: Geometry and respiratory displacement of human ribs. J Appl Physiol 62:1872-1877, 1987

134. Winter RB: The Spine. Pediatric Orthopaedics. Volume 2. Edited by WW Lovell, RB Winter. Philadelphia, JB Lippincott, 1978

135. Wynne-Davies R: Familial (idiopathic) scoliosis: A family survey. J Bone Jt Surg 50B:24-30, 1968

136. Yamada H: Strength of Biological Materials. Edited by FG Evans. Baltimore, Williams & Wilkins, 1970

Appendix A

Glossary of Anatomical & Biomechanical Terms Related to Spine

1. Planes: [44] (see Fig. A1)

median (midsagittal) plane - plane which divides body into a right and left half

sagittal plane - any vertical anteroposterior plane parallel to the median plane

coronal (frontal) plane - any vertical plane at right angles to the sagittal plane

transverse (horizontal) plane - any plane at right angles to both the sagittal and coronal plane

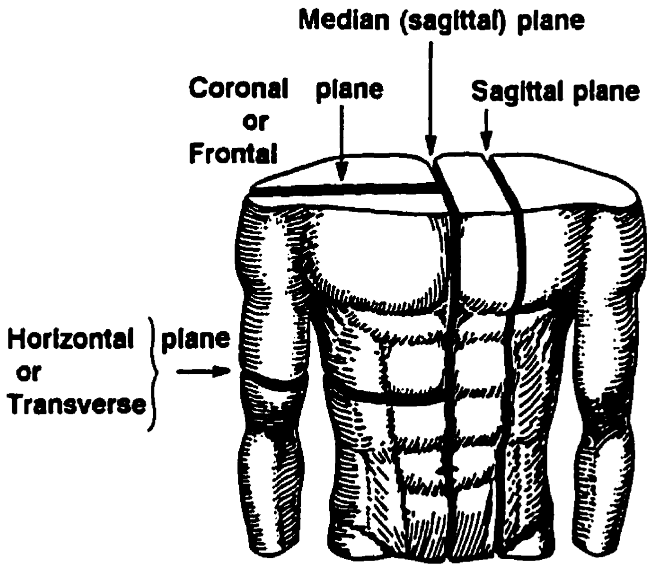

Fig. A.1 Fundamental planes in body. After Grant [44].

2. Terms of Relationship: [44]

anterior - nearer the front surface of the body
posterior - nearer the back surface of the body

superior - nearer the crown of the head
inferior - nearer the soles of the feet

medial - nearer the median plane of the body
lateral - farther from the median plane of the body

cranial - superior end
caudal - inferior end

ipsilateral - refers to the same side of the body
contralateral - refers to opposite sides of the body

3. Miscellaneous Terms Related to Spine:

intervertebral joint - joint inbetween adjacent vertebra in spinal column comprised of intervertebral disc, ligaments, and facet joint

motion segment - usually consists of two vertebrae and the intervertebral joint inbetween. Used in particularly for testing flexibility or stiffness of intervertebral joint

flexion - in reference to the spine, forward or anterior bending in sagittal plane

extension - in reference to the spine, backward or posterior bending in sagittal plane

lateral bending - in reference to the spine, bending in frontal plane to the right or left

lordosis - curvature of the spine in the sagittal plane with its convexity anterior, i.e. longer anterior length than posterior length of spine

kyphosis - curvature of the spine in the sagittal plane with its convexity posterior, i.e. longer posterior length than anterior length of spine

ligamentous spine - spine with its rib cage and muscles removed

thoracolumbar - pertaining to thoracic and lumbar regions of the spine

coupling - phenomenon in which motion along or about an axis is consistently associated with motion along or about another axis [88]

main motion - motion produced in same direction as applied load [88]

coupled motion - motion produced in direction(s) other than direction of applied load

Appendix B

Formula used to calculate equivalent sectional properties for 3-element model based on the approximation of 3 equal length elements

1. Notation used in formulas:

   1 denotes lateral plane
   2 denotes anterior-posterior (sagittal) plane
   eq denotes equivalent property
   i denotes inside segment ie. central
   o denotes outside segment ie. anterior and posterior
   β denotes % of full element to inside element
   α denotes % of full element to outside elements such that $2\alpha + \beta = 1$
   property definitions are found in List of Symbols

2. Figures defining additional notation and making correspondence between the 1-element and equivalent 3-element representations.

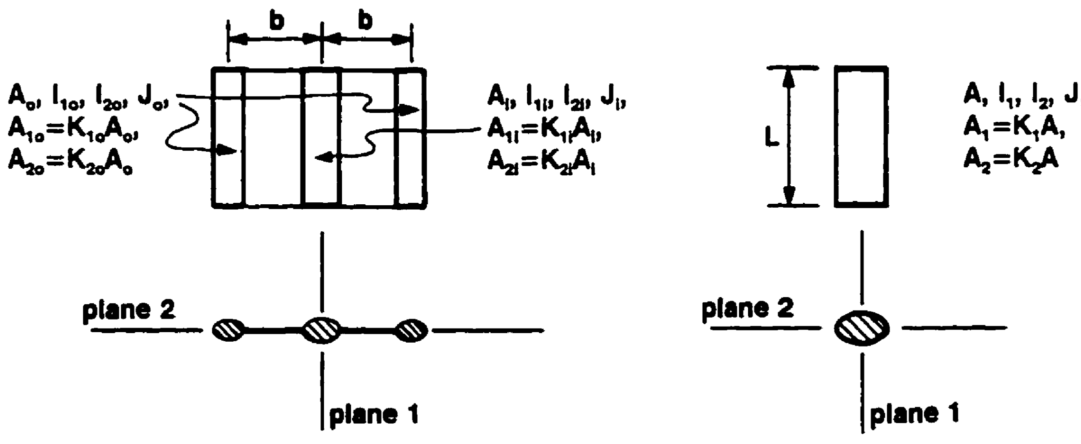

3. **Properties of the 3-element equivalent model in terms of the 1-element model. α and β are chosen appropriately in a particular instance.**

Axial Area:
$$A_t = \beta A$$
$$A_e = \alpha A$$

Lateral Bending Inertia:
$$I_{1_t} = \beta I_1$$
$$I_{1_e} = \alpha I_1$$

Lateral Shear Area:
$$A_{1_t} = \beta A_1 \qquad K_{1_t} = \frac{A_{1_t}}{A_t} = \frac{\beta A_1}{\beta A} = K_1$$
$$A_{1_e} = \alpha A_1 \qquad K_{1_e} = \frac{A_{1_e}}{A_e} = \frac{\alpha A_1}{\alpha A} = K_1$$

Ant-Post Bending Inertia:
$$I_{2_{eq}} = I_2 - 2b^2\alpha A$$
$$I_{2_t} = \beta I_{2_{eq}}$$
$$I_{2_e} = \alpha I_{2_{eq}}$$

Ant-Post Shear Area:
$$A_{2_{eq}} = \frac{1}{G\left[\dfrac{L^2}{3EI_2} + \dfrac{1}{GA_2} + \dfrac{b^2L^2\alpha A}{2EI_{2_{eq}}I_2} - \dfrac{L^2}{3EI_{2_{eq}}}\right]}$$
$$A_{2_t} = \beta A_{2_{eq}} \qquad K_{2_t} = \frac{A_{2_t}}{A_t} = \frac{\beta A_{2_{eq}}}{\beta A} = \frac{A_{2_{eq}}}{A}$$
$$A_{2_e} = \alpha A_{2_{eq}} \qquad K_{2_e} = \frac{A_{2_e}}{A_e} = \frac{\alpha A_{2_{eq}}}{\alpha A} = \frac{A_{2_{eq}}}{A}$$
$$\therefore \quad K_{2_t} = K_{2_e} = \frac{A_{2_{eq}}}{A}$$

Torsional Constant:
$$J_t = J - \frac{2b^2}{G}\left[\frac{1}{\dfrac{L^2}{12E\alpha I_1} + \dfrac{1}{G\alpha A_1}}\right]$$
$$J_e = 0$$

4. **Tables for the properties of the 1-element model used in calculating equivalent 3-element properties. α is chosen such that I_{2eq} is a positive value. This is a restriction on input data required in NASTRAN. In this case, α choosen to be 0.12 (i.e. β=0.76).**

Table B.1 Values Used to Calculate Equivalent Properties for 3-Element Vertebra

Vertebra	E (N/cm^2)	G (N/cm^2)	A (cm^2)	I_1 (cm^4)	I_2 (cm^4)	J (cm^4)	K_1,K_2	Avg. (central) length, L (cm)	Avg. sag. radius, b (cm)
T1	1030000	431000	4.24	2.651	0.773	2.395	1	1.679	0.853
T2	1030000	431000	4.72	3.061	1.030	3.083	1	1.791	0.937
T3	1030000	431000	5.08	3.036	1.390	3.813	1	1.848	1.05
T4	1030000	431000	5.50	3.181	1.822	4.633	1	1.905	1.1535
T5	1030000	431000	6.05	3.631	2.342	5.695	1	1.957	1.244
T6	1030000	431000	6.68	4.240	2.965	6.980	1	1.993	1.3295
T7	1030000	431000	7.44	5.198	3.728	8.685	1	2.021	1.4165
T8	1030000	431000	8.23	6.386	4.566	10.650	1	2.073	1.4895
T9	1030000	431000	8.98	7.853	5.250	12.586	1	2.134	1.527
T10	1030000	431000	9.97	10.407	6.022	15.258	1	2.304	1.554
T11	1030000	431000	11.15	13.896	7.036	18.684	1	2.43	1.5925
T12	1030000	431000	12.00	16.789	7.813	21.327	1	2.574	1.615
L1	1030000	431000	12.81	19.659	8.692	24.108	1	2.72	1.6545
L2	1030000	431000	13.57	22.346	9.624	26.908	1	2.793	1.6895
L3	1030000	431000	14.58	26.430	10.853	30.774	1	2.8	1.7285
L4	1030000	431000	15.25	28.846	11.896	33.690	1	2.747	1.7655
L5	1030000	431000	14.73	26.207	11.366	31.710	1	2.653	1.756

Table B.2 Values Used to Calculate Equivalent Properties for 3-Element Intervertebral Joint

Superior Vertebra	E (N/cm^2)	G (N/cm^2)	A (cm^2)	I_1 (cm^4)	I_2 (cm^4)	J (cm^4)	K_1,K_2	Avg. (central) length, L (cm)	Avg. sag. radius, b (cm)
T1	929.7	1376.0	4.39	0.826	1.932	0.697	0.4375	0.449	0.887
T2	732.7	1535.4	4.98	1.384	2.962	0.667	0.4375	0.31	0.9935
T3	746.7	1593.0	5.36	1.716	3.643	0.779	0.4375	0.272	1.106
T4	800.9	1656.4	5.71	2.176	3.177	0.928	0.4375	0.222	1.1995
T5	745.0	1523.5	6.28	2.544	4.013	1.154	0.4375	0.251	1.289
T6	820.2	1666.3	6.89	2.946	4.912	1.362	0.4375	0.32	1.3755
T7	645.7	1650.0	7.61	4.788	4.646	1.741	0.4375	0.4	1.4535
T8	776.1	1537.5	8.38	4.584	6.834	2.471	0.4375	0.442	1.5155
T9	806.8	1646.2	9.02	4.681	5.394	3.062	0.4375	0.473	1.5395
T10	775.3	1577.4	10.09	7.353	10.790	4.511	0.4375	0.507	1.573
T11	920.7	1484.3	11.30	6.810	9.232	10.787	0.4375	0.68	1.611
T12	1060.1	1562.4	12.07	7.469	13.736	41.265	0.4375	0.841	1.6295
L1	1042.8	1564.1	12.98	6.174	15.802	34.163	0.4375	1.006	1.6755
L2	998.8	1493.1	13.78	5.592	25.453	42.473	0.4375	1.147	1.7095
L3	1225.6	1494.0	14.66	4.946	23.332	50.101	0.4375	1.221	1.7415
L4	1251.2	1429.8	15.38	6.478	16.797	47.705	0.4375	1.401	1.7775
L5	1164.3	1451.7	14.55	15.514	14.833	43.081	0.4375	1.57	1.733

Appendix C

Model of Normal Spine and Rib Cage: MOE

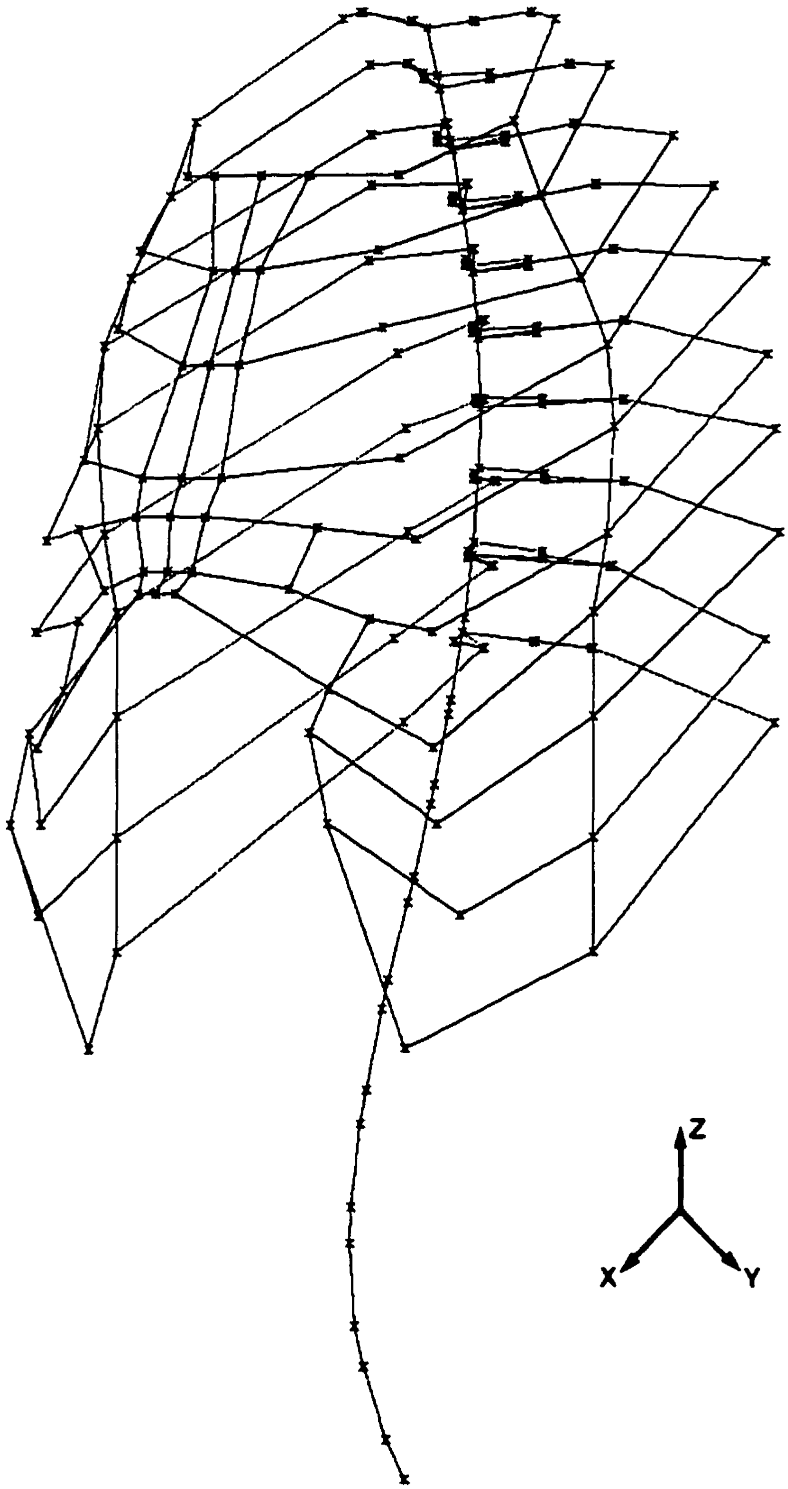

Fig. C.1 Oblique view of the 3-dimensional model (MOE) of the normal spine and rib cage. Nodes are denoted with an x.

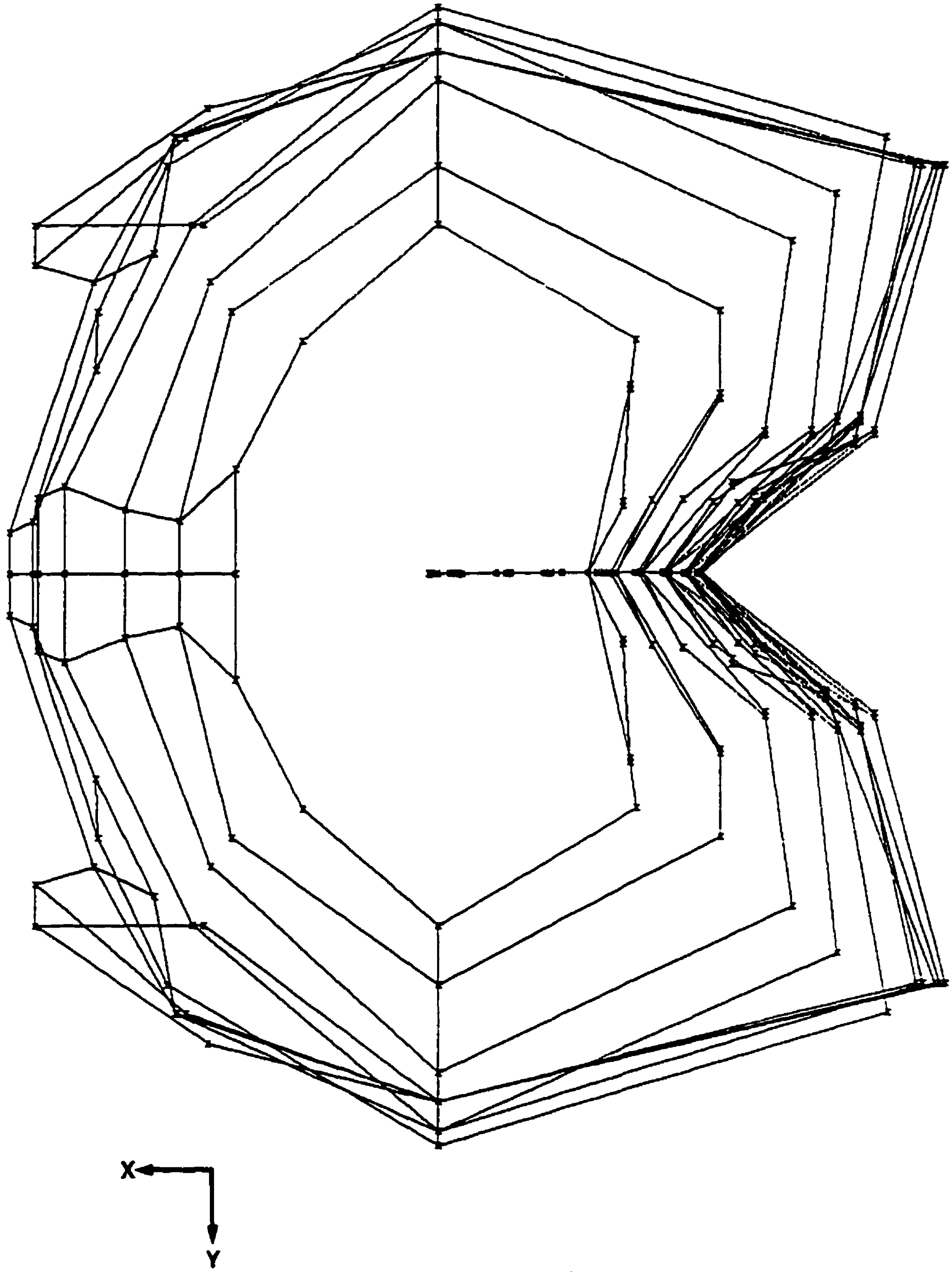

Fig. C.2 Top view of model.

Table C.1 Legend for Spine and Rib Cage Model

Element no.	Description of element	Element type	Property no.
1-33 odd 2-34 even	Centerline of vertebrae Centerline of i.v. joint	beam	101-117 1-17
35-67 odd 36-68 even	Anterior face of vertebrae Anterior face of i.v. joint	beam	118-134 18-34
69-101 odd 70-102 even	Posterior face of vertebrae Posterior face of i.v. joint	beam	118-134 18-34
103-137 138-172	Endplates on anterior side Endplates on posterior side	beam	100 (rigid)
173-190 191-208	Left vertebrae links to facets Right vertebrae links to facets	beam	150
209-218 219-228	Left transverse processes Right transverse processes	beam	151
229-246 247-264	Left CV joints Right CV joints	beam (axial only)	60
265-274 275-284	Left CT joints Right CT joints	beam	61
285-364	Ribs (10 pairs - 4 elements ea.)	beam	153-162 (Rib 1-10)
365-382 383-400	Left CC Right CC	beam	71-88
401-412 413-418	Sternum (quad. elements) Sternum (beam elements)	quad beam	152 100 (rigid)
421-429 430-438	Left IC Right IC	beam (axial only)	62-70
500-525	Loading arms (from bottom center of vertebra to C.G.)	beam	100 (rigid)

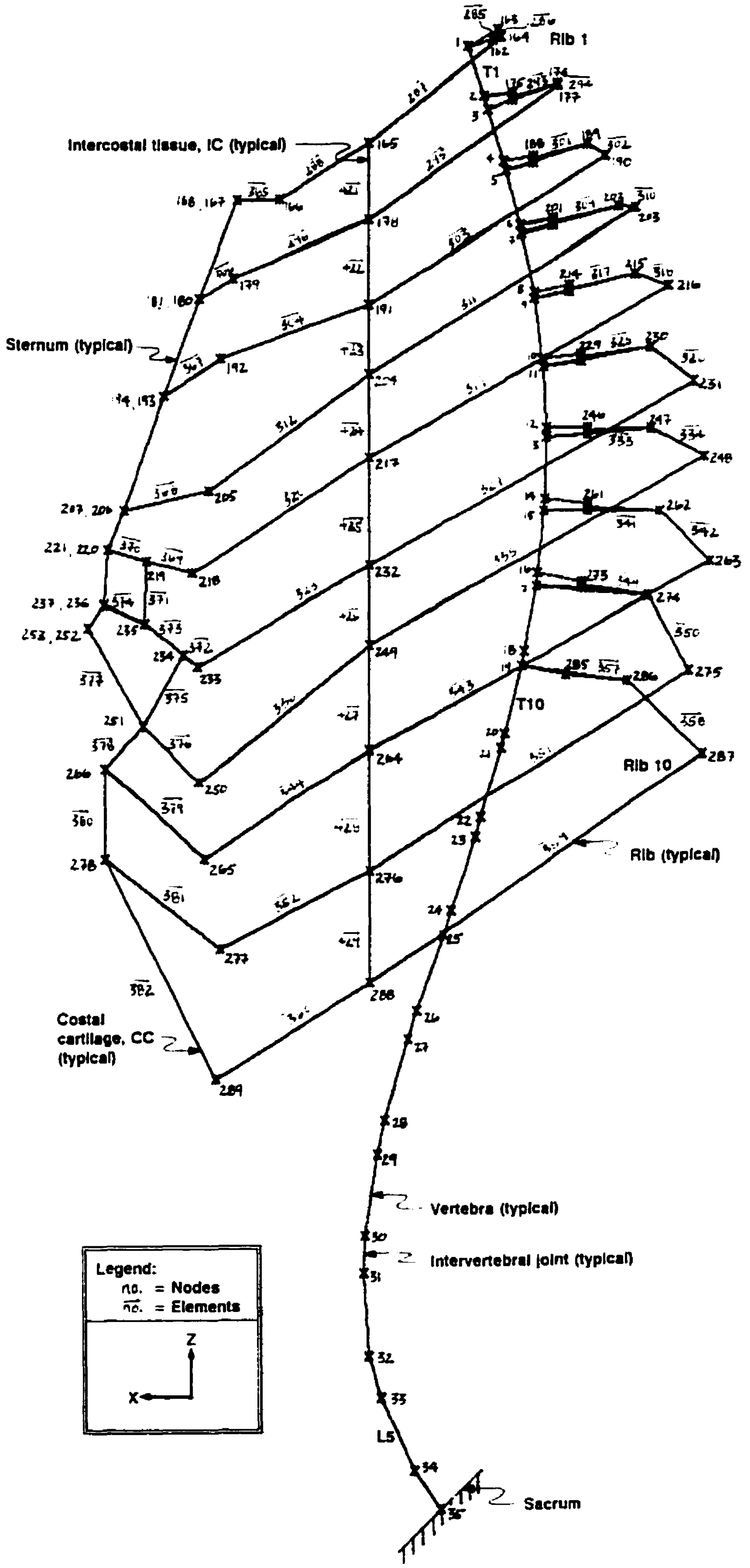

Fig. C.3 Left lateral view of model illustrating nodes and elements of the spine and left side of (symmetrical) rib cage.

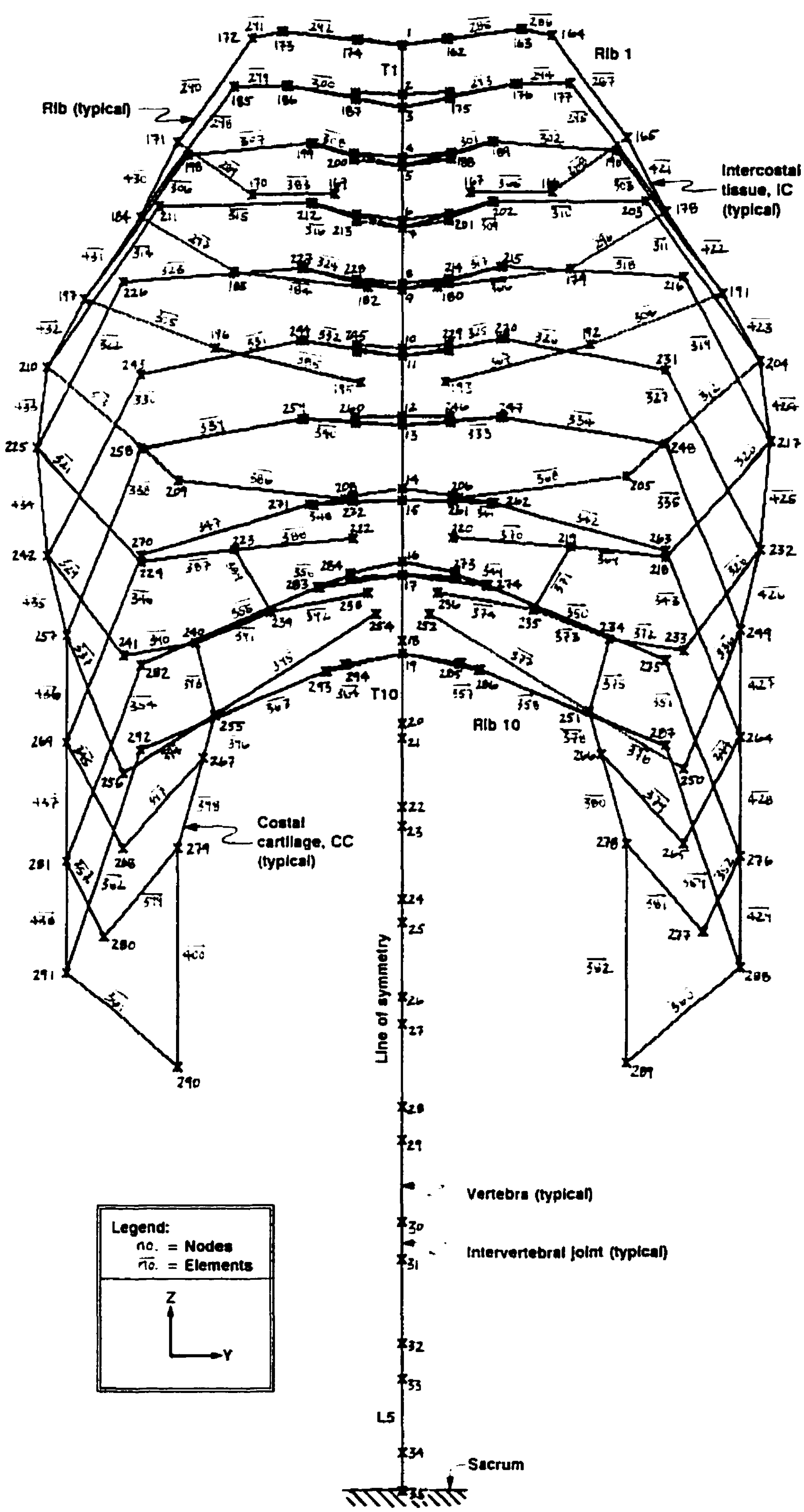

Fig. C.4 Anterior (front) view of model illustrating nodes and elements of the spine and rib cage. Stermun removed to simplify figure.

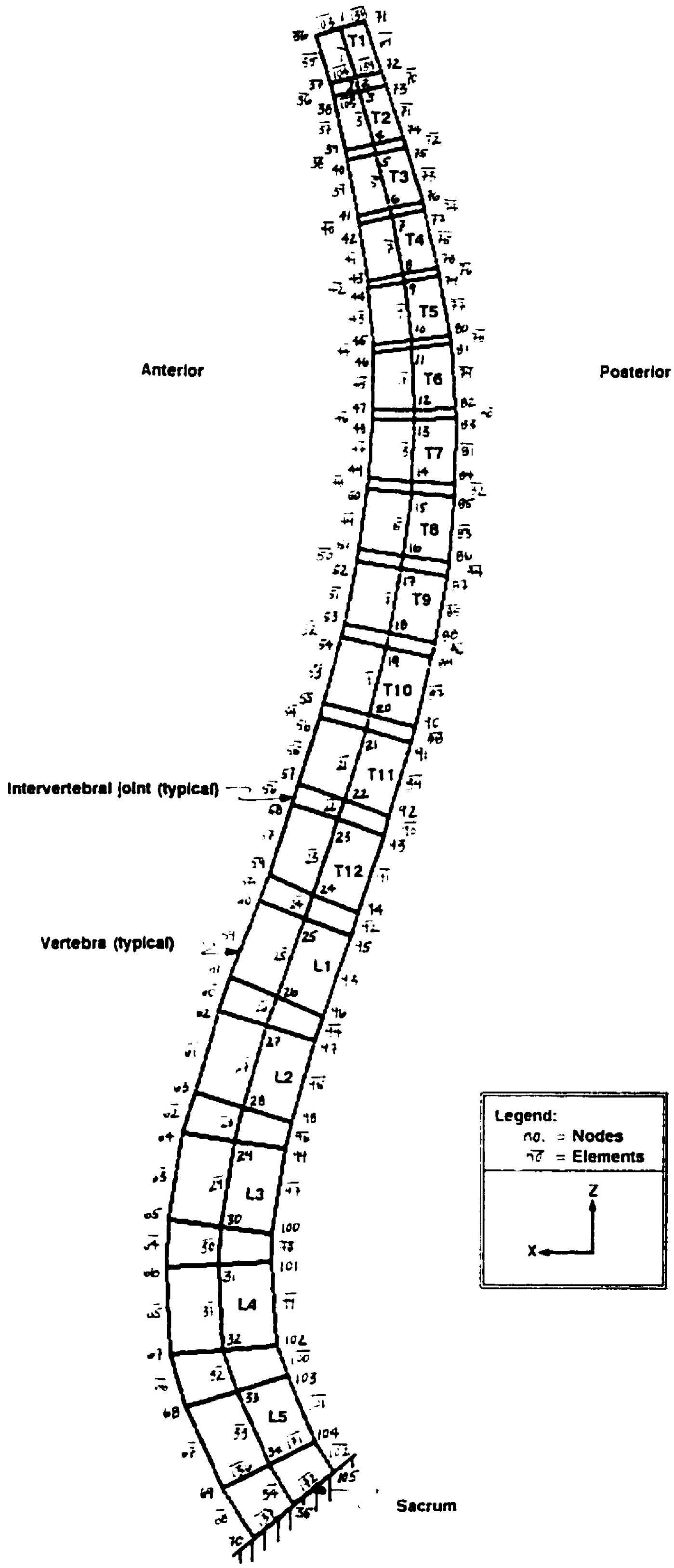

Fig. C.5 Left lateral view of the 3-element model of the spine illustrating nodes and elements. Rib cage (left out to simplify figure) is attached to central elements as shown in 1-element model, Fig. C.3.

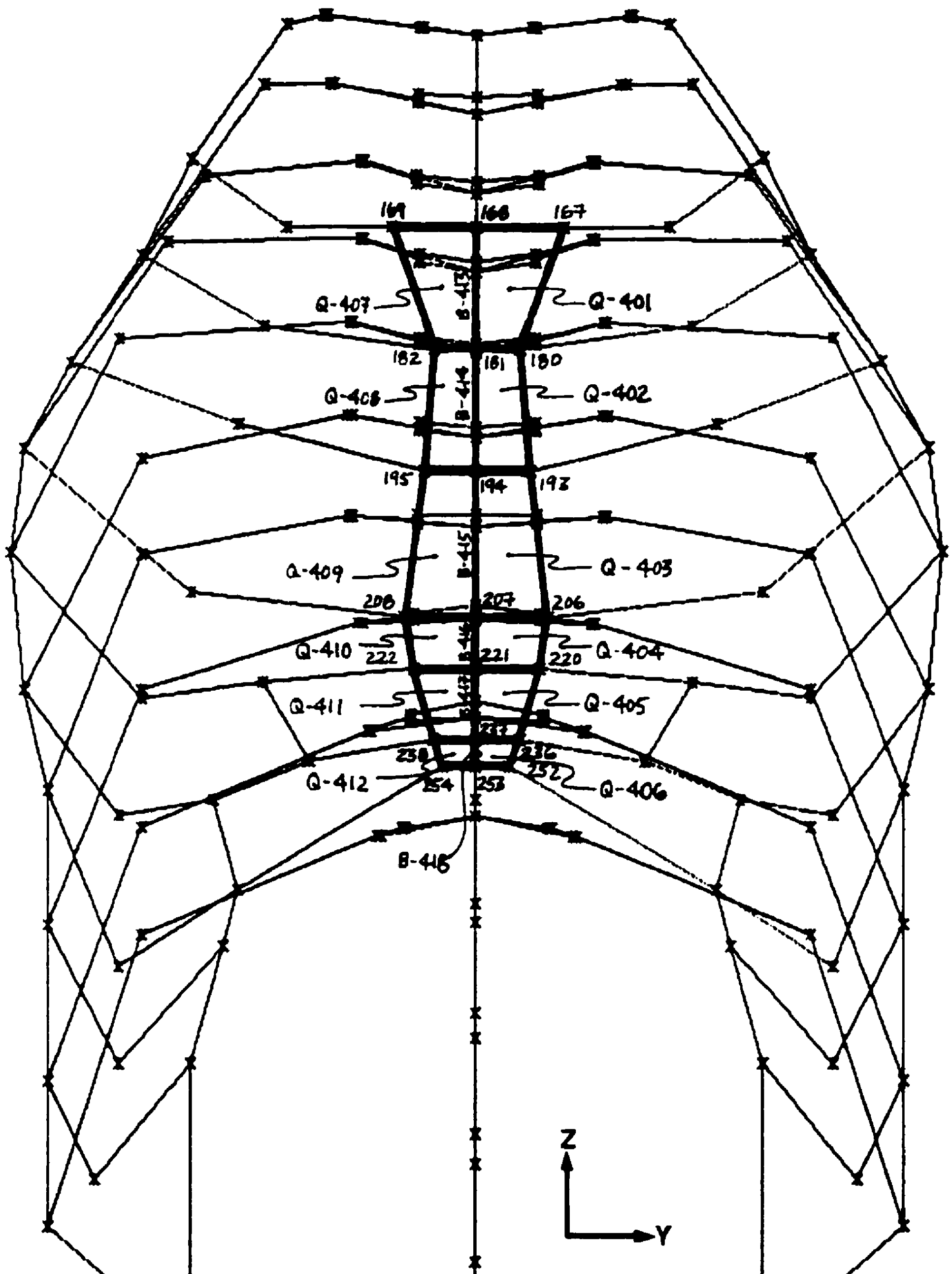

Fig. C.6 Anterior view of model illustrating nodes and elements of the sternum. Q-no. = quadrilateral elements, B-no. = beam elements, no. = nodes.

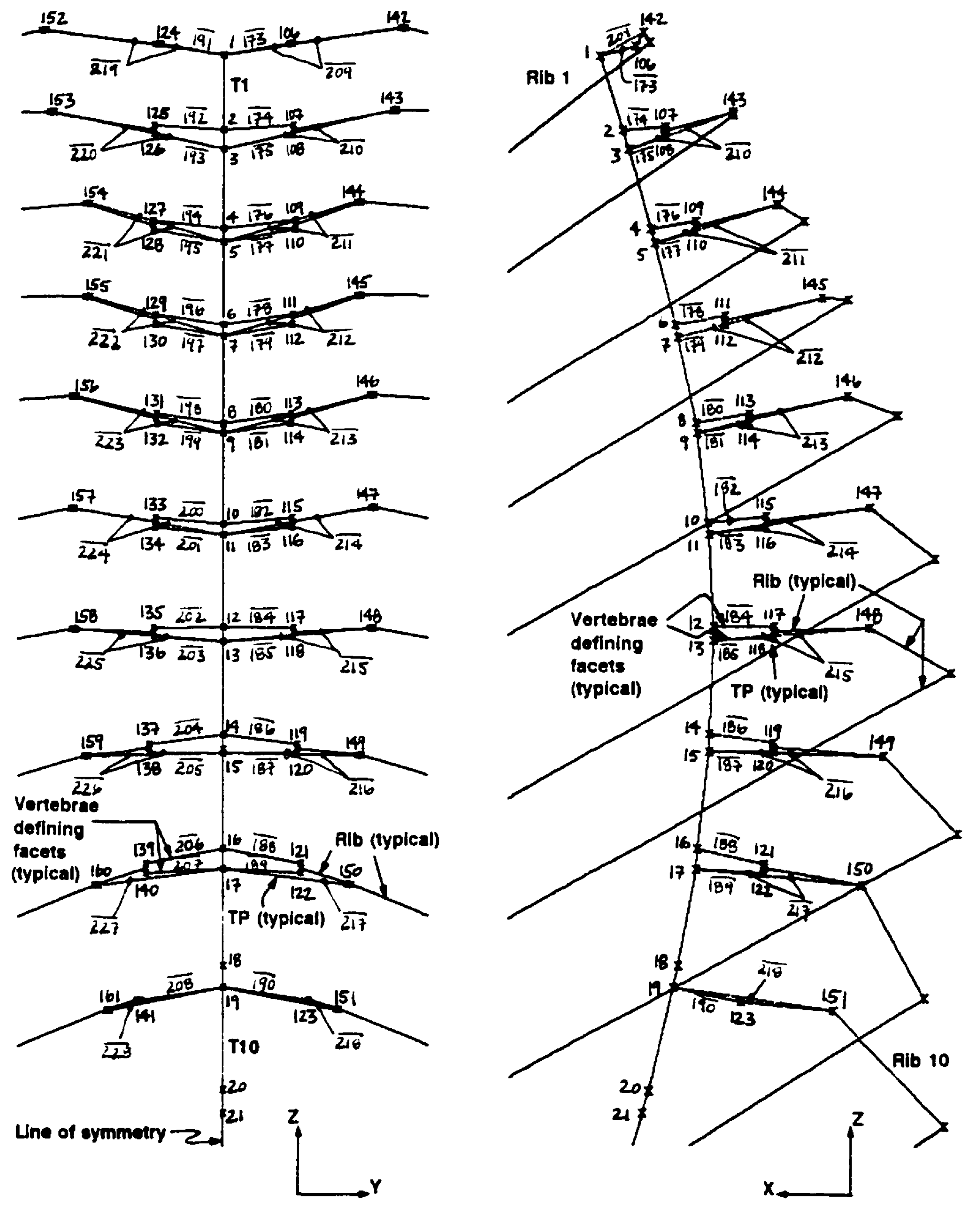

(a) (b)

Fig. C.7 Transverse process elements and elements positioning vertebral body facets shown in (a) anterior view, and (b) left lateral view. These elements define the location on the vertebrae where ribs are attached. $\overline{no.}$ = elements, no. = nodes.

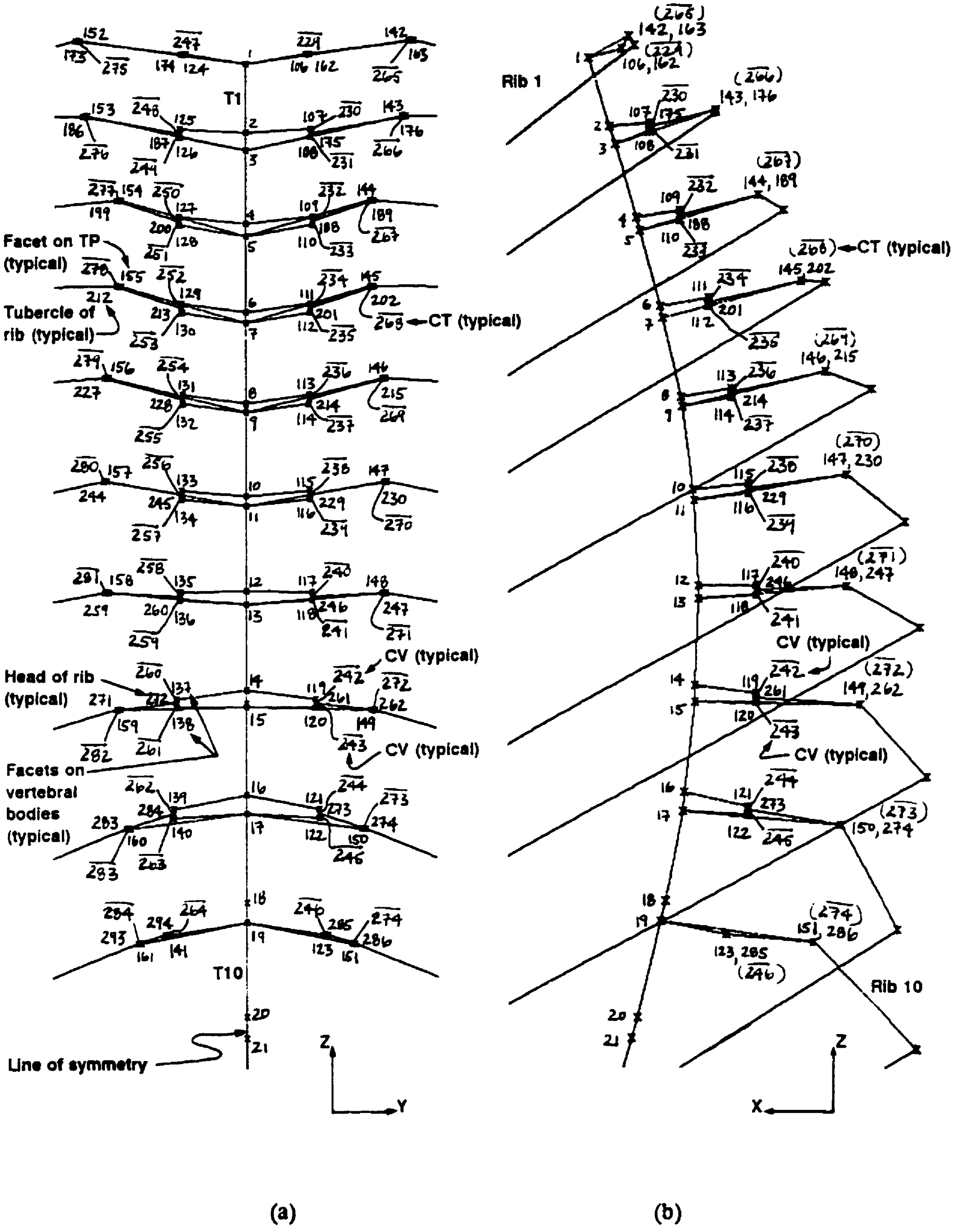

Fig. C.8 Costovertebral (CV) and costotransverse (CT) elements shown in (a) anterior view, and (b) left lateral view. These elements provide connections between vertebrae and ribs. CV connects head of rib to vertebral body, and CT connects tubercle of rib to transverse process. $\overline{no.}$ = elements, *no.* = nodes.

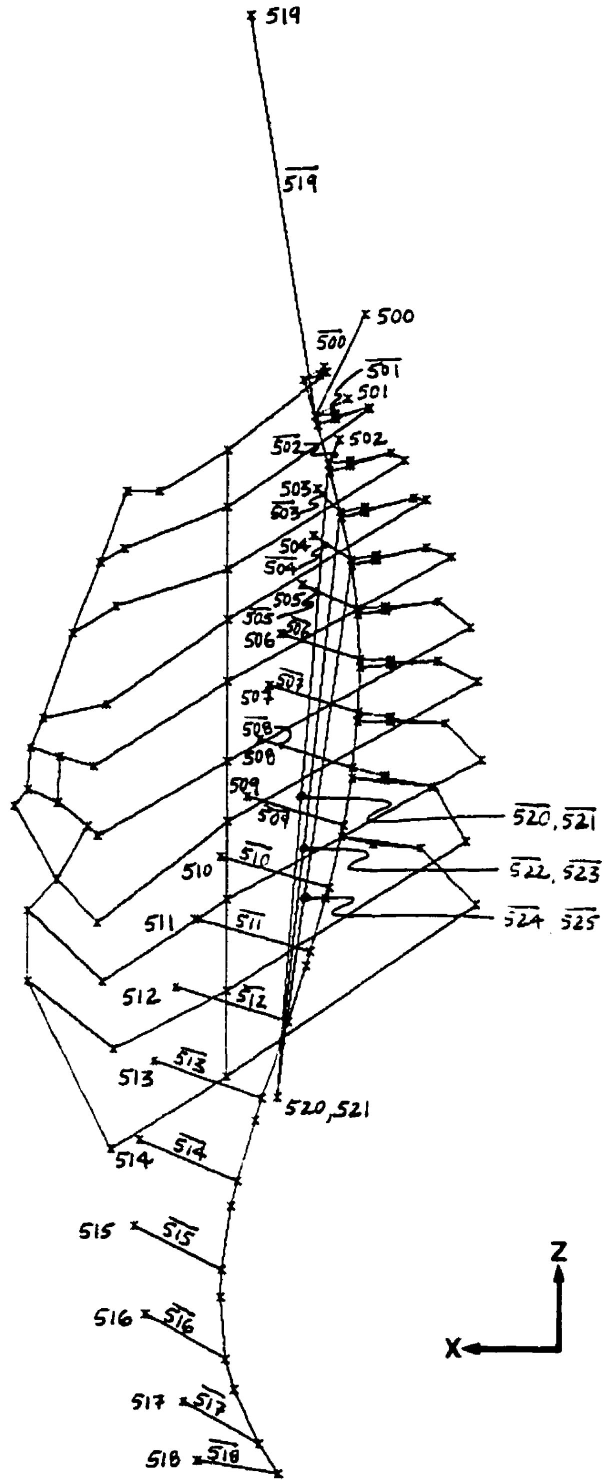

Fig. C.9 Left lateral view of model illustrating nodes and elements used for distributed-type loading. $\overline{no.}$ = elements, no. = nodes.